Development and characterisation of a heparinised fibrin hydrogel as a delivery vehicle for regenerative medicine

By

Miss Silindile Ngcobo

NGCSIL005

This thesis is presented for the degree

Doctor of Philosophy (PhD) in Biomaterials

In the Department of Surgery

Chris Barnard Division of Cardiothoracic Surgery

University of Cape Town

2023

Supervisor: Prof. Neil Davies

Plagiarism declaration

I, **Silindile Ngcobo**, hereby declare that the work on which this thesis is based is my original work (except where acknowledgements indicate otherwise) and that neither the whole work nor any part of it has been, is being, or is to be submitted for another degree at the University of Cape Town or any other University. I authorise the University of Cape Town to reproduce, for the purpose of research, either the whole or any portion of the contents in any manner whatsoever.

Signature:

Signed by candidate

Date: 20 December 2023

Acknowledgements

I extend my gratitude to my supervisor, Professor Neil Davies, for his invaluable academic guidance, unwavering support, and full presence throughout the PhD journey.

I thank the late Professor Deon Bezuidenhout for all his contributions and insights towards this thesis as a co-supervisor. He never lacked a good word of encouragement and support.

Mrs. Helen Isley is acknowledged for all her efforts in ensuring that the reagents needed for this study were available in the lab. I also thank her for assistance with the Histology work. Equally, I thank Mrs. Anel Oosthuizen of the Polymer Lab for her assistance and patience when sourcing specific reagents, allowing me to use the Polymer Lab's equipment whenever I needed them, and making time to advice on my questions.

I acknowledge Dr. Jandré De Villiers of the Polymer Lab for his initial assistance with thromboelastography, Mrs. Miranda Waldron of the Electron Microscope Unit for scanning electron microscopy assistance, Associate Professor Dirk Lang of the Confocal & Light Microscope Imaging Facility for training and advice in confocal microscopy, and Ms Janet MacCallum together with Dr. Chima Ofoegbu for all their assistance with animal surgical procedures in the Research Animal Facility.

All fundings from the South African National Research Foundation (including travel grants), University of Cape Town's Merit Awards and Doctoral Research Scholarship, as well as the Department of Surgery PhD Studentship are hereby acknowledged.

I also thank all my lab and office mates, past and present, who made my time at the Cardiovascular Research Unit a pleasant experience. Similarly, I thank every single individual that walked this journey beside me through prayers, conversations, hugs, hearty meals, and writing treats.

Lastly, I give praises to the Lord God Almighty whose steady hand took hold of my right hand till the end.

Dedication

I dedicate this thesis to my family:

My parents Mrs. Ntombi Margret “maDlamini” Ngcobo and Mr. Norman Jabulani Ngcobo who modelled the value of education and made sacrifices to see it realised for us.

My siblings Nompumelelo Patience Ngcobo who is late, Khululiwe Ngcobo and Thulisiwe Ngcobo for their friendship, and support.

Thank you for everything ♥

Abstract

Fibrinogen is an attractive hydrogel candidate for regenerative medicine due to its inherent biocompatibility, biodegradability, and clinical approval. It is the precursor protein cleaved by the protease thrombin that polymerises into a fibrous network known as fibrin. The present study sought to modify fibrinogen through covalent attachment of heparin to form heparinised fibrin hydrogels. Heparin is known to bind a significant number of growth factors and its anti-coagulative characteristic plays a role in minimising thrombotic events. We therefore developed a novel method for attaching heparin to fibrinogen that allowed for retention of thrombin-based polymerisation. Additionally, the potential of co-modification with polyethylene glycol (PEG) enhancing heparinisation and improving fibrin resistance to proteolytic degradation was assessed. The modified forms of fibrin hydrogel were then assessed for their potential as regenerative hydrogels.

To conjugate heparin to fibrinogen, we explored the utility of an acrylated form of heparin (developed in Professor Bezuidenhout's Polymer Laboratory) that preferentially binds to thiol groups (such as cysteine side chains in proteins) via a Michael-type addition reaction. As additional free thiols might increase heparin binding, we also modified the fibrinogen with a n-hydroxysuccinimide-PEG-thiol (NHS-PEG-SH) molecule, and a maleimide based assay confirmed that 0.75 free thiols were successfully bound to fibrinogen to form modified fibrinogen-PEG-SH (FP). This represented a greater than 100-fold increase in free thiols present in native fibrinogen. This binding was further confirmed with a Fourier-transform infrared spectroscopy. Fibrinogen and FP were then assessed for hep-acr binding.

Two assays were used for heparin quantification, namely calorimetric 3-Methyl-2-Benzothiazolinone Hydrazone assay modified for quantification of protein bound heparin, and a commercial fluorescent probe-based assay. Both assays showed that hep-acr was successfully conjugated to fibrinogen and FP at 0.2-0.3 molecules of heparin bound per either molecule to form fibrin(ogen)-heparin (FH) and fibrin(ogen)-peg-heparin (FPH) respectively. Binding through the acrylate moiety was confirmed

with non-acr hep binding at 10 times lower levels. All modified forms of fibrinogen retained the ability to polymerise via the action of thrombin.

Though not amplifying heparinisation, PEGylation and heparinisation combined strongly protected fibrin from spontaneous *in-vitro* degradation at 37ºC compared to all other hydrogel formulations (fibrin and FH were 100% degraded by day 5; FP by day 6 and FPH only by 57% at day 15). Micrographs from scanning electron microscopy (SEM) revealed a more fibrillar structure after polymerisation for FH closer in morphology to that of fibrin, while FP and FPH both formed more sheet like structures. Rheology showed a reduction in storage modulus/ mechanical stiffness for FP (18.3 ± 1.3 Pa) and FPH (17.6 ± 2.7 Pa) compared to normal fibrin (42.1 ± 1.5 Pa) and FH (36.7 ± 1.9 Pa). Despite these differences, both FH and FPH were anti-thrombotic as determined by the attached heparin completely impeding clot formation for the duration of analysis (2 hours) with thromboelastography, as compared to whole blood, fibrinogen, and FP which formed clots within 1.4 ± 0.1, 1.5, and 1.3 ± 0.1 min respectively.

All the hydrogels were biocompatible, with viability percentages not less than 70% after three days of 3D culture for all three cell lines evaluated, namely human umbilical vein endothelial cells (HUVECs), human dermal fibroblasts and adipose tissue-derived stem cells (ADSCs) as indicated by live/dead assays. A 3D HUVEC spheroid-based angiogenesis assay found that FH substantially stimulated formation of capillary-like structures relative to fibrin. When evaluated for growth factor release *in-vitro*, the burst release in the first day was reduced by 5-fold for both basic fibroblast growth factor (bFGF) and vascular endothelial growth factor (VEGF) in the presence of heparin. Both FH and FPH further prolonged and sustained bFGF and VEGF release *in-vitro* relative to their unheparinised counterparts. The FH and FPH released 16 ± 0.7 and 16 ± 0.7 ng bFGF per day, and 20.5 ± 2.2 ng and 18.4 ±1.6 ng VEGF per day up to 15 days respectively with bioactivity maintained.

An initial *in-vivo* subcutaneous rat model study of fibrin formulations loaded with 1 µg of VEGF showed pronounced vessel formation into all forms of fibrin independent of VEGF after 10 days. A significant increase in vessel ingrowth for either heparinised form of fibrin was not observed. This dosage of VEGF has previously been seen to stimulate neovascularisation into heparinised PEG hydrogels in our laboratory and it

was hypothesised that the high levels of vascularisation stimulated by fibrin alone may have obscured the VEGF induced angiogenesis. Further studies exploring VEGF dosage and concentration of fibrin hydrogels should be carried out.

As delivery of stem cells within hydrogels is a key present function of regenerative hydrogels, the impact of the heparinised fibrinogens on ADSC differentiation underwent preliminary investigation. The impact of heparin on mesenchymal stem cell differentiation is presently unclear with several contradictory reports in the literature. Predictably the soft fibrin hydrogels in all formulations strongly promoted adipogenesis relative to stiff tissue culture plastic (TCP). More surprisingly, osteogenesis was also increased on the fibrin hydrogels relative to TCP. Additionally, heparinisation altered differentiation, where osteogenic differentiation in FH was significantly increased against all groups, while this increase was observed in FH when compared to the FP group for adipogenic differentiation.

In conclusion, this study presents two methods of conjugating heparin to fibrinogen to form anti-thrombotic heparinised fibrin hydrogels where polymerisation via thrombin activity was retained. The bound heparin in both hydrogel systems substantially reduced burst release of bFGF and VEGF and allowed for sustained release of bioactive growth factors. The FPH was advantageous in that it reduced inherent fibrin degradation, and provided a transparent physical appearance that was useful in viewing encapsulated cells. The FH did not significantly reduce mechanical stiffness compared to unmodified fibrin, and further encouraged more HUVEC invasion in 3D. All formulations of fibrin hydrogels proved to be significantly better matrices for ADSC adipogenic and osteogenic differentiation as compared to TCP. These findings are crucial for applications in stem cell and, growth factor delivery and ultimately tissue regeneration.

Table of Contents

Plagiarism declaration II

Acknowledgements III

Dedication IV

Abstract V

List of figures ..... XIII~~XVIII~~

List of tables ..... XVI~~XXI~~

List of appendices ..... XVII~~XXII~~

CHAPTER 1: LITERATURE REVIEW 1

1.1. Regenerative medicine 1

1.2 Hydrogels 1

1.3 Synthetic hydrogels 5

1.4 Natural hydrogels 8

1.4.1 Polysaccharides 9

1.4.1.1 Cellulose 9

1.4.1.2 Chitin ..... 10~~11~~

1.4.1.3 Alginate 12

1.4.2 Decellularised tissues 15

1.4.3 Proteins 18

1.4.3.1 Collagen ..... 18~~19~~

1.4.3.2 Fibrinogen ..... 20~~21~~

1.4.3.3 Fibrin in wound healing ..... 23~~24~~

1.4.3.4 Mechanism of fibrin formation and branching ..... 27~~28~~

1.4.3.5 Fibrinolysis 30

1.5 Fibrin hydrogels ..... 30~~31~~

1.5.1 Hydrogel micro-structure ..... 30~~31~~

1.5.2 Hydrogel mechanical properties 3233
1.5.3 Applications in wound sealing 3435
1.5.4 Applications in cell support and delivery 3637
1.5.5 Applications in growth factor delivery 3940
1.5.6 Fibrin hydrogel functionalisation through PEGylation 4243
1.5.7 Fibrin hydrogel functionalisation with heparin 4647
1.5.7.1 Growth factor localisation for controlled release 4950
1.6 Study rationale 5556
1.7 Aim 5657
1.8 Hypothesis 5657
1.9 Objectives 5657
CHAPTER 2: HEPARIN CONJUGATION TO FIBRINOGEN AND CHARACTERISATION 5758
2.1 Introduction 5758
2.2 Results and discussion 6061
2.2.1 Method development: Fibrinogen heparinisation 6061
2.2.2 Fibrinogen bound heparin quantification 6768
2.2.3 Characterisation 7273
2.2.3.1 Fourier Transform Infrared Spectroscopy 7273
2.2.3.2 Thromboelastography 7475
2.2.3.3 In-vitro hydrogel degradation 7677
2.2.3.4 Turbidity analysis 7778
2.2.3.5 Scanning electron microscopy for microstructure 7980
2.2.3.6 Rheological analysis for stiffness 8283
2.2.4 *In-vitro* cytocompatibility 8485
2.2.5 Endothelial cell invasion with 3D spheroids 8991
CHAPTER 3: SUSTAINED GROWTH FACTOR RELEASE 9597

3.1 Introduction 9597
3.2 Results and discussion 99101
3.2.1 bFGF binding and release 99101
3.2.2 VEGF binding and release 101103
3.2.3 Bioactivity of eluted bFGF and VEGF 104105
3.2.4 *In-vivo* subcutaneous rat implants for neovascularisation. 105107
3.2.4.1 Influence of heparin on collagen deposition 109111
CHAPTER 4: ADIPOSE DERIVED MESENCHYMAL STEM CELL DIFFERENTIATION ON HYDROGELS 111113
4.1 Introduction 111113
4.2 Results and discussion 115117
4.2.1 Functional characterisation 115117
4.2.2 *In-vitro* cytocompatibility 119122
4.2.3 Influence of bound heparin on ADSCs differentiation 122125
CHAPTER 5: CONCLUSION 126129
CHAPTER 6: MATERIALS AND METHODS 129133
6.1 Heparin acrylate preparation 129133
6.2 One step fibrinogen heparinisation 129133
6.3 Two step fibrinogen Heparinisation 130134
6.3.1 PEGylation 130134
6.3.2 Free thiol quantification 130134
6.3.3 Heparin acrylate conjugation to free thiols 131135
6.4 Size exclusion chromatography 131135
6.5 Dialysis 132136
6.6 Bound heparin quantification 132136
6.6.1 3-Methyl-2-benzothiazolinone hydrazone hydrochloride hydrate heparin (MBTH) assay 132136
6.6.2 Heparin Red® assay 133137

6.7 Lyophilisation and storage 133137
6.8 Characterisation 134138
6.8.1 Fourier transform infrared analysis 134138
6.8.2 Thromboelastography 134138
6.8.3 *In-vitro* degradation 135139
6.8.4 Turbidity analysis 135139
6.8.5 Scanning electron microscopy 136140
6.8.6 Rheology 136140
6.8.7 Growth factor release 137141
6.8.7.1 Bioactivity 137141
6.9 *In-vitro* cell culture 138142
6.9.1 Cell culture stocks 138142
6.9.2 Cell culture conditions 138142
6.9.2.1 Culture media 138142
6.9.3 Thawing of cells 138142
6.9.4 Cell passaging 138142
6.9.5 Cryofreezing of cells 139143
6.9.6 Live/Dead® viability assay 140144
6.9.7 CellTiter-Glo® luminescent cell viability assay 140144
6.9.8 3D spheroid sprouting invasion assay 141145
6.9.8.1 Methylcellulose preparation 141145
6.9.8.2 Siliconising plates 142146
6.9.8.3 Assaying spheroids 142146
6.9.8.4 Fixation, staining, and visualisation 143147
6.9.9 Adipose derived mesenchymal stem cell characterisation 143147
6.9.9.1 Alizarin Red Stain 144148
6.9.9.2 Oil Red O Stain 144148

6.9.10 Adipose derived mesenchymal stem cell differentiation on hydrogels 145~~149~~

6.10 *In-vivo* rat subcutaneous implant assay ..... 145~~149~~

6.10.1 Porous polyurethane discs sterilisation ..... 146~~150~~

6.10.2 Hydrogel preparation in polyurethane discs ..... 146~~150~~

6.10.3 *In-vivo* Subcutaneous implants ..... 146~~150~~

6.10.4 Histology ..... 148~~152~~

6.10.4.1 Wax processing and embedding ..... 148~~152~~

6.10.4.2 Staining ..... 149~~153~~

6.10.5 Microscopic analysis ..... 149~~154~~

6.10.6 Statistical analysis ..... 150~~154~~

6.11 Data analysis ..... 150~~155~~

6.12 Reagents, equipment, and consumables ..... 151~~155~~

References ..... 158~~162~~

Appendices ..... 195~~199~~

List of figures

Figure 1.1: Polyethylene glycol chemical structure with hydroxyl groups 6

Figure 1.2: Chemical structure of cellulose, a polysaccharide high carboxyl (COOH) and hydroxyl (OH) group content 9

Figure 1. 3: Chemical structure of chitin and chitosan with 2-amino-2-D-glucopyranose and 2-acetamido-2-deoxy-D-glucopyranose units 11

Figure 1.4: Chemical structure of calcium alginate with 1,4-β-D-mannuronic acid and 1,4-α-L-guluronic acid units 13

Figure 1.5: Fibrinogen structure showing two sets of fibrin polypeptide chains 21

Figure 1.6: Three pathways of the coagulation cascade 25

Figure 1.7: Four stages of the wound healing process 27

Figure 1.8: Fibrinogen polymerisation process and resultant fibrous structure 28

Figure 1.9: Cell interaction with fibrin matrix 38

Figure 1.10: Growth factor entrapment in fibrin systems 40

Figure 1.11: Highly sulphated heparin chemical structure with uronic acid and glucosamine residues and their carboxylic acid groups 46

Figure 2.1: General EDC reaction chemistry mechanism 58

Figure 2.2: An illustration of a Michael addition reaction between a thiol and an acrylate 59

Figure 2.3: Thiol binding optimisation 61

Figure 2.4: Molar ratio dependent binding of NHS-PEG-SH to fibrinogen 62

Figure 2.5: Optimisation time for heparin coupling to free -SH on PEGylated fibrinogen 64

Figure 2.6. Size exclusion elution profiles for heparin and fibrinogen 65

Figure 2.7: Optimisation for bound heparin quantification with MBTH 68

Figure 2.8: Bound hep-acr quantification with MBTH 69

Figure 2.9: Bound hep-acr quantification with heparin red assay 70

Figure 2.10: FTIR spectra for fibrinogen and modified fibrinogen 73

Figure 2.11: Parameters for clotting kinetics of the different hydrogel precursors measured with a thromoelastogram 75

Figure 2.12: Unmodified and modified fibrin hydrogel degradation measured with Bradford protein assay for samples collected over 15 days 77

Figure 2.13: Optical properties of native and modified fibrin hydrogels 79

Figure 2.14: SEM micrographs for unmodified and modified fibrin hydrogels set in PU discs 81

Figure 2.15: Rheological analysis of fibrin and modified fibrin hydrogels with average elastic modulus, G' (Pa), for each hydrogel type 83

Figure 2.16: Live/ Dead viability assay for 3D hydrogel encapsulated HUVECs and human dermal fibroblasts 85 - 86

Figure 2.17: 3D HUVECs cell activity in the different hydrogel types from 24 hours to 7 days 89

Figure 2.18: Sprout invasion from HUVEC spheroids 93 - 94

Figure 3.1: VEGF signaling pathway induced by VEGF binding to VEGFR that is a receptor tyrosine kinase 97

Figure 3.2: Sustained cumulative release of bFGF from heparinised fibrin hydrogels 100

Figure 3.3 Sustained cumulative release of VEGF from heparinised fibrin hydrogels 102

Figure 3.4: Bioactivity of the released bFGF and VEGF on day 15 104

Figure 3.5: Subcutaneous implant neovascularisation after 10 days 107

Figure 3.6: Picrosirius red stains for the non-VEGF treated samples 110

Figure 4.1: ADSC functional characterisation with adipose induction for 14 days 116 - 117

Figure 4.2: ADSC functional characterisation with osteogenic induction for 21 days 118 - 119

Figure 4.3: Live/ Dead cell viability assay for 3D hydrogel encapsulated ADSCs at 3 and 7 days 121

Figure 4.4: 2D seeded ADSCs after 24 hours seeding 123

Figure 4.5: Adipogenic and osteogenic ADSC differentiation on hydrogels compared to tissue culture plastic 125

Figure 6.1: Illustration of the positions for the subcutaneous implant model in rats 148

List of tables

Table 1.1: Heparin binding growth factors and their functions 48

Table 2.1: Summary results for heparin dialysis optimisation 67

Table 2.2: Clotting kinetics for fibrinogen and modified fibrinogen measured with a thromboelastogram 75

Table 3.1: Summary of bound VEGF and bFGF to the different hydrogel formulations 103

Table 3.2: Summary VEGF and bFGF released per day from the different hydrogel formulations 103

Table 6.1: Table of reagents 151

Table 6.2: Table of equipment 153

Table 6.3: Table of general consumables 155

List of appendices

Appendix A: Slow heparin release from FH and FPH quantified from degradation eluates 195

Appendix B: Example rheology Scans 196

Appendix C: 2D ADSC differentiation on hydrogels – adipogenic 7 days 190

Appendix D: 2D ADSC differentiation on hydrogels – osteogenic 14 days 197

List of abbreviations

2D	Two-dimensional
3D	Three-dimensional
SDMSCs	Synovium-derived mesenchymal stem cells
ADSCs	Adipose-derived stem cells
aFGF	Acidic fibroblast growth factor
ALPL	Alkalike phosphatase
AM	Adipogenic media
AT	Antithrombin
ATP	Adenosine triphosphate
bFGF	Basic fibroblast growth factor
BMMNC	Bone marrow derived mononuclear cells
BMP-2	Bone morphogenetic protein-2
BMP-4	Bone morphogenetic protein-4
BTC-PEG-BTC	Benzotriazole-PEG-benzotriazole
Ca^{2+}	Calcium ion
CHF	Congenital heart failure
ECs	Endothelial cells
EDC	1-ethyl-3-(3-dimethylaminopropyl) carbodiimide
EDC/s-NHS	Carbodiimide/N-hydroxysulfosuccinimide
EF	Ejection fraction

EGF	Epidermal growth factor
ELISA	Enzyme-linked immunosorbent assay
EthD-1	Ethidium homodimer-1
F	Fibrin
FDA	Food and Drug Administration
FGF	Fibroblast growth factor
FH	Fibrinogen-acrylate heparin
FGFR	Fibroblast growth factor receptor
FTIR	Fourier transform infrared spectroscopy
FP	Fibrinogen-PEG-SH
FPA	Fibrinopeptide A
FPB	Fibrinopeptide B
FPH	Fibrinogen-peg-acrylate heparin
FVII/FVIIa	Factor VII/VIIa
Gp	Glycoprotein
HBD	Heparin binding domain
HB-EGF	Heparin binding epidermal growth factor
Hep-acr	Acrylated heparin
HEPES	Phosphate, 2-(4-(2-hydroxyethyl)-1-piperazinyl)-ethanesulfonic acid
HGF	Hepatocyte growth factor
HGF	Hepatocyte growth factor

HUVECs	Umbilical endothelial cells
NHS-PEG-SH	Hydroxysuccinimide-PEG-sulfhydryl
IGF	Insulin growth factor
IGF-1	Insulin growth factor like-1
IL-10	Interleukin 10
IL-6	Interleukin-6
LMWH	Low molecular weight heparin
LVEF	Left ventricular ejection fraction
MBTH	3-Methyl-2-benzothiazolinone-hydrazonehydrochloride
Mg^{2+}	Magnesium ion
MI	Myocardial infarction
miRNA	microRNA
MMP	Matrix metalloproteinase
mRNA	Messenger ribonucleic acid
MSC	Mesenchymal stem cell
MW	Molecular weight
NaCl	Sodium chloride
NHS	N-Hydroxysuccinimide
NHS-PEG-SH	N-Hydroxysuccinimide-PEG- sulfhydryl
NMR	Nuclear magnetic resonance
Non-hep acr	Non-acrylated heparin

OM	Osteogenic media
PBS	Phosphate buffered solution
PDGF	Platelet-derived growth factor
PEG	Polyethylene glycol
PLA	Poly (lactic acid)
PlGF	Platelet-derived growth factor
PRP	Platelet rich plasma
PU	Porous polyurethane
PVA	Polyvinyl alcohol
RAS/ MAPK	Ras/mitogen activated protein kinase
RGD	Arginine–glycine–aspartic acid
rhBMP-2	Recombinant human bone morphogenetic protein-2
SEC	Size exclusion chromatography
SEM	Scanning electron microscopy
starPEG	star-shaped poly(ethylene-glycol)
SG-PEG-SH	Succinimidyl Glutarate-PEG- sulfhydryl
TCP	Tissue culture plastic
TEG	Thromboelastogram
TGF-β	Transforming growth factor-β
TNF- α	Tumour necrosis factor-α
tPA	Plasminogen activator

UFH	Unfractionated heparin
uPA	Urokinase
VEGF	Vascular endothelial growth factor
VEGFR	Vascular endothelial growth factor receptors
VS	Vinyl sulfone
vWF	Willebrand Factor

CHAPTER 1: LITERATURE REVIEW

1.1. Regenerative medicine

Tissue and organ loss or damage due to trauma, disease, and injury are a global concern. Pharmaceutical interventions are often not curative in nature (1), and thus necessitate the need for transplants as a cure. Transplants are however highly invasive, limited by donor availability and require lifelong commitments to immunosuppressants following the transplant (1, 2). Regenerative medicine has presented as an alternative therapeutic approach for repairing damaged or diseased or even lost tissue (3). This approach aims to repair or replace injured and diseased tissue for restore normal function. It leverages stimulating the human body's innate cellular and molecular repair mechanisms to heal damaged tissue (3, 4). For this, various approaches have been explored and include delivery of exogenous cells, genetic material, bioactive biomolecules such as growth factors, biomaterials, or a combination thereof (4, 5, 6). Biomaterials have drawn the attention of researchers due to their ability to co-exist with human tissue and are thus good candidates for structurally and functionally supporting healing tissue during the regeneration process (7). Particularly, hydrogels have been a crucial component of regenerative medicine strategies (including tissue engineering) due to their ability to mimic the extracellular matrix (ECM) of tissues (7).

1.2 Hydrogels

Hydrogels are among the first biomaterials designed for use in the human body (8, 9). They are distinguished from all other gel types by their ability to absorb large volumes of water (at least 10% of their weight/ volume) (10). Wichterie & Lim in 1960 reported the first hydrogel, a poly-2-hydroxyethylmethacrylate based hydrogel that was used to manufacture contact lenses for correcting vision (8). This hydrogel was investigated extensively and obtained Food and Drug Administration (FDA) approval by 1971 (8). It was subsequently investigated for ocular drug delivery (8, 11). Numerous hydrogels have since been identified and are to date a crucial component of regenerative medicine and

tissue engineering strategies. These hydrogels have been defined in various ways over the years, with the most common definition being that they are three-dimensional (3D) hydrophilic polymeric (linked monomers) networks that can absorb and retain large amounts of water without rapidly dissolving in the water (12). They have also been defined according to their mechanism of formation, that is, they are a swollen (from water absorption) 3D network formed by reacting one or more monomers (12, 13, 14). Both these definitions highlight the most crucial characteristic of hydrogels; their ability to absorb large amounts of water (hence hydrophilic properties), swell and form a 3D network. For example, hydrogels that have carboxylic acids in their main chain, when placed in water these become deprotonated at neutral pH and resultantly leave negative ions down the length of the polymer chain (15, 16, 17). These negative charges ultimately cause the polymer to repel each other causing it to uncoil and open. This then attracts water molecules for hydrogen bonding allowing the hydrogel to absorb high amounts of water (15, 16). Additionally, hydrogels are ideal biomaterials for human use as they can mimic the structure and function of natural human tissue (16). This characteristic is ideal as water content/ body fluid in human body tissue can similarly be absorbed and used for tissue hydration (15, 16). They can also be designed with flexibility to mimic the structures and characteristics of natural tissue (13), enabling seamless integration into the body. Furthermore, some hydrogels can further naturally bind cells, and biomolecules (18, 19) thus acting as a reservoir like the extracellular matrix (ECM) while others can be functionalised to possess these abilities (13, 18, 19).

To achieve their desired functions, hydrogels must of course exhibit specific physical and biological characteristics that are determined by their intended applications at target environments. Firstly, they must withstand forces from the surrounding tissue, whilst in most instances also permitting efficient diffusion of nutrients and gases for ingrowing tissue or cellular cargo (20). The biomechanical needs vary widely with hydrogels needing to function either in soft tissue such as cardiac tissue, or hard tissue such as cartilage or bone. Additionally, hydrogels need to be biocompatible and able to coexist with living tissue without inducing severe and/or chronic inflammatory and immunogenic responses (21, 22). They should also be able to support crucial cellular processes such as cell

adhesion, proliferation, and migration (13, 21). Equally, hydrogels used in regenerative medicine should be biodegradable (e.g. to match tissue invasion), with biodegradation profiles that ideally match the rate of new tissue formation and degradation products should further be non-cytotoxic (13, 21, 23). Injectability is further another desirable aspect in hydrogels (24)as it lends itself to a minimally invasive delivery approach. An ability to polymerise after delivery is attractive not only for facilitating minimal invasiveness but also for the potential to fill irregular and deep wounds (24). It can be attained by controlling gelation kinetics such that the hydrogel's precursors can be injected as a liquid to form a solid hydrogel *in-situ* (21, 24). Double barrelled syringes are an example of such injectables whereby two components are mixed just prior to injection to allow for further control of gelation kinetics (e.g. commercial fibrin systems such as Tisseel) (25). Other commonly used approaches to allow for injectability exploit specific properties of the particular hydrogel system such as thermal initiation, pH responsiveness, ionic triggering and thixotropy (21). These characteristics enable diverse hydrogel usage in tissue repair.

To support tissue regeneration, as indicated above, hydrogels need to enable adequate nutrient and gas supply as well as metabolic waste removal (13). This is needed to ensure survival of cells either being delivered or those surrounding the hydrogel in the tissue being repaired and/or are migrating into the hydrogel (13). Hydrogels thus need to have good permeability for diffusion, while also limiting cells from moving out of the hydrogel prematurely when used for cell delivery (13). This characteristic is often governed by the cell's (or any molecule being transported) overall 3D size in relation to the hydrogel's pore size (21, 26). As defined by the International Union of Pure and Applied Chemistry's classification and slight adaptations by Foudazi et al., 2023, hydrogels with pore sizes <1.4 μm (with a dominant water state as primary bound water) are known as microporous hydrogels, those with pore size between 1.4 − 3 μm (with a dominant water state as primary water state and secondary bound water) are super-microporous hydrogels, between 3−50 μm (with a dominant water state as primary water state, secondary bound water and free water) mesoporous and if the pore sizes are >50 μm (with mainly free water) they are known as macroporous hydrogels (26). These characteristics are significant in designing and understanding target hydrogel function. Pore size can be

regulated by controlling factors that control gelation kinetics such as polymer and crosslinker concentration ratios (**section 1.5.1**), as well as gelation conditions, e.g., temperature and pH (27). To further understand hydrogel behaviour, they are classified into groups. For this, there are several means of classification based on a range of parameters. These include classification based on the type of cross-linking that occurs when forming the hydrogel (e.g. chemical cross-linking or physical crosslinking such as hydrogen bonds, ionic interaction or hydrophobic interactions), polymer configurations/ crystallinity (i.e., amorphous, semicrystalline or crystalline), polymeric network charge (ionic, non-ionic, amphoteric or zwitterionic), type of network (i.e., single, semi-interpenetrating, interpenetrating, double network, or mechanically interlocked origin), and origin of the polymer forming the hydrogel (13, 28). In the latter case, hydrogels can be classified as either being natural, or synthetic based on the polymer forming the hydrogel (13).

Hybrid hydrogels have been proposed as another class of hydrogels. It should be noted that ongoing discussions persist regarding the hybrid concept , with a range of definitions proposed for hybrid hydrogels. For instance, Zhang, 2018 (29) defined them as complexes that are constituted by hundreds of nanoparticles (<100 nm) that are either physically or chemically crossed linked.. They have also been defined as systems composed of different polymers or (and) nanoparticles (30). Other authors have presented them to be composed of chemically, morphologically, or functionally different building blocks from at least two classes of molecules including biologically active polymers, nano or microstructures interconnected chemically or physically, maximising the characteristics of each component (30, 31). This underscores the versatility of biomaterials for enhanced functionality and how they have been defined.

In overall, the advancement of hydrogels has progressed significantly, enabling the manipulation of environmental factors to optimise delivery at target sites (32, 33).For example, several polymers have been explored in context of stimuli responsive hydrogels (smart hydrogels) for tissue targeted delivery (34, 35). These hydrogels are engineered to detect surrounding environmental factors such as pH, temperature, and ionic strength. Subsequently, they react to alterations in these factors by adjusting their intrinsic physical

and/or chemical properties, such as hydrophilicity, permeability, and/or structure, facilitating the release of the loaded drug. (34, 35). A change in environmental stimulus prompts a phase volume transition in the hydrogel (35), facilitating drug release, while retaining the capability to revert to its original state once the stimulus is removed. This transition typically involves swelling and relaxation or change of the hydrogel structure (35). Overall, the method holds promise for tissue-specific delivery, with pH being one of the most extensively studied environmental stimuli. A pH-sensitive hydrogel can be designed based on the understanding that various body parts or organs exhibit different pH levels, such as stomach pH (1-3), blood pH (7.35-7.45), and lysosome pH (4.5-5.0), with diseased tissue tending to be more acidic compared to healthy tissue (36). A pH responsive hydrogel can thus be tailored to release drugs at the intended site based on that tissue's particular pH (37), and this enables reduced dosing frequency, maintains the desired drug concentration and prevents non-specific accumulation of the drugs in non-target tissue (37, 38, 39). Further optimisation studies are still required for the application of both synthetic and natural hydrogels.

1.3 Synthetic hydrogels

Synthetic hydrogels are hydrogels polymerised from chemically manufactured monomers or polymers (13, 40). These polymers are often attractive for their stronger mechanical properties, as compared to natural hydrogels (**section 1.4**), and thus produce hydrogels with good durability (13, 40). Because the materials used to construct synthetic hydrogels are chemically produced, their molecular weights, and structures can be manipulated such that the resultant hydrogel properties have specific mechanical properties, gelation kinetics, and degradation patterns (22, 41). This thus makes synthetic hydrogels attractive as they are more likely to have higher levels of reproducibility and low batch to batch variability.

A well investigated and widely used synthetic monomer is polyethylene glycol (PEG) (**Figure 1.1**). PEG is an inert synthetic monomer used since the late 1970s to polymerise into hydrogels (42). These hydrogels are attractive due to their well-defined chemical nature, hydrophilicity, and overall reproducibility (13, 40, 43).

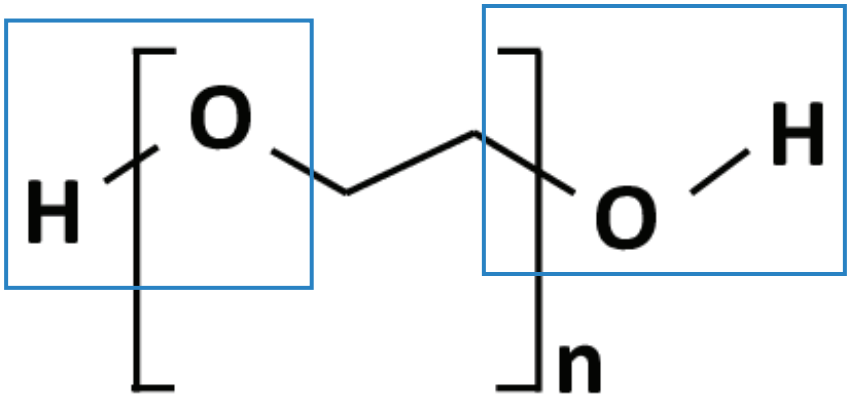

Figure 1.1: **Polyethylene glycol chemical structure with hydroxyl groups (in blue)**

The PEG hydroxyl groups (**Figure 1.1**) at each terminal end of the PEG monomer permit modification and functionalisation with various chemical groups (42). As a result, numerous PEG based hydrogels with unique characteristics are known to date and are useful for engineering hydrogels that allow for improved biocompatibility, enzymatic degradation, more controlled release, and specific cellular invasion patterns (44, 45, 46). For example, Lutolf and Hubbell, 2003 (47) developed a highly engineered PEG system where multivalent PEG monomers with vinyl sulfone terminals were crosslinked with bi-cysteine oligopeptide sequences. The crosslinking was driven by a Michael-type addition reaction between the peptide sulfhydryls and the vinyl sulfones and allowed for the introduction of enzymatic degradation of the PEG hydrogel. Mono-cysteine peptides also allow for the attachment of cell adhesion sequences such as arginine-glycyl-aspartic acid (RGD). This system could also covalently entrap growth factors, such as vascular endothelial growth factor (VEGF), that contain exposed sulfhydryls or have been engineered to contain them (47). This development was crucial in improving PEG hydrogel's bioactivity as PEG alone is naturally bioinert. It was further used to deliver recombinant human bone morphogenetic protein-2 (rhBMP-2) in rat crania with defects where bi-cysteine matrix metalloproteinase (MMP) recognition site peptides were used as crosslinkers (48). RGD peptides were also added for cell attachment and the MMP cleavage site peptide crosslinkers conferring enzymatic degradability on the hydrogel network. The PEG hydrogels bound 90% of the loaded dose of rhBMP-2, compared to collagen sponge that bound 60%. When polymerised in critical-size calvarial defects in

rats, the rhBMP-2 loaded PEG hydrogels stimulated newly formed bone after five weeks accompanied by hydrogel degradation. PEG hydrogels without rhBMP-2 or MMP degradability however had a significantly much less pronounced effect. These findings showed the applicability of PEG hydrogels in growth factor delivery, and new tissue formation. More recent work on PEG hydrogels has demonstrated that the rate of tissue invasion could be modulated through a two-mechanism type hydrogel system (49), where one aspect of the hydrogel is hydrolytically degradable and the other enzymically degradable (49). This hydrogel was formed by incorporating PEG-vinyl sulfone and PEG-acrylate monomers that respectively form hydrolytically stable and unstable bonds with bi-cysteine MMP sensitive crosslinking peptides. Tissue invasion into subcutaneous implants in rats was modulated by controlling the ratio of the hydrolytically stable and unstable components (49). This system reflects the growing application of synthetic hydrogels such as PEG hydrogels.

Other synthetic polymers have also been explored, for instance, polyvinyl alcohol (PVA) is attractive for its hydrophilicity and biocompatibility (50), with pure PVA hydrogels showing good promise as support in knee chondral and osteochondral defects (51). When these hydrogels kind of hydrogels were placed in between a damaged region and opposing cartilage surface of osteochondral defects of patients' knees, they provided pain relief and improved joint function relative to the baseline scores for at least six years (51). Pure PVA hydrogels are however considered mechanically weak with poor elasticity and thermal instability (52). They are further non-bio-adhesive (53) and for these reasons PVA is thus often used in conjunction with other polymers as a co-polymer (52, 53). For instance, a natural/ synthetic (PVA/chitosan) hybrid hydrogel at a 6:4 ratio was used to treat osteochondral defects in rabbits (54). Three groups were formed: one with only defects, one treated with the hydrogel alone, and another treated with the hydrogel and bone marrow-derived mesenchymal stem cells (BMSCs). After 12 weeks, the hydrogel with bone marrow-derived mesenchymal stem cells (BMSCs) group exhibited significantly better healing, indicating the potential of PVA for cartilage repair and BMSC delivery (54). This highlights the need to enhance PVA properties by combining it with other materials.

In addition to PVA, other biomaterials under investigation include poly (lactic acid) (PLA). Poly (lactic acid) is particularly attractive due to its reduced likelihood of inducing immunological responses (55). However, pure poly (lactic acid) (PLA) has limited functionality because of its high hydrophobicity that stems from its non-functional and hydrophobic lactides (56). Additionally, it exhibits a very low degradation rate (55, 56). To overcome this, PLA has been combined with hydrophilic copolymers like PEG or to create hydrogels with improved and interesting characteristics (56). For example, one of the most interesting attributes of certain PEG–PLA hydrogels is their thermo-responsive characteristics (56). At ambient temperature, the copolymer solution retains its solubility, but as the temperature rises to around 37°C, it undergoes gelation, forming a solid matrix (56). These hydrogels have shown promising hydrolytic degradation properties, but further evaluations are still necessary.

Despite synthetic biomaterials for hydrogels showing good promise, there are drawbacks to their utilisation. Their bio-inert nature (low biological activity), and potential immune response induction, limits their application and thus require extensive functionalisation for improvement (57). For example, PEG hydrogels alone are not ideal for supporting cell adhesion and tissue formation (58). Additional ECM peptides such as the RGD sequence (described above), are often required to improve cellular interaction and it is likely that this type of approach does not completely recapitulate the information contained in the ECM (58). This is in contrast to most natural hydrogels, which are intrinsically more biocompatible (59).

1.4 Natural hydrogels

Natural hydrogels are prepared from natural polymers and are thus classified as such. These polymers are sourced from animals, plants, or even microorganisms (59). As natural resources, they are readily available and have inherent biocompatibility. Known natural hydrogels are grouped either as polysaccharides or proteins. Decellularised tissue (a combination of both protein and polysaccharides) has also been used to form hydrogels (59).

1.4.1 Polysaccharides

Due to the typically high content of carboxyl and hydroxyl groups in their backbones, polysaccharides have a high capacity for absorbing water and swelling (60). These functional groups enable them to absorb biological fluids (exudate) leaking out from wounded tissue, without adhering to the healing tissue and thus ideal for supporting the wound healing process (61). Additionally, these functional groups present as opportunities for modifying the polymer (60). The most used polysaccharides for hydrogels include cellulose, chitosan, and alginate (61).

1.4.1.1 Cellulose

Cellulose is the most abundant natural polymer**.** It is made up of linear repeating glucose units, joined by β-1,4 glycosidic links (**Figure 1.2**) (62). The polymer is sourced from plant cell walls, where it provides structural support, as well as certain bacteria such as *Acetobacter xylinum* (34, 36, 63). Bacterial sourced cellulose is considered the purest form of cellulose and possesses good physicochemical characteristics such as mechanical strength and thermal stability. When forming hydrogels, hydroxyl groups in the cellulose polymer chains crosslink via the weak hydrogen bonds (60). These cellulose hydrogels, mostly bacterial cellulose-based (60), have been incorporated in diapers, napkins (Klemm, Heublein et al. 2005), and wound dressings due to their biodegradability and ability to absorb large water volumes (35, 64, 65).

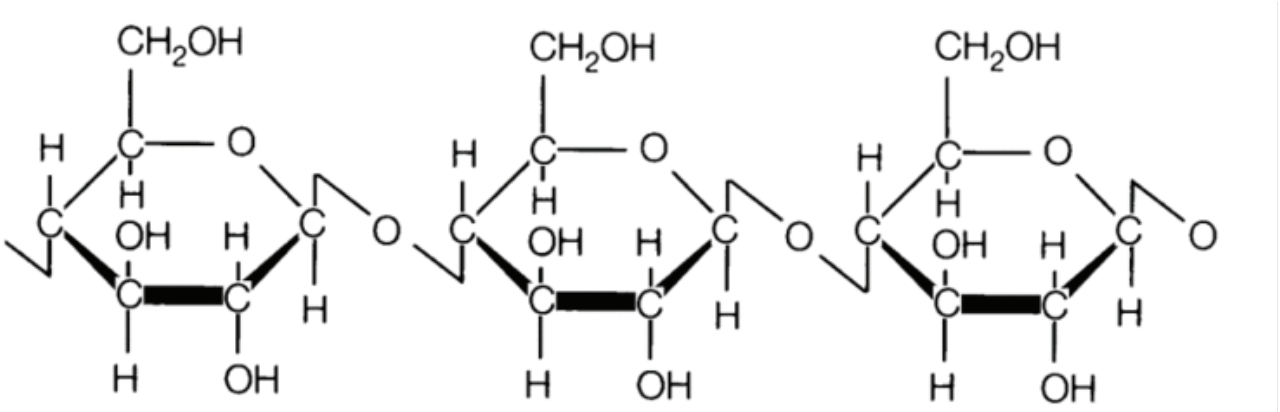

Figure 1.2: Chemical structure of cellulose, a polysaccharide high carboxyl (COOH) and hydroxyl (OH) group content.

Despite cellulose's use in manufacturing products, few studies have explored its application in regenerative medicine, and even fewer studies have been conducted *in-vivo*. In a pre-clinical study by Simeoni et al., 2021, a bacterial cellulose patch containing co-cultured bone marrow MSCs, and skeletal myoblasts was surgically inserted in the epicardial region of the left ventricle in an acute myocardial infarction (MI) rat model (66). Analysis of the left ventricular function, at seven and 30 days after infarction showed that the patch with cells could protect the myocardium from pathological remodelling compared to the control groups (cells and patch only) and further improved left ventricular ejection fraction (LVEF) while the patch and cell only groups showed no improvement (66). Koike, Sha, Bai, Yuhei Matsuda, 2019 (67) also indicated bacterial cellulose's usefulness by showing that it has good efficacy for binding and delivering BMP-2 in bone regeneration.. This study used critical frontal bone defects in rabbits to show that a combination of bacterial cellulose hydrogel and BMP-2 significantly increased bone formation, compared to the groups with BMP-2 only in the defects. This was indicated by the accumulation of osteoblasts in the area, and positive staining for osteocalcin (67). While these studies show promise for application as a vehicle for cells, there are still significant concerns with immunogenicity from hydrogels prepared from both micro-organisms and plant sources (68). This has been a disadvantage for translation to the clinic.

1.4.1.2 Chitin

As the second most abundant natural polymer in nature, chitin (**Figure 1.3**) occurs in most living organisms including insects, and fungi (69). It is a tough fibrous polysaccharide observed in the exoskeleton of anthropoids and cephalopod insects (such as spiders, crickets) (70). This polysaccharide is a major structural component of the insects' outer covering (exoskeleton) that keeps their soft bodies protected from injury and further gives them overall structure and shape (70). Chitin is however not widely used in its original form and is rather utilised primarily as a precursor in the formation of the polysaccharide chitosan after extensive deacetylation (59, 71). Structurally, chitosan is comprised of unbranched repeating units of 2-amino-2-D-glucopyranose and 2-acetamido-2-deoxy-D-

glucopyranose linked by β-(1–4) glycosidic bonds, resembling other glycosaminoglycans of the ECM (**Figure 1.3**) (59, 71) (69) and is often used to form hydrogels (59, 71).

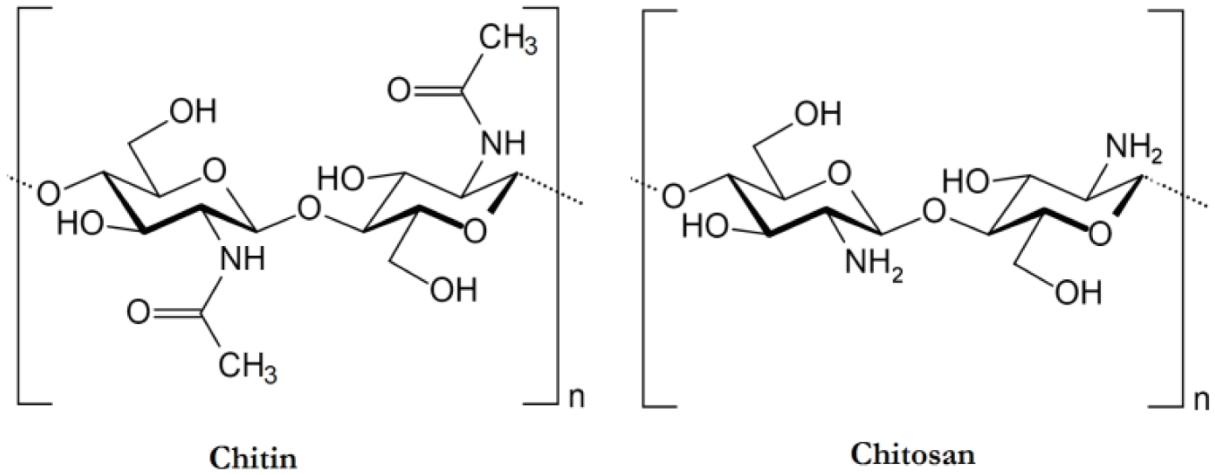

Figure 1. 3: **Chemical structure of chitin and chitosan** with 2-amino-2-D-glucopyranose and 2-acetamido-2-deoxy-D-glucopyranose units

Most chitosan-based hydrogels are formed through chemical cross-linking (72). In this, covalent bonds link amines and hydroxyl groups in between chitosan macromers. This cross-linking occurs either through cross-linkers, such as dialdehyde compounds (glutaraldehyde) or photo-polymerisation (i.e. ultraviolet) (72). Chitosan may be an appealing choice of polymer for regenerative hydrogels due to several beneficial effects, including anti-microbial activity (73). As an anti-microbial, its polycationic (positive charges) structure can bind bacteria with negatively charged surfaces through electrostatic interaction, whereafter it disrupts their cell membranes (via increasing outer and inner membrane permeability) through mechanisms still under study (73). It has also been reported to present with antioxidant activity though here again mechanisms of action are yet to be understood (74). Moreover, it has been shown that chitosan can also activate macrophages to remove dead cells and tissue through phagocytosis (59), and also to secrete cytokines that promote the activation, proliferation, and differentiation of various cells e.g. endothelial cells, fibroblast, and epithelia cells, involved in the wound healing process (59, 75). This has thus been proposed as a potential mechanism by which chitosan could accelerate wound healing.

Regardless of the attractive properties of chitosan, its production for use as a polymer for hydrogel systems requires laborious and prolonged processing for activation (76). The deacetylation reactions require harsh conditions with high temperatures, and concentrated acid solutions to dissolve (77). As a result, chitosan hydrogels are formed from an overly processed polymer with weak mechanical properties (including mechanical strength and slow gelation time) and are thus challenging to characterise for use (77). The produced chitosan further has a high molecular weight and strong intramolecular hydrogen bonds which render it insoluble in water (76) (77) and thus needs several additional steps of dissolving it in salt solutions in the preparation of hydrogel liquid solutions. It also has immunogenicity, a high degradation rate and cytotoxicity (77). For these reasons, its application has been limited and it is more often used as a co-polymer.

1.4.1.3 Alginate

Following alginate's discovery by Sandford in the early 1980s, methylation studies by Hirst and colleagues revealed that it is an anionic polymer of 1,4-β-D-mannuronic acid and 1,4-α-L-guluronic acid (**Figure 1.4**) (78, 79, 80). Alginate is sourced mostly from brown algae (81). Various methods are used to cross-link alginate for hydrogels, and these include covalent-crosslinking, ion interaction, and thermal gelation in the presence of divalent cations such as calcium ions (Ca^{2+}) and magnesium ions (Mg^{2+}) that facilitate the crosslinking of the carboxylate groups in the guluronate groups of the polymer's backbone (82) (83, 84). These hydrogels have been explored extensively for replacing the old wound gauze-based dressings for severe skin burns and chronic wounds. The older dressings have over time shown that they are prone to induce secondary injury when they are peeled off the wounds due to the gauze material absorbing the exudate without any form of moisturisation (83, 84). In contrast, alginate hydrogels can absorb the exudate without adhering to the wound (85), and further provide a moist environment to support the wound healing process. The ability of alginate as a polymer to dissolve in water, without the need of harsh conditions and acids for processing, makes it an interesting polymer of choice for wound dressing compared to other polysaccharides (85, 86). It is further reported to possess the ability to stimulate monocytes to release cytokines such as interleukin-6 (IL-6) and tumour necrosis factor-α (TNF- α). These cytokines

further stimulate the release of anti-inflammatory factors e.g., interleukin 10 (IL-10) that play a role in vascular and tissue repair (85, 86).

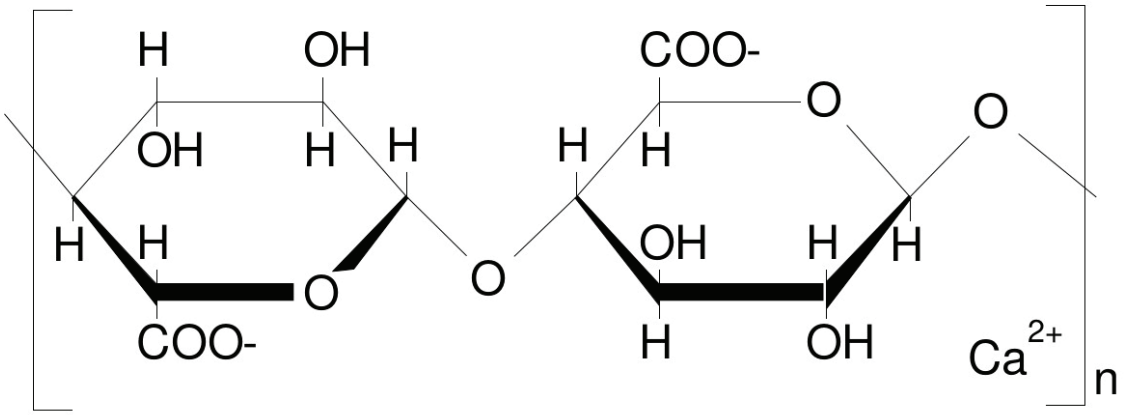

Figure 1.4: **Chemical structure of calcium alginate** with 1,4-β-D-mannuronic acid and 1,4-α-L-guluronic acid units

In addition to its use in wound dressing, alginate has been investigated in a clinical study as a potential carrier for islets of Langerhans in tissue transplant for patients with type 1 diabetes (87). In this, islets of Langerhans isolated from human cadaveric pancreas were transplanted in a case subject with insulin dependent diabetes. Prior to transplantation, alginate microcapsule (hydrogel protective capsules) from purified alginate were used to encapsulate the islets, before being injected peritoneally. Insulin secretion was observed within 24 hours after injection, a reduction in the need for insulin medication was observed, and later an improvement in diabetic ulcers at nine months (87). Later evaluations in clinical trials have further proven their safety. For instance, in a phase one clinical trial conducted by Tuch et al., 2009 (88), four type 1 diabetic patients with no detectable C-peptide levels received an intraperitoneal infusion of islets (1.1 m U/ islet equivalents) encapsulated within microcapsules made of barium alginate for a maximum of 19 months (88). The results indicated that urinary C-peptide was detected six weeks after the third infusion and remained detectable at 2.5 years (C-peptide levels ranged from 0.06 to 0.34 nmol/l or 0.02 to 0.06 nmol/mmol creatinine). A tissue biopsy further revealed that the alginate capsules used were still intact and surrounded by fibrous tissue

containing thin-walled capillaries with mild histiocytic activity indicative of healing tissue(88). However, challenges persist, including the scarcity of donor organs, the acquisition of reliable and consistent islet preparations, as well as immune responses (89). Products such as ViaCyte's candidates are addressing these challenges by utilising pancreatic progenitor stem cells implanted using alginate-based hydrogels (89). Once implanted and matured, these cells are engineered to secrete insulin and other pancreatic hormones in response to blood glucose levels (90). Subsequent phase 1 and 2 clinical trials have demonstrated promising results (91).

In cardiac diseases, clinical studies have also supported the use of alginate hydrogels. In context, Algisyl-LVR™ is a commercially available alginate hydrogel and has been shown effective in clinical trials for gradual remodelling of the left ventricle in patients with MI and congenital heart failure (CHF) (92, 93). When its safety and efficacy was evaluated as a left ventricular augment in patients with dilated cardiomyopathy (advanced heart failure) and undergoing open-heart surgery, outcomes showed that there were no adverse effects with Algisyl-LVR™ use, and LVEF improved by ±7.3% from baseline in 24 months (93). It also showed positive results when implanted in conjunction with coronary artery bypass graft treatment, with significant decrease in myofiber stress, and improved left ventricular function (92). Furthermore, a clinical trial by Anker et al., 2015 injected Algisyl-LVR™ intramyocardially in combination with heart failure standard treatment in 40 patients with advanced heart failure (94). After a year, the patients in the treatment group showed a 16% increase in the LVEF, a 4% decrease in left ventricular end-diastolic diameter and 9% decrease in left ventricular mass. The hydrogel was still present at the end of the study (94). Further to this, intracoronary injection of a calcium cross-linking alginate hydrogel in pigs has shown to reverse left ventricular remodelling post MI (95). This hydrogel was prepared by mixing alginate into calcium D-gluconate solution, and thereafter injected as a liquid to transition into a hydrogel, the transition facilitated by increasing Ca^{2+} at the infarct site. After 60 days, it significantly reversed left ventricular enlargement, compared to a saline control that had an increase in the left ventricular diastolic area, left ventricular systolic area as well as the left ventricular mass by 44%, 45% and 35% respectively (95, 96). Later work has attempted to explore its application

in microfluidic organ “on a chip” devices that model tissue organs in various disease states, due to its key feature of delayed hydrogel gelation (97). In this, alginate hydrogels are explored as potential scaffolds and matrices that can assist with providing support for cell and tissue adhesion. Alginate however still faces the challenges of poor cell adhesion (needing additional RGD sequences or other co-polymers) (59, 98). It further has high mechanical instability, and slow degradation as it is not naturally degradable in mammals (59, 98). This has prompted the exploration of more biomaterial sources including decellularised tissue.

1.4.2 Decellularised tissues

Recently, ECM hydrogels have drawn the attention of researchers. These hydrogels are derived from ECM components, such as collagen, fibronectin, or hyaluronic acid (99). They mimic the natural environment found in tissues and organs, providing a supportive matrix for cell growth and function (99). In regenerative medicine, they are attractive for their biocompatibility and ability to promote cell adhesion, proliferation, and differentiation (100). They can further be tailored to specific tissue types and can be used alone or in combination with cells to regenerate damaged tissues or organs (101). In essence, they are ideal due to their resemblance to target tissue as they are isolated from native tissue, and decellularised for use as ECM hydrogels following their decellularisation (102, 103).

Various methods are employed to achieve decellularisation and they include chemically and mechanically removing all cells from the chosen native tissue, leaving only the ECM with its macro- and micro-structure maintained (104, 105). Briefly, the tissue decellularisation process starts with harvesting the desired tissue from a donor, followed by fixation with a substance like formaldehyde to preserve tissue structures (101). Decellularisation begins with the use of enzymes e.g. trypsin, detergents e.g. sodium dodecyl sulfate, or other agents to remove cells, leaving behind the ECM. The tissue is then rinsed and washed to remove any remaining debris or decellularisation agents (101). In the final steps, the decellularised ECM into a hydrogel matrix, achieved by mixing it with hydrogel precursors, or a crosslinking agent (101). The process of forming the hydrogels comprises of two primary stages: firstly, solubilising the ECM material into

protein monomers, and secondly, neutralising the solution under controlled temperature and/or pH conditions to trigger the spontaneous reformation of intramolecular bonds, resulting in a uniform gel (101, 106). The predominant approach for generating an ECM hydrogel involves pepsin-mediated solubilisation of a pulverised ECM (also referred to as ECM digestion) (107). Pepsin is able to cleave the telopeptide bonds within the collagen triple helix structure, leading to the unravelling of collagen fibril aggregates (107). The mechanism of hydrogel formation is a collagen-based self-assembly process (fibrillogenesis mechanism with collagen above) influenced by the presence of glycosaminoglycans, proteoglycans, and ECM proteins (108). Consequently, polymerization kinetics are affected by the native biochemical profile of the source tissue and the proteins that are retained after decellularisation and solubilisation (108).

A desire during decellularisation is to limit damaging the ECM so to retain as many potentially regenerative characteristics such as cell adhesion sites (104, 105). For instance, much research has been conducted on forming myocardial matrix hydrogels from decellularised tissue (109, 110, 111). In a commonly utilised approach, a heart is dissected to remove all major veins and arteries. The myocardium is then minced into smaller pieces, and decellularised with the detergent sodium dodecyl sulfate. It is then lyophilised and further converted into a powder through milling (112). To form a hydrogel, pepsin is added to a suspension of decellularised cardiac tissue to solubilise the powder. After neutralisation, a hydrogel can be formed at 37 ˚C (112).

Injectable hydrogels from decellularised tissue have shown promise in post-MI treatment pre-clinically (109). For example, Singelyn et al., 2011 produced a self-assembling injectable hydrogel from ventricular porcine ECM (113). When injected in the left coronary artery in the myocardium of rats two weeks post MI induction, the hydrogel appeared to reduce cardiomyocyte death. End-diastolic-volume, end-systolic-volume and ejection fractions (EF) were also preserved post-MI (113). Similar observations were reported by Chen at al., 2016 where a matrix derived from zebrafish ventricle ECM was used to induce cardiac regeneration in mice post-acute MI. Only mechanical disruption was needed for decellularisation, avoiding the use of detergent, and thus ECM integrity was well preserved. Proliferative cardiomyocytes were observed as indicated by a

positive detection of co-localised cardiac troponin T and proliferation marker protein Ki-67 at the infarct and peri-infarct areas three days post injection (114). These findings showed that decellularised tissue has great potential to use as a natural ECM, prompting the first first-in-human study.

Traverse et al.,2019 (115) conducted the first-in-human study exploring the safety and viability of transendocardial injections of VentriGel . VentriGel is a hydrogel derived from cardiac ECM in patients who had experienced myocardial infarction (MI) and were dealing with LV dysfunction, both in the early and late stages following the event. The VentriGel was administered to 15 individuals with moderate left ventricular (LV) dysfunction (where the LV ejection fraction fell between 25% and 45%), who were within 60 days to 3 years post-MI and had undergone percutaneous coronary intervention for revascularisation. The primary focus of the study was on tracking adverse events and any unusual findings in clinical laboratory results. This pioneering study marked the first use of VentriGel in humans and successfully established its safety and feasibility in post-MI patients, indicating the necessity for further investigation through larger-scale, randomised clinical trials (115).

Similarly, another in-human clinical trial by Diaz et al.,2021 (116) with a myocardial-derived decellularised ECM hydrogel suggested VentriGel's potential effectiveness for patients with chronic MI, though precise mechanisms responsible for its efficacy in chronic MI are not well understood. This study aimed to explore both the effectiveness and the mechanism by which myocardial matrix hydrogel alleviates adverse remodelling of the left ventricle in a rat model of chronic MI. Assessment of cardiac function using magnetic resonance imaging were conducted at baseline measurements taken two days before injection of either the matrix or saline (8 weeks post-MI), with subsequent assessment at 12 weeks post-MI (4 weeks post-injection). The results showed significant differences in myocardial wall thickening at the apical segment, indicating a marked reduction in LV apical wall thickening in the saline control group ($\Delta = -0.344 \pm 0.122$, $n = 5$) compared to matrix-treated animals ($\Delta = 0.107 \pm 0.080$, $n = 5$). These differences were not observed in the saline control group (116). Analysis of differential gene expression revealed that the matrix could prevent further negative remodelling of the LV in the chronic MI model

by modulating the immune response, reducing pathways associated with the progression of heart failure and fibrosis, and increasing the expression of genes essential for cardiac muscle contraction (116). Both these studies demonstrated the usability of tissue to form hydrogels. There is still however a need to standardise methods for decellularisation to improve efficacy and batch to batch variability and further to evaluate it clinically (103). Furthermore, decellularised ECM hydrogels present with reduced mechanical strength relative to the native tissue (117).

1.4.3 Proteins

Some naturally occurring and inherently biologically active proteins can be used as a polymer source for hydrogel synthesis. These proteins include collagen, and fibrin (118). Due to the biological activity of the proteins used in forming these hydrogels (59), they present some specific intrinsic advantages over synthetic hydrogels. These advantages (unique to each protein) include the ability to bind and present biomolecules such as growth factors, cell adhesion and supporting cellular activities such as proliferation and differentiation (59). Despite these advantages, there are still challenges including weak mechanical properties and batch to batch variability (59, 118).

1.4.3.1 Collagen

Collagen is the most ubiquitous protein in the ECM and contributes a third of all protein content in the human body (119). It is the main ECM protein of tissue such as connective tissue (i.e., ligaments, cartilage and tendons), skeletal muscle, bone, blood vessels and avascular tissue of the cornea (120). In these tissues, it provides structural support, including mechanical support (tensile strength), tissue shape and organisation due to its rigidity and resistance to stretching (120). Collagen is synthesised mainly by fibroblasts of the connective tissue (121, 122) and degraded naturally by metalloproteases, serine proteases and collagenase (120). It also plays a role in wound healing (described in **section 1.4.3.3**) where during the hemostasis phase, collagen exposure induces the activation of platelets and their aggregation, which then leads to the deposition of the fibrin clot that acts as a temporary haemostatic plug (120, 123). In the inflammatory

phase, collagen further activates immune cells i.e., neutrophils which then secrete pro-inflammatory cytokines e.g., IL-6 that stimulate macrophages and also fibroblasts, endothelial cells and epithelial cell migration (123). Fibroblasts actively synthesise and deposit a collagen matrix that ultimately replaces the temporary fibrin clot (121). Collagen degradation fragments further have the ability to stimulate fibroblasts proliferation and growth factor synthesis for angiogenesis and tissue re-epithelialisation (123). In the remodelling phase of wound healing, collagen type III, is synthesised and gradually replaced by the high tensile strength (type I) in order to form scar tissue (123). Disturbances at this step can lead to abnormalities such as keloid scars, where there is excess accumulation of collagen (124).

At least 29 forms of collagen have been identified, and they all share a typical triple helix structure (119). This triple helix structure is formed by three cords of α peptide chains, held together by covalent and hydrogen bonds forming stable fibers (119). Type I collagen is the most common of all collagens and thus widely used in hydrogel applications due to its ready availability (119, 125, 126).Type I collagen hydrogels are prepared (and kept soluble) in acidic solutions and formed at neutral pH and physiological temperatures in the presence of sodium chloride (NaCl) (127, 128). They are formed through the fibrillogenesis mechanism, which is the process of forming fine fibrils (129). This mechanism is induced by increasing the temperature (usually to 37°C) of collagen solution in buffer at required concentration, while the pH remains neutral (129). This then leads to collagen fiber self-assembly (129), and this assembly increases with increasing temperature. Although polymerisation at extreme pHs and lower temperatures has been reported, these conditions compromise mechanical properties and are impractical for cell and tissue application as they are detrimental to cell viability (130).

Collagen hydrogels have been mostly explored as matrices for cell differentiation *in-vitro* with most studies focussing on optimising their mechanical properties as it has been a limiting factor in application (131). In a study investigating the impact of stiffness in chondrocyte differentiation for cartilage formation, chondrocytes seeded in 2D, and 3D were cultured on or in collagen hydrogels of different stiffnesses (2 – 20 Pa) for up to seven days (132). At the end of the experiment, chondrocytes in 3D proliferated better

than those in two-dimensional (2D). Cartilage markers (aggrecan, type II collagen and sex determining region-box transcription factor 9 were also more upregulated in softer hydrogels while in stiffer hydrogels there was a loss of chondrogenic phenotype indicated by actin cytoskeleton expression (132). Surprisingly and inconsistently, the stiffness range used in this study was much lower than that of normal articular cartilage (± 20 MPa), and those reported in other studies (133, 134). These findings indicated collagen's meaningful contribution in regenerating tissue and highlighted further need to optimise pure collagen hydrogels for use as differentiation matrices for clinical evaluation.

Attempts to evaluate collagen hydrogels in clinical trials have been limited. Some trials are in the recruitment stage (135), while others have been terminated with no reported results (135, 136). A collagen matrix, Oasis®wound matrix, is currently clinically approved for use in wound dressing (137). This collagen matrix was evaluated in a randomised, open-label, controlled clinical trial for treatment of chronic pressure ulcers in patients with Stage III and Stage IV full-thickness pressure ulcers (137). After 12 weeks of weekly treatment with the matrix, complete wound healing was achieved in 40% of patients that received the matrix in addition to standard treatment. In the control group that received only the standard treatment, complete wound healing was only at 29%. The study demonstrated that collagen has promise as a therapy that accelerates wounds healing (137). There is still however a need to improve collagen's mechanical properties. Despite it being a strong structural protein in the ECM, pure collagen hydrogels have weak mechanical properties (135), with difficulty in producing hydrogels stiffer than 1 KPa due to several factors such as processing (131). It further has poor binding capacity for growth factors, and thus a limited application as a delivery vehicle (131).

1.4.3.2 Fibrinogen

Fibrinogen presents as a good candidate biomaterial compared to other natural hydrogels. This is due to the fact that it is inherently able to rapidly form the hydrogel fibrin, it is biocompatible, as well as biodegradable, and can further bind several biomolecules of the ECM involved in tissue repair (138). This protein is produced mainly by hepatocytes of the liver, and as indicated above, is the precursor protein for fibrin

(139). As an acute phase protein, its production and circulation is increased during inflammation (140), with an increase up to 10 times the normal plasma concentration to mediate the inflammatory response associated with innate immunity (140). It is proposed to promote leukocyte migration (recruitment) and induce cytokines i.e., TNF-α, interleukin (IL)-1β and IL-6 production by triggering the respective cell's onward signalling pathway (141). Additionally, the fibrinogen fragment, Bβ15–42, possesses anti-inflammatory effects and contributes to preventing the loss of the endothelial barrier function due to stress (141).

Naturally, fibrinogen is a fibrous glycoprotein with a 340 kDa molecular weight, a fiber length of about 45 nm, and diameter of about 2 – 5 nm (139, 142). As a dimer (**Figure 1.5**), it consists of two sets of polypeptide chains (monomers) that are linked together by 29 disulfide bonds to form the dimer (143). Each polypeptide chain set is made up from three polypeptide chains, namely Aα, Bβ, and γ uniquely attached to the E-region (centre) of the two sets (138, 139). The two α-chains are each linked to the E-region through fibrinopeptide A (FPA) and fibrinopeptide B (FPB) (**Figure 1.5**). In contrast, the Bβ and γ chains together form the D-region and link to the E-region through a coiled segment extending from the Bβ chain portion (138, 139).

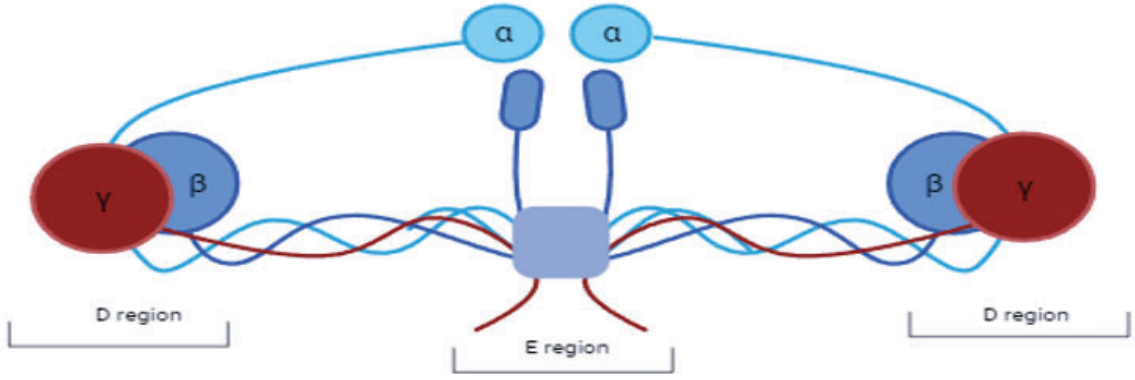

Figure 1.5: **Fibrinogen structure showing two sets of fibrin polypeptide chains** (black). Each has α, β, and γ polypeptide chains linked to the E-region (centre). The βC and γC chains on each peptide together form a D-region and link to the E-region through a coiled segment extending from the β portion. The α chains (known as αC domain) link to the E region through small fibrinopeptides and to each β and γ portions. Image created with BioRender.com.

At molecular level, fibrinogen is encoded by a three gene cluster, *FGB, FGA and FGG,* located on chromosome four (chromosome 4q31.3) (144, 145). This gene cluster is expressed mainly in the hepatocytes under co-ordinated gene expression that ensures the correct ratios of each gene product and overall fibrinogen plasma levels (144). This occurs both in basal states and during inflammatory stress (144). Complete mechanisms of this regulation are still under study. At present, there is strong evidence of regulation by proximal promoters and enhancers with binding sites for hepatocyte transcription factors that then initiate transcription for messenger ribonucleic acid (mRNA) production (144). In humans, these promoters are located at –59 to –47 nucleotides from the fibrinogen gene transcription start site for *FGA,* –91 to –79 for *FGB* and –77 to –66 for *FGG* (146, 147, 148). All these three promoters have interleukin-6 responsive elements (short sequences within the promoter) enabling immediate increased gene expression in response to an acute-phase inflammatory stimulus (144, 147). They can also bind liver loop forming enhancers (cis-regulatory elements) such as fibrinogen enhancer 2 that interact with transcription factors and co-activators for a further level of regulation (144).

Fibrinogen gene regulation plays a crucial role in determining circulating levels of the protein (144). This is important as elevated levels are a risk for cardiovascular diseases and low levels for bleeding disorders such as hypofibrinogenemia. Therefore, hepatocytes must be able to produce fibrinogen at about 1.7 – 5 g per day and through tight gene expression control maintain blood plasma at a concentration between 1.5 – 3.5 g/ L (139, 144). Fibrinogen has a half-life of three to five days in plasma (139, 144). This regulation occurs at various levels including at post-translational level (144). In post-transcriptional regulation, small (~22 nucleotides) non-coding RNAs, known as microRNA (miRNA)s have been reported to repress or up-regulate the clustered gene's translation (144). Fort, Borel, Migliavacca et al., 2010 (149) conducted an *in-vitro* study to gain insight into the miRNAs involved in fibrinogen regulation. For this, 470 known human miRNA precursors were first screened in HuH7 human hepatomas that produce fibrinogen in culture media and their effect on fibrinogen synthesis was quantified by enzyme-linked immunosorbent assay (ELISA) (149) . 39 miRNAs showed significant down regulatory effects (1.46 log fold change) and 11 showed significant up regulatory effects (1.2 log fold

change) (149). These identified miRNAs were then further evaluated and quantified with qPCR and multiplex analysis. From this, 23 of the 39 down regulating miRNAs (1.46 log fold change) were confirmed for down regulatory effects e.g., has-miR 29a, while four of 11 miRNAs (1.2 log fold change) were confirmed for up regulatory effects e.g., has-miR 365 in human liver hepatocytes. This investigation confirmed the miRNA post-transcriptional mechanism of fibrinogen regulation and further identified specific miRNAs involved (149). As a result of these layers of control, fibrinogen production in the hepatocytes and resultant abundance in the blood is well maintained under normal physiological conditions. Therefore, blood can be used as a source of fibrinogen. In addition to miRNAs, genome-wide association studies have further linked several polymorphic markers (e.g., single nucleotide polymorphisms) to circulating fibrinogen levels in humans and, these polymorphs are suggested to contribute to the plasma concentration levels (144).

1.4.3.3 Fibrin in wound healing

Fibrin is a long fibrous blood protein polymerised rapidly from circulating fibrinogen as a natural defence mechanism against blood loss due to tissue injury (150). Once polymerised, it plays an indispensable role in the final step of the coagulation cascade's (**Figure 1.6**) common pathway where together with platelets it forms a stable, insoluble, and temporary haemostatic plug that enables wound healing (139, 143, 150). Briefly, wound healing is a well-co-ordinated process that occurs in four phases, namely, haemostasis, inflammation, proliferation and maturation/ remodelling as indicated in **Figure 1.7** (151, 152). The haemostasis phase (**Figure 1.7 (1)**) begins immediately after injury to prevent blood loss. When blood leaks out of the blood vessels, blood vessels initially constrict in response to vasoconstrictors such as endothelin from the damaged endothelium acting on vascular smooth muscle in attempt to preserve blood loss (151, 152). Platelets, normally protected from untimely release by an intact endothelium (152), are also immediately recruited to the injury site where they adhere to the exposed sub-endothelium that contains collagen (151, 152). They release platelet-derived growth factor (PDGF) which activates mesenchymal cell proliferation and vascular smooth muscle constriction (151, 152). Once platelets are activated, they adhere to the injury site

mediated by von Willebrand Factor (vWF) released by endothelial cells (ECs), through G protein-coupled receptors on their surface and integrins i.e., α2β1 Integrin (152), to exposed collagen which binds to glycoprotein (Gp) Ib-IX in the platelet membrane. They further recruit, through compounds such as thromboxane A_2, other platelets to this site that also aggregate at this site to form a platelet plug (151, 152). Activated platelets in this plug release growth factors such as transforming growth factor-β (TGF-β), PDGF, epidermal growth factor (EGF), and insulin growth factor (IGF) that play a role in the subsequent wound healing phases as cellular mediators (151, 152).

The wound healing platelet plug is stabilised by fibrin production in the coagulation cascade which helps to form a more stable haemostatic plug (153, 154). For this, the coagulation cascade is activated either through extrinsic (tissue factor) or intrinsic (contact) pathways, with the extrinsic pathway believed to be the primary pathway for blood coagulation (154). In the extrinsic pathway (**Figure 1.6**), extravascular tissue factor forms a complex with plasma factor VII/VIIa (FVII/FVIIa) released by the hepatocytes in response to the damaged endothelium with tissue injury (154). This complex activates factor X to factor Xa. Alternatively, factor VII can activate factor IX, which, in turn, activates factor X. Factor X then activates prothrombin (factor II) to thrombin (factor IIa) in a reaction catalysed by the prothrombin complex (factor V) (154). Pro-thrombin is synthesised in the liver and thrombin is responsible for converting circulating fibrinogen (factor I) to a fibrin hydrogel network in the presence of Ca^{2+} (139, 154). This occurs in the common pathway which stabilises the initial platelet plug (154).

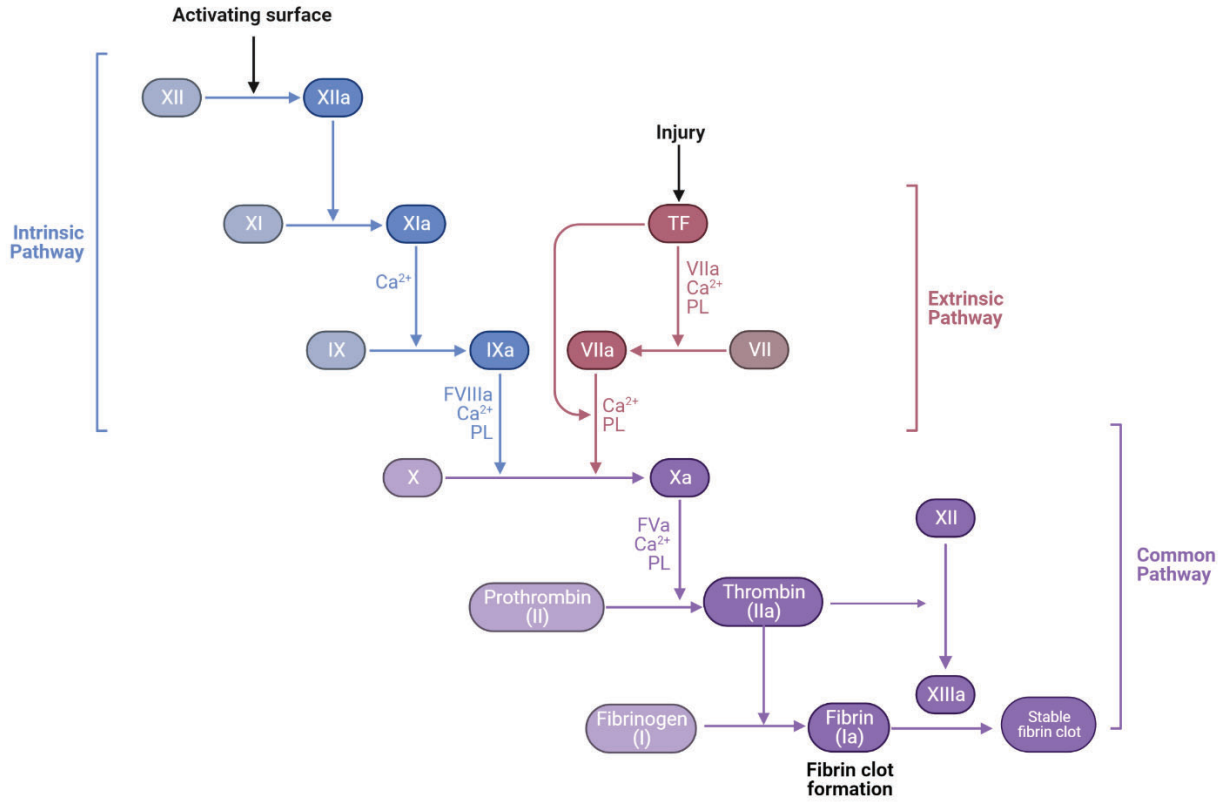

Figure 1.6: **Three pathways of the coagulation cascade**. The intrinsic pathway is activated by negatively charged surfaces such as glass and leads to the activation of factor Xa, which in turn activates thrombin for fibrinogen polymerisation. All the factors needed for the intrinsic pathway are present in the blood. In contrast, the extrinsic pathway needs external factors such as tissue factor. It is activated by tissue injury and leads to the activation of factor Xa that activates prothrombin for thrombin. X: Stuart-Prower factor, serine endopeptidase, Xa: thrombokinase, XI: Plasma thromboplastin, antecedent serine protease, XII: Hageman factor, serine protease, XI: plasma thromboplastin antecedent, IX: Christmas factor, serine protease, VII: Stable factor, serine protease, XII: Fibrin stabilising factor, a transglutaminase, PL: Platelet membrane phospholipid, TF: Tissue factor. Image created with BioRender.com.

In contrast to the extrinsic pathway, in the intrinsic pathway all factors needed for coagulation are present in the blood and do not need tissue factor (154). The pathway is triggered when blood encounters negatively charged surfaces such as glass and kaolin, which then activates factor XII to XII_a (**Figure 1.6**) (154, 155). It is believed to play a role in thrombotic diseases and not normal haemostasis. Factor XII_a catalyses the conversion of factor XI to factor XI, which in turn catalyses the conversion of IX to factor IXa in the presence of Ca^{2+} (154, 155). Factor IXa then forms a complex with factor VIII and this complex plays a role in stabilising membrane proteins in the presence of Ca^{2+} (**Figure 1.6**). This complex also activates factor Xa when factor X binds to the complex in the

presence of Ca^{2+} (154, 155). Factor Xa complexes with factor V to convert prothrombin to thrombin, and thrombin converts fibrinogen to fibrin (155). Thrombin also converts factor XIII to factor XIIIa that is responsible for stabilising the formed fibrin clot by crosslinking the fibers, preventing premature clot degradation (155). Factor XIIIa, a transglutaminase, also catalyses cross-linking (intermolecular gamma-glutamyl-epsilon-lysyl bonds) between the formed fibrin and other ECM proteins (e.g. fibronectin) for a stable network needed for homeostasis and ultimately wound healing (156). It also catalyses the formation of intra-fibrin bonds (isopeptide bonds) between free amine groups of lysine residues and acyl groups at the terminal end of the side chain of the glutamine residue (157).

In the inflammatory phase (**Figure 1.7 (2)**) of wound healing which occurs within 24 hours of injury, neutrophils are recruited to the injury site in response to cellular mediators (151, 152) and chemoattractants (such as growth factors, and cytokines), released by platelets, and parenchymal cells as the first line of defence against infection (151, 152). They release inflammatory meditators such as TNF-α and IL-1 that recruit and activate fibroblasts and epithelial cells (152). They also release oxygen free radicals that kill bacteria and foreign material and further release proteases, including neutrophil collagenase and elastase, which remove dead tissue and old ECM components damaged by injury (152). Monocytes are also recruited to the injury site in response to chemoattractants such as TGFβ-3, and monocyte chemoattractant protein-1(151, 152). These monocytes are activated to macrophages which have a dual role; first to phagocytose dead tissue, remove dead neutrophils, kill any remaining bacteria and secondly to further release growth factors and cytokines such as vascular endothelial growth factor, platelet-derived growth factor, fibroblast growth factors TGF-β , NFα, IL-1, and IL-6 which play a role in synthesising, depositing and organising a new ECM (together with the recruited fibroblasts) and promote angiogenesis before the proliferation phase (151, 158).

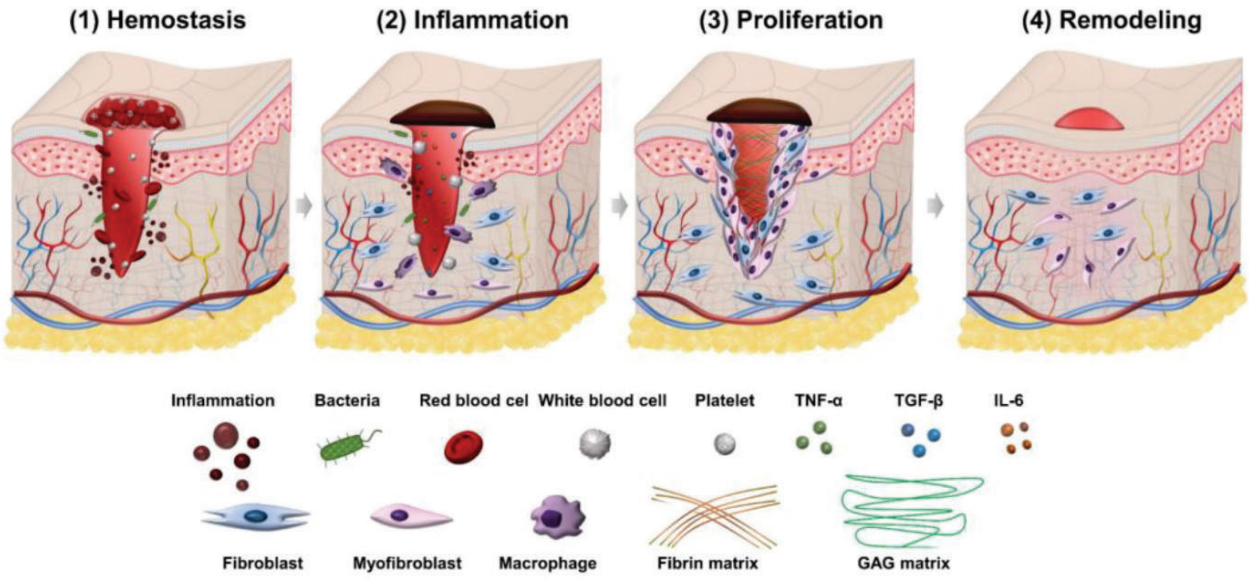

Figure 1.7: Four stages of the wound healing process. The goal of phase 1 in the hemostasis phase is to stop any bleeding. In phase 2 activation of the innate immune system occurs, while in the proliferation phase, granulation tissue becomes evident and consists of high number of neovessels to heal the injured tissue. The remodelling phase is marked by granulation tissue maturing into scar. Image reproduced from Trinh et al.,2022 (159) with permission to use. (159).

In the proliferation phase **Figure 1.7 (3)**, the collagen matrix produced by fibroblasts (predominantly in the form of myofibroblasts) completely replaces the fibrin matrix previously produced (151). The collagen matrix is rich in fibronectin and proteoglycans that helps to restore the ECM (123, 158). As the collagen is deposited and becomes abundant, a new connective tissue, granulation tissue, forms. This tissue is rich in blood vessels and can support fibroblasts in forming scar tissue. It matures to form a scar in the remodelling phase (**Figure 1.7 (4)**), indicative of healed tissue (123, 158).

1.4.3.4 Mechanism of fibrin formation and branching

Fibrinogen polymerisation to fibrin begins when the serine protease thrombin binds to the central E-domain of fibrinogen through exosite 1 and cleaves off FPA and FPB from the amino-terminal of the Aα chains (139, 160). The FPA is cleaved off first (Arg-Gly bond hydrolysis) and initiates the formation of protofibrils. It is then followed by FPB, which results in the α-chain being released from the E-region such that it is left only attached to the Bβ chain (143). This is followed by lateral aggregation (association), through knob:

hole interaction of two stranded protofibrils that eventually twist to form fibrin fibers (**Figure 1.8**) (139, 160). The γ chains have high affinity binding sites for Ca^{2+} (161). Calcium ions, accelerate the process of protofibril aggregation and thus decrease the time required to form a stable clot, while the proteolytic activity of thrombin remains unchanged (139). The exact mechanism for lateral aggregation to form a 3D network is yet to be fully understood. Although research in this field is scarce, Yang, Mochalkin et al., 2000 (162) proposed that it could be through the interaction of two β-nodules of each joining protofibrils at β330-375 residues (162, 163). Further studies are needed.

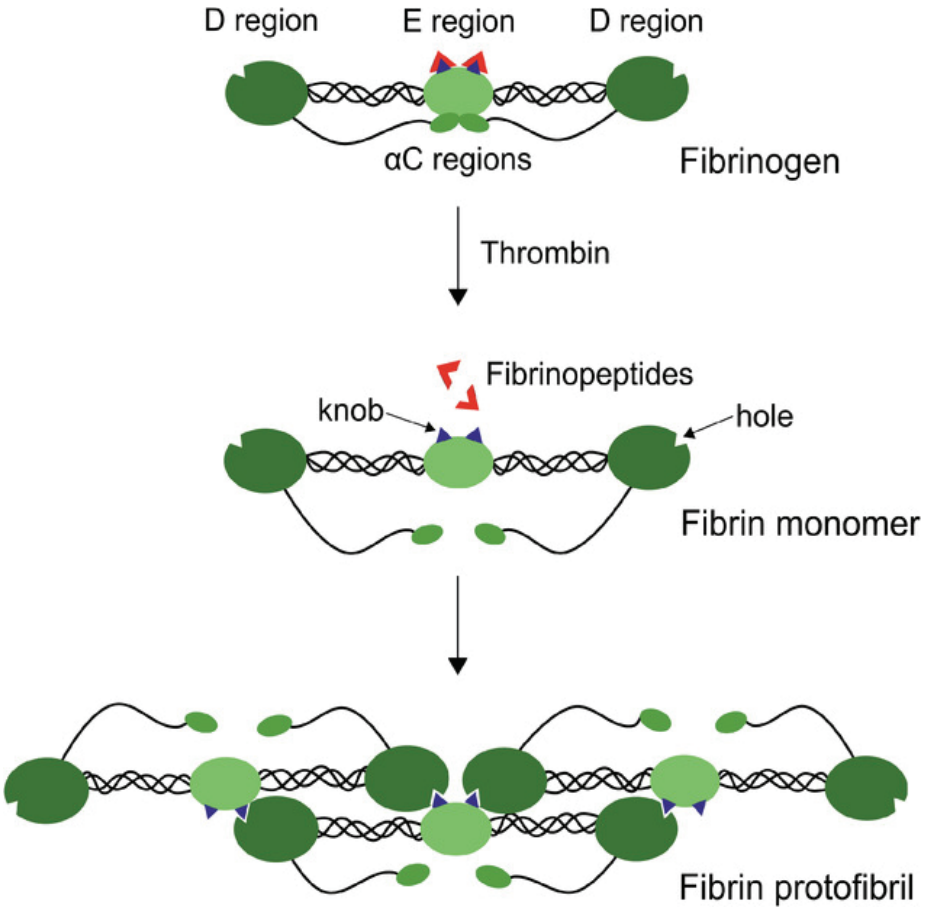

Figure 1.8: Fibrinogen polymerisation process and resultant fibrous structure. (A) An illustration of the process of fibrin protofibril formation from fibrinogen upon enzymatic cleavage by thrombin. The steps for fibrin clot formation can be divided into three steps Firstly the cleavage of the fibrinopeptides by thrombin from fibrin monomers. Secondly formation of two stranded protofibrils from the monomers and finally the aggregation of the protofibrils into fibers that then branch to form a clot (Lateral and bilateral aggregation).Image reproduced from Stamboroski et al.,2021 with permission to use (164).

As fibrin fibers elongate, they also branch out to assemble into a paracrystalline 3D network (139). This occurs through a rapid and modified polycondensation reaction, at ambient temperatures (139). Branching occurs mainly through two mechanisms, namely bilateral and trimolecular junction (163). In bilateral junction, two protofibrils laterally aggregating assemble to form a four stranded fibril that further diverges into two protofibrils (163). In contrast, a trimolecular junction occurs when a fiber molecule attaches to the end of a protofibril such that these protofibrils grow as two stranded protofibrils (163). It has been observed that regardless of the branching mechanism, most branch points in the network have three fibers with the same diameter, suggesting that the initial branching mechanism is negligible in determining the overall 3D network structure (163).

The formed fibrin 3D structure binds various ECM components with its different binding domains (165). It contains a heparin binding domain (HBD) for binding ECM heparin and thereby growth factors possessing a HBD such as the VEGF family e.g., VEGF-165, fibroblast growth factor (FGF) family e.g., FGF-2, and some TGF-β and neurotrophin (165). In humans the Aα-chain naturally contains two RGD sequences at positions Aα95–97 and Aα572–574. These are absent in bovine fibrinogen and are instead compensated for by RGD at Aα-252–254 (144, 166). These sequences are sites of interaction with cells through integrins that serve as transmembrane cell adhesion molecules (167). Integrins with a- and b-subunits including, αIIbβ3 on platelets, aMb2, on leukocytes, and αVβ3, αVβ5, and α5β1 occurring on both EC as well as fibroblasts have been shown to bind to the RGD sequences (167, 168, 169, 170). This then makes fibrin adhesive for endothelial cells, fibroblasts, smooth muscle cells, platelets, and leukocytes. Furthermore, non-integrin receptors such as vascular endothelial cadherin, intercellular adhesion molecule-1, P-selectin, and glycoprotein Ib (GPIba) are also known to provide cellular interaction with fibrin(ogen) (168) for cell adhesion. In addition, plasma proteins such as vitronectin and fibronectin can bind to fibrin(ogen). Vitronectin directly binds to the carboxy-terminal of the γ chain, while fibronectin binds through the αC-domain, which is only in accessible in fibrin and not fibrinogen (165). Thus, fibrin provides multiple points of interaction with proteins and cells that are integral to wound healing.

1.4.3.5 Fibrinolysis

Once the fibrin has served its function as a haemostatic plug in wound healing, it is degraded through fibrinolysis (171). Fibrinolysis occurs via plasmin activity, a protease converted from plasminogen by tissue plasminogen activator (tPA) and urokinase (uPA) through cleavage at Arg561-Val562 (171). The tPA is produced by endothelial cells and has higher affinity for plasminogen, while uPA is produced in monocytes, macrophages, and urinary epithelium cells and has a lower affinity (171). Plasmin also prevents new clot formation by digesting factor II, V, VII, XII, prothrombin and precursor fibrinogen (171). As a result of fibrinolysis, fibrin(ogen) degradation products (FDPs) including FPB and d-dimer fragments are released as by-products (172, 173). The FDPs have been reported to have significant immunomodulatory and regenerative effects (171). For instance, FPB has been shown to act as a chemoattractant for monocytes, macrophages and neutrophils (174, 175). The Bβ 15-42 peptide fragment in the N-terminal B chain is proposed to have cytokine-inducing and immunosuppressive attributes that protect endothelial barriers and may also protect organs from shock-related ischemia (176, 177) (171). Once fibrinolysis is complete, plasmin is degraded in the liver.

1.5 Fibrin hydrogels

1.5.1 Hydrogel micro-structure

Fibrin hydrogels for use in the clinic and research are formed from fibrinogen and thrombin in a manner that mimics the last step of the blood coagulation cascade **(Figure 1.6**) (178). For these hydrogels, the microscopic structural features (micro-structure) play a pivotal role in determining cell spreading, migration, proliferation, nutrient transfer, and biomolecule exchange (179). They are influenced by factors such as starting fibrinogen and thrombin concentrations, Ca^{2+} levels, ionic strength, and pH. These factors drive gelation and polymerisation kinetics (179, 180). Chernysh and Weisel 2008 distinguished gelation time from polymerisation time as the point at which 15 – 20% of fibrinogen has been converted to fibrin, while polymerisation time relates to the time taken to form a pure fibrin hydrogel (181). Controlling gelation and polymerisation rates allow for regulation of fibrin hydrogel characteristics (24).

The influence of fibrinogen and thrombin concentrations on micro-structural characteristics is understood to be a combination of the rate of fibrinogen cleavage by thrombin, lateral aggregation, and fiber branching (182). Early kinetic modelling studies that investigated the reaction of thrombin on fibrinogen concluded that this reaction follows Michaelis-Menten kinetics (183, 184, 185, 186). In these investigations, altering fibrinogen concentration as a substrate impacted the rate of FPA cleavage and overall lag phase. In this, FPA cleavage increased with increasing fibrinogen concentration and led to a shorter lag phase for clot formation. Equally, at lower thrombin with constant fibrinogen concentrations, the rate of FPA cleavage lowered resulting in a longer lag phase for clot formation (183, 184, 185, 186). Conversely, at high thrombin and constant fibrinogen concentrations the rate of cleavage increased leading to a shortened lag phase (183, 184, 185, 186). This reaction has been proposed to follow zero order Michaelis-Menten kinetics where the rate of the reaction increases with increasing enzyme concentration and decreases with decreasing enzyme concentration independent of the substrate (187, 188). Subsequently, increased FPA cleavage results in increased fibrin protofibril formation that further associate to form fibers.

With fibrin fiber aggregation, a new protofibril is added to a fiber for lateral aggregation at 22.5-nm repeats to form protofibrils (143). Because lateral aggregation and branching compete, at high concentrations branching is proposed to supersede lateral aggregation and resultantly form more branch points with thinner fibers as the fibers branch before they aggregate (139, 189). Fibrin fibers have been proposed to possess some degree of elasticity, and due to this, more branch points lead to more stretching and thus formation of longer fibers (190). Resultantly, a highly branched and dense network (less permeable) with thinner fibers forms at high thrombin concentrations. At lower thrombin concentrations, fibrinopeptide cleavage is slower, resulting in a lower rate of protofibril formation that pack to form thicker fibers with less branch points and thus a loose and more porous microstructure 3D network (190).

Fibrinogen and thrombin concentration and the resultant micro-structure has been shown to impact cell behaviour. Ho et al., 2006 (191) studied human mesenchymal stem cell (MSC) behaviour in fibrin hydrogels of varying concentrations.. For this, single MSC were

encapsulated in fibrin hydrogels from fibrinogen concentrations ranging from 5 - 50 mg/ml, and thrombin concentration ranging from 1 to 250 units/ml. The cells were then cultured in the hydrogels for 12 days and viability quantified with a live/ dead assay. At high fibrinogen concentrations (17 and 50 mg/ml), thrombin changes had no obvious effects on human MSCs proliferation. Higher fibrinogen concentrations decreased cell proliferation, regardless of thrombin concentrations. At lower fibrinogen concentrations (5 mg/ml) however, thrombin had influence on proliferation. There was a consistent decrease in proliferation as the thrombin concentration increased. This was observed at high, middle, and low concentrations (167, and 250 units/ml). Formulations of 5 mg/ml with 1 unit/ml thrombin were better performing hydrogels, as they supported proliferation and yielded more viable cells with an elongated and spindle- like structure (191). The cells further established filopodia and intercellular (fibrous) connections and formed a 3D cell network. At high concentrations (50 mg/ml) cells appeared rounded and did not indicate proliferation at further time points. This was probably due to structural differences (e.g. pore sizes) where confocal and scanning electron microscopy (SEM) images showed a more porous structure and more structural homogeneity for the 5 mg/ml, and a less porous and dense structure at 50 mg/ml. Proliferation was shown to be highly dependent on fibrinogen concentration. Although cell-matrix and cell-cell interaction mechanisms explaining this phenomenon within a hydrogel matrix are unknown and remain an active research area, this study was in agreement with the hypothesis that fibrin hydrogel micro-structure impacts cell behaviour (191). Similar observations, to those seen with MSCs, have been observed with single fibroblasts (192). The short coming of these studies (191) (192) is however that they did not directly consider mechanical stiffness of the different formulations and its impact on both proliferation and migration rates.

1.5.2 Hydrogel mechanical properties

Fibrin possesses both viscous and non-linear elastic properties rendering it viscoelastic (193). Its viscosity is commonly characterised by the shear energy loss during deformation modulus, called G”, while elasticity (determining stiffness) is characterized by the shear energy storage during deformation modulus, G’, also known as Young’s

modulus (139, 194). These two parameters are commonly measured with a rheometer, which quantifies response to deformation. The elastic component is often much larger than the viscous component but decreases with increased deformation rates. Resultantly, at higher or repeated deformations, fibrin hydrogels lose water through syneresis. Both Litvinov & Weisel, 2017 (143) as well as Britton et al., 2019 (193) have attested to these findings and further confirmed fibrin's non-linear elasticity as well as its high deformation observed in stress-strain curves, where at low strains stress is directly proportional to strain while stiffness is constant (139, 143, 193). Conversely, at higher strains, stiffness increases significantly (143). For these reasons, correct optimisation of both G' and G'' is therefore crucial for fibrin hydrogels with good mechanical properties, as well as cell invasion for tissue formation (143, 194). Specifically, these hydrogels need to be dense enough to bear the required load at their implant position and loose enough to support cellular activities (194). Overall, properties of single fibers and their 3D assembly, i.e., fiber stretching, orientation, number of fibers, branching and packing arrangements, contribute to determining the mechanical behaviour of the final hydrogel (143, 194). Fibrinogen and thrombin concentrations, which inform micro-structure, ultimately determine mechanical properties. A loose 3D network is more likely to result in less stiff hydrogels, compared to a densely packed network which produces stiffer hydrogels (143, 194).

Salam et al., 2018 (195) evaluated the influence of both fibrinogen concentration and hydrogel stiffness on 3D human MSC migration at different fibrinogen concentrations (5, 10, 30, 40, and 50 mg/ml) and standard thrombin concentration at 5 units/ml.. Microstructural results from SEM confirmed a dense network with smaller pore sizes at the higher concentrations (50 mg/ml; ± 0.8 μm), whilst pore sizes increased with lower fibrinogen concentration (5 mg/ml, ± 3.8 μm). Storage modulus also increased with increasing fibrinogen concentration (195). Similar to the findings by Ho et al., 2006, at lower concentrations, individually encapsulated cells were elongated with a spindle fiber shape, while they were more round and smaller at higher concentrations indicating limited spreading (191). Further results from sprouting spheroids showed that 5, 10 and 20 mg/ml hydrogels had some sprouting by 24 hours, while at 40 and 50 mg/ml there was no

outgrowth. By 72 hours, 5 and 10 mg/ml had the highest migration index (i.e., fold increase) at 0.6 and 0.5 respectively, while that of 40 and 50 mg/ml were below 0.2 and 20, and 30 mg/ml were at 0.3 and 0.28 respectively. The study concluded that an increase in fibrinogen concentration results in increased hydrogel density that reflects as increased hydrogel stiffness, represented by G' (191). This characteristic limit 3D cell migration perhaps due to less porosity for cell invasion. This is likely due to encapsulated cells migrating by physically moving through pores and/or secreting enzymes that can remodel or degrade the matrix e.g., MMPs. Therefore, while high stiffnesses hydrogels may be useful for immobilising cells such as in surgical sealants (191), these are may not be useful where cell migration/ invasion is required i.e., vascularisation. Similar studies, also using different concentrations, with other cell types such as ECs and co-cultures could be beneficial in gaining a more nuanced understanding.

1.5.3 Applications in wound sealing

The first applications of fibrin were fibrin sealants, also known as fibrin glues (196). Following testing in clinical trials, they were approved by the FDA for use as tissue sealants, hemostats, and adhesives in 1998 (it is still the only material licensed as a such) and today have versatile functions in surgery (196, 197). These non-autologous formulations are available in liquid formats that can be topically sprayed onto the injury or surgical site using mostly double barrel syringes for greater control of gelation time (196, 197). One barrel of the double syringe contains fibrinogen liquid at concentrations typically between 67 - 106 mg/ml (198). The second barrel will contain of thrombin at about 400-1200 units/ml and the co-factor $CaCl_2$ (36 – 44 µmol/ml). It can also contain the serine protease inhibitor aprotinin (2250 - 3750 K units/ml) to prolong glue duration (198, 199). Aprotinin use in the clinic was temporarily suspended from 2008 to 2012 due to safety concerns, but has however since been reinstated (200). These concentrations, volumes and units, within these ranges, vary depending on the application.

Upon applying pressure to the plunger of the syringe, these components are sprayed as a unit at their target surgical site and thereafter polymerise to form a covering clot that acts either as a sealant, hemostat or adhesive (198). The fibrinogen mixture can also be

delivered using a catheter directed to the surgical site (201). Tisseel is an example of an FDA approved commercial fibrin for use in surgery and many other competitors are also being explored for wound sealing (201).

As tissue sealants, fibrin forms a clot that acts as a sealing barrier that prevents liquid or exudate from leaking out the wound or surgical site, (202) and ultimately preventing wound drainage. For example, fibrin sealants have been used to seal and augment stapled anastomoses after oesophageal atresia surgery as well as assist in the healing process of post-surgical enterocutaneous fistulas (202). Anastomoses leakage often extends hospital stays and requires reoperation, while untreated fistulas may have complications such as sepsis, and organ damage (202, 203). For example, when commercial Tisseel was used in a clinical trial to seal an enterocutaneous fistula (around the anastomosis) formed post oesophageal atresia surgery, it could assist with controlling leakage (204). Oesophagograms showed that the sealant also sped up the healing process and closure, reducing the time frame from 32 and 37 days respectively in the control group to 12 and 15 days respectively in those who received the fibrin sealant (204). Oral intake also began sooner in the fibrin sealant group compared to the control group without the sealant (204). Similarly, a phase I/II non-randomized trial showed that a fibrin sealant could improve chronic venous ulcers, with at least 50% reduction in the ulcerated area and overall quality of the ulcerated area in 22% of the participants followed up till the end of the trial (205). These findings indicate the potential of fibrin to also enhance wound healing.

Fibrin is also known to function as an adjuvant hemostat where the clot specifically assists in controlling bleeding during surgical procedures (206). The clot precursors are again applied by spraying or using catheters, and thereafter form a clot at the bleed point and then acts as a barrier (139, 206). In a prospective randomised control trial, fibrin was used as a hemostatic agent at concentrations 100 - 300 mg/ml, with thrombin at 50 - 350 units/ml, and factor XIII at 40 units/ml (25). It was used to help control bleeding in neonates undergoing extracorporeal membrane oxygenation because of failing lung and heart function. The procedure helps with inducing gaseous exchange to sustain their lives. In this study, fibrin was applied either through spraying or using a two-channel

device, one with fibrinogen and the other with thrombin. The two components were mixed via a double-barrelled syringe and further delivered at the target site using a haemedics device with a short cannula. The fibrin was delivered at the vessel cannulation site if there was a bleeding wound. The fibrin hemostat was given in addition to electrocauterisation treatment and compared to a control group that only received electrocauterisation. In the first 24 hours, the fibrin population showed significantly less frequent bleeding (18.2%, compared to 42.2%) and volume of blood lost (12.6 ml/ kg compared to 18.7 ml/ kg) compared to the control group (25). These findings proved fibrin's efficacy as an adjuvant hemostat. Similar observations have been noted when the hemostat was used in surgery for vascular surgery (207, 208).

As an adhesive, fibrin has been used in surgery to glue tissue structures together (209). For this, it is prepared at lower thrombin concentration (5 units/ ml) to control for gelation time at target site. It then acts as an interface that connects two tissue surfaces, i.e., wound side tissue, and helps to stop them from separating. It is often used in skin grafts for burns and as a flap attachment in wound closure (209). This indicates the diverse applications of fibrin, and its role has expanded beyond use as a sealant, hemostat, and adhesive in surgery, to a hydrogel delivery vehicle for cell delivery.

1.5.4 Applications in cell support and delivery

Due to its biocompatibility, fibrin has been shown to be an ideal vehicle for supporting and delivering viable cells (165). Naturally, fibrin supports cell migration, vessel formation and vascular infiltration during wound healing (152, 165). Additionally, it has been shown that it can maintain the paracrine functions of cells and is thus advantageous for less invasive clinical procedures (210, 211). In implanting cells for therapeutic purpose, the effectiveness of the implant and ultimately tissue regeneration is dependent on cell viability upon engraftment (210). It is common that cell death occurs within a few days of implantation, and cells directly injected into an injured site can also be washed away, and this loss often needs to be compensated for (212, 213). For instance, poor engraftment and high rates of cell death have been reported when MSCs were transplanted in environments with harsh conditions such as in large wounds with extensive tissue damage (214). In line with this, high concentration (1 million cells) of fluorescently labelled

MSCs were injected intramyocardially into healthy porcine hearts using an injection catheter (215). When these cells were tracked microscopically, it was found that these cells were washed out into veins immediately following implant. This venous drainage was found to be more pronounced during systole when the myocardium contracts (215). A vehicle for cell delivery thus ideally needs to be effective in retaining cells at the delivery site and supporting their viability.

To prepare fibrin for cell delivery, cells are often suspended into a fibrinogen solution, followed by thrombin addition to the cell suspension and the solution embedded or injected into the target site (138). Cells can bind to fibrin through an RGD and integrin interaction (**Figure 1.9**) (165). Fibrin fibers possess RGD sequences, while integrins are present on the surface of the cells (**section 1.4.3.3**). In application, fibrin has shown promising findings as a cellular micro-environment in cardiac and bone tissue. For instance, Christman et al., 2005 (216) showed that skeletal myoblasts mixed with fibrin and injected into the left ventricle of MI induced rats reduced infarct scar size in ischemic myocardium, with good preservation of wall thickness and survival of transplanted cells. Infarct size was also decreased, and tissue perfusion increased after five weeks compared to cell alone control. Interestingly, fibrin alone also showed similar outcomes as the fibrin group with cells, and this was thought to potentially reflect the pro-angiogenic nature of fibrin. Likewise, Ryu et al., 2005 (217) demonstrated that rat bone marrow derived mononuclear cells (BMMNC) mixed with fibrin matrix resulted in more extensive tissue regeneration in infarcted myocardium compared to BMMNC implantation without matrix, after eight weeks *in-vivo*. Here a fibrin alone control was not incorporated.. Additionally, the implantation also resulted in neovascularisation, with higher micro-vessel density (350 microvessels/mm^2) compared to BMMNC implantation without fibrin matrix (262 microvessels/mm^2). The average internal diameter of microvessels was also significantly larger in BMMNC implantation with fibrin matrix group (14.6 μm) than BMMNC implantation without matrix group (10.2 μm) (217).

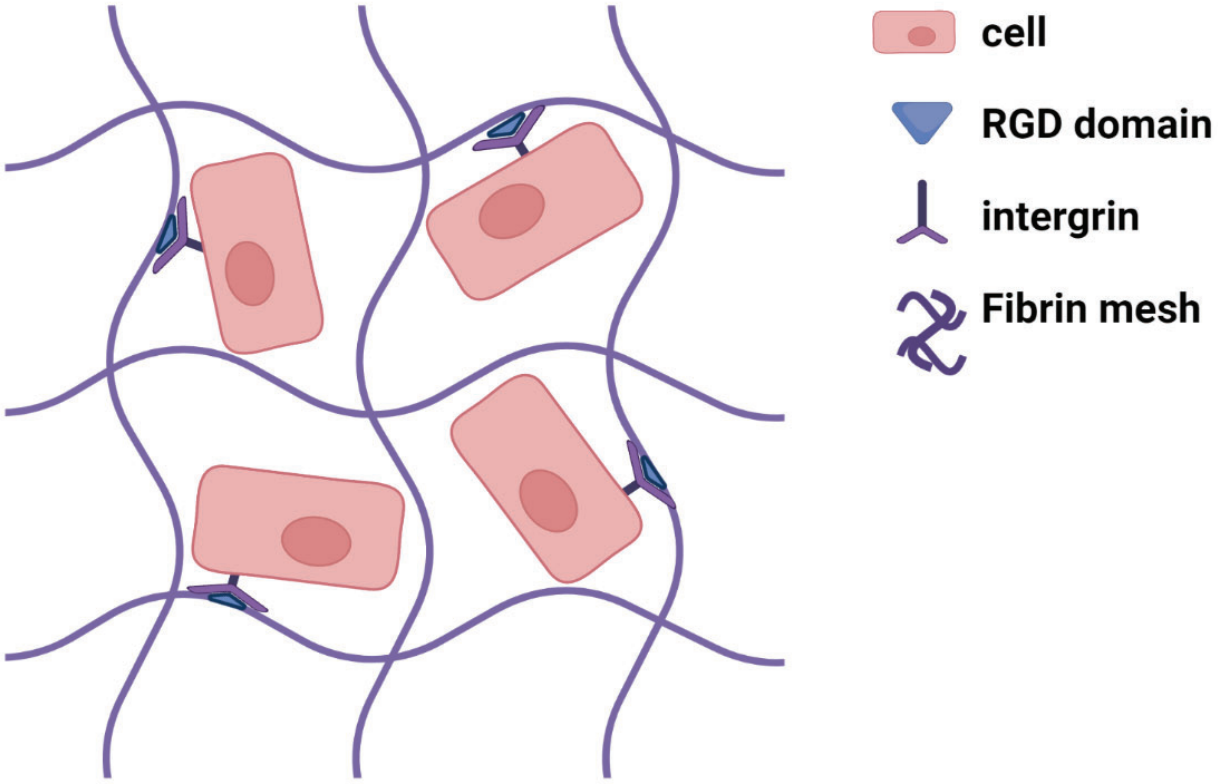

Figure 1.9: Cell interaction with fibrin matrix. The cells interact through their integrins which bind RGD sequences on the fibrin. Image generated with Biorender.

In a pilot clinical study, bone marrow MSCs delivered with fibrin spray were effective in healing human acute and chronic wounds (218). In this, the MSCs were isolated from the patients' bone marrow's iliac crest. Fibrinogen was then prepared at 5 mg/ml and 25 units/ml thrombin and then mixed with the isolated bone marrow MSCs and delivered to the wound beds (2×10^6 cells/ cm^2). Acute wounds from post-surgical skin cancer healed after three applications (a week apart) and by eight weeks all wounds were healed and remained healed at 12 weeks observation. Similarly, the fibrinogen and the bone marrow MSC solution was sprayed unto leg and foot chronic wounds (more than a year old) from diabetic neuropathy and venous insufficiency patients that had failed to heal with standard care, and topical application of PDGF. The wounds were completely closed by six months, with healing that began at three months (218). Further clinical studies with larger sample sizes and careful controls are necessary for more conclusive results.

1.5.5 Applications in growth factor delivery

In recent years, fibrin has shown potential as a growth factor delivery system for more controlled delivery (219), curbing the side effects experienced with a systemic bolus delivery. The range and distribution of pore sizes within the hydrogel network are crucial for achieving controlled release kinetics and uniform distribution of growth factors (220). A narrow size distribution ensures consistent release rates and avoids burst release effects, which are critical for maintaining therapeutic efficacy over time. In this study, a narrow size was desired (221). For delivery,growth factors are loaded into fibrin in various ways including simply mixing fibrinogen (**Figure 1.10**) with the growth factor prior to polymerisation or modifying the growth factor to facilitate attachment (219). The simplest, quickest, and most common growth factor delivery hydrogel system is formulated by adding the desired growth factor to the precursor solution (commonly fibrinogen) and allowing it to distribute within the solution and thereafter crosslinking it with thrombin to sterically entrap the factor within the fibrin mesh (219). The hydrogel is thereafter placed/ injected at the target site where the growth factor diffuses out overtime (219). In an *in-vitro* study that prepared fibrin hydrogels in a similar manner and evaluated growth factor retention and release from the fibrin hydrogel, it was found that fibrin has different affinities for the different growth factors, and this impacted their release and retention (222). Fibrinogen was prepared at 10 mg/ml, in the presence of aprotinin, with thrombin at 10 units/ml. A total of 6 ng of bFGF, $VEGF_{121}$ and $VEGF_{165}$ were individually pre-mixed with fibrinogen and thereafter polymerised to form hydrogels. The hydrogels were then incubated at 37˚C in media for four days and the media eluates for each day assayed for growth factor using enzyme-linked immunosorbent assay (ELISA). The $VEGF_{121}$ had the lowest affinity with the highest release rate (about 2.8 ng/ day) followed by $VEGF_{165}$ at ±1.7 ng/day, and bFGF at ± 0.1 ng/day. This showed that growth factors are not only sterically entrapped but also bind to fibrin with different affinities, and that fibrin hydrogels can be prepared simply to release growth factors at different rates thus adding another level of control (222).

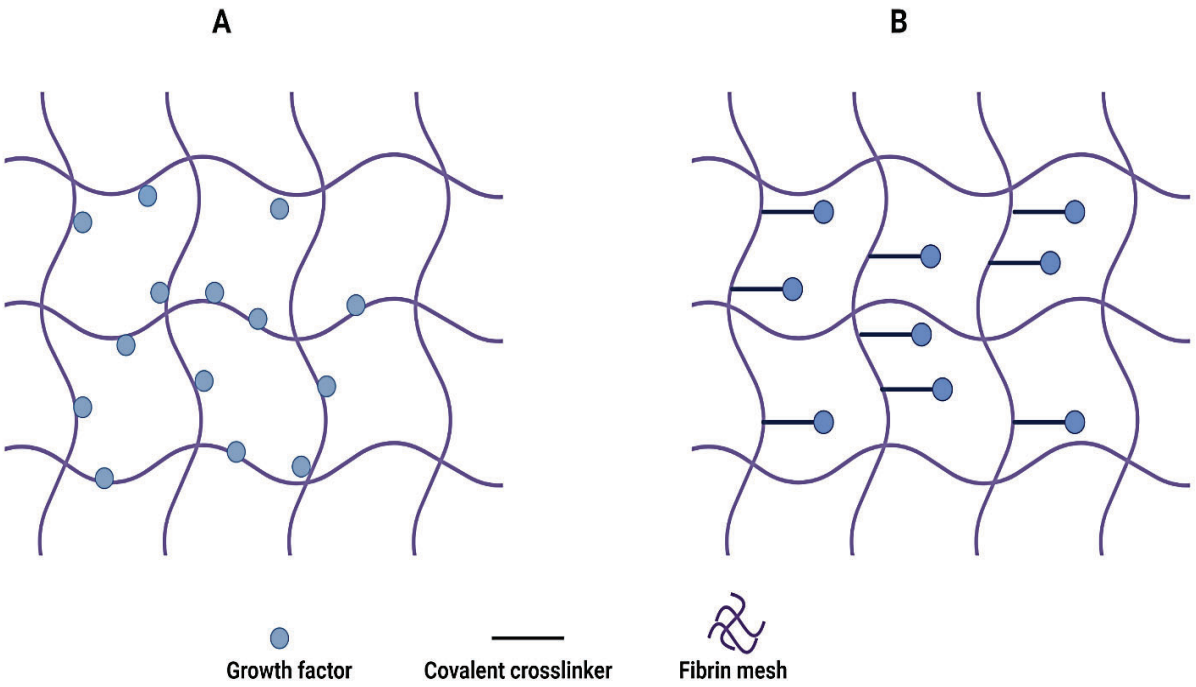

Figure 1.10: **Growth factor entrapment in fibrin systems**. (A) Growth factor simply mixed with fibrinogen and polymerised together (219). (B) Growth factors attached to fibrin through covalent crosslinkers that naturally crosslink with fibrin during the clotting process (222). Image generated with Biorender.

More sophisticated systems have also been explored to tether growth factors covalently to fibrin for delivery where transglutaminase, that naturally crosslinks fibrin during clotting (**Figure 1.10**), activity is exploited to couple a modified growth factor (219). The growth factors are then released either through hydrogel degradation, or breakdown of covalent linkages (219). A mutant of $VEGF_{121}$ was created which contained a N-terminal fragment with a factor XIII substrate sequence NQEQVSPL (223). The impact of the covalently attached $VEGF_{121.}$ on HUVECs growth was then assessed by seeding HUVECs in 2D onto polymerised fibrin hydrogels. It was proposed that the growth factor was released through hydrogel degradation by cells and resulted in increased proliferation. A dose response pattern was observed, with an optimal response at 1 µg $VEGF_{121}$/ ml fibrin hydrogel as compared to fibrin alone. This effect was reduced at higher concentrations (5 – 10 µg/ ml) possibly due to receptor saturation (223). These findings demonstrated a fibrin delivery system with covalently immobilised growth factor that could be released to act as a mitogen for HUVECs.

Establishing required growth factor doses, and timing of release for optimal capillary formation however remains a challenge. As observed in the above study, a moderate dose was needed to induce optimal HUVEC growth response. At lower doses, a minimal response was observed, while the highest doses decreased response. Similarly, Sacchi et al. 2014 (224) determined a dose dependant effect and further confirmed its impact on angiogenesis (224). In this study, $VEGF_{164}$ was covalently cross-linked to fibrinogen as described for $VEGF_{121}$ above, in the presence of aprotinin, using an $\alpha 2\text{-PI}_{1-8}$ plasmin inhibitor, a sequence that interacts with Factor XIII, (similar to Zisch et al., 2001) to form a 25 mg/ml fibrin hydrogel with 2 U/ml thrombin (224). A 50 µl volume of hydrogels with $\alpha 2\text{-PI}_{1-8}\text{-VEGF}_{164}$ concentrations at 0.01; 0.1; 1, 5 and 100 µg/ml were then injected intramuscularly (gastrocnemius muscle) in mice (224). After four weeks, angiogenesis was observed across all four concentrations but with varying degrees of induction and morphologies. The 5 µg/ ml $\alpha 2\text{-PI}_{1-8}\text{-VEGF}_{164}$ was the optimal concentration that induced morphologically normal angiogenesis characterised by skeletal muscle capillaries ensheathed in pericytes. More homogenous vessels, 90% within 10 µm diameter, were also observed at this $VEGF_{164}$ concentration compared to vessels in the control group (no $VEGF_{164}$) (224).

In contrast, capillaries observed by Sacchi et al. 2014 (224) at 100 µg/ml had more abnormal structures that resembled angiomas and had no mural cells.. Functional improvement of ischaemia was tested with a hind limb ischemia model where 50 µl of the hydrogel was injected at the determined optimal concentration, 5 µg/ml $\alpha 2\text{-PI}_{1-8}\text{-VEGF-A}_{164}$, or a low concentration of 0.5 µg/ml. The findings showed that when 0.5 µg/ml $VEGF_{164}$ was delivered over four weeks, capillary formation increased (two-fold) higher than the control groups (fibrin alone) and resulted in improved blood flow and collateral arteriogenesis. Interestingly, these observations were however not apparent at 5 µg/ml and angiogenesis was only induced in normal non-ischaemic muscle. The authors hypothesised that this effect could be attributed to the effect of increased inflammatory cells and proteases in the ischemic limb that ultimately accelerated hydrogel degradation rate, which directly impacted growth factor release rate. Of course, effective released growth factor dose per unit time is directly proportional to the degradation rate, and also

the duration of release is inversely proportional to it (224). This then enables more growth factor release with increasing degradation rate for a shorter period without sustained release. These findings emphasise the importance and difficulty of optimising and determining the therapeutic window for growth factor delivery and investigating a range of fibrinogen and growth factor concentrations.

In an effort to gain greater insight into the influence of fibrin concentration and growth factor dosage, Arkudas et al., 2009a (225) used an *in-vivo* subcutaneous rat angiogenesis model to study the impact of growth factor concentration at 10 and 40 mg/ml fibrin (500 µl) with 2 units/ml thrombin and 25 ng/ml aprotinin, with 100 ng/ml or 250 ng/ ml VEGF alone or in combination with bFGF (100 ng/ml) delivery (225). A significant increase in vessel numbers at 100 ng/ml $VEGF_{165}$ only group was observed at one and two weeks with 10 mg/ml fibrin, but a 40 mg/ml concentration was not associated with increased vessel formation. Furthermore, stimulation of vascularisation was decreased at the higher VEGF concentration. Delivery of the combination of VEGF and bFGF had no significant impact on vessel growth. It is possible that the 10 mg/ml fibrin hydrogel in conjunction with 100 µg/ml VEGF allowed for an optimal growth factor dosage due to a faster degradation, but these findings emphasise the difficulties in achieving the desired rate (225). Surprisingly, in an arteriovenous loop model with 500 µl fibrin (10 mg/ml at 2 units/ ml thrombin) hydrogel filled in a custom made Teflon isolation chamber and the loop embedded in the medial thigh of rats, Arkudas et al., 2009b (226) showed that 100 ng/ml $VEGF_{165}$ alone had little meaningful effect on vascularisation whilst here a combination of both $VEGF_{165}$ and bFGF at 100 ng/ml showed a significant increase by two weeks.. These conflicting findings perhaps indicate that the position of implant of fibrin releasing growth factors might also impact the outcome.

1.5.6 Fibrin hydrogel functionalisation through PEGylation

PEGylation is an established process for improving protein stability and half-life by shielding it from proteolytic degradation (227, 228). This is achieved by attaching the terminal hydroxyl groups of PEG to the amino sidechains of protein whilst endeavouring to retain protein function (227, 228). This in turn increases the protein's size and

hydrophilicity. Early work by Frank Davis in the late 1970s showed that conjugating methoxy-PEG to proteins shields them from lysis by proteases, thus extending their half-life with an added advantage of reduced immunogenicity (227, 228, 229). This is due to PEG's ability to sterically block proteases and thus shield the protein from degradation (227). PEGylation has resultantly been applied extensively in pharmaceuticals and explored for fibrinogen(227, 228, 229).

Fibrinogen PEGylation has shown to be a promising tool in tissue engineering. Suggs and colleagues (Suggs Laboratory) have comprehensively studied PEGylated fibrin hydrogels using a range of molecular weight PEG crosslinkers and attachment chemistries (e.g., N-Hydroxysuccinimide (NHS) ester terminal (230, 231, 232, 233). Their hydrogels are typically prepared by adding the PEG crosslinker solution to fibrinogen so that they are bound to fibrinogen through primary amine groups (233). Prior to crosslinking with thrombin, the solutions are added at varying molar ratios to the fibrinogen solution, under specific conditions e.g., room temperature and pH between 7.2 – 8.5 using phosphate, 2-(4-(2-hydroxyethyl)-1-piperazinyl)-ethanesulfonic acid (HEPES) buffer, carbonate-bicarbonate or borate buffers to assist the NHS ester reaction chemistry (233). Zhang et al.,2006 (233) first developed a benzotriazole-PEG-benzotriazole (BTC-PEG-BTC) (3.4 K) PEGylated fibrin (at 10 mg/ml fibrinogen) patch for transplanting MSCs.. After 48 hours of seeding, the MSCs within the hydrogel formed a tube-like network that stained positive for both CD31 and vWF, suggesting that the PEGylated fibrin hydrogel stimulated the ability of MSCs to differentiate towards endothelial cell phenotypes without the addition of any exogenous biomolecules (233). The PEGylated fibrin further maintained this endothelial phenotype until the patch degraded. There was however no fibrin alone control group, and in a later study Rytlewski, Geuss, Anyaeji, 2012 (from the same group) (234) found comparable results to Zhang et al.,2006 (233), with fibrin alone group control stimulating a similar but less pronounced effect in MSC differentiation. PEGylation resulting in delayed thrombin induced gelation times (low thrombin to fibrin ratio), which was however insignificant at molar ratios of PEG to fibrinogen below 10:1, raising the possibility of altered stiffness (which was not evaluated in the study) and its impact on migration (234). Perhaps at low

stiffness (softer matrices) migration was favoured, and higher stiffness it was obstructed. It was proposed that the resultant endothelial phenotype in PEGylated fibrin is thus due to a combination of factors, that is fibrin's inherent angiogenic characteristics, and the influence of structure where PEGylated fibrin forms semi-amorphous sheets that might maintain the tubes whilst fibrous fibrin tends to collapse them with time (232).

A subsequent study by Zhang et al, 2008 (235) again used BTC-PEG-BTC (3.4 KDa) PEGylated fibrinogen (as with Zhang, 2006) and covalently mixed it with hepatocyte growth factor (HGF).. It was then applied as an injectable to determine whether such a formulation could enhance the therapeutic effect of bone BMNCs delivery to an infarcted mouse heart. Encapsulating BMNCs in the injectable PEGylated fibrin together with HGF reduced cell death by almost 15-fold compared to directly injecting them to the infarcted area and to PEGylated fibrin plus cells without HGF after two - four weeks. It further reduced apoptosis of the transplanted cells. Fibrosis was also significantly reduced with HGF plus PEGylated fibrin delivery (15.9.6%), compared to PEGylated fibrin alone (17.2%) (235). In this, the effectiveness of PEGylated fibrin was shown as a potential matrix for cell delivery though the lack of native fibrin controls does limit the conclusions that can be drawn.

Subsequently, fibrinogen PEGylation has also been found to slow fibrin hydrogel degradation. Drinnan et al., 2010 (230) (Suggs Laboratory) showed that fibrin hydrogels PEGylated with PEG-succinimidyl α-methylbutanoate $(SMB)_2$ had a slower plasmin degradation rate compared to unmodified fibrin. Non-PEGylated fibrin was completely degraded by plasmin at day four while PEGylated fibrin was still present. A similarly reduced degradation rate was observed by Dadashzadeh, Moghassemi & Amorim, 2021 using the same crosslinker (236). Drinnan et al 2010 (230) further showed that that PEG-PEG-$(SMB)_2$ PEGylated fibrin hydrogels could release TGF-β1 over 10 days *in-vitro*, with bioactivity of the released growth factor maintained for eight days. It was further observed that its release rate was congruent with the hydrogel's degradation rate that was in turn dependent on the degree of PEGylation indicating the multiple functions of PEGylated fibrin (230).

PEGylated fibrin has also been found to improve skeletal muscle function through delivery of growth factor, enhance stem cell delivery, improve tissue vascularisation for wound healing, and maintain cardiomyocyte function (237). When human conditions of insulin-like growth factor-I (IGF-I) (25 µg/ml) was conjugated to fibrinogen with SG-PEG-SG crosslinker (3.4 KDa) and injected *in-vivo* in the lateral gastrocnemius limb muscle of mice that had had ischaemia/ reperfusion injury induced, there was significant improvement in muscle structure and function after four days. In contrast, there were no difference between the injected saline, bolus IGF-I, and PEGylated fibrin alone control groups (237). Additionally, human adipose-derived stem cells (ADSCs) encapsulated and delivered within these PEGylated hydrogels could enhance wound vascularisation in a rat skin excision model, confirmed by early collagen deposition, and wound healing in contrast to PEGylated fibrin alone without cells (238). It was further shown that PEGylated fibrin with ADSCs mixture could significantly encourage tube network formation more than collagen and fibrin with ADSCs *in-vitro*. The ADSCs in PEGylated fibrin had significantly longer network length, and branch number per network. Gene expression evaluations indicated that conditioned media, after seven days of culture, from PEGylated fibrin with ADSCs had significantly high levels of angiogenic factors (VEGF mRNA) and pro-inflammatory factors such as VEGF, IL-6, and IL-8 compared to collagen, and significantly higher von Willebrand factor (a key glycoprotein in haemostasis during wound healing) compared to both fibrin and collagen (239). This suggested that PEGylated fibrin has a superior role in supporting cells for vascularisation and paracrine secretion of angiogenic and immunomodulatory factors. While the exact mechanisms for greater elongation and network formation are unknown, and the extent to which the hydrogel formulations can modify cellular activities remains poorly understood, it can be postulated that a combination of structural changes (where PEGylated fibrin is observed to form sheets as opposed to fibers), and varying storage moduli could have also contributed to encouraging the more elongated morphology compared to fibrin alone and collagen (239). In this study, collagen had a storage modulus of 175 Pa, fibrin of 25 Pa and 1:1 SG-PEG-SG PEGylated fibrin of 50 Pa. Here the 1:1 SG-PEG-SG PEGylated fibrin was stiffer than unmodified fibrin. Detailed mechanisms are yet to be understood on the interplay of stiffness, paracrine factors, and hydrogel micro-structure on vascularisation. In addition,

both Ricles et al., 2016 (240) and Chung et al., 2015 (239) similarly observed improved tissue neovascularisation when PEGylated fibrin was used to deliver MSCs in a rat hind limb ischemic model and burn injury model respectively compared to PEGylated fibrin and cells alone (239, 240). PEGylated fibrin was also shown to be a good matrix for cardiomyocyte cell spreading, with cell contraction being higher in less stiff (indicated by lower concentration) hydrogels. These findings show several potential benefits of PEGylating fibrin, though further modification of fibrin might allow for greater control of growth factor release.

1.5.7 Fibrin hydrogel functionalisation with heparin

Heparin is a linear polysaccharide consisting of 1-4α linked disaccharide repeating units of uronic acid and glucosamine residues (**Figure 1.11**) and is thus known as a glycosaminoglycan (241). It was discovered in 1916 as a naturally occurring anticoagulant, able to prevent blood from clotting too fast (242). It is produced mainly by mast cells and, forms a crucial component of the heparans lining the inner walls of the vascular system (241). In the ECM, it can bind a variety of proteins, such as fibrinogen, fibronectin, vitronectin, and heparin-binding growth factors (**Table 1.1**) that possess a HBD (discussed below) to help to modulate processes such as wound healing and angiogenesis (241).

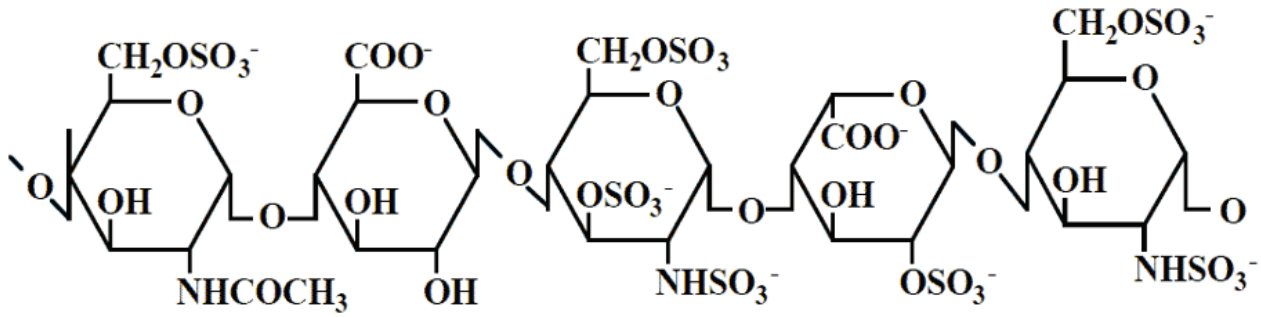

Figure 1.11: Highly sulphated heparin chemical structure with uronic acid and glucosamine residues and their carboxylic acid groups

As a glycosaminoglycan (**Figure 1.11**), heparin is highly sulphated and contains carboxylic acid groups which give it its overall negative charge (total net charge of about -75, about - 2.7 sulfate groups per disaccharide monomer) (241). It is this negative charge

that makes heparin attractive for binding several proteins (243, 244). Heparin has been widely used as an anticoagulant in the clinic since 1935 (245) and is today listed as an essential drug by the World Health Organisation (246). It is available in two forms, unfractionated heparin (UFH) and low molecular weight heparin (LMWH). The UFH has an average molecular weight (MW) of around 15 KDa, while LMWH is a much shorter chain, with a MW less than 8 KDa and is less highly sulfated. The LMWHs have gradually replaced UFH due to their more predictable pharmacokinetics, and reduced side effects (247, 248). Regardless, both these forms of heparin have anticoagulative properties due to their pentasaccharide sequence that binds the serine protease inhibitor, antithrombin (AT), to inhibit thrombin action and ultimately coagulation through the anticoagulation pathway (249, 250). The LMW heparin however has lower binding and retention efficiency than UFH for most growth factors (251).

Several target proteins that bind heparin, such as growth factors and chemokines, possess a region known as the HBD that directly interacts with heparin (252, 253). Research has sought to understand this region and determine whether there are shared amino acid sequence features among target proteins' HBDs or even specific arrangements of the amino acids (i.e., folding patterns). Though the mechanism are still poorly understood and limited progress has been made in this area, HBDs have thus far been found to be unique to each protein and are independent of specific arrangements of amino acids or protein fold orientations (252, 253). The HBDs rather typically contain some positively charged amino acids, commonly arginine and lysine, that ionically interact with negatively sulfo or carboxyl groups of the heparin (253). In addition to these electrostatic interactions, hydrophobic interactions and hydrogen bonds have been found to provide stability to this heparin-HBD interaction (253). Arginine has been found to bind heparin approximately 2.5 times tighter than lysine forming more stable hydrogen bonds and stronger electrostatic interactions with the sulfo groups (253, 254, 255). The binding sites have been proposed to contain clusters of 1, 2, or 3 basic amino acids (XB_nX, where n=1, 2, or 3), commonly spaced with 1 or 2 non-basic residues (BX_mB, where m=1 or 2) (253, 256). Non-basic amino acids such as serine and glycine have been found to be the most common in the HBD where their small side chains provide less steric hinderance

and more flexibility for interaction with heparin (253). Further and more recent studies are imperative to identify specific consensus sequences, crucial for heparin binding growth factors utilised in regenerative medicine (253, 255, 256).

Table 1.1: Heparin binding growth factors and their functions

Heparin binding growth factor	Function	Reference
Basic fibroblast growth factor (bFGF)	bFGF stimulates the release of other angiogenic growth factors that regulate angiogenesis. It plays a role in vessel maturation, especially endothelial junction formation, and mural cell proliferation and migration.	(257, 258, 259, 260, 261)
Vascular endothelial growth factor (VEGF)	Main regulator of angiogenesis. It stimulates EC proliferation, migration, and survival.	(260, 261)
Heparin binding epidermal growth factor (HB-EGF)	Stimulates nitric oxide synthase 3 and nitric oxide (NO) production for angiogenesis.	(262, 263, 264, 265, 266)
Bone morphogenic protein (BMP)	Key regulator of bone forming cells, e.g. osteoblast, differentiation.	(264, 265, 266, 267, 268, 269)
Transforming growth factor beta (TGF)-β	Promotes collagen production by fibroblasts for ECM synthesis and remodelling required in stabilising newly formed blood vessels. Regulates osteoclast and osteoblast differentiation and is thus a role player in maintaining mass (balance formation and bone resorption).	
Insulin growth factor like (IGF)-I	Stimulates myoblast, satellite, osteoblast cell proliferation for skeletal muscle regeneration, and bone matrix formation.	(269, 270, 271, 272)
Platelet-derived growth factor (PDGF)-BB	Recruits pericytes and vascular smooth muscle cells to cover newly formed blood vessels ensuring blood vessel maturation and stability during angiogenesis.	(269, 272, 273, 274, 275, 276)
Hepatocyte growth factor (HGF)	Anti-fibrotic action in the liver and contributes to the liver's regenerative capacity. Serves as a growth factor for mature parenchymal hepatocytes. Stimulates motility of epithelial cells and keratinocytes	(274, 275, 276, 277, 278, 279)
Placental growth factor (PlGF)	Directly and indirectly stimulates angiogenesis through the vascular endothelial growth factor receptor 1 (VEGFR-1) and ultimately vascular endothelial growth factor 2 (VEGFR-2) with vascular endothelial growth factor A (VEGF-A).	(277, 278, 279)

1.5.7.1 Growth factor localisation for controlled release

There have been several investigations into incorporating heparin into biomaterials particularly hydrogels due to its potential to localise heparin binding growth factors with an HDB for longer term sustained release. Covalently attaching heparin on the surface of porous polyurethane (PU) discs is one approach that has been explored (280). After 28 days of being subcutaneously implanted in rats, explants of heparinised disc samples showed significantly increased vascularisation (number of vessels) compared to control PU groups. This vascularisation was observed without any increased inflammatory response. Davies et al., 2012 (44) further showed that this scaffold could be used to stage the release of VEGF and platelet-derived growth factor PDGF-BB for sustained vascularisation. It bound and released both VEGF and PDGF-BB *in-vitro* at a rate of 75 ng/h for 24 hours and 86 pg/h for at least seven days respectively. In subsequent rat subcutaneous implants, the heparin alone PU discs again resulted in significantly increased vessel ingrowth at 10 days, which increased even more in the presence of VEGF, while no additional effect was observed in the PDGF-BB group. When the combination of growth the growth factors were added, a similar effect to the VEGF addition group was observed. At a two-month time point, more vascularisation was observed in the PDGF-BB group addition group compared to the VEGF. The combination effect was similar to the PDGF-BB group addition group. Thus, this staged release allowed for a rapid initiated neovascularisation due to VEGF, that was then sustained by the gradual release of PDGF-BB. It was then shown that the VEGF and PDGF-BB combination was useful in stimulating endothelisation of porous PU vascular grafts in a rat infrarenal aortic loop model where vessels were stimulated to invade through the graft wall and reach the blood surface after 12 weeks accelerating vascular graft healing (281).

Heparin has also been covalently incorporated into PEG hydrogels for growth factor release. PEG–heparin hydrogels formed by crosslinking amino end of four-arm amine functionalised star-shaped poly(ethylene-glycol) (starPEG) with carbodiimide/*N*-hydroxysulfosuccinimide (EDC/s-NHS) activated carboxylic acid groups of heparin were shown to be effective in releasing bFGF and VEGF (282). After four days, 16 ng (4 ng/ day) bFGF and 9 ng (2.25 ng/ day) VEGF were released, with a higher release rate

surprisingly observed for bFGF despite bFGF having a higher affinity (Kd = 23 nM) for heparin compared to VEGF (Kd = 165 nM). This was proposed to be due to the fact that VEGF is a larger molecule than bFGF and possibly diffuses out of the hydrogel more slowly than bFGF due to steric hinderance.

Equally, heparinised and hydrolytically degradable PEG hydrogels with covalently bound heparin were prepared by binding hep-acr to the thiol groups of 10 KDa four arm PEG thiol crosslinkers. The heparinised crosslinkers were then used to crosslink 20 KDa 8 arm PEG with acrylated terminal. Heparin was shown to increase binding of VEGF to the PEG acrylate hydrogels and result in a more sustained release rate (45). *In-vivo* subcutaneous rat models further showed that heparin presence resulted in an increase of capillary growth into implants, which increased even further with the presence of VEGF (45). Ciuffreda et al., 2018 (283) further demonstrated that a similar approach could be used to generate enzymatically degradable and heparinised PEG hydrogels using 20 kDa eight arm PEG with vinyl sulfone termini. Here the hep-acr was coupled to the PEG hydrogel via MMP-1 recognition peptide sequence. *In-vitro*, these hydrogels were shown to bind significantly more growth factor compared to the same hydrogel without heparin, binding 1.6-time VEGF and 3.15 times bFGF. Intramyocardial injection of rat bone marrow mesenchymal stem cells MSCs ($1x10^6$ cells) encapsulated in these heparinised hydrogels in rats with induced MI improved left ventricular remodelling as indicated by increased fractional shortening and ejection fraction (EF) and decreased scarring relative to rat bone marrow MSC alone and hydrogel alone (283). Increases in neovascularisation and cardiomyocyte survival was observed for the rat bone marrow MSC plus heparinised PEG hydrogel. It was considered likely that the presence of heparin had amplified the paracrine effect by capturing and stabilising the growth factors secreted by the mesenchymal stem cells. This study further supported the value of heparin in synthetic hydrogels, and warrants exploration in natural hydrogels, with fibrin being a promising candidate due to its biocompatibility, biodegradability and angiogenic characteristics (283).

Immobilising heparin on fibrinogen has been explored in several ways for enhancing growth factor delivery from fibrin hydrogels. Early work by Sakiyama-Elbert & Hubbell,

2000 (284) systematically designed a hydrogel system utilising a bi-domain peptide consisting of a heparin binding site on its C-terminal and an N-terminal transglutaminase substrate that allowed the peptide to be coupled to fibrinogen through the transglutaminase activity of factor XIIIa during polymerisation (284). This peptide could non-covalently bind heparin, which was then used to entrap bFGF, and thereafter mixed with thrombin and polymerised. Upon evaluation *in-vitro* for localised delivery of bFGF for neural extension, bound bFGF was found to enhance neural extension of dorsal root ganglia in a dose dependant manner at 1 µg/ml and 5 µg/ml (400 µl hydrogel) bFGF, and no significant neural extension increase at 10 ug/ml presenting a dose response effect (284). Control samples where free bFGF in fibrin were assessed found no enhancement of neural extension. The VEGF, which is a heparin binding growth factor but does not stimulate neural growth biologically, also did not stimulate neural growth in this system (284). Although complex and requiring several steps, it supports the premise of fabricating fibrinogen with heparin for localised growth factor delivery but needs further evaluation beyond *in-vitro* experiments.

More work has explored means of directly and covalently attaching heparin to fibrinogen. Work by Yang and colleagues employed standard carbodiimide chemistry to couple low molecular weight heparin to the amine groups of fibrinogens (285). For this, heparin was prepared by first activating its carboxylic acid groups by dissolving heparin in 2-morpholinoethanesulfonic acid, hydroxysuccinimide, 1-ethyl-3-(3- dimethylaminopropyl)-carbodiimide hydrochloride and reacting for 12 hours at 4˚C. This solution was then precipitated with excess anhydrous acetone. Fibrinogen was prepared next by dissolving it in buffered solution (PBS) at pH 7.4 at 4˚C, thereafter, reacted with heparin for 3 hours at 4˚C through the activated carboxylic acid groups of and the resultant product precipitated in acetone before being lyophilised. Excess heparin was removed by reconstituting the lyophilised product in PBS and dialysing at 4˚C for 24 hours. The resultant product was then lyophilised for a further 48 hours in preparation for storage. Bound heparin was quantified to 42 mg/g fibrinogen using the toluidine blue method. The modified fibrinogen could not be polymerised with thrombin and required the addition of an excess of modified fibrinogen to form heparin conjugated fibrin (HCF) (285, 286). *In-*

vitro release of BMP-2 from three delivery systems were then compared: (1) HCF formed by mixing 40 mg/ml of the heparin conjugated fibrin and 60 mg/ml additional fibrinogen (standard composition for all studies reported by this group) (2) fibrin only and (3) fibrin with free heparin all dissolved in aprotinin containing PBS and then polymerised with thrombin dissolved in calcium chloride (287). The HCF reduced BMP-2 initial burst release in the first six hours to 28% of BMP-2 loaded as compared to fibrin alone as well as fibrin with free heparin at 44% and 45% released respectively. By day three, fibrin and fibrin with free heparin had released 84% and 81% of the loaded BMP-2, in contrast to the HCF which was able to release a similar amount (89%) over 13 days indicating a more sustained release. In addition, the released BMP-2 was still bioactive (indicated by alkaline phosphatase (ALP) activity when osteoblasts were induced with the released BMP-2) by day seven in all systems, comparable to fresh BMP-2. When BMP-2 loaded HCF, BMP-2 loaded unmodified fibrin with free heparin and HCF alone were set in polyester cylindrical tubes and evaluated in hind limb muscle pockets of rats. After eight weeks, it was shown that significantly more bone mineralisation (about 10 times) (with increased osteocalcin and osteopontin) was observed in explants of HCF loaded BMP-2 compared to either BMP-2 alone, fibrin with BMP-2 and fibrin with free heparin and BMP-2 (287).

When the release of bFGF from HCF was investigated, long-term delivery of bFGF and angiogenesis stimulation could be achieved (285). *In-vitro*, the initial burst release for the first 12 hours from normal fibrin was 52% compared to HCF which was reduced to 8%. A more controlled release profile was observed with 100% of the loaded bFGF released from normal fibrin in 10 days whilst it took 21 days to release 89% of bFGF from HCF. When bioactivity of the released bFGF was evaluated by measuring its ability to stimulate human dermal fibroblast proliferation over nine days, bFGF released from HCF was consistently shown to increase proliferation in serum free medium, while that from fibrin with free heparin decreased sharply from day three up to day nine. It would be of interest to compare these findings to bFGF released from fibrin as this control was not included in these experiments. When 25 µg bFGF was loaded in a 200 µl HCF hydrogel and evaluated for neovascularisation in a hind limb ischaemic mouse model, after 28 days it

was shown that when all groups were normalised against the HCF plus bFGF group, that this group had increased capillary formation relative to HCF alone. This was however not observed for fibrin with free heparin groups loaded with bFGF. The study was thus able to achieve neovascularisation with high levels of bFGF (285).

HCF was further evaluated for *in-vitro* delivery of bioactive factors of PRP for wound healing. In this, PRP containing 1628 ng/ml PDGF-BB, 76.2 pg/ml VEGF, and 37.9 pg/ml bFGF was mixed with equal volume of HCF or fibrin (288). The HCF with PRP was shown to significantly sustain the release of PDGF-BB and VEGF compared to fibrin and calcium gelled PRP. When bFGF was evaluated significant differences were not observable between the different hydrogel formulations (288). In mice with full-thickness skin wounds, HCF qualitatively demonstrated an increase in involucrin expression (indicative of keratinocyte proliferation) in immunohistochemical stains (like normal skin), and this was significantly reduced in fibrin with PRP as well as calcium gelled PRP. Additionally, HCF with PRP was shown to significantly increase capillary density, indicated by von Willebrand Factor staining, over 12 days compared to calcium gelled PRP: fibrin with PRP and no treatment (288). The levels obtained were however significantly below the observations in normal skin, indicating a further need optimise delivery for improved neovascularisation. (288).

HCF has further been evaluated for its therapeutic value with delivery of synovium-derived mesenchymal stem cells (SDMSCs) and growth factors. Sarsenova et al., 2022 (289) showed pre-clinically that a combination of HCF (70 µl) with SDMSCs (1×10^6 cells), TGF-β1 (200 ng) and bone morphogenetic protein-2 (BMP-4) (200 ng) could significantly enhance hyaline cartilage regeneration and subchondral bone plate in a rabbit osteochondral defect model at 12 weeks after surgery. This was observed qualitatively as white fibrous tissue indicating complete healing over 100% of the defect compared to HCF alone where healing only covered about 25%. When quantified with cartilage scores, a score of 12 for SDMSC+TGF-β1+BMP-4 in HCF was significantly increased relative to 10 for HCF with SDMSC, 7 for TGF-β1+BMP-4 in HCF and 2 for HCF alone attesting to the beneficial effects of cell and growth factor delivery in HCF in cartilage regeneration. This effect was however not compared to other hydrogel types such as fibrin alone and

fibrin with free heparin in order to ascertain that the beneficial effects were associated with HCF. Growth factor and SDMSC concentrations were also not stated for *in-vivo* experiments. In a recent clinical trial, HCF was prepared at a higher fibrinogen concentration using 91 mg additional fibrinogen and 20 mg HCF. This HCF formulation was again combined with SDMSC ($2x10^7$) and growth factors (TGF-β1 and bone morphogenic protein 4 (BMP-4) at 1 µg/ml) and delivered with a double barrel syringe for treating articular cartilage defects in patients with osteoarthritis (290).In the study, 15 patients with an average age of 44 years and average articular cartilage defect size of 4.9 cm were recruited. Safety was assessed based on the absence of infection, loose body presence (cartilage or bone fragments in synovial fluid), inflammation, adhesion, and any tumour formation in the knee joints. After eight weeks post implantation, no severe adverse effects were reported indicating safety at this early timepoint. After six months of treatment, articular cartilage repair was evaluated and, 73% patients had complete graft integration into the border zone of the defects with an appearance of intact surface tissue indicative of regenerating articular cartilage. As this was a safety study there were no controls and the long-term benefits for cartilage repair will need further evaluation in phase 2 and 3 trials.

Regardless, covalent attachment of heparin to fibrinogen presents benefits of growth factor localisation, their sustained released and cell delivery in hydrogels. The methods employed for covalent attachment are however quite laborious and require extensive processing of fibrinogen. For instance, the method employed by Yang et al (287), with covalent attachment of heparin, requires excessive processing of both heparin and fibrinogen in order to activate the heparin and attach it to fibrinogen resulting most likely in significant loss of biological information contained in the heparinised fibrinogen. As a result, the product is unable to polymerise without the addition of substantial amounts of native fibrinogen in order to form a hydrogel. For these reasons, a more efficient process of conjugating heparin to fibrinogen, retaining its ability to polymerise without additional fibrinogen would be useful.

1.6 Study rationale

Regenerative medicine holds promise as an alternative therapeutic strategy for diseased and injured tissue. Piloted clinical trials have been limited by several factors including pro-angiogenic growth factor half-life seen with bolus administration. As a result, high concentrations must be administered to achieve the desired potent effects at the target site. These high concentrations however induce undesirable side effects including hypotension and are a risk for over-vascularisation which is a trigger cancer. Equally, mesenchymal stem cell therapy has shown great promise in clinical trials. The greatest challenge has however been cell survival and proliferation upon transplant. This raised a need for effective delivery strategies, of which hydrogels have been explored with promising results. For this purpose, synthetic hydrogels have shown to be bio-inert, and as a result, natural hydrogels are being investigated as alternatives. Although most of these natural hydrogels are biocompatible and biodegradable, they have poor cell adhesion abilities and can induce a certain degree of immunogenicity. In contrast, fibrin is a natural reservoir for growth factors, cells, and receptors which acts as a temporary ECM during tissue repair due to due to the respective binding sites on the fibrinopeptide chains. It is therefore a suitable candidate matrix for supporting cell migration, proliferation or (and) growth factor delivery and ultimately vascularisation as seen in the natural wound healing process. In this regard, it is a good candidate biomaterial compared to other natural hydrogels. Furthermore, it is the only biomaterial approved by the FDA for use as a haemostat, sealant, and adhesive in surgery. Heparin on the other hand is a negatively charged heparin glycosaminoglycan known to bind and localise several growth factors possessing a heparin biding domain in the ECM. Limited research has been conducted on immobilising heparin to fibrin, as described in the literature above. The methods used have been laborious, and the fibrinogen fabrication process has been found to be damaging, resulting in fibrinogen that cannot polymerise to form a hydrogel (285, 287, 290).

1.7 Aim

This study therefore aimed to employ less laborious and gentler methods (with fewer and less harsh processing steps to fibrinogen) to establish a fibrin hydrogel covalently modified with heparin, that retained the ability to polymerise with thrombin and to assess its regenerative capabilities.

1.8 Hypothesis

It was hypothesised that a polymerisable heparinised fibrin hydrogel would form, and the presence of covalently bound heparin would facilitate sustained delivery of growth factors.

1.9 Objectives

To achieve the aim, four objectives were pursued:

1. Determining the potential of acrylated heparin (hep-acr) as a reagent for covalent heparinisation of fibrinogen such that thrombin-based polymerisation is retained.
2. Assaying the mechanical and structural properties, and biocompatibility of the heparinised fibrin.
3. Assessing the potential for controlled release of angiogenic growth factors *in-vitro* and angiogenic stimulation *in-vivo with the* heparinised fibrin.
4. Evaluating the influence of the heparinised fibrin on mesenchymal stem cell differentiation.

CHAPTER 2: HEPARIN CONJUGATION TO FIBRINOGEN AND CHARACTERISATION

2.1 Introduction

Heparin's polyanionic nature due to its carboxylate groups, *O*- and *N*-sulfates, makes it an ideal candidate for binding a wide range of proteins. This highly negative charge attracts positively charged proteins mainly through lysine and arginine in the HBD, and histidine under more basic pH conditions for electrostatic interactions (252, 253, 291). In the ECM, this interaction enables cell adhesion, regulates smooth muscle proliferation and sequesters growth factors that regulate crucial cellular activities such as angiogenesis (250, 292). Heparin incorporation into biomaterials thus presents with these potential benefits in regenerative medicine. Fibrin is an attractive biomaterial as it is a naturally occurring protein in the ECM that is bioactive, biodegradable and has attained FDA-approval for use. In wound healing, it is also an effective reservoir for storing and releasing growth factors and cytokines that guide the wound healing process (159, 165). Heparin's interaction with these proteins is largely electrostatic, with contributions from hydrophobic interactions, hydrogen bonding, as well as secondary structure interaction of the heparin binding proteins (252, 253).

Early methods used peptides to covalently attach heparin to proteins for heparinised hydrogels, while recent methods directly bind them. As described in the literature review, Sakiyama-Elbert and Hubbell (2000) (284) developed a hydrogel system using a bi-domain peptide for delivering heparinized growth factors with enzymatic biodegradation capability. Conversely, more recent approaches use 1-ethyl-3-(3-dimethylaminopropyl) carbodiimide (EDC)/NHS chemistry (to crosslink proteins by linking carboxylic acids to primary amines **(Figure 2.1**). Further, Wissink et al.,2001 (293) showed that collagen, which is thrombogenic, could be covalently heparinised using EDC chemistry and bound heparin quantified with radiolabelling (^{3}H-heparin). For this, heparin's carboxylic groups were activated using EDC and NHS, and thereafter primary amine functionalised collagen added to the activated heparin solution, allowing the carboxylic groups to first bind to the EDC and the intermediate product swiftly reacting with the amines for an amide

bond that stabilises/ crosslinks the intermediate product (293). A thrombin inhibition assay proved that this heparinised collagen had anti-coagulation activity, confirming heparin binding (293).

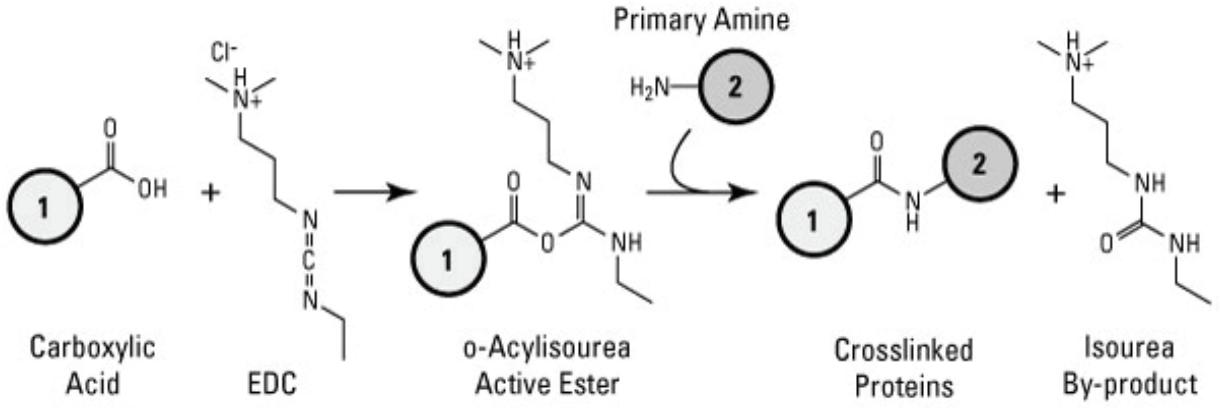

Figure 2.1: **General EDC reaction chemistry mechanism**. (1) Carboxylic acid reacts with the EDC to form an active ester. (2) This active ester is displaced by the more stable primary amine (in proteins) to form a crosslinked protein and a urea by product. Image adapted from Thermofisher, 2022 (294).

Yang and colleagues also explored covalent conjugation of heparin to fibrinogen with EDC chemistry where the carboxylic groups of heparin were activated with EDC, and the product reacted with the primary amino groups of fibrinogen for 3 hours at 4˚C and dialysed to remove access heparin (285, 287, 295). The heparinised fibrinogen was further precipitated with acetone prior to lyophilisation (for storage) for 48 hours. This method was however laborious and did not yield a thrombin clottable heparinised fibrinogen for a hydrogel and required an excess of unmodified fibrinogen to polymerise. Furthermore, due to the fact that most proteins, such as fibrinogen, possess both carboxylates and amines, there is the potential for self- polymerisation with this method (296).

We therefore aimed to conjugate heparin to fibrinogen in a manner that retains thrombin-based polymerisation without the necessity of additional unmodified fibrinogen. For this, we explored the utility of an acrylated form of heparin, acrylated heparin (hep-acr), developed in Professor Bezuidenhout's laboratory. This hep-acr preferentially binds to

thiol groups such as cysteine side chains in proteins via spontaneous thiol-acrylate Michael-type addition reactions (**Figure 2.2.)** that produce no by-products (297) . We also explored modifying fibrinogen with a n-hydroxysuccinimide-PEG- sulfhydryl (NHS-PEG-SH) molecule prior to heparinisation as additional free thiols might be expected to increase heparin binding. The products, fibrinogen-hep (FH) and fibrinogen-peg-hep (FPH), were then characterised to gain insight on their nature and potential applications.

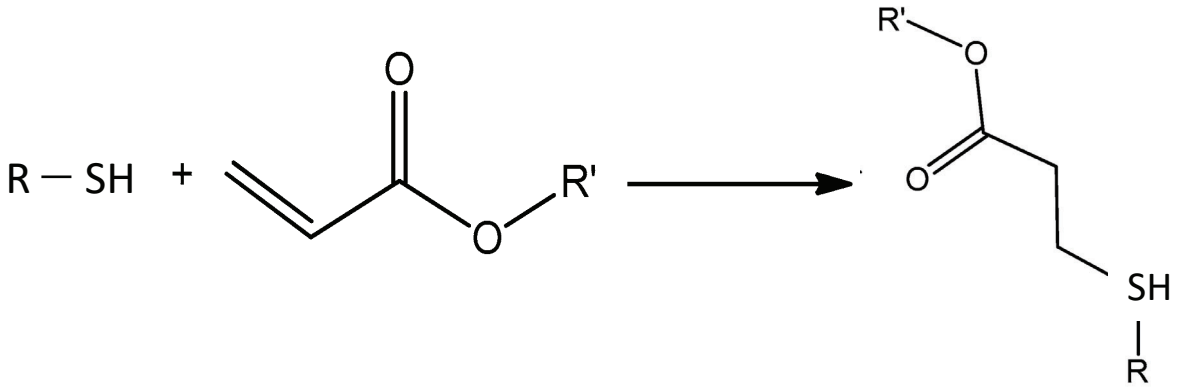

Figure 2.2: **An illustration of a general Michael addition reaction between a thiol and an acrylate** (ester), forming a secondary amine/ amino carbonyl compound, that is an alkene as a product.

2.2 Results and discussion

2.2.1 Method development: Fibrinogen heparinisation

We sought a relatively simple, and efficient method for attaching heparin to fibrinogen which maintained polymerisation into fibrin via thrombin activity without the need of supplementation with unmodified fibrinogen. Two methods were explored that relied on the reaction of hep-acr with free thiols in the fibrinogen polypeptide. In one approach, a one-step method where direct heparinisation of fibrinogen with hep-acr was investigated. In another approach, a two-step method was investigated whereby additional free thiols were introduced into the polypeptide via reaction with bifunctional PEG molecules with a primary amine reactive N-hydroxysuccinimide ester terminus and a thiol end. The PEGylated (fibrinogen-PEG-SH hereafter referred to as FP) version would then be reacted with hep-acr through the thiols. It was hypothesised that PEGylation itself would directly improve fibrin's resistance to proteolysis (**section 1.4.3.5**) thus improving its half-life. For this, four PEG molecules with free end thiols were first compared for their binding efficiency to fibrinogen. These four molecules were n-hydroxysuccinimide-PEG-thiol (NHS-PEG-SH, 3.4 kDa), succinimidyl glutarate-PEG-thiol (SG-PEG-SH, 3.4 kDa), succinimidyl propionate-PEG- thiol (SPA-PEG-SH, 3.5 kDa), and NHS-PEG-SH,10 kDa). They were used for PEGylation reactions which were carried out in PBS at pH 7.8 for 1.5 hours as these are optimal conditions as determined from the literature (231, 233, 298). After 1.5 hours, unbound PEG molecules were removed by dialysis using a 100 kDa molecular weight cut off cellulose ester membrane for 24 hours. Free PEG molecules were found to be efficiently removed over this time period of dialysis (**Figure 2.3C**: dialysis control row) with over 99.8% removed for all PEG molecules. The molar binding ratio used here to compare the different PEG molecules was chosen as 1:10 as this is a widely used binding ratio for PEGylation of fibrinogen that has been found not to impact substantially on its polymerisation. Molar ratios that are too high (e.g. 1:20) often result in fibrinogen oligomerisation which could ultimately comprise its polymerisation. Equally, lower molar ratios may not provide sufficient protease protection (299).

Free thiols of the bound PEG molecules were quantified with an optimised Thiostar® assay (**Figure 2.3A**), a highly linear maleimide based fluorescent assay that generates a

fluorescence signal when the maleimide binds to the free thiols. NHS-PEG-SH (10 kDa) yielded the highest number of bound thiols at 0.8 thiols per fibrinogen molecule, and this was more than double compared to the other PEG molecules (**Figure 2.3B**). The SPA-PEG-SH (3.5 kDa) had 0.3 thiols, SG-PEG-SH (3.4 kDa) 0.2 thiols and NHS-PEG-SH (3.4 kDa) 0.1 thiols per fibrinogen molecule.

A

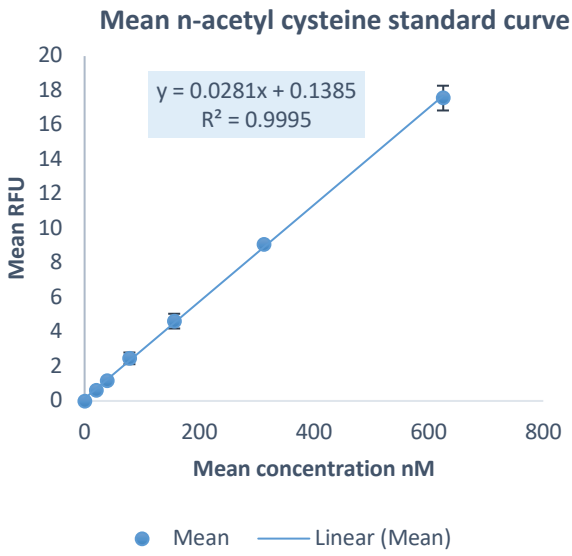

B

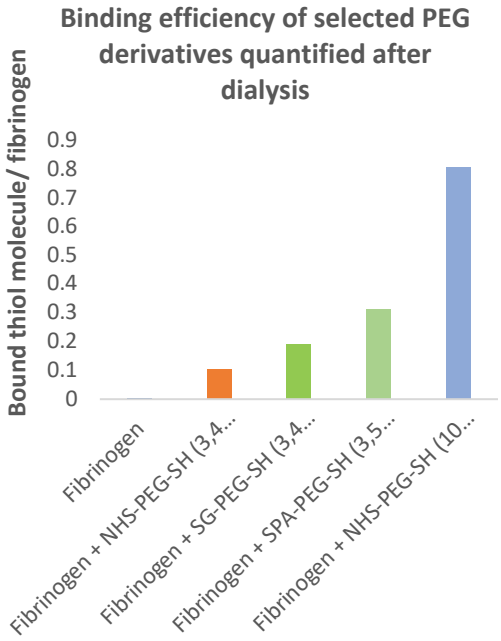

C

	NHS-PEG-SH	SG-PEG-SH	SPA-PEG-SH	NHS-PEG-SH
PEG concentration (μM)	294.1	294.1	285.7	290.9
Post dialysis -SH concentration (μM)	3.1	5.7	9.396	23.8
Dialysis control (nM)	33.4 (0.01 %)	33.4 (0.01 %)	33.5 (0.01 %)	465.0 (0.16 %)
Fibrinogen: -SH-PEG	0.21 per 2 Fibrinogen molecules	0.39 per 2 Fibrinogen molecules	0.64 per 2 Fibrinogen molecules	1.6 per 2 Fibrinogen molecules

Figure 2.3: **Thiol binding optimisation**. (A) Strong linearity of Thiostar® fluorescent detection assay for detection of thiols with n-acetyl cysteine as a standard. Measure in relative fluorescent units (RFU), n = 3 biological repeats. (B) Binding efficiency of the four different PEG molecules, with NHS-PEG-SH (10 kDa) having the highest number of bound thiols, n=1. (C) Dialysis efficiency with 100 kDa dialysis cellulose ester membrane of free PEG molecules (% remaining indicated), n=1.

Because NHS-PEG-SH (10 kDa) yielded the highest number of thiols per fibrinogen molecule, it was chosen for further exploration. Lower ratios of fibrinogen: PEG binding

were then assessed to determine whether the binding was saturated at levels lower than 1:10 but this was found not to be the case (**Figure 2.4**) where substantial drops in thiolation were observed with reduced ratios of PEG to fibrinogen. The PEGylation with NHS-PEG-SH (10 kDa) was reproducible with 0.8 free thiols per fibrinogen, as with the experiment above (**Figure 2.3**). As we wished to retain polymerisation of fibrinogen, higher ratios than 1:10 were not explored. Because unmodified fibrinogen is known to have thiols in its backbone, it was assayed as a control to determine their contribution to the detected thiols. The results showed that fibrinogen had 0.007 free thiols per fibrinogen (± 7 thiols per every 1000 fibrinogens), more than 100-fold lower than NHS-PEG-SH (10 kDa) and therefore negligible. This low level might be expected due to disulfide bridges formed between the cysteine residues (300).

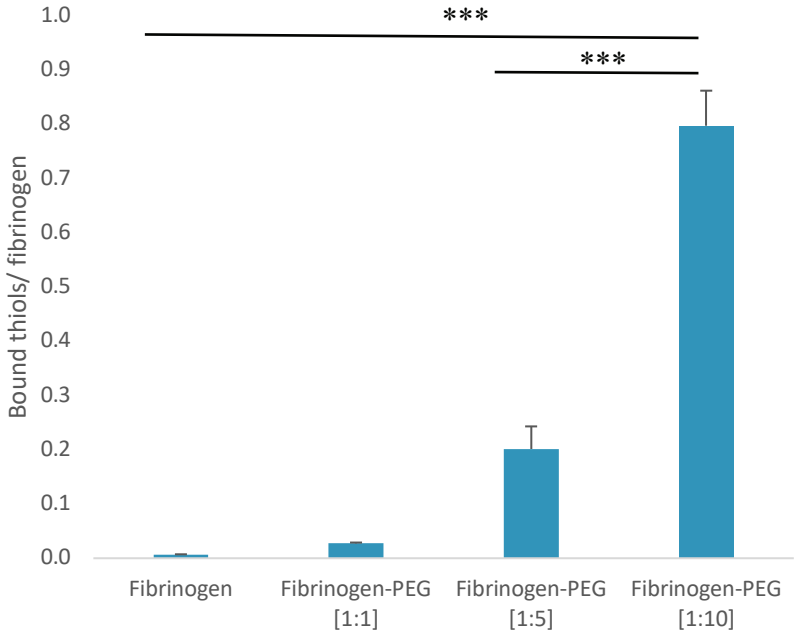

Figure 2.4: **Molar ratio dependant binding of NHS-PEG-SH to fibrinogen.** Highest number of bound thiols was achieved at the highest molar ratio, 1:10, that was higher than at 1:1 and 1:5. Free thiols contributed by fibrinogen alone were significantly very low. ***p<0.001 vs fibrinogen, 1:1 and 1:5, n = 3 technical repeats. Data represented as mean

Both unmodified fibrinogen (hereafter referred to as F) and FP (0.8 thiol per fibrinogen) were then reacted with hep-acr. This hep-acr was produced in Prof Bezuidenhout's laboratory through the Schotten-Baumann reaction using acryloyl chloride, and yielded

40% acrylation of the heparin disaccharide units (45, 297). Acrylates were desired for their reactivity and highly preferential binding to the thiol groups in cysteine side chains via 1,4-addition Michael type additions (301). The concentration of hep-acr in the reaction with fibrinogen and FP was at a 1.3:1 ratio (0.6 mg/ml). Previous work (44, 48, 278, 284, 285) with pure PEG hydrogels found that this concentration resulted in levels of heparin modification that effectively captured and controlled the release of growth factors whilst higher concentrations of heparin resulted in modification levels that caused bleeding in rats after implantation, also supported by unpublished data from our lab). For both heparinisation approaches, the fibrinogen concentration was 10 mg/ml.

As the level of heparinisation could potentially be tracked by assaying the loss of free thiols using the simple Thiostar® fluorescent assay, effective but convenient incubation times were determined with FP. The assumption was made that a decreasing thiol signal would indicate covalent binding to heparin. As indicated in **Figure 2.5**, a decrease in the amount of free thiol was observed with time, with the hours' time point (time points beyond this were not favourable for fibrinogen as a protein) at 37°C showing the highest decrease in thiol signal (51%, equivalent to a reduction in 0.4 thiol per FP molecule). This was assumed to be indicative of 0.4 heparin molecules per fibrinogen molecule. This equated to approximately 0.2 mg heparin per ml in a 10 mg/ml fibrin hydrogel. As indicated above, PEG hydrogels at 0.6 mg/ml heparin previously achieved effective controlled release of growth factors (49, 283). It is important to note that heparin concentration in said PEG hydrogels was likely lower as efficiency of heparin binding was not determined in these previous studies. The 6 hours' time point was thus used for all experiments in this study as it achieved a desirable level of heparinisation modification to be carried out in a day.

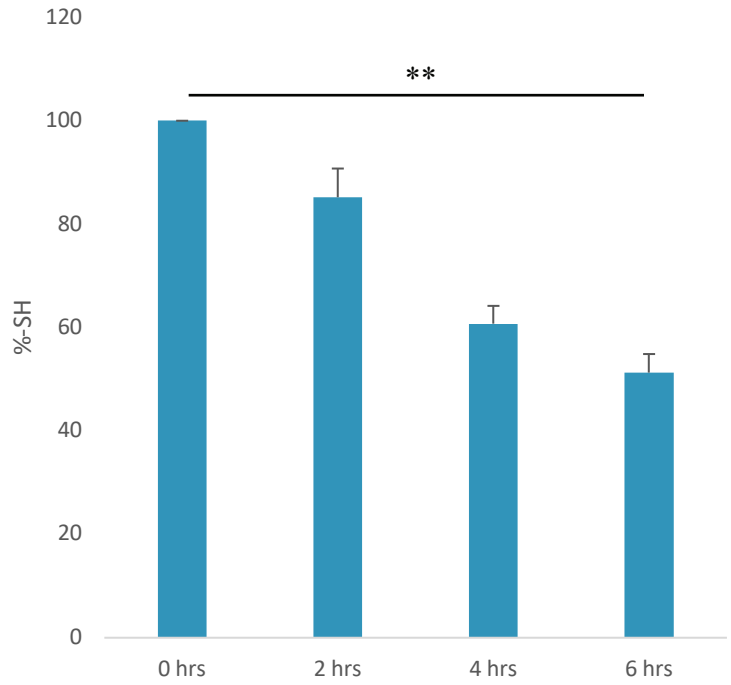

Figure 2.5: Optimisation time for heparin coupling to free -SH on PEGylated (10 KDa) fibrinogen. The 6 hours' time point showed to be a reasonable time as it yielded the highest -SH reduction effect. ** $p<0.01$ vs 0 hours, n = 3 biological repeats.

Fibrinogen or FP (10 mg/ml) were incubated for 6 hours at 37°C with hep-acr at 0.6 mg/ml. Then a variety of approaches were investigated for removal of unreacted heparin, monitored with the 3-Methyl-2-benzothiazolinone-hydrazonehydrochloride (MBTH) assay. In all instances, separation methods were assessed by loading the equivalent to that in the heparinisation reaction of the relevant molecule alone. Size exclusion chromatography (SEC) with Sephadex-G100 medium was the first technique explored for removing excess heparin as this is a more rapid method than dialysis which was used above to remove unreacted PEG during formation of FP. However, it was not possible to separate heparin and fibrinogen as they both eluted at similar points (**Figure 2.6**). Additionally, there was substantial dilution of the loaded fibrinogen possibly reflecting separation of the alpha, beta, and gamma chains during passage through the column of SEC.

A

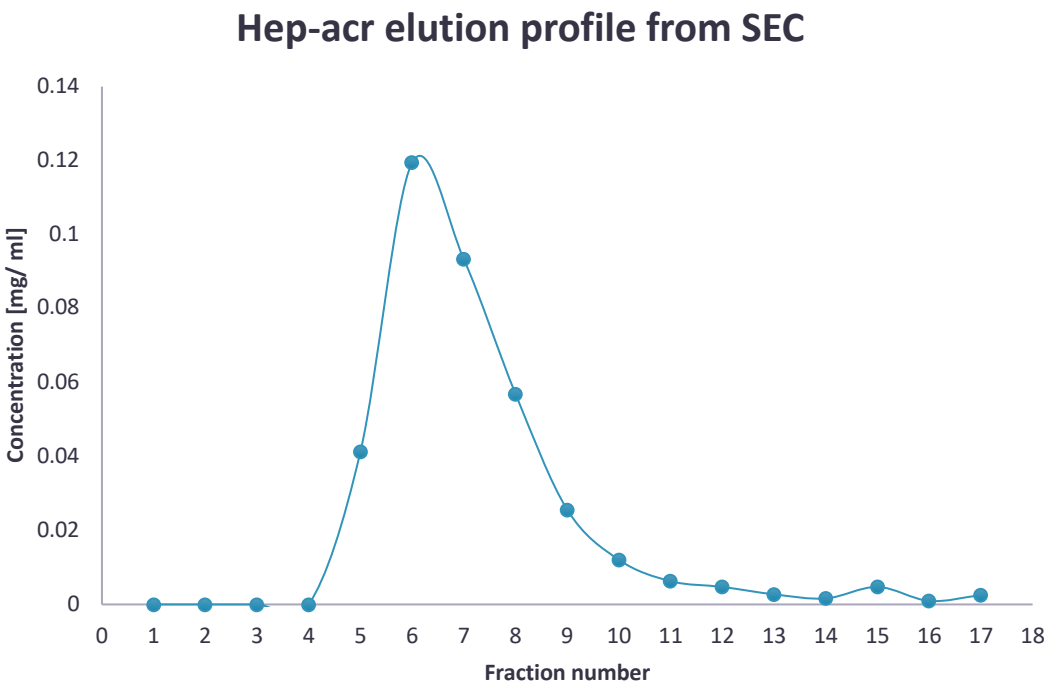

B

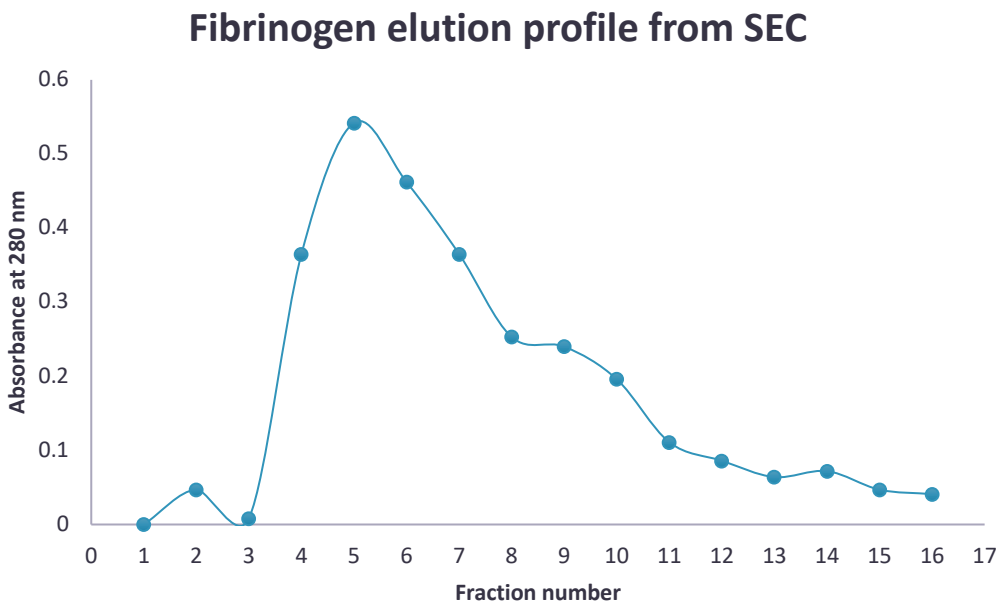

Figure 2.6. **Size exclusion elution profiles for heparin and fibrinogen**. (A) Elution profile of heparin peaking at fraction 6 as determined with an MBTH assay. (B) Fibrinogen elution profile showing substantial eluant from fraction 4-13, with absorbance measured with a nano-drop at 280 nm.

Dialysis was the next technique investigated to remove unbound hep-acr and unmodified/ non-acrylated heparin (non-acr hep) as a control. The latter was included as it's binding to fibrinogen was also assayed. Dialysis using the 100 kDa molecular weight cut-off (MWCO) dialysis membrane (used for removal of PEG above) showed a high % of hep-acr remaining (45.6 ± 11.8%) and non-acr-hep (48.5 ± 1.2%) as indicated in **Table 2.1**. This was after 24 hours dialysis against a 1000x excess volume with four changes of dialysis buffer (PBS). In principle, dialysis is affected by buffer volume (and composition), the number of buffer changes, time of dialysis, temperature and dialyses particle size vs. pore size. Through extensive troubleshooting whereby number of buffer changes were increased, the volume of the buffer solution was increased, and the dialysis process extended for up to 48 hours, no meaningful change in % heparin remaining in the dialysate with the 100 kDa MWCO membrane was achieved. As a large molecule (MW 15.5 - 18 kDa), heparin proved challenging to dialyse with a 100 kDa MWCO (302). In principle, MWCO should be at least 10x greater than the protein to be reserved for effective dialysis though the 10 kDa PEG (as described above) was very effectively removed indicating that dialysis inefficiency might be due to shape and/or the highly negative charge of heparin (302).

A membrane with a larger MWCO (300 kDa) was then assessed. At 24 hours, dialysis with this 300 kDa MWCO membrane removed 94.5% of hep-acr (**Table 2.1**). When the time was increased to 36 hours, significantly improved results were obtained, removing 99. % for both hep-acr and non-acr-hep respectively. Therefore, dialysis with a 300 kDa MWCO for 36 hours at room temperature with the buffer at pH 7.4 was effective and used for all preparations in this study. Dialysis was against PBS (>1000x dialysate volume) and the buffer was changed three times every 12 hours and once one hour before the end of the dialysis cycle. Fibrinogen loss with the 300 kDa MWCO membrane was also checked by spectroscopy at 280 nm and no significant loss was observed. The MBTH assay also indicated good accuracy when an undialysed hep-acr control sample was detected with 98.3 ± 2.5% accuracy.

Table 2.1: Summary results for heparin dialysis optimisation, n=3 biological repeats

	%hep-acr reserved	% Heparin reserved
Dialysed 0.6 mg/ml hep-acr or heparin (100 kDa MWCO for 24 hours)	45.6 ± 11.8	48.5 ± 1.2
Dialysed 0.6 mg/ml hep-acr or heparin (300 kDa MWCO for 24 hours)	5.5 ± 0.3	5.3 ± 0.2
Dialysed 0.6 mg/ml hep-acr or heparin (300 kDa MWCO for 36 hours)	0.7 ± 0.8	0.9 ± 0.3

2.2.2 Fibrinogen bound heparin quantification

Once unbound hep-acr could be efficiently removed with dialysis, bound hep-acr was then quantified. There are limited assays for suitable quantification of bound heparin and at low concentration. We modified the MBTH assay, used above, to detect heparin bound to fibrinogen as it had been, originally developed for free heparin (**section 2.2.1**). When using the unmodified assay, substantial precipitation was observed where fibrinogen formed yellowish foam with threads upon addition of nitrous acid. Upon the MBTH reagent addition, dark purple/ black precipitates developed (**Figure 2.7**) and these interfered with absorbance readings when assayed in the spectrophotometer. Several procedures were then assessed to try overcoming this issue. These included sonicating the precipitated solution to dissolve the precipitants, as well as centrifuging the solution to pellet the precipitates. These were without success. It was hypothesised that the amino acids of fibrinogen (constituting the large protein chains) were undergoing nitration when the acid was added and perhaps forming the precipitate when the peptides clumped together. Often, aromatic amino acids react with nitric acid in xanthoproteic reactions to form xanthoproteic acid which is yellow/ orange in colour (also observed in our reactions) (303). Fibrinogen has aromatic amino acids such as tyrosine present in its backbone, and this justified our hypothesis (304). Discovering this piece of information then led to brainstorming strategies that could possibly assist in overcoming this issue. Enzymatic removal on the fibrinogen polypeptide was then investigated as it seemed likely that the

large protein chains might contribute to the precipitation. Proteinase K was chosen as a proteolytic agent as it is a potent and non-specific protease. Following dialysis, samples were incubated for 12 hours with proteinase K. After the 12 hours, the proteinase K was inactivated by increasing heat to 95˚C and the samples cooled down before assaying in the MBTH assay. Proteinase K successfully degraded the fibrinogen protein to overcome precipitation when nitrous acid solution and the MBTH reagents were added. In this, it was able to degrade the heparinised fibrinogen such that when nitrous acid was added, a strong foam did not form, and the dark (black/ purple) threads did not form upon MBTH reagent addition.

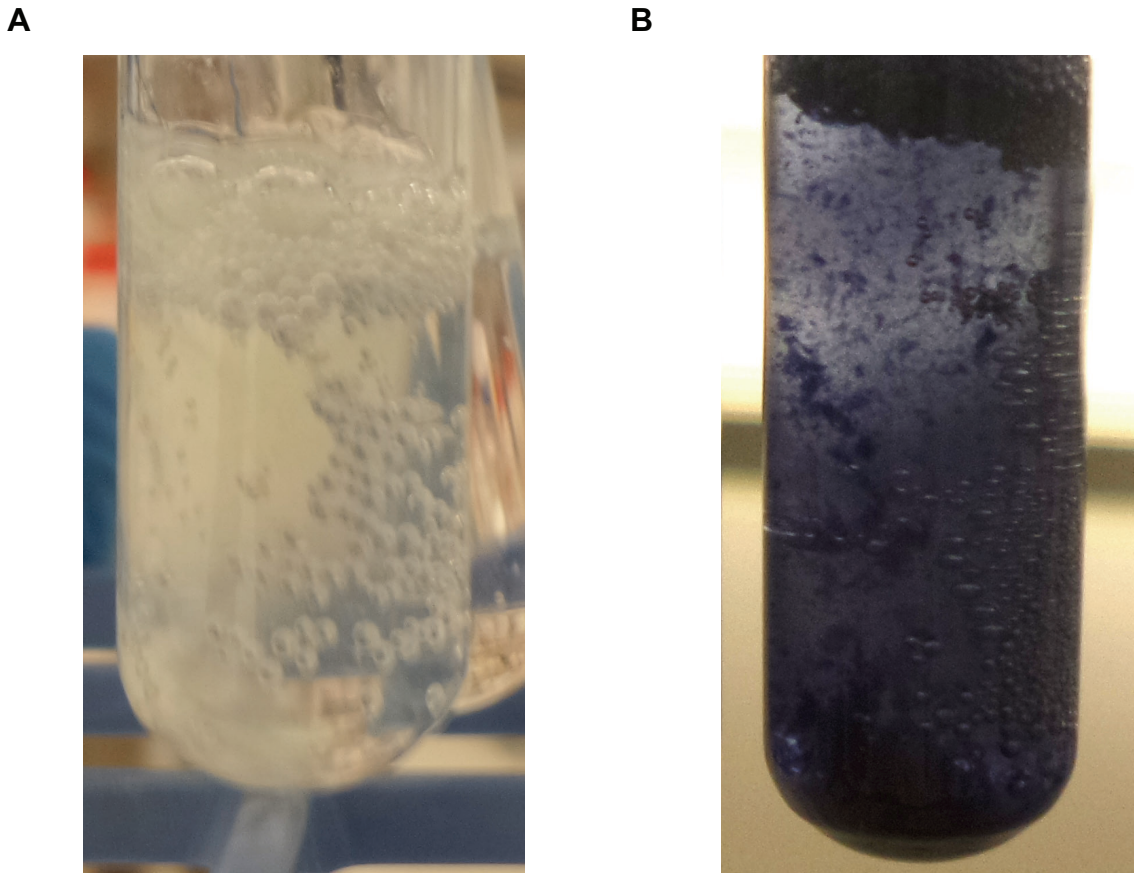

Figure 2.7: Optimisation for bound heparin quantification with MBTH. (A) Fibrinogen precipitated with the addition of nitrous acid solution forming bubbles, and a yellow colour. (B) Dark precipitates visible with the addition of the MBTH solution.

After digesting the samples with proteinase K, they were assayed with the MBTH assay, and bound heparin calculated. One heparin molecule was found to be bound every third

fibrinogen for both fibrinogen and FP. This was 9-fold higher compared to when non-acr hep was used as a control (**Figure 2.8**). This non-acr was found to not be able to bind effectively to fibrinogen validating that most of the binding was through the acrylates. Normal (non-acr-hep) heparin has been reported before to bind to fibrinogen perhaps through the HBD forming electrostatic interactions (165). This binding was however observed to be much lower (9-fold lower) in the present study (**Figure 2.8**).

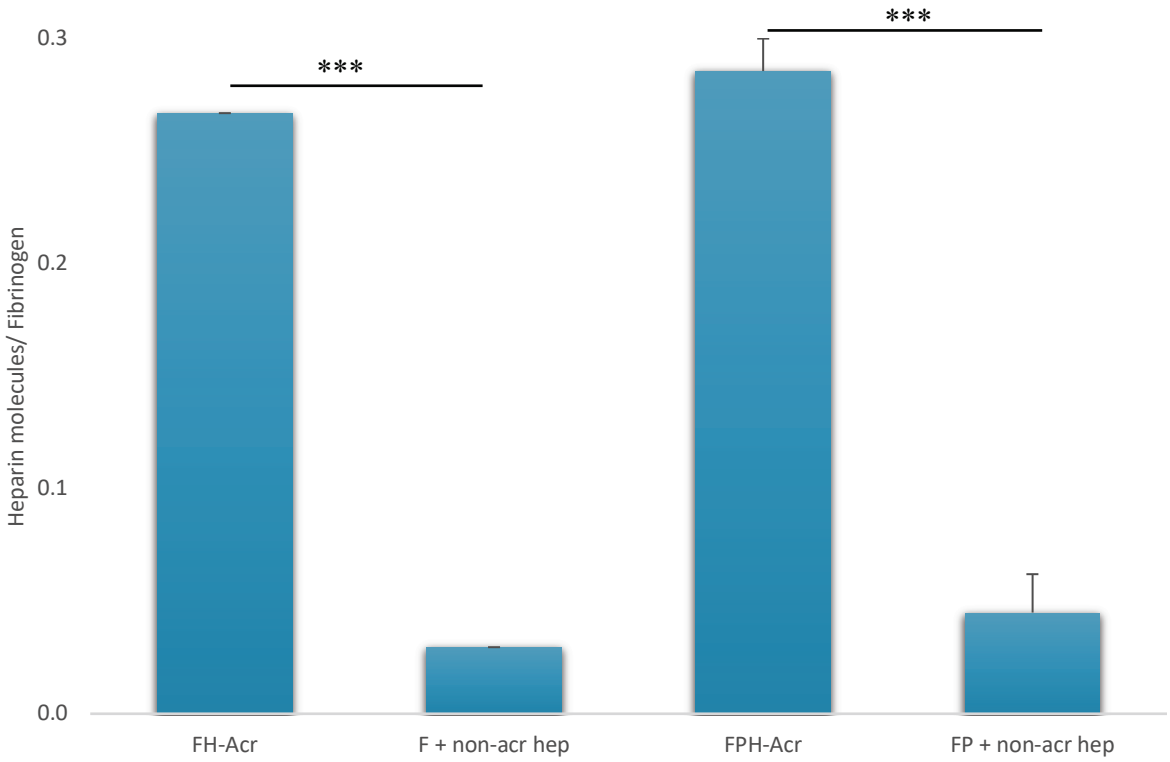

Figure 2.8: **Bound hep-acr quantification with MBTH.** More heparin was bound using hep-acr compared to non-acrylate heparin, Hep-acr binding to fibrinogen to form the FH was 9-fold higher than non-acrylate heparin. ***p<0.001, n = 3 biological repeats (three separate experiments, on three different days)

Although the MBTH was useful as a first line quantification assay, it was a laborious assay, requiring several processing steps and a large sample volume. A more sensitive and direct fluorescent assay, Heparin Red® assay was used as a second line screen. This assay was imported from Germany with great difficulty thus limiting its availability for use (limited number of reactions could be conducted). It was however convenient as it could directly measure heparin without additional processing steps. Quantification with this assay revealed that one heparin molecule was bound every second fibrinogen for

both method one and two. This amount was significantly higher ($p<0.001$) than the amounts detected with the MBTH. It was hypothesised that this was due to the fact that Heparin Red® allows for direct detection, with specificity only for heparin (proteoglycan) while the main detection component of the MBTH assay (MBTH) can bind other substances, other than heparin, such as phenol oxidases, carbohydrates, and proteins. Similar to the MBTH, the bound hep-acr amount was also found to be 9-fold higher when compared to when bound non-acr heparin was used as a control (**Figure 2.9**), validating that binding was through the acrylates (165).

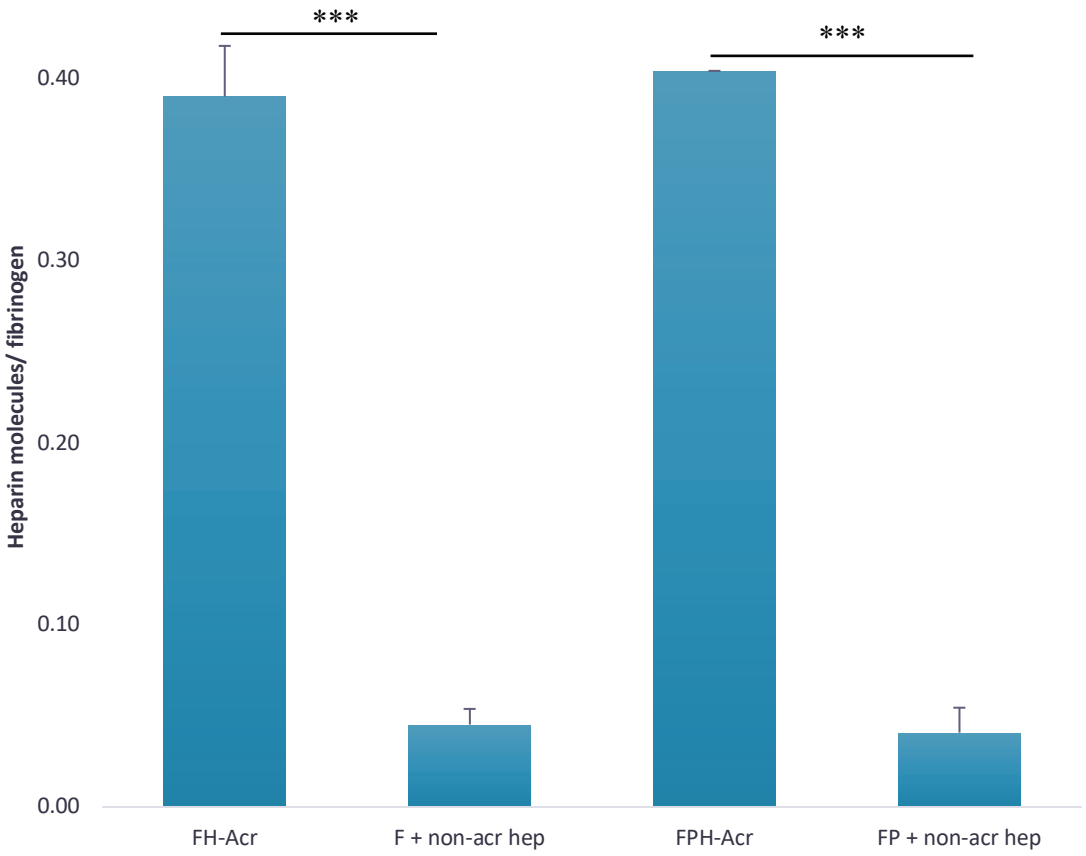

Figure 2.9: **Bound hep-acr quantification with heparin red assay**. More heparin was bound using hep-acr compared to non-acrylate heparin. Hep-acr binding to fibrinogen through NHS-PEG-SH was 9-fold higher than non-acrylate heparin. ***$p<0.001$, n = 3 biological repeats.

Both the MBTH and the Heparin Red® assay were consistent in revealing that both method one and two yielded similar amounts of bound hep-acr, approximately 30% bound

relative to the starting amount It was also expected that not all the hep-acr would bind to fibrinogen as the initial hep-acr of the disaccharide units were only 40% acrylated, suggesting a relatively good yield for the fibrinogen heparisation reaction (297, 305). Additionally, the amount bound to fibrin is similar to that calculated to be bound to PEG hydrogels as reported by our lab (45, 49, 283, 297, 306). This amount was sufficient to bind and sustain the release of bFGF and VEGF for more than 20 days, and further significantly induce vascularisation (relative to the hydrogel only control) over four weeks. It was interesting that both the one step and the two step methods bound a similar amount of heparin to fibrinogen despite the increased number of free thiols present on FP. It was challenging to discern why both fibrinogen and FP yielded similar amounts with hep-acr. The Michael addition reaction of acrylate with thiols is highly selective relative to amines (the other possible reactant present in proteins) and PEG-acrylates have been found to react very slowly with proteins (307). Thus, the addition of almost one free thiol per fibrinogen molecule (a 100X increase in free thiols) would be expected to substantially enhance binding of hep-acr. Furthermore, the number of free thiols that were lost after reaction with hep-acr are almost similar to the number of heparin molecules bound. Therefore, possibly fibrinogen reacted with hep-acr through amine groups in a much slower reaction and FP via the added free thiols. However, it is difficult to discern why this scenario would still not have resulted in FPH not achieving approximately double the level of heparin modification rather than the non-significant increases observed here. Though the specific reaction mechanism for successful covalent modification of fibrinogen with heparin, (both FH and FPH), could not be discerned, all hydrogels successfully polymerised without the need of additional fibrinogen as required in previous studies (285). All hydrogels polymerised with 1 unit/ ml without delaying gelation, while the FPH needed 4 units/ml fibrinogen thus suggesting a possible modification in structure that influenced thrombin action and the polymerisation process. Regardless, hydrogels formed successfuly from both FH and FPH, and were thus characterised in the next chapters for features such as thrombotic actvity, biodegradation, cytocompatibility and biocompatibility.

2.2.3 Characterisation

2.2.3.1 Fourier Transform Infrared Spectroscopy

Once fibrinogen was PEGylated, Fourier transform infrared spectroscopy (FTIR) was conducted on lyophilised samples. This was to confirm fibrinogen PEGylation, usually indicated by the insertion of the C-O bond into fibrinogen and further profile FH and FPH to possibly gain insight into the unclear hep-acr binding mechanisms to fibrinogen. The resultant spectra (**Figure 2.10A**) indicated that fibrinogen was successfully PEGylated using the SH-PEG-NHS molecule. This was first confirmed by the absence of the characteristic succinimidyl ester triplet band (specific for PEG-NHS) in the FP and FPH but present in the SH-PEG-NHS stock as three peaks at 1739 cm^{-1}, 1782 cm^{-1} and 1813 cm^{-1} (marked with arrows in **Figure 2.10A**) in the FP and FPH. This indicated a successful reaction of the primary amino groups in native fibrinogen with the NHS group resulting in the opening of the amide ring. Additionally, the insertion of the C-O bond in the FP and FPH was indicated by the peak between 1100 - 1103 cm^{-1} (marked with an arrow in **Figure 2.10A**) and these peaks are reported to be concentration dependant. Previous studies (Shpichka, 2017 & Shpichka, 2020) have suggested that the increased amide (one and two) peaks at 1650 and 1530 cm^{-1} in **Figure 2.10A** are indicative of NHS-PEG binding which amplifies the amides already present in native fibrinogen (299, 308). However, these peaks are reported to generally reflect protein conformational changes and unfolding thus exposing amides (308, 309). For such a reason, it is possible that the addition of PEG triggers fibrinogen conformational changes (308, 309). Confirming the exact bonds by which hep-acr was bound to F and FP proved to be challenging due to the overlap of spectra. However, comparing the F, FH, FPH and hep-acr spectra, a unique peak around 1600 cm^{-1}(**Figure 2.10.1B**) that is much reduced in fibrinogen alone was observed. This peak (indicated with an arrow in **Figure 2.10B**) completely disappeared for FH and was reduced for FPH, suggesting a disappearance of the available acrylates with insertion of hep-acr to fibrinogen and FP. The acrylate peak around 1600 cm^{-1} (**Figure 2.10B**) has been suggested as a characteristic C=O in acrylates (310, 311).This however requires further investigation with techniques such as nuclear magnetic resonance (NMR), which could not be conducted in this study due to limited samples.

A

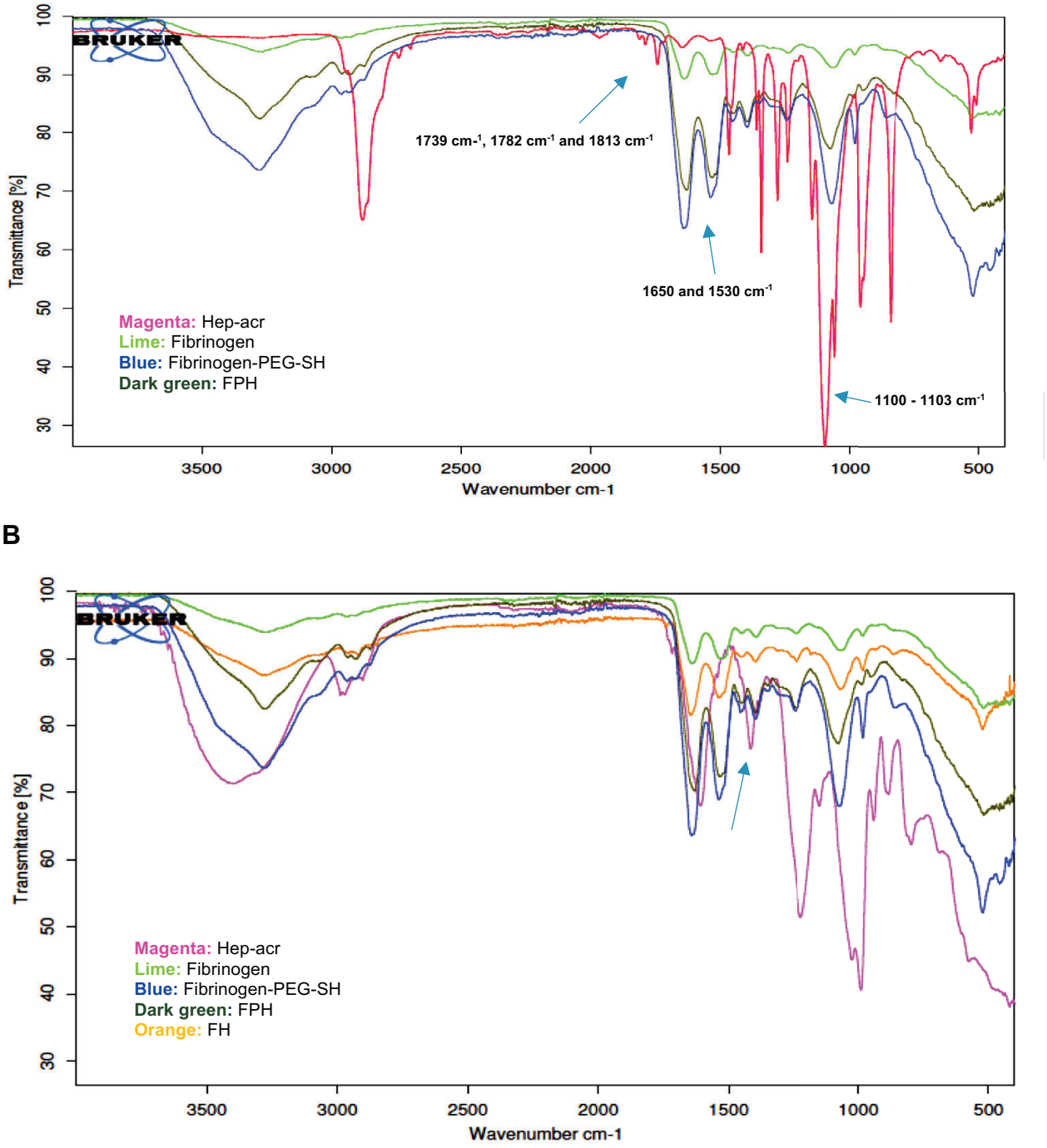

Figure 2.10: FTIR spectra for fibrinogen and modified fibrinogen. (A) PEGylation was confirmed by the absence of the three peaks at 1739 cm^{-1}, 1782 cm^{-1} and 1813 cm^{-1} in FP (blue) and FPH (dark green), which are present in the SH-PEG-NHS stock (pink); insertion of the C-O bond was indicated by the peaks at about 1100 - 1103 cm-1 (FP and FPH, blue and dark green) and heightened amide peaks at 1650 and 1530 cm^{-1} (blue and dark green). (B) The unique peak around 1600 cm-1 for FH (orange) and FPH (dark green) suggested hep-acr binding to fibrinogen.

2.2.3.2 Thromboelastography

The heparinised fibrin, FH and FPH, were then evaluated for their clotting kinetics that are indicative of potential thrombotic effects. For this, thromboelastography was conducted with a TEG® haemostasis analyser using the researcher's own blood. The FP, FH and FPH unpolymerised samples were placed in oscillating cups pre-warmed to 37°C, and thereafter citrated whole blood with kaolin and 0.2 M $CaCl_2$ added. These were then assayed for 120 minutes in the thromboelastogram (TEG) that looked for the fibrinogen's ability to clot using thrombin present in the blood. Unmodified bovine fibrinogen and whole blood were assayed as control samples. Unmodified fibrinogen, whole blood control and FP clotted swiftly within 1.4 ± 0.1 min, 1.5 ± 0 min, and 1.3 ± 0.1 min (**Table 2.2 and Figure 2.11**) respectively forming stable clots with strengths at 55.6 ± 0.3 mm, 58.8 ± 0.59 mm, and 58.1 ± 1.0 mm respectively. No significant differences were observed in both clotting times and strength. In contrast, FH and FPH samples did not clot at all and this was indicated by no values for average kinetic time and clot strength for the duration of the experiment (2 hours) (**Table 2.2**). The significantly delayed average kinetic times for FPH and FH ($p<0.001$ vs fibrinogen and FP), taken together with no clots formed for the duration of the experiments as well as the much lower angles (representative of the rate at which the clot forms) revealed the anti-thrombotic property of FH and FPH. It further confirmed that the method employed to attach heparin to fibrinogen was successful, with the quantity attached sufficient for safe anti-thrombotic hydrogels.

Interestingly, FP was observed to have a significantly ($p<0.001$) higher angle (72.9 ± 1.0°) compared to unmodified fibrinogen (49.0 ± 10°) (**Figure 2.11**), indicating delayed fibrinolysis and suggesting that the clot formed by FP lasted longer than that formed from unmodified fibrinogen. No studies have conducted research with the TEG assay on modified and unmodified fibrin as this is an assay that's used mostly in the clinical setting and minimally for research purposes.

Table 2.2: Clotting kinetics for fibrinogen and modified fibrinogen measured with a thromboelastogram, n= 3 biological repeats

	Whole blood fibrinogen	Bovine fibrinogen	Fibrinogen - PEG	Fibrinogen-PEG-heparin-acr	Fibrinogen-Heparin-acr
Clotting time/ R (min)	6.6 ± 0.1	5,1 ± 0,1	5.0 ± 0,1	117.0 ± 1	116.0 ± 1
Kinetic time / K (min)	1.4 ± 0,1	1.5 ± 0	1.3 ± 0.1	-	-
Angle/ α (°)	58.5 ± 1,6	49.0 ± 1	72.9 ± 1,0	0.2 ± 0	0.2 ± 0
Clot strength/ maximal amplitude/ MA (mm)	55.6 ± 0,3	58.8 ± 0,59	58.1 ± 1,0	-	-

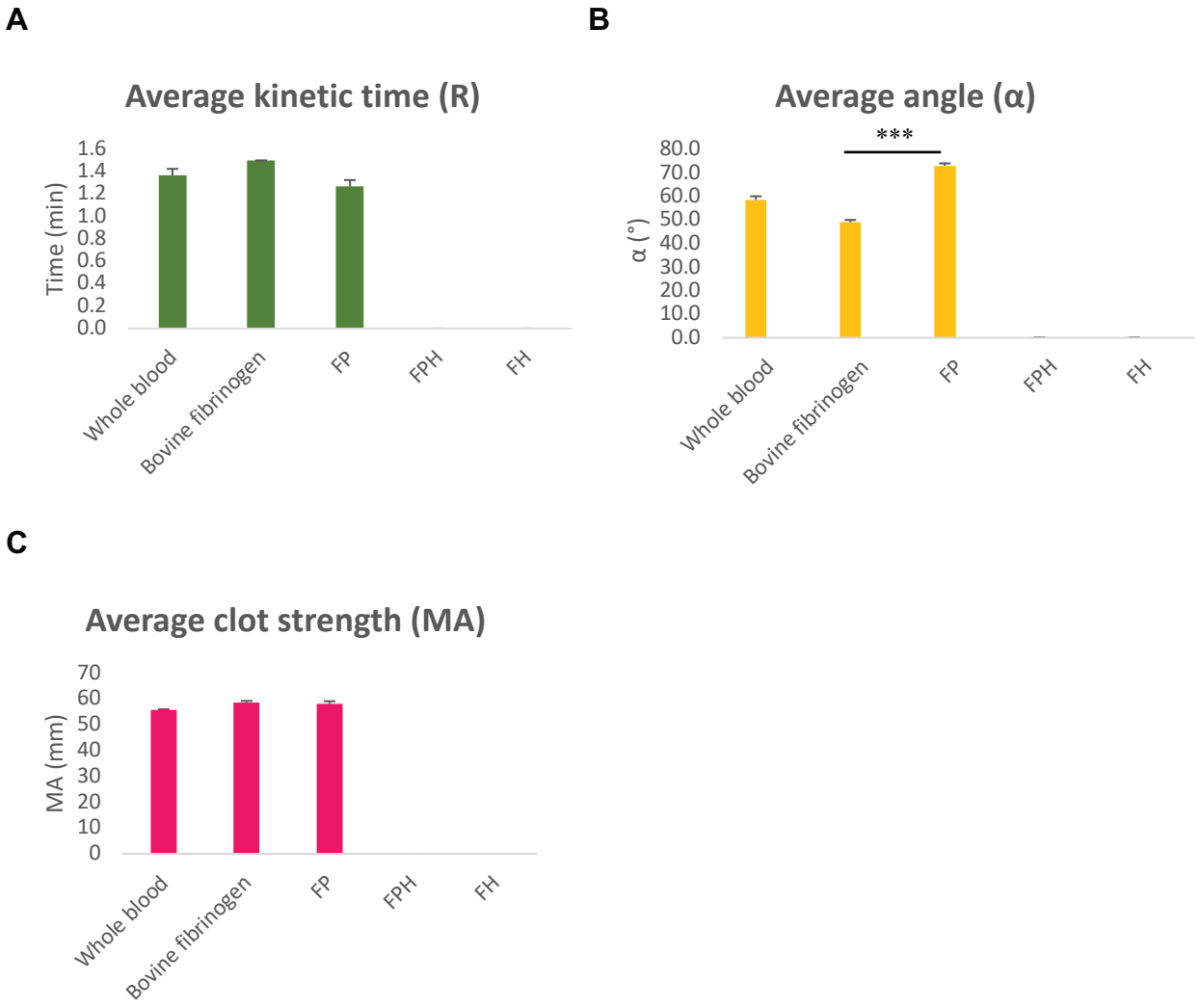

Figure 2.11: Parameters for clotting kinetics of the different hydrogel precursors measured with a thromoelastogram.(A) Delayed average kinetic time observed for heparinised fibrin compared to non-heparinised fibrin.(B) Heparinised fibrin groups with no clot formation angle (indicative of the absence of a clot) whille the non-heparinised groups had. FP had a significantly higer clot angle.(C) No significant differences in clot strength were observed among the non-heparinised fibrin, and heparinised groups did not form a clot indicating anti-thrombotic activity. ***p<0.001, n=3 biological repeats, .

2.2.3.3 *In-vitro* hydrogel degradation

In-vitro degradation rates of fibrin and modified fibrin hydrogels were investigated to determine whether PEGylation could shield fibrinogen from proteolytic degradation to provide more stable hydrogels for longer periods of function *in-vivo*. For the assay, hydrogels were set and incubated in PBS with a neutral pH at 37°C. Buffer eluates were then collected every day for 15 days and thereafter the degradation by-products assayed in the Bradford protein assay. The results (**Figure 2.12**) revealed that by day four, unmodified fibrin had rapidly degraded (91.8 ± 2.8%) with complete degradation (100 ± 3.6%) at day five, while FP degradation was delayed with complete degradation at day nine (100 ± 3.4%). In contrast, FH had delayed degradation leading up to day four whereby 82.8 ± 28% of the hydrogel had degraded and this was significantly different ($p<0.05$) to F at day four. On day five however, 100 ± 6.5% had degraded, and this was not significantly different to fibrin at day five. For FPH, by day 15, only 57.5 ± 6.2% of the hydrogel had degraded, suggesting that covalently bound heparin in the presence of bound PEG had a greater effect on slowing unmodified fibrin's degradation rate. When the FH and FPH degradation eluates were successfully assayed for cumulative heparin release in the MBTH, heparin presence was confirmed but proved challenging to quantify accurately (data shown in **appendix A**).

The presence of aprotinin delayed degradation and all hydrogels were still present by day 15 (**Figure 2.12**). This strongly suggested that the rate of degradation was slowed through PEGylation, and heparin inhibition of proteases present in the commercial fibrinogen. The ability of PEG molecules to slow fibrin degradation has been reported previously using PEG crosslinkers (230, 236). It was an interesting finding that in this present study, a similar effect was achieved using a PEG molecule that is not a crosslinker, suggesting a similar protein shielding mechanism as in PEGylation with a crosslinker. Protein PEGylation is a well-established mechanism for shielding proteins from proteinases (**section 1.5.6**). It achieves this by reducing the overall protein charge through surface amine groups modification and/ or by increasing the protein's molecular size and weight, which in turn decreases its accessibility to proteases (steric hindrance) (312, 313). These findings have implications in growth factor delivery, where longer and more sustained

release is desired, while limiting burst releases. They further support the use of fibrin as a natural biomaterial due to the potential for controlling its degradation rate.

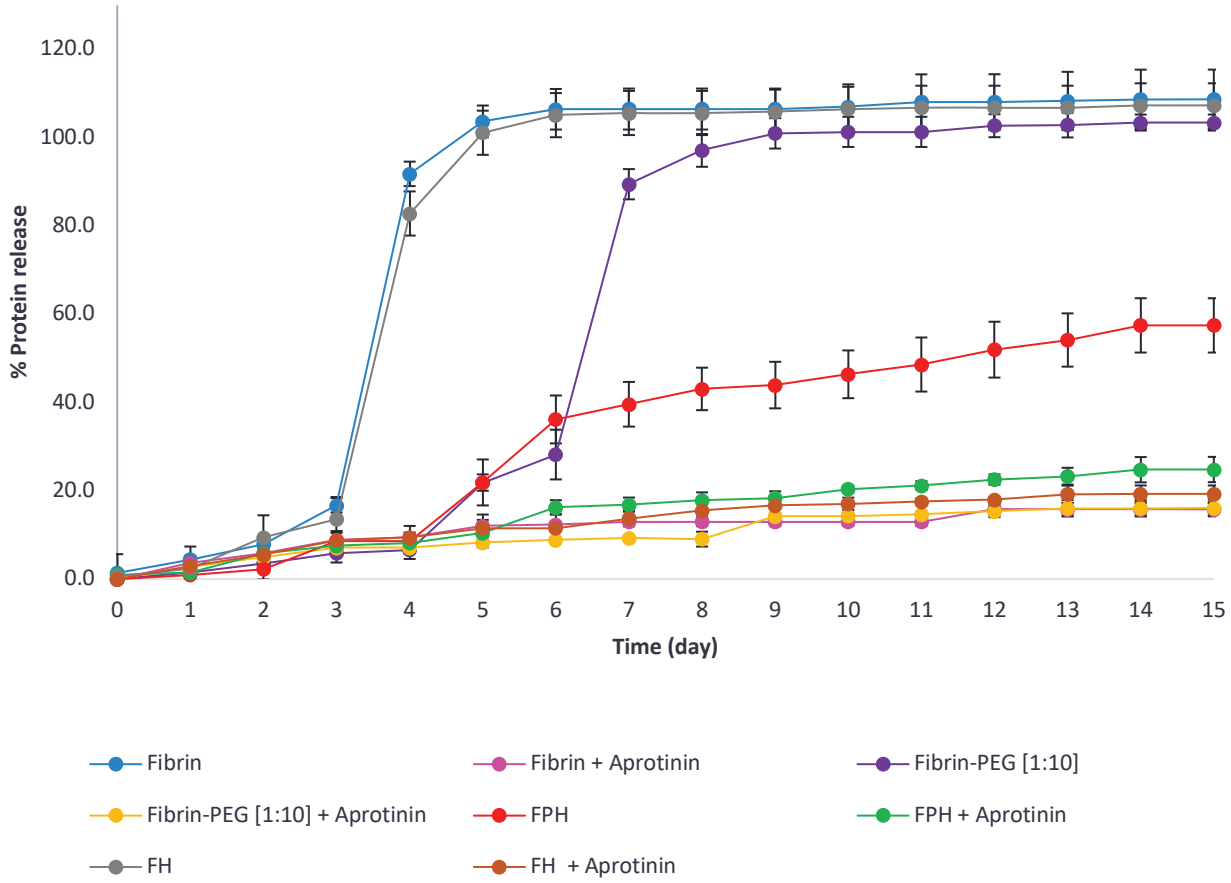

Figure 2.12: Unmodified and modified fibrin hydrogel *in-vitro* degradation measured with Bradford protein assay for samples collected over 15 days. Compared to unmodified fibrin, hydrogels with PEG and hep-acr lasted longer and aprotinin delayed degradation in all hydrogels. n= 3 technical repeats.

2.2.3.4 Turbidity analysis

To assess the turbidity of the different hydrogel, a transmission spectrum was measured using a spectrophotometer**.** In principle, samples that allow visible light to pass through it have high transmission, and absorb less light, as transmission is inversely proportional to absorbance. For the measurements, 100 µl hydrogels were set in clear 96 well

microplates and thereafter assayed in a spectrophotometer. The resultant spectra confirmed unmodified fibrin's turbid nature and revealed that FPH and FP were more transparent, while FH was more turbid (**Figure 2.13**). That is, unmodified fibrin and FH absorbed more light compared to FPH and FP. This was indicated by fibrin's increasing light absorbance for the duration of the spectra, from visible light's percentage transmission of 8.2 ± 0.8% at 380 nm that increased gradually (only 66.8 ± 0.9% at 780 nm) to peak to 73.8 ± 0.8% at 900 nm. In contrast, FPH and FP hydrogels had a sharp increase in visible light transparency between 300 nm - 380 nm. By 380 nm, visible light transmission was > 80% for both FP (80.6 ± 2.7 %) and FPH (82.4 ± 1.8%) and remained around this transmission percentage till about the end of the spectra, peaking between at 780 nm – 900 nm at > 90.2 ± 0.9% for FP and 90.1 ± 0.7% for FPH. This indicated that these hydrogels were generally far more transparent than fibrin and FH, with the transmission peaks around 780 nm - 900 nm corresponding to that of water. This transparent characteristic of FP and FPH has been reported in literature and is postulated to be due to the protein self-associating through hydrophobic interaction (299, 308). It is advantageous for studying cell behaviour in 3D tissue culture compared to turbid fibrin hydrogels where it is challenging to visualise embedded cells at higher concentrations (236). Interestingly, the turbidity characteristic of FH was closer to unmodified fibrin compared to FP and FPH, perhaps suggestive of some degree of self-association through hydrophobic interactions. Light transmission percentage was at 37.7 ± 32.5% at 380 nm, steeper than fibrin and 66.5% ± 15.5% at 780 nm similar to fibrin. This demonstrated that transmission was similar to fibrin (higher absorbance, and at lower wavelengths), with fibrin showing an earlier effect compared to FH.

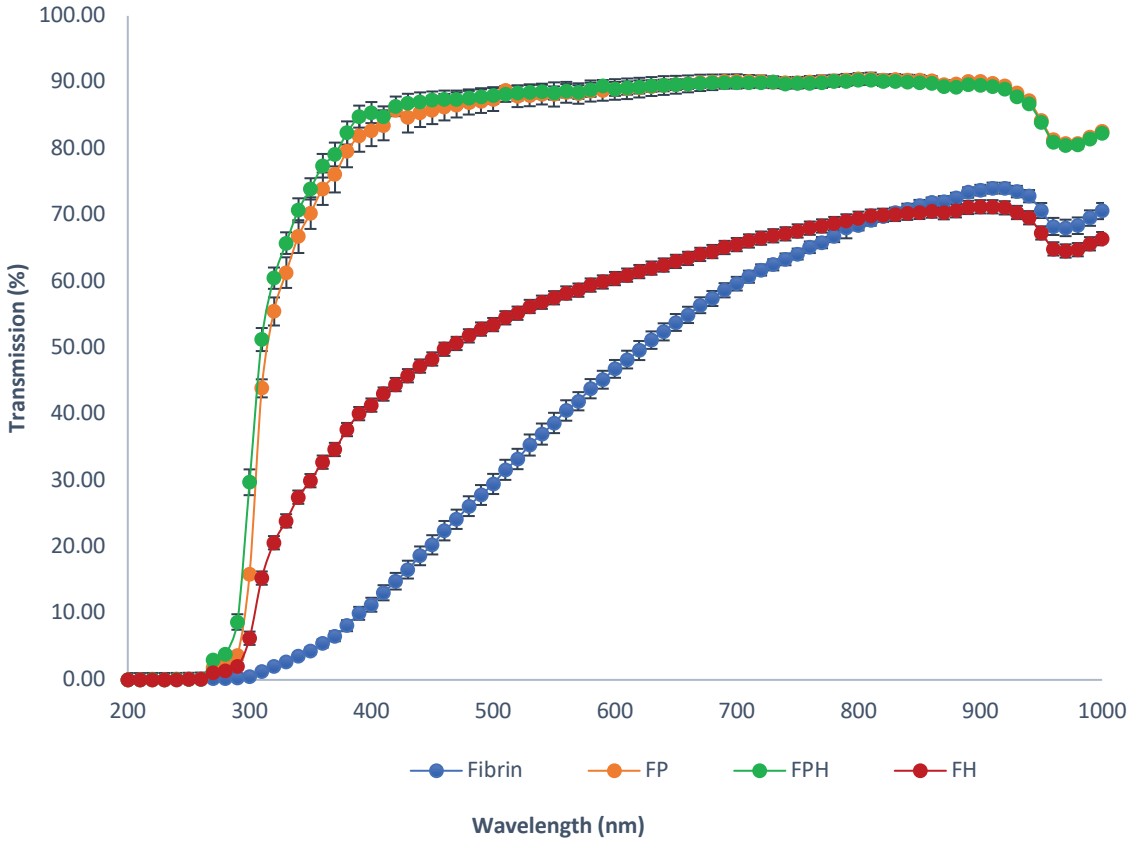

Figure 2.13: Optical properties of native and modified fibrin hydrogels. Compared to unmodified fibrin, PEGylated hydrogels transmissed more light from around 300 nm upwards compared to fibrin and FH. This result confirmed previous findings of unmodified fibrin's turbid charateristic and PEGylated fibrin's transparent charateristic. FH (red) and FPH (green) were charaterised for the first time and FH found to be more closer to fibrin's turbid nature, while FPH was transparent indicating no impact of hep-ar on optial properties. n=3 technical repeats with each hydrogel set in its individual well .

2.2.3.5 Scanning electron microscopy for microstructure

A scanning electron microscope (SEM) was used to gain insight into the structures of the different hydrogel formulations. The hydrogels were prepared by polymerising the precursors with thrombin in porous polyurethane foams (**Figure 2.14A**) with diameter pores between 150 -180 µm and 80-90 µm interconnections (314). This was done to support the hydrogels during the freeze-drying process in preparation for SEM viewing. Micrographs showed that FP (**Figure 2.14D and E**) and FPH (**Figure 2.14F and G**)

hydrogels had similar amorphous sheet-like layers, while unmodified fibrin had a typical fibrous structure with randomly oriented fibers (**Figure 2.14B and C**), with pore sizes (distance between two opposite walls of a pore/ void space in the hydrogel) were not uniform throughout the hydrogels. These findings were comparable with previously published literature that also observed the sheet-like structures with PEG molecule addition to fibrinogen. Furthermore, Benavides et al.,2015 (315) found that in PEGylation, the overall pore sizes are much smaller compared to fibrin, which could explain the sheet-like layers observed in this study.

In contrast to FP and FPH, FH hydrogels (**Figure 2.14 H and I**) had a structure that was closer to that of fibrin. It exhibited a more fibrous nature with fibers that looked denser and thicker than fibrin most likely due to the heparinisation of fibrinogen. Additionally, dialysed unmodified fibrinogen (forming a fibrin hydrogel) did not have a different structural change to undialysed unmodified fibrinogen (J) (forming a fibrin hydrogel) indicating the modifications itself rather than the process was responsible for any structural change. As this was the first observation of its kind with no literature to compare it to, it was hypothesised that the milder structural changes in FH could have resulted from the interaction of acrylates with fibrinogen's amides or thiols.

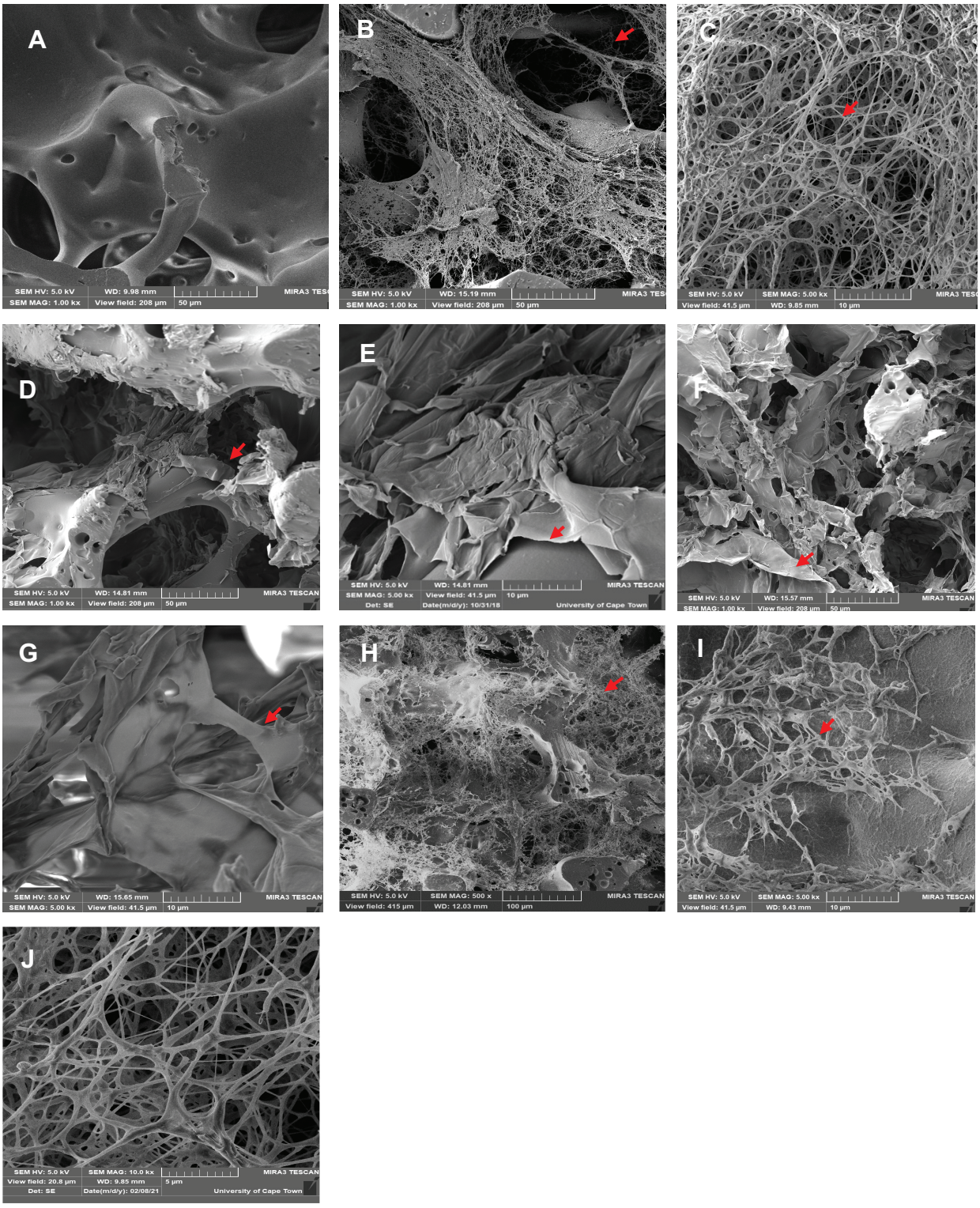

Figure 2.14: SEM micrographs for unmodified and modified fibrin hydrogels set in PU discs (empty disc at A) at 1.00kx, scale bar = 50 µm. (B) Fibrin hydrogel microstructure at 1.00 kx, scale bar =50 µm. (C) fibrin fibers at 5.00 kx, scale bar = 10 µm. (D) FP hydrogels at 1.00 kx, scale bar = 50 µm. (E) More defined sheet-like structures for FP hydrogels at 5.00 kx with arrow indicating fibers with a sheet-like structure, scale bar = 10 µm. (F) FPH microstructure at 1.00 kx with arrow indicating sheets, scale bar = 50 µm and (G) FPH more defined sheet-like structure (arrow) at 5.00kx, scale bar = 10 µm. (H) FH microstructure fibers at 500 x, scale bar = 100 10 µm. (I) FH microstructure fibers with better defined fibrous structure at 5.00 kx, scale bar = 10 µm. (J) Undialised fibrin, 10.00kx, scale bar = 10 µm.

2.2.3.6 Rheological analysis for stiffness

To characterise the hydrogels' stiffness, rheological analysis was conducted for each hydrogel type using a rheometer. With each run, fibrinogen precursors for the different hydrogels were carefully mixed with thrombin in a tube and the mixture immediately transferred to the lower plate geometry of the rheometer set to 37°C. The upper geometry was swiftly lowered according to the gap set, and the hydrogels allowed to fully polymerise and thereafter frequency sweeps run between 0.1 – 10 Hz. Average G' readings at 1Hz were used for stiffness values. The complete scan examples are given in **appendix B**.

Fibrin hydrogels had the highest average G' at 42.1 ± 1.5 Pa; followed by FH at 36.7 ± 1.9 Pa (**Figure 2.15**). These two hydrogels' formulations were not significantly different from each other in stiffness. In contrast, FP and FPH had lower stiffnesses (**Figure 2.14**), 18.3 ± 1.3 Pa and 17.6 ± 2.7 Pa respectively and these were significantly different ($p<0.01$ for FP vs F, FP vs FH; FPH vs F and $p<0.05$ for FPH vs FH) to both unmodified fibrin and FH, but not from each other. This suggested that the incorporation of PEG reduced stiffness significantly. Few studies have reported rheological data on both fibrin and PEGylated fibrin and the reported findings are somewhat inconsistent. For instance, Shpichka et al.,2020 (299) and Rytlewski et al., 2015 (239) reported similar observations of PEGylation reducing stiffness to form softer hydrogels at a 10:1 molar ratio as used in the present study. Shpichka et al., 2020 (299) reported a 50% reduction in stiffness with PEGylation, from 600 Pa unmodified fibrin to 300 Pa with PEG-NHS PEGylation, while Rytlewski et al., 2015 (239) observed a small, but significant, reduction with PEG-SG_2 (500 Da) from 140 Pa unmodified fibrin to 130 Pa after PEGylation (232). The PEG molecular weight sizes in Shpichka and colleagues' study were not mentioned for more detailed comparison with our findings. The PEG addition to fibrinogen is proposed to modify fibrin fibers, where a more fibrous and denser network leads to stiffer hydrogels, while less fibers yield softer hydrogels. PEGylated fibrin hydrogels have been reported, similar to the present study, to have sheet-like structures as opposed to fibers of unmodified fibrin as described above (232, 299).

In contrast to Shpichka et al.,2020 (299) and Rytlewski et al., 2015's (239) findings, Koroleva et al., 2016 (316) observed no significant decrease in stiffness when a 10:1

(PEG: fibrinogen) PEG-NHS-PEGylated (bifunctional PEG which can crosslink) fibrin hydrogel was compared to unmodified fibrin (298, 316). Surprisingly in the same study, at a lower PEGylation ratio, 5:1, a 30% increase in stiffness was observed. Further, cross-linking with different types of PEGs (NHS-PEG, BTC-PEG, SC-PEG and SMB-PEG), showed that storage moduli is potentially PEG molecule dependant, where a small NHS-PEG (0.5 kDa), and BTC-PEG (3.4 kDa) significantly decreased storage modulus, while SC-PEG (3.4 K) induced no significant changes and SMB-PEG (3.5 kDa) increased it with varying moduli (32 - 173 Pa) with fibrin at 105 Pa. It was concluded that small molecule (0.5 kDa) PEGs resulted in a decrease in stiffness, while larger molecules increase stiffness (3.4 kDa) (317). The influence of PEGylation thus appears to be dependent on several factors such as the PEG molecule, and molar ratio. In this study, Both FP and FPH (**Figure 2.15**) were not significantly different to each other in stiffness, similarly, FH was not significantly different to F. This suggested that the incorporation of heparin neither reduced nor increased stiffness whilst incorporation of the PEG-SH did influence stiffness. It was considered that though stiffness was reduced by almost 50%, the relative actual decrease from ±40 Pa to ±18 Pa was unlikely to have any major biological effect.

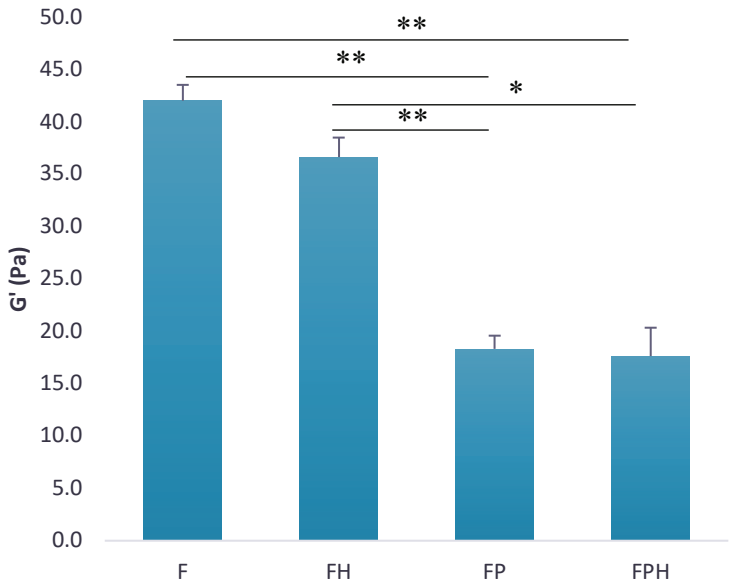

Figure 2.15: Rheological analysis of fibrin and modified fibrin hydrogels with average elastic modulus, G' (Pa) at 1Hz, for each hydrogel type. Average elastic modulus significantly decreased with NHS-PEG addition, while there

were no significant differences when unmodified fibrin. Results represented as mean ± SD, ***p<0.001, **p<0.01, *p<0.05, n=2 independent biological repeats with three technical repeats each.

2.2.4 *In-vitro* cytocompatibility

To assess whether the incorporation of either PEG or heparin had any effect on the cytocompatibility of fibrin, cell viability was assessed with a live/ dead cell viability assay with HUVECs. This assay distinguishes live cells from dead cells using calcein AM and ethidium homodimer-1 (EthD-1). In live cells, intercellular esterase is active and the plasma membrane intact. Calcein AM is cleaved by the esterases of live cells resulting in green fluorescence (ex: 495 nm and em: 515 nm). The EthD-1 is unable to cross the cell membrane of live cells, while in dead cells it crosses the damaged plasma membrane and binds to their DNA resulting in a bright red fluorescent signal (excitation at 525 nm and emission at 617 nm). For the experiments, cells were encapsulated in 3D, and thereafter cultured for three and seven days in 10% FBS HUVEC culture media. After staining, cells were imaged within the fibrin hydrogel using a confocal microscope and quantified by ImageJ analysis.

The results showed that on day three, HUVECs exhibited a more rounded shape (compared to their cuboidal shape in a monolayer) (**Figure 2.16A**), and there were more live cells than dead with average viability percentage ≥ 70% for all the hydrogels (**Figure 2.16B**), indicating that all the hydrogels were non-cytotoxic at this time point. When the incubation period was extended to seven days however, there were significantly ($p<0.001$) more dead HUVECs than alive (**Figure 2.16B**) with an average viability percentage of below 50% for all hydrogels (**Figure 2.16B**). However, although 50% and less were alive by day seven, it is likely that a huge percentage of cells were dead by then and were not being detected by EthD-1 due to total loss of cell structure. The fact that there were no major differences between HUVECs in fibrin hydrogels, and the modified hydrogels suggested that the cell death was rather related to cells and not the hydrogels. Fibrin with unattached heparin (F and H) presented with similar findings of cell death, indicating that the cell death was also not influenced by the presence of attached heparin in FPH and FH.

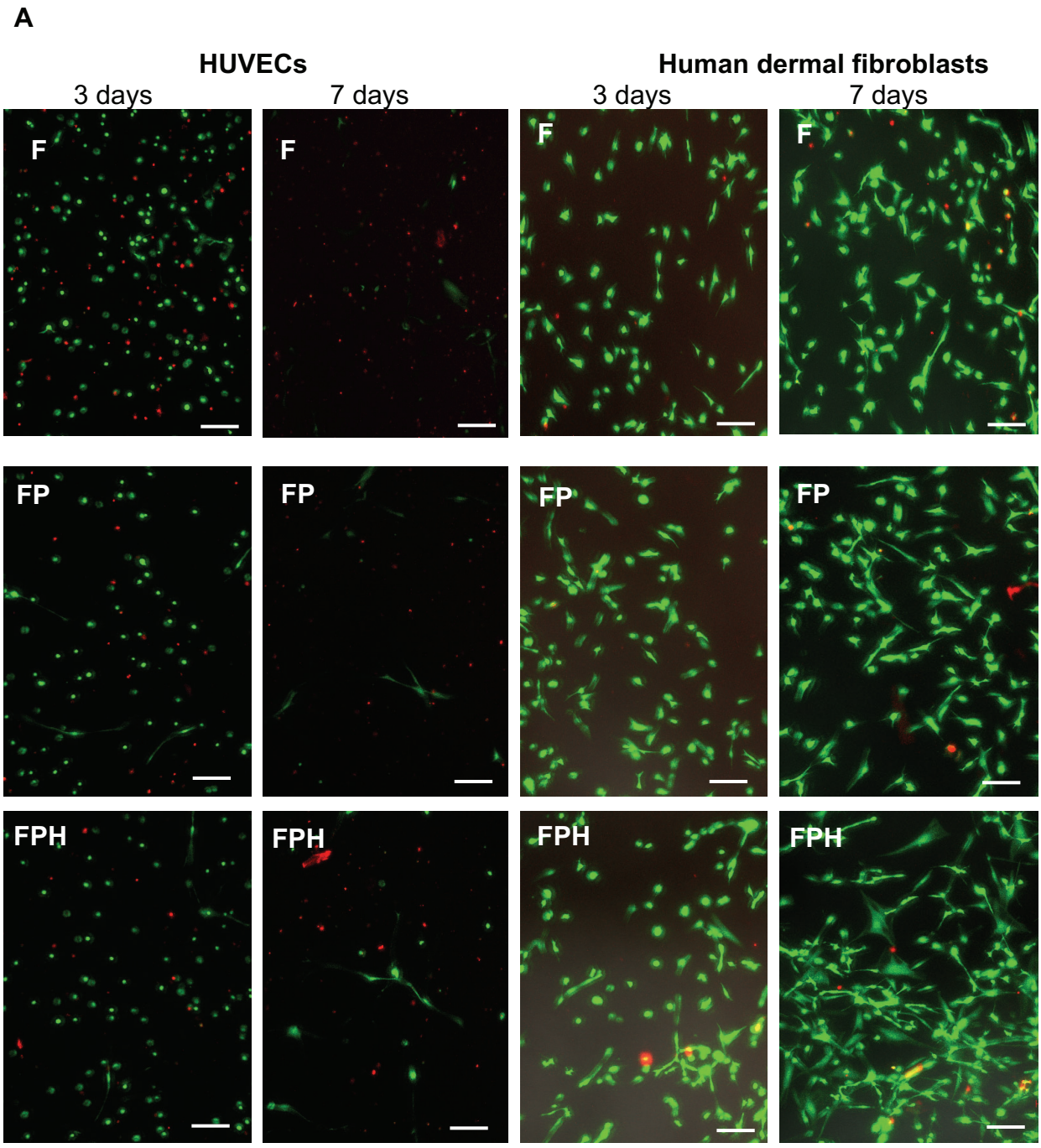
A
HUVECs
Human dermal fibroblasts
3 days
7 days
3 days
7 days
F
F
F
F
FP
FP
FP
FP
FPH
FPH
FPH
FPH

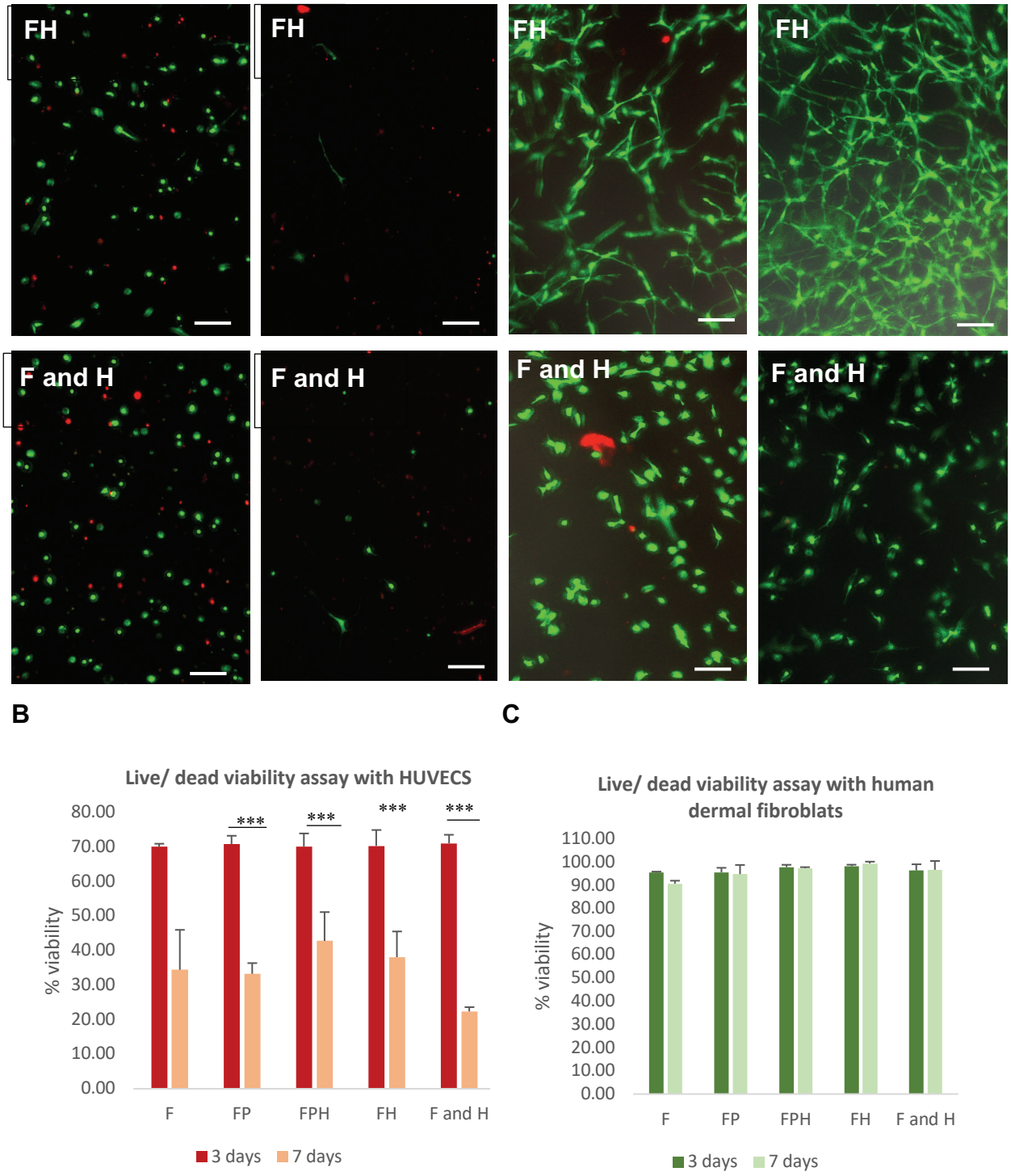

Figure 2.16: Live/ Dead viability assay for 3D hydrogel encapsulated HUVECs and human dermal fibroblasts. (A) Micrographs of encapsulated HUVECs and HdFBs at day 3 and day 7 imaged with a confocal microscope, red = dead cells, green = live cells. (B and C) Day 3 and 7 HUVEC and HdFBs viability quantified with ImageJ's particle/ cell counter plugin. At day 3, HUVECs were viable, above 50% and HdFBs above 90%. By day 7, % viability in HUVECS gels was below 50%, while for HdFBs was still above 90%. Results presented as mean ± SD, n = 3 technical repeats. Red = dead cells, green = live cells. ***p<0.001, scale bar = 100 µm

To gain greater insight into the cause of HUVEC death at day seven, HdFBs were cultured in the same experimental conditions as the HUVECs with different media (10% MCBD culture media), and a live/dead assay conducted at three and seven days. The HdFBs survived with a viability average ≥90% for both days three and seven in all hydrogels (**Figure 2.16C**). Compared to HUVECs, HdFBs were flatter and elongated, especially in the FH and FPH groups (**Figure 2.16A**). These results indicated that the hydrogels were more biocompatible with HdFBs compared to HUVECs for extended culture periods. This is congruent with the robust characteristic of HdFBs that play a supportive role to ECs *in-vivo.* They are often used in *in-vitro* co-culture systems with ECs where they play several roles including that of supporting endothelial network development through paracrine mechanisms (318). Therefore, no differences in cell viability were observed for any of the modified hydrogels and the observed cell death for ECs was most likely due to their fragile nature.

The live/ dead findings (reduced % viability over time in HUVECs) prompted further investigation of HUVEC activity in 3D. For this, the cells were encapsulated in the same manner as described for the cytocompatibility studies above and cultured for 24, 48 and 72 hours and seven days. At the end of each incubation time, cell activity was measured with a CellTiter-Glo® Luminescent cell viability assay that quantified the amount of adenosine triphosphate (ATP) in viable cells. The ATP content is considered to be relatively stable in cells and thus can be used to approximate cell number (319). HUVEC numbers in all fibrin types were observed to increase between 24 and 48 hours and decreased between 48 and 72 hours followed by a substantial reduction at seven days (**Figure 2.17**). Between 24 and 48 hours, cell number increase was highest in the fibrin hydrogels at 1.19-fold increase, followed by FH at 1.13-fold increase and FP and FPH at 1.06 and 1.07 respectively.

Hydrogels with higher stiffness (F and FH) had the highest proliferation rate, while hydrogels with the lowest stiffness (FP and FPH) had the lowest proliferation rate between 24 and 48 hours. Yeh et al., 2012 (320) similarly reported matrix stiffness to regulate EC proliferation through septin 9 inhibition, where a stiffer matrix was conducive for increased

proliferation, while a softer matrix led to lower proliferation (320). Similar effects have been reported by other authors using different cell lines in 3D (321, 322). Moreover, scar tissue that forms during the remodelling phase of wound healing is much stiffer than the original tissue's ECM. This scar tissue is a successor of granulation tissue, a provisional ECM of the proliferation phase that is characterised by increased cell proliferation (323, 324).Congruent to this, both F and FH had a higher proliferation rate compared to FP and FPH between 24 and 48 hours, supporting the impact of stiffness on proliferation. There were also no significant differences between the proliferation rate of F and FH as well as FP and FPH, between 24 and 48 hours. The presence of hep-acr thus appeared to play no role in proliferation, but the PEG molecule seemed to influence cell division.

For all the hydrogel formulations, HUVEC numbers decreased significantly ($p<0.001$) at 72 hours and were even more drastically reduced by day seven indicating substantial cell death (**Figure 2.17**). This was congruent with the live/ dead assay results above (**Figure 2.16**), and thus supporting that HUVECs were not robust for long term culturing. These findings were crucial for HUVEC application in subsequent experiments. The repetitive low cell numbers (above) in both the FP and FPH require further investigation in future studies.

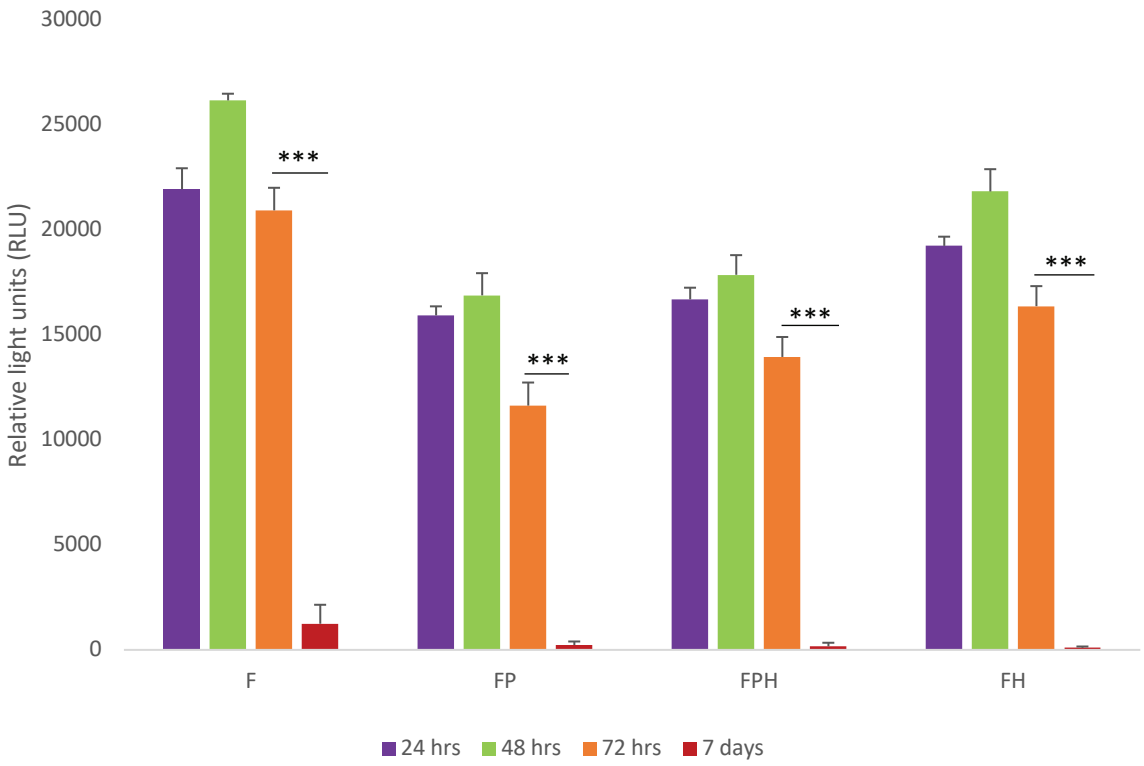

Figure 2.17: 3D HUVECs cell activity in the different hydrogel types from 24 hours to 7 days. Cell activity in all hydrogels decreased from 24 hours up to day 7, with significant decrease observed between 72 hours and day 7. RLU = relative light unit. (***p<0.001), Results presented as mean ± SD, n = 3 biological repeats.

2.2.5 Endothelial cell invasion with 3D spheroids

During angiogenesis, EC sprouting is pivotal for neovascularisation of implanted hydrogels. Equally, hydrogels that are intended to support tissue repair and regeneration should possess certain characteristics, i.e., porosity, and biocompatibility that support adequate nutrient exchange and cell activity. As in the ECM, the hydrogel should enable cell migration into the surrounding tissue. Therefore, this aspect was studied with a well-established *in vitro* 3D angiogenesis assay (49, 325, 326). For the assay, spheroids of HUVECs (750 cells) were formed overnight in non-tissue culture treated round bottom plates and cultured in methylcellulose containing media, and thereafter embedded in the different hydrogel groups. Once the hydrogels had set, culture media containing 2% FBS was added, and the 3D constructs cultured for 48 hours. For better visualization, the sprouted spheroids were stained with ActinRed (stains cytoskeleton) and the nuclei counterstained with Hoechst 33258.

Analysed images revealed that all hydrogel formulations permitted HUVEC invasion though at different rates, confirming fibrin's pro-angiogenic characteristic and porosity that supports HUVEC migration. There were higher numbers of sprouts of shorter length (short and fanned out as indicated in **Figure 2.18A**) for F, FP and F and H, whilst FH had fewer but longer sprouts. For FPH, spheroids repeatedly disintegrated by 24 hours, and by 48 hours longer but fewer sprouts emerged from those remaining. Resultantly, measured cumulative sprout length was similar for all groups except FPH, and measured average sprout number was higher in F, FP as well as in F and H, and lower in FPH and FH. This allowed for calculation of average sprout length per spheroid which was found to be highest in FH. Average sprout length per spheroid in the FH hydrogels was 161.0 ± 16.8 μm (**Figure 2.18C**). This was significantly higher when compared to 80.9 ± 0.5 μm in FP ($p<0.01$), 74.5 ± 6.2 μm in F ($p<0.01$) and 72.2 ± 0.9 μm in F and H ($p<0.001$). The lower average sprout length per spheroid in F as well as in F and H led us to postulate that the significantly longer sprouts in the FH were due to hep-acr directly attached to fibrinogen. As this was the first study to successfully attach heparin to fibrinogen in this manner, this was an interesting finding. Heparin is known to trap several growth factors possessing heparin binding sites and induce/ augment angiogenesis (327). This finding thus has implication in the hydrogel's potential utility in therapeutic angiogenesis.

Although analysis in the FPH hydrogels proved challenging, cumulative sprout length (107.6 ± 22.6 μm) was second to that seen in FH. For these hydrogels, spheroids repeatedly changed shape by 24 hours, looking more oval, condensed, and lost their defining edges (**Figure 2.18A** By 48 hours, longer sprouts had emerged inconsistently from the condensed spheroids of which some were disintegrated (and not included in the analysis). This disintegration of spheroids was not observed for FP, FH or F and H indicating that separately neither modification nor the presence of heparin were responsible for this behaviour. This suggested that the combination of heparin with PEG attached to fibrinogen was not a favourable 3D microenvironment for HUVEC invasion. Published literature rigorously exploring a plausible rationale for this interaction is scarce. However, Kim, Kim and Tae, 2013 reported findings with human ADSCs encapsulated in hydrogels, at varying elasticity, containing free heparin attached to PEG (328). In their study they observed a less efficient differentiation capacity for ADSCs in 3D culture

relative to in 2D culture. Though not directly comparable, perhaps this suggests a less optimal outcome for some cellular functions when cultured within fibrin in the presence of these two reagents.

The above cytocompatibility studies did not indicate any major issue though cell numbers were perhaps somewhat reduced in FP and FPH hydrogels. In the present study, as cytotoxicity of individual HUVEC at 48 hours (**Figure 2.16**) was not observed, it was speculated that perhaps an interaction between PEG and hep-acr promoted protein oligomerisation which ultimately impacted spheroid shape over 48 hours, and overall sprouting. Interestingly, the lower sprout length and total cumulative sprout observed in the F and H group was comparable to F and FP individual groups, with no significant differences. This suggested that the differences in stiffness between the F and FP groups were not large enough to impact HUVEC 3D invasion.

Furthermore, the sheet-like layers, observed in both FP and FPH groups (**Figure 2.14**), have been proposed to influence 3D cell migration and ultimately tube formation. Shpichka et al., 2020 (299) hypothesised that PEGylation can possibly improve 3D cell migration, compared to unmodified fibrin, by covering the RGD cell adhesion sites present in the α-chain of fibrin. With this, the primary amino group of arginine can be bound to the PEG via the NHS moiety, and thus covers the adhesion sites allowing cells to migrate faster. In the present study, both FP and FPH had similar amorphous sheet-like layers while FH was fibrous like fibrin (**Figure 2.14**). There were however no significant invasion differences observed between F and FP, comparable to findings reported previously at lower PEGylation ratios (1:10) (232, 299, 316). This finding strengthened the evidence that the high cumulative sprout length in the FPH, and FH was due to covalently bound heparin. It further confirmed that our binding molar ratio for SH-PEG-NHS to fibrinogen was enough to support invasion.

Regardless, the FH positively allows for more rapid and sustained invasion by sprouting EC than unmodified fibrin. This is presumably due to bound heparin as F and H did not elicit a similar response. There was some evidence of deleterious outcomes from a combination of PEG and heparin with difficulties in maintaining HUVEC spheroid integrity

in FPH, but there was equally some evidence for more rapid and sustained HUVEC invasion. This coupled with its greater stability (see **section 2.2.3.3**) suggested continued investigation of FPH potential regenerative properties.

A

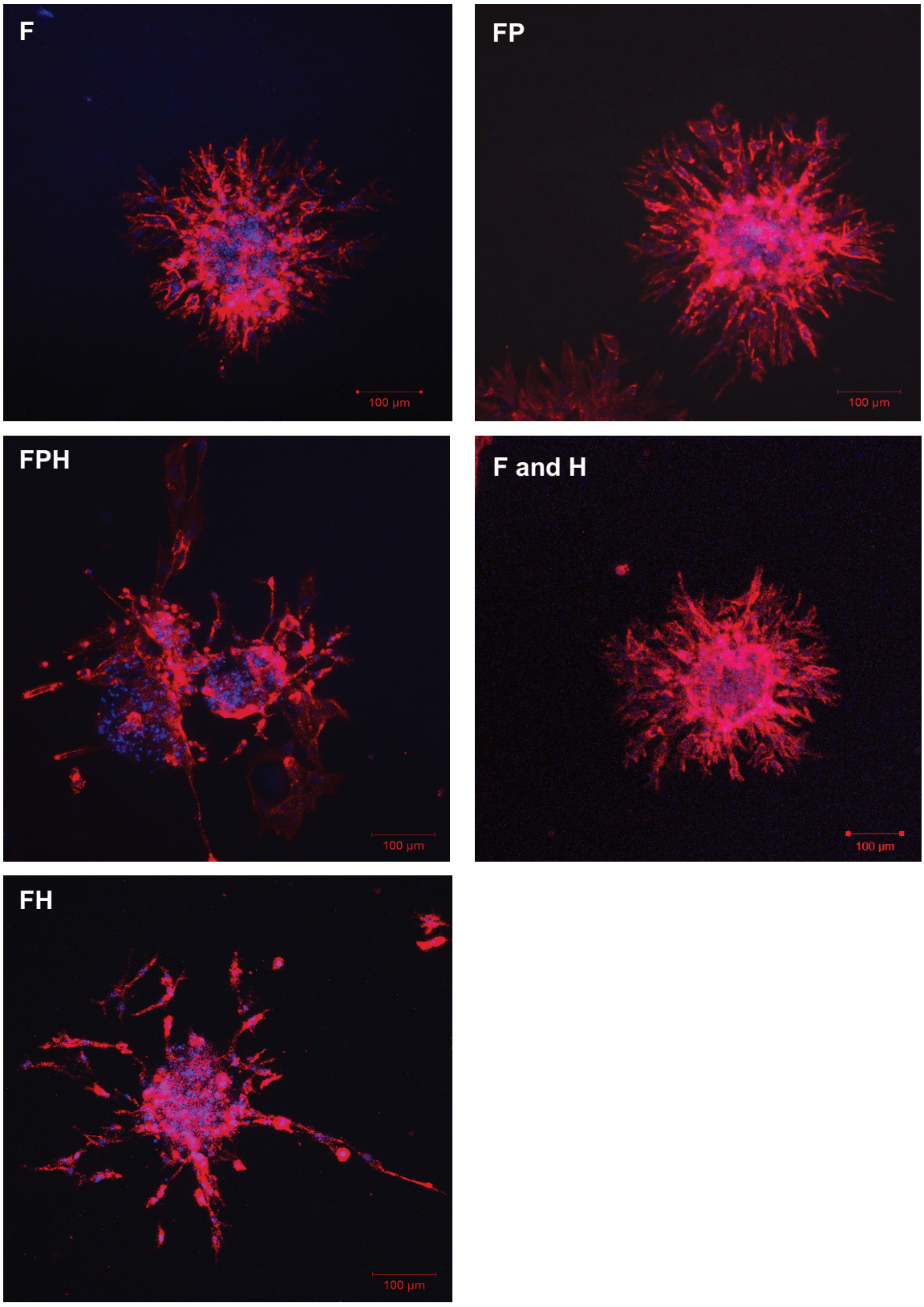

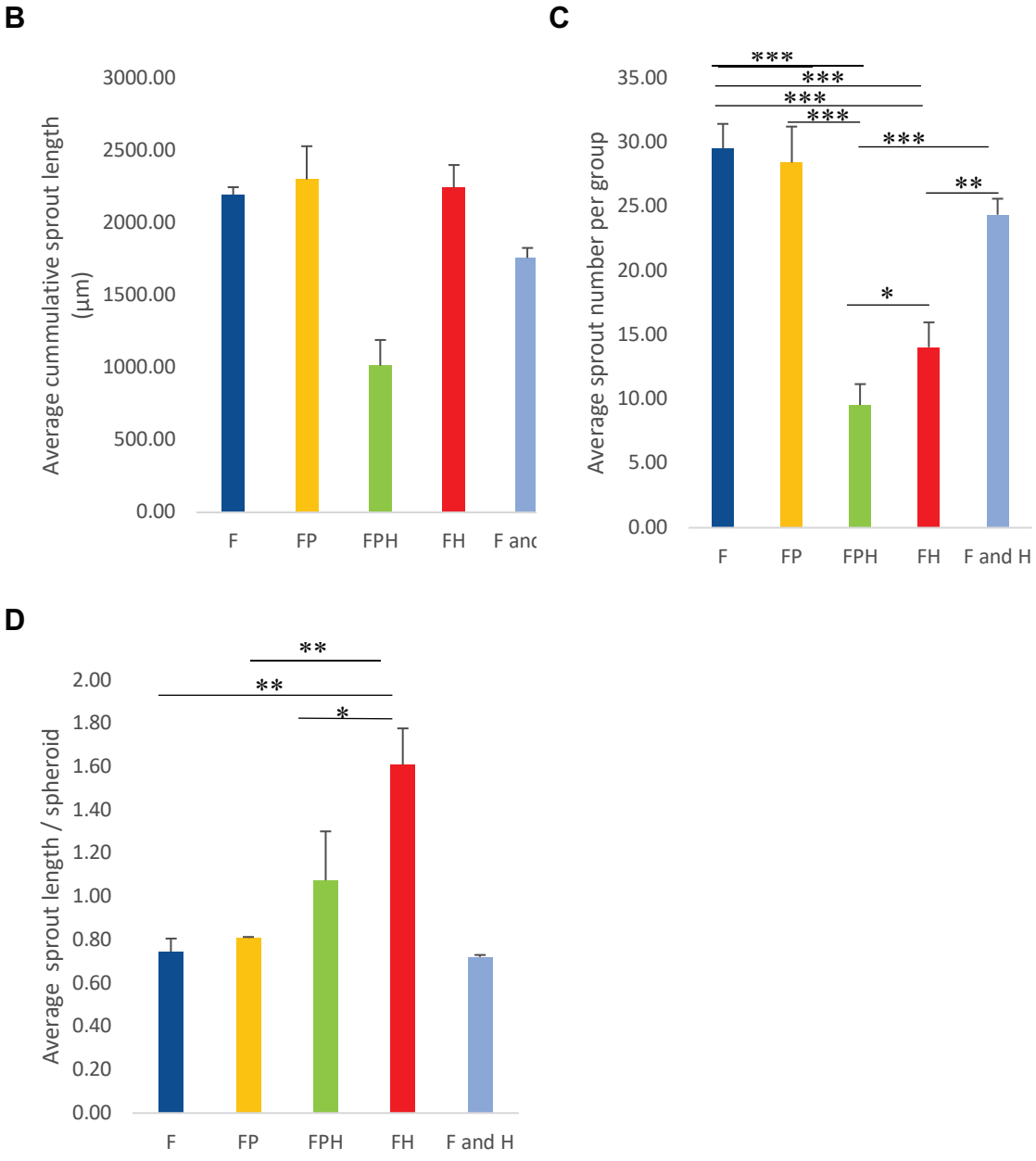

Figure 2.18: Sprout invasion from HUVEC spheroids. (A) Sprouting spheroid representative confocal fluorescent images after 48 hours incubation (magenta = phalloidin-stained cytoskeleton, blue nuclei) are blue, scale bar =100 µm.(B) Cummulative sprout length for the different hydrogel group. (C) Average sprout number was higher in F, FP as well as F and H compared to FH and FPH. (D) Average sprout length per spheroid where FH was signifiantly increased compared to F as well as F and H.. *p<0.05, **p<0.01, ***p<0.001, n = 3 technical repeats, with no less than 4 spheroids per hydrogel.

CHAPTER 3: SUSTAINED GROWTH FACTOR RELEASE

3.1 Introduction

Growth factors are crucial soluble proteins secreted by cells to regulate cellular processes such as proliferation, migration, and differentiation (329). Judah Folkman et al., 1971 (330) first identified and implicated angiogenic growth factors and demonstrated that these growth factors were able to contribute to concentration dependant tumour development by encouraging new blood vessel formation. Subsequent work by Takeshita et al., 1994 (331) confirmed this effect, and further demonstrated that it was mainly regulated by VEGF. In regenerative medicine, angiogenic growth factors such as VEGF are being investigated for their therapeutic potential where exogenous angiogenic growth factors are administered to damaged/ ischaemic tissue to stimulate new blood vessel formation from an existing vasculature in a process called angiogenesis (6).

Angiogenesis is the formation of new blood vessels from a pre-existing vasculature and the main process by which adult's blood vessels are formed (332, 333). Almost all physiological and pathophysiological processes such as wound healing, cancer, and tissue repair hinge on optimal angiogenic response for their successful resolution (334, 335, 336). For instance, in the proliferation stage of the wound healing process, angiogenesis is required to re-establish nutrient and oxygen supply, encourage fibrous tissue formation, and prevent hypoxia. This vessel formation and vessel growth occurs mainly through sprouting angiogenesis, predominantly regulated by VEGF, a 45 kDa heparin-binding glycoprotein and homodimer that almost exclusively targets endothelial cells(337). The VEGF is secreted by almost all cell types and its secretion is triggered mainly by tissue hypoxia where it is upregulated 30-fold higher than all other pro-angiogenic growth factors (338, 339). Due to its substantial ability to increase permeability of the blood vessel's endothelium in preparation for angiogenesis, it was originally known as the vascular permeability factor (340, 341). It is known to date that in mammals, VEGF has five main members in its family, namely VEGF-A, VEGF-B, VEGF-C, VEGF-D and PLGF (342, 343, 344, 345, 346). In this family, VEGF-A is the original/ first member, and

it is the most highly conserved among animals. It is therefore considered as the main VEGF necessary for a functional vasculature (347, 348). It has been shown that a single *VEGF-A* allele deletion results in immature and deficient cardiovascular and angiogenesis development that ultimately leads to embryonic lethality, attesting to the indispensable role of VEGF-A(349).

The VEGF-A has four main isoforms namely $VEGF_{121}$, $VEGF_{165}$, $VEGF_{189}$, and $VEGF_{206}$ encoded by exons in the VEGF-A gene (350). Evidence suggests that $VEGF_{165}$ and $VEGF_{121}$ are the most ubiquitous isoforms. The $VEGF_{121}$ is however the only VEGF-A isoform that does not possess the HBD for heparin binding to enhance affinity for VEGF receptor signalling, while $VEGF_{165}$ possesses the HBD (260, 350). As a resultant, $VEGF_{165}$ is the most potent and biologically active VEGF for vascular endothelial growth factor receptors (VEGFRs). The VEGF signals through VEGFRs, namely VEGFR-1, VEGFR-2, and VEGFR-3, with major angiogenic activities generated through VEGFR-2 that is expressed by ECs. VEGFR-1 has greater affinity (about Kd = 1-10 pM) for VEGF-A than VEGFR-2 (Kd=10 - 100 pM), however its tyrosine kinase activity (for signalling, **Figure 3.1**) is 10-fold weaker than that of VEGFR-2 (351). Consequently, it cannot effectively activate the receptor for angiogenesis regulation though it has a higher binding affinity. The exact role of VEGFR-1 remains unknown, with propositions that it may play a role in sequestering VEGF-A for negative regulation of angiogenesis (351).

While extensive data exists on VEGF for diseases such as cancer (352) and age-related macular degeneration (353), the focus of this thesis was to investigate VEGF in its therapeutic, stimulating context for diseased or injured tissue. Therefore, the doses used in this study were carefully considered and not excessively high. This may contribute to the improvement of products like Regranex® (354) which are used in

chronic wound healing but have faced regulatory challenges.

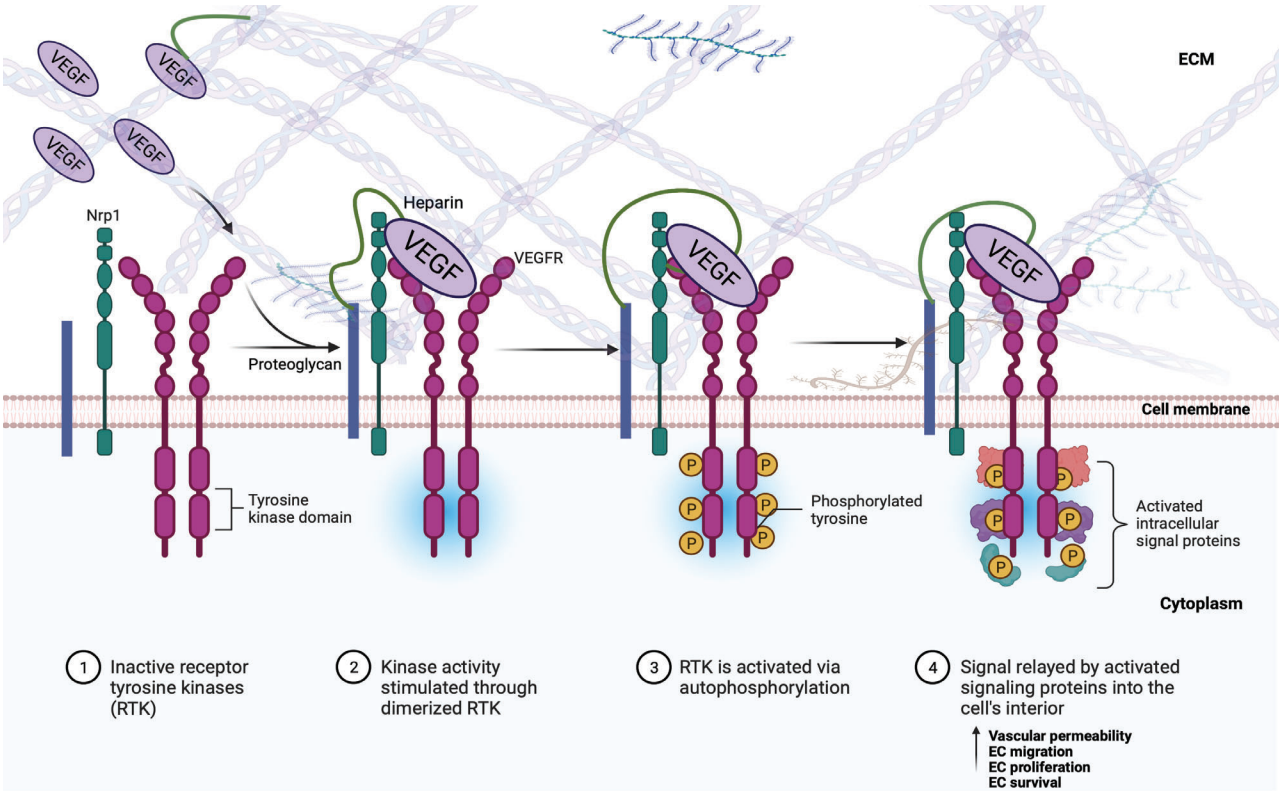

Figure 3.1: VEGF signalling pathway induced by VEGF binding to VEGFR that is a receptor tyrosine kinase. The VEGF-VEGFR complex signals in the presence of Neuropilin-1 (Nrp) 1 and heparin. Image created with BioRender.com.

The acidic fibroblast growth factor (aFGF) and bFGF of the FGF1 family are another group of heparin binding angiogenic growth factors with molecular size between 17 – 34 kDa (257). These angiogenic growth factors signal through four main heparin binding receptors, namely fibroblast growth factor receptor (FGFR)1, FGFR2, FGFR3 and FGFR4 that are 56% - 71% homologous (355). These four receptors all have a HBD and are present at varying degrees in several cell types including fibroblasts, smooth muscle cells and ECs (356, 357, 358). It has been shown that FGFR-1 is unique to mediating proliferation, migration, protease production and tubular morphogenesis, while FGFR-2 mediates only cell motility (359). The aFGF binds to all FGFRs, while bFGF only binds to FGFR-1 and 2, and this resultantly broadens the role of aFGF and keeps that of bFGF more specific as it can only bind two receptors (360, 361). Several angiogenic effects are induced by bFGF, directly through the FGFR-1 and FGF-2 and indirectly by triggering the release of other angiogenic factors such as VEGF. In context, for direct receptor

signalling, bFGF binds to its respective receptors, in the presence of heparan sulphate proteoglycan co-factors such as heparin, and induce Ras/mitogen activated protein kinase (RAS/ MAPK) pathway which promotes EC proliferation, and migration (362). Indirectly, recent evidence suggests that bFGF has a specific role of triggering the release of angiogenesis regulators such as VEGF-A and proteases such as MMPs (362, 363). The bFGF thus has a significant role in activating angiogenesis.

For tissue repair mechanisms that induce angiogenesis, free form administration of exogenous angiogenic growth factors, either systematically or locally, without a delivery vehicle has shown to result their half-life reduction. As a result, low concentrations reach the target site due to degradation by protease and mononuclear phagocyte system elimination (364). To compensate for this loss, higher concentrations or repetitive administrations are often administered to improve efficacy at the target site (365, 366, 367). Higher concentrations are however not ideal due to costs and are opportunistic for overstimulation. For these reasons, hydrogel systems have been explored as growth factor delivery systems that localise and shield them from degradation.

Having established two heparinised fibrin hydrogel systems in chapter 1, the goal of this chapter was then to investigate the systems' potential to bind, localise and sustain bFGF and VEGF release over time. Although fibrin alone binds these growth factors, it can only release them for a short period of time without a sustained release (165, 368). Heparinised fibrin (FH and FPH) pre-mixtures were then loaded with 1 µg of each growth factor individually, VEGF and bFGF, in tubes and thereafter allowed to polymerise with thrombin at 37°C for 30 minutes 1 hour, before PBS was added. After three hours, the PBS was aspirated out into a collection tube as a wash eluate to remove unbound growth factor. The PBS was replaced with fresh PBS and further incubated for 15 days. Eluates were collected on day one and every second day for 15 days and thereafter assayed with an ELISA for release rates.

3.2 Results and discussion

3.2.1 bFGF binding and release

Heparinised fibrin hydrogels significantly bound more bFGF compared to the non-heparinised (F and FP) hydrogels. After a 3-hour wash, FH and FPH bound 975 ± 9.9 ng (98% of loaded bFGF) and 972 ± 7.4 ng (97%) respectively with no significant differences between these two groups (**Figure 3.2**). In contrast, F and FP bound 721 ± 44.3 ng and 705 40.2 ng respectively, with no significant differences between these non-heparinised groups (**Figure 3.2B** and **Table 3.2)**. This represented a significant additional binding of 254 ng (25%) by FH relative to fibrin ($p<0.01$) and 267 ng by FPH (27%) relative to FP ($p<0.001$). These findings indicated as evidence that covalent addition of heparin to fibrin enhanced bFGF binding and that PEGylation did not influence bFGF binding.

The presence of heparin in both FH and FPH was also found to slow the rate of bFGF release. After the release of unbound bFGF in the first 3 hours, a further burst type release of 374 ± 8.2 ng (52% of bound bFGF) and 366 ng ± 11.2 (52% of bound bFGF) was observed on the first day from F and FP respectively. In contrast, this was 63 ± 17.7 ng (8 % of bound bFGF) and 77 ± 12.0 ng (9% of bound bFGF) for FH and FPH respectively. Both F and FP were observed to release no more bFGF after day three. However, FH and FPH released 16 ± 1.2 ng and 16 ± 0.7 ng bFGF per day over the 15 days assayed respectively, both at 6 % of the bound bFGF. These release rates were not significantly different between the two heparinised fibrin hydrogels. A similar effect on bFGF binding and release was observed when heparin was covalently bound to fibrin using carbodiimide chemistry where fibrin alone released 52% of the bound bFGF within 12 hours, in contrast to 9% when it was conjugated to heparin (42.7 mg per 1 g fibrinogen) (285). About ± 3% bFGF was released rate per day over 21 days from the heparin conjugated fibrin, and this rate was similar to that observed in this study for FH and FPH. It should be noted however that the concentration of fibrinogen in the hybrid fibrin was high at 40 mg/ml HCF and 60 mg/ml unmodified fibrinogen, and the volume used per

sample to load 100 ng bFGF was not given. The binding and release characteristics did however appear similar.

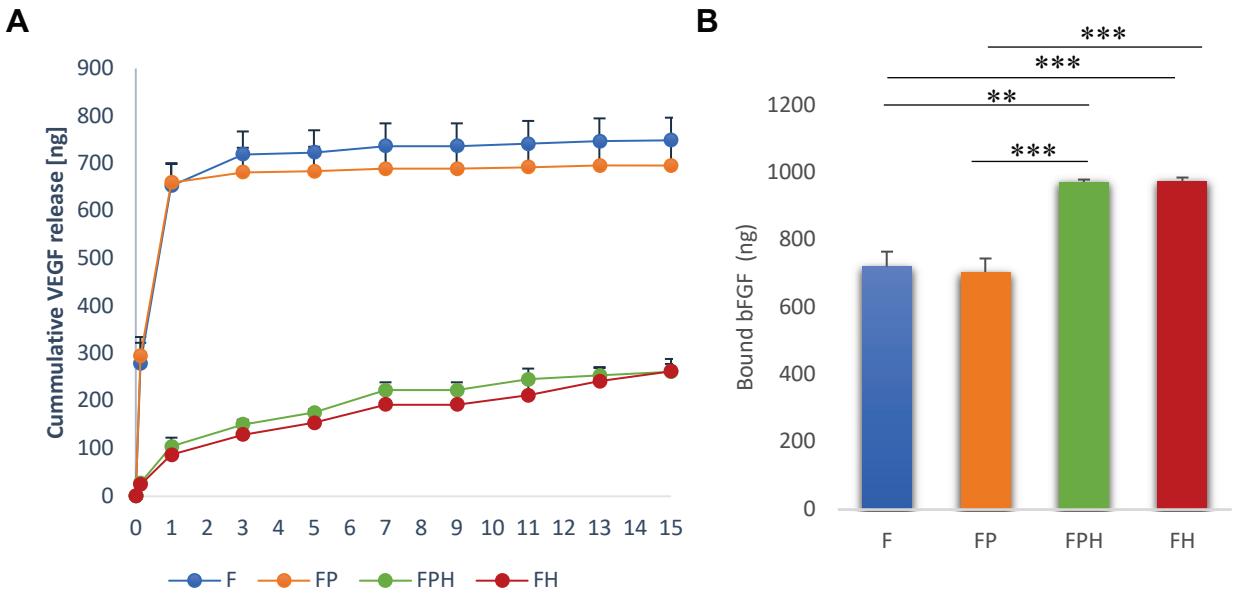

Figure 3.2 Sustained cumulative release of bFGF from heparinised fibrin hydrogels. (A) Cumulative bFGF release over 15 days from unmodified fibrin(F), fibrin-PEG (FP), fibrin-PEG-heparin (FPH) and fibrin-heparin (FH). Heparin incorporation slowed the initial bFGF burst release and sustained the release at 16 ± 1.2 ng for FH and 16 ± 0.7 ng for FPH per day up to 15 days. (B) Total bFGF binding to F, FP, FPH and FH. Bound heparin significantly increased bFGF binding in FH and FPH relative to both F and FP. ***p<0.001, n=3 technical repeats.

In total, 263 ± 26.1 ng cumulative bFGF was released from FH and 262 ± 16.5 ng from FH through day 1 to day 15. In contrast, F and FP released ± 70% of the loaded bFGF by day three, and this remained at ± 70% up to day 15 (**Figure 3.2A**). This suggested that 30% remained bound to the hydrogel system without release. This finding was similar to that observed by Martino et al., 2013 (165) where different heparin binding growth factors were evaluated for their affinity to fibrin(ogen). The findings showed that bFGF had a significantly stronger binding affinity, compared to other heparin binding growth factor classes ($VEGF_{165}$), with only a ± 30% total release of the loaded growth factor, retaining ± 70% from day one to day seven. It was hypothesised that the sequestering of bFGF was due to its strong complexation to the promiscuous HBD of fibrin(ogen). This binding is proposed to occur with high affinity and to saturation where it cannot bind any more bFGF. The lack of difference in binding between F and FP suggests PEGylation

does not interfere with this inherent interaction. However, with heparin present, additional bFGF could be trapped into the fibrin covalent delivery system. It is also proposed that there are two binding sites; with one having a much stronger affinity and thus explaining the trapped (not released) 30% (369). In this present study, this is supported by the observed finding of heparin presence enabling more bFGF binding and sustained release compared to its absence.

3.2.2 VEGF binding and release

ELISA revealed that heparinised fibrin hydrogels bound more $VEGF_{165}$ than the non-heparinised hydrogels. After a 3-hour wash, 932 ± 11.8 ng (93%) and 940 ± 0.7 ng (94%) $VEGF_{165}$ was bound for FH and FPH with no significant differences between these two groups (**Figure 3.3B)**. This was significantly less for F and FP at 593 ± 51.5 ng (59% of bound VEGF) and 604 ± 37.6 ng (60% of bound VEGF) respectively, signifying that heparin presence enabled additional $VEGF_{165}$ entrapment of 339 ng by FH relative to F($p<0.01$); and 347 ng by FPH relative to FP ($p<0.001$). Again, there were no significant binding differences between the F and FP groups. After the release of unbound $VEGF_{165}$ in the first 3 hours, the F and FP further had a burst release close to half of the loaded $VEGF_{165}$ (493 ± 70.2 ng at 49% and 492 ± 46.3 ng at 49% respectively) by day one, and by day three, all (100%) the $VEGF_{165}$ had been released from both hydrogels. In contrast, the FH and FPH were able to generate a controlled release of 21 ± 2.2 ng and 18 ± 1.6 ng $VEGF_{165}$ released per day, respectively, for 15 days as indicated in **Figure 3.3A.** Thus, heparin incorporation demonstrated the ability to enhance $VEGF_{165}$ binding and release. In total, FH released375 ± 43.6 ng, and FPH released 337± 23.5 ng between day one and day 15, compared to F and FP that released 100% (total 1µg) by day three. There were no significant differences between the FH and FPH groups in both the amount released per day and total cumulative $VEGF_{165}$ release. This more sustained growth factor delivery profile is beneficial for enhancing tissue repair (288, 370).

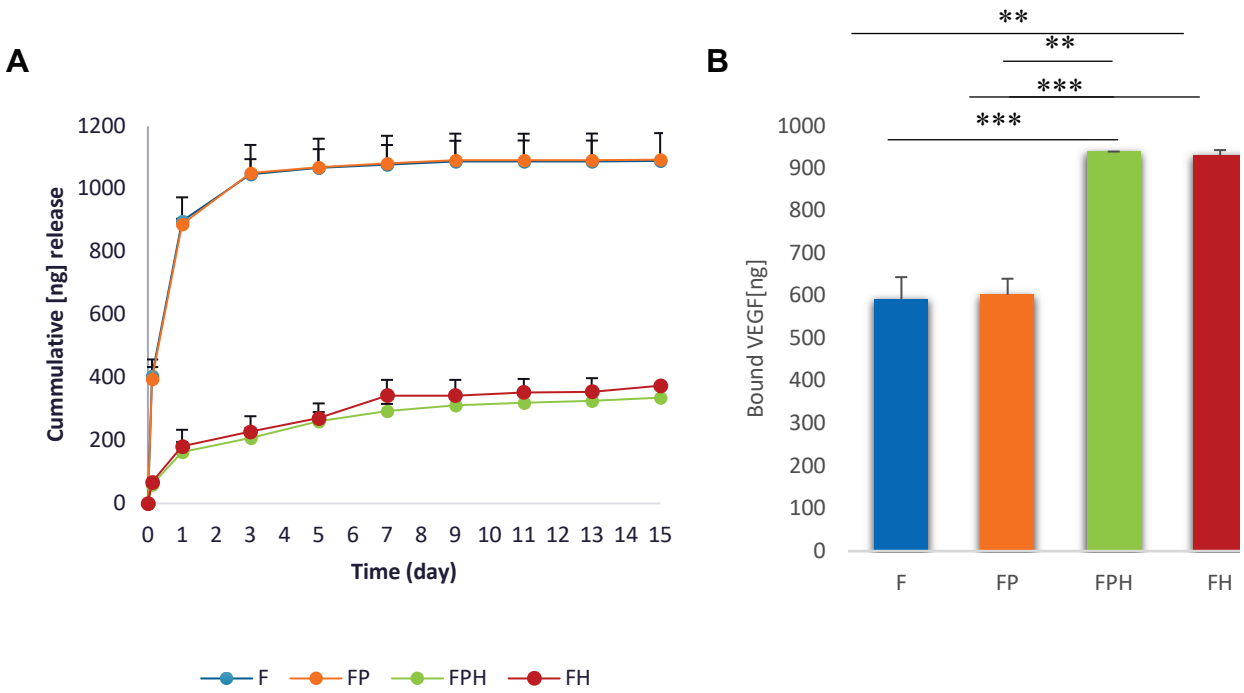

Figure 3.3 Sustained cumulative release of VEGF from heparinised fibrin hydrogels. (A) Cumulative $VEGF_{165}$release over 15 days from unmodified fibrin (F), fibrin-PEG (FP), fibrin-PEG-heparin (FPH) and fibrin-heparin (FH). Heparin incorporation slowed the initial VEGF burst release and sustained the release at 21 ± 2.2 ng for FH and 18 ± 1.6 ng for FPH per day up to 15 days. (B) Total VEGF binding to F, FP, FPH and FH. Bound heparin significantly increased bFGF binding in FH and FPH relative to both F and FP. **p<0.01, ***p<0.001, n=3 technical repeats.

In overall, both bFGF and VEGF showed similar patterns in the binding and release to and from the different hydrogel systems (summary **Table 3.1 and Table 3.2**). In all groups (F, FP, FPH and FH), more bFGF was bound compared to VEGF. VEGF had a higher release rate compared to bFGF. In this, 100% VEGF was released by day three in the F and FP groups, and only ± 70% of bFGF by this timepoint. FPH and FH released VEGF at higher rate over the 15 days, compared to bFGF. This could be due to the fact that bFGF binds more tightly to both fibrin and heparin compared to VEGF. For instance VEGF has a dissociation constant (K_D) of 60.9 nM while that of bFGF is 39 nM for heparin, and this limits bFGF from both fibrin and heparin for release compared to VEGF (371, 372). Generally, as the growth factor affinity increases (decrease in K_D value), binding is

enhanced and the ease of growth factor release decreases (165). This likely explains the slower release rate of bFGF compared to VEGF. It should be noted that heparin dissociation from fibrin through hydrolysis of the bond formed with a thiol could further facilitate growth factor release (45, 373).

Table 3.1: **Summary of bound VEGF and bFGF to the different hydrogel formulations**, n=3 technical repeats (three different hydrogels)

	VEGF [ng]	bFGF [ng]
F	593 ± 51.5	721 ± 44.3
FP	604 ± 37.6	705 ± 40.2
FPH	940 ± 0.7	972 ± 7.4
FH	932 ± 11.8	975 ± 9.9

Table 3.2: Summary VEGF and bFGF released per day from the different hydrogel formulations, n = 3 technical repeats (three different hydrogels).

	VEGF [ng]	bFGF [ng]
FPH	18 ± 1.6	16 ± 0.7
FH	21 ± 2.2	16 ± 1.2

For both bFGF and VEGF, release rates seemed not to be impacted by thrombin concentrations as, both FH and FPH were formed at the same fibrinogen concentrations (10 mg/ ml) but with different thrombin concentrations. For F, FP and FH thrombin concentration was 1 unit/ml, and for FPH it was at 4 units/ ml. This further supported that heparin was responsible for the sustained release of the growth factors and not thrombin and fibrinogen concentrations. Fibrin is known to bind various angiogenic growth factors that mediate the wound healing process, and the binding of bFGF and VEGF to fibrin in this study confirms this. Importantly, heparinisation was found to substantially increase binding of both growth factors and generate sustained release which is a very desirable modification for a regenerative hydrogel.

3.2.3 Bioactivity of eluted bFGF and VEGF

It crucial that growth factor bioactivity is retained after binding and release from a delivery system. Although several studies have investigated bFGF and VEGF sustained release, fewer studies have subsequently investigated their stability and bioactivity following release. The bioactivity of bFGF and VEGF released from heparinised fibrin hydrogels was thus evaluated by assaying the eluted bFGF and VEGF ability to stimulate HdFB, and HUVEC proliferation respectively. The eluates released in the final release period (day 15) were used to prepare media containing 10 ng/ml bFGF or VEGF that were then used to culture HdFB and HUVEC respectively. Fresh growth factors were used as positive controls, and growth factor free medium as negative experimental control (2% serum was used for the sensitive HUVECs and serum free for HdFB). These were then incubated for 72 hours, and cell proliferation measured.

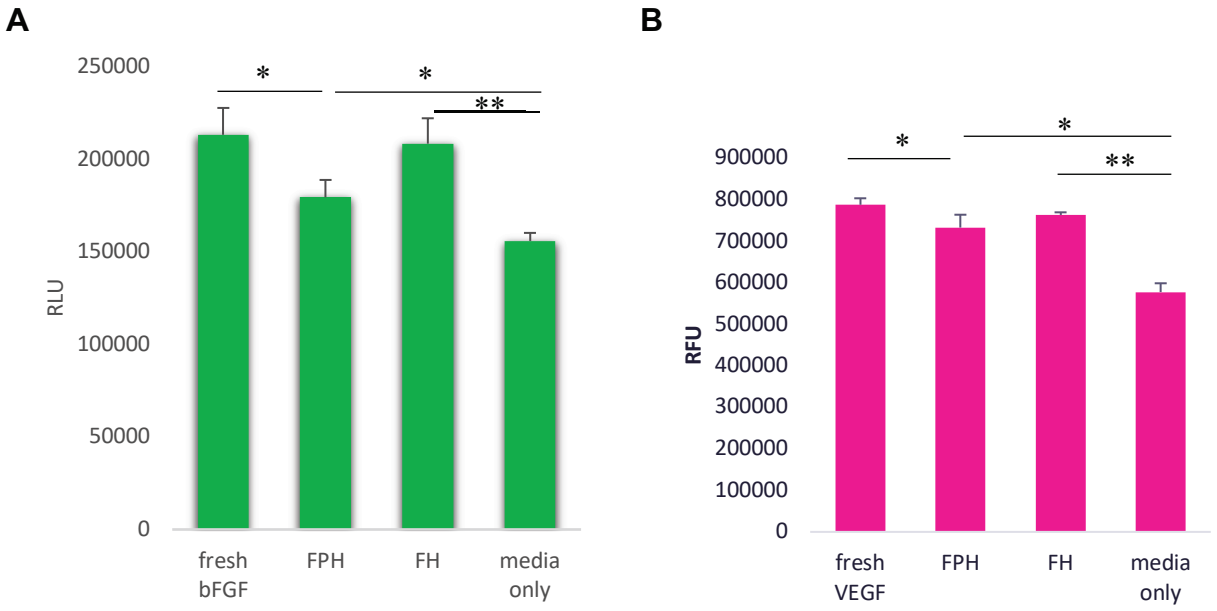

Figure 3.4: Bioactivity of the released bFGF and VEGF on day 15. CellTiter-Glo® Luminescent Cell Viability Assay responses **for: (A)** HdFBs stimulated with fresh bFGF or bFGF eluted from FPH and FH at 15 days. (B) HUVECs stimulated with fresh VEGF or VEGF eluted from FPH and FH at 15 days. *p<0.05 and **p<0.01, n= 3 technical repeats,

At 72 hours, significant 34% and 15% increases in HdFBs numbers relative to the negative control (media only) were observed for bFGF eluted from FH ($p<0.01$) and FPH ($p<0.05$) respectively, while a 37% increase was observed from fresh bFGF ($p<0.01$). Similarly, significant 32% and 27% increases in HUVEC numbers relative to the negative

control were observed for VEGF released from FH ($p<0.01$) and FPH ($p<0.05$), and a 36% increase from fresh VEGF ($p<0.01$). These findings indicated that both VEGF and bFGF released from FH and FPH on day 15 were still bioactive as they were able to induce cell activity significantly above the negative controls that contained no growth factors. Surprisingly, both VEGF and bFGF from FPH showed a significant reduction ($p<0.05$) in bioactivity as compared to fresh bFGF and VEGF indicating a possible moderate denaturation. It is not clear what aspect could be responsible for this as almost all unbound PEG was removed by dialysis and any remaining would no longer have active NHS termini due to prolonged incubation at pH 7.4. However, future analysis of these growth factors eluted from an FP hydrogel might shed some light on this anomaly.

3.2.4 *In-vivo* subcutaneous rat implants for neovascularisation.

In-vitro assays evaluating angiogenesis often aim to induce EC capillary-like tubes, representative of the final stages of angiogenesis with matrix degradation (invasion), new lumen formation and anastomoses. These assays however do not represent the entire angiogenesis process; often using one cell type and overlooking the contribution of other cell types and ECM components. A minimally invasive, rat subcutaneous model assay that is well established in our laboratory was used in this study to evaluate neovascularisation in the different hydrogel formulations (44, 45, 49, 280, 374, 375, 376). This model enables a smaller number of animals to be used as it allows for analysis of up to 6 groups per animal. For this, the different hydrogel formulations, (F, FH and FPH) were polymerised in porous PU discs (described in **section 2.2.3.5**) either with 1 µg VEGF or without VEGF as controls. The PU discs served a supportive function where they enabled hydrogels to be set within pores with diameters that allow vessel ingrowth, and ease of immunocytochemistry preparation post explant and thus more accurate analysis and precise demarcation of the neovascularised area. The prepared samples were thereafter implanted subcutaneously in surgical incisions at the dorsal region of the rats and explanted after 10 days. Since FP behaved similar to F *in-vitro* with growth factor release (**section 3.2.1 and 3.2.2**), F only was used as a control for FPH and to further limit use of animals. After 10 days, the samples were explanted, fixed in zinc, and thereafter processed for endothelium staining (CD31) with immunocytochemistry.

Analysis was then conducted with Visiopharm Integrated Systems software program which was trained to automatically detect CD31 positive ($CD31^+$) structures on imaged cross-sectional samples, and vessel density (vessel per mm^2 and vessel%) was quantified. This approach allowed for detection of vessel ingrowth across the entire cross-section of the centre of the implanted disc thus avoiding the need to select areas with the potential for unconscious bias. To further remove the possibility of bias, when confirming the accuracy of the automated detection the researcher was blinded to the identity of the samples.

Following immunohistochemical staining, $CD31^+$ vessels were observable in all samples (**Figure 3.5A**) explanted after 10 days, indicative of vascularisation into all discs. When these vessels were quantified, an increase in vessel density for all hydrogels containing VEGF, relative to the relevant hydrogel alone, was observed (**Figure 3.5B**). The FH with VEGF had the highest fold increase (**Figure 3.5C**) at 1.2, and this was followed by both FPH (1.1) and F (1.1) VEGF respectively suggesting an increased effect with heparin presence These increases were however not significant ($p=0.23$ for FH; $p=0.34$ for FPH; and $p=0.45$ for F respectively) in relation to the controls. Furthermore, no obvious influence on vascularisation area was observed for VEGF.

A

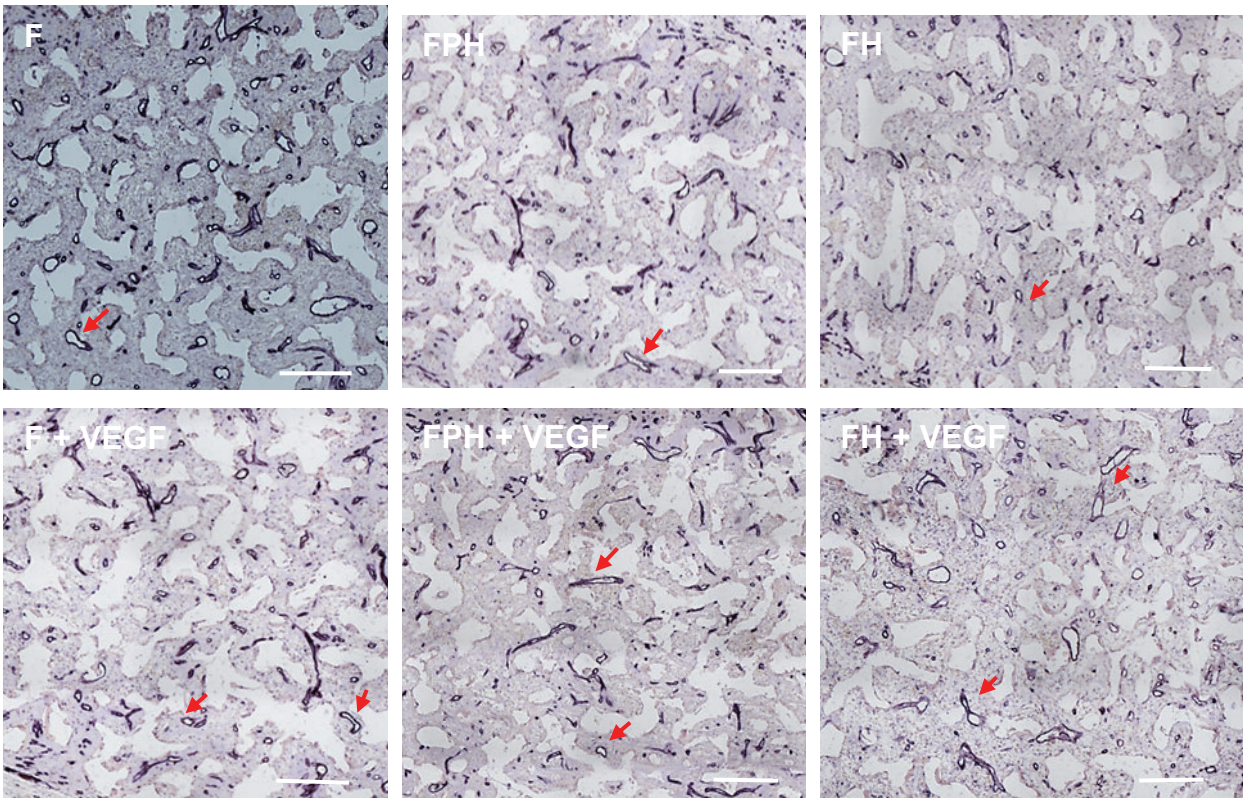

B

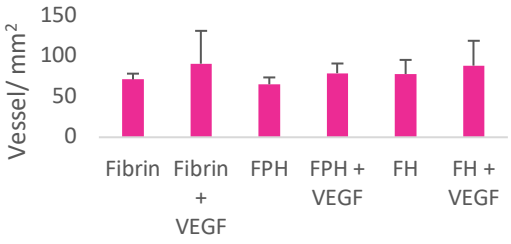

C

	Fold increase (with and without growth factor)
Fibrin + VEGF	1.1
FPH + VEGF	1.1
FH + VEGF	1.2

D

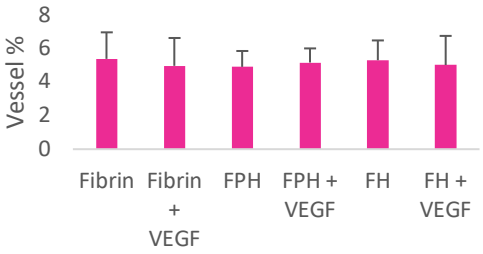

Figure 3.5: Subcutaneous implant neovascularisation after 10 days. (A) Representative cross sectional area micrographs of CD31⁺ stained vessels for F, FPH and FH with and without VEGF. Vessels (red arrows) are observed in all the groups, slightly more pronounced in the FH+VEGF group. (B) Vessel density for F, FPH and FH with and without VEGF. (C) Fold increase indicating a slight increase with FH and VEGF combination. (D) Vascularised area indicated by vessel %. Scale bar = 1000 µm, n=6 samples per group.

This experiment was powered to detect a 20% increase in vessel numbers or vessel area based on variances observed in previous PEG hydrogel growth factor release studies carried out in our laboratory (44, 49). The high fibrin alone baseline neovascularisation (**Figure 3.5D**, 5.5 ± 1.5%) is hypothesised to have contributed to no significant differences being observed between the respective VEGF groups and no VEGF groups. This level of vascularisation is substantially higher than that in empty PU discs or PEG alone or filled discs observed in previous PU and PEG studies in our laboratory (2.2 to 3.2 %). It is even higher than or the same as the growth factor loaded groups (4.5 to 6%). It is possible that such high vessel ingrowth could be due to the pro-angiogenic characteristic of fibrin and might require higher levels of VEGF or a more sustained release (44, 49). The delivery systems in this present study, FH and FPH, were found to deliver 21 ± 2.2 and 18 ± 1.6 ng per day *in-vitro* respectively (**section 3.2.2** and **3.2.3**), and it is possible that these quantities were not sufficient for a significantly higher vascularisation *in-vivo* relative to their respective controls. In a study investigating the effect of VEGF on vascularisation using PU scaffolds, short term (10 days) VEGF released/ osmotically pumped 15 ng/day and generated no significant differences ($p<0.05$) in vascularisation relative to the control PU scaffolds (0 ng/day). Significant differences were only observed at higher concentrations, 150 and 1500 ng/day, with vascularisation directly proportional to the VEGF concentration (374). In the same study, it also was observed that vascularisation can rapidly regress after growth factor withdrawal and this may have been another contributing factor to the results observed in this study. In a heparinised PEG study however, at a lower release rate of 8.75 ng VEGF per day, a significant increase in neo-vessel area was observed (44, 49). These findings require further investigations.

It should be noted that no trace of fibrin could be observed in any discs explanted at 10 days, suggesting that the release rate may have been higher than the *in-vitro* rate due to release caused by hydrogel degradation, but perhaps of a too limited duration. These findings indicate that future studies might need to increase the VEGF concentration or perhaps more usefully the fibrin concentration to delay degradation and thus prolong the release of VEGF over a longer period.

3.2.4.1 Influence of heparin on collagen deposition

During the last phase of the wound healing process, collagen is secreted by wound cells, particularly fibroblasts, to create a scar. In the above *in-vivo* angiogenesis assay, collagen is produced in the pores of the implanted scaffold replacing the hydrogel that was present (49). This likely due to the resemblance of the progression of tissue ingrowth in this angiogenesis model to that observed in the wound healing process and also a foreign body reaction to the PU (377). In regenerative medicine and with the implantation of biomaterials, excessive scarring is undesirable (378). It has been proposed that heparin may be anti-fibrotic, particularly in the liver, but also potentially through limiting collagen production by fibroblasts (378, 379, 380). Therefore, it was considered opportune to determine the density of collagen in the various explants.

The results showed that there was a slight but non-significant downward trend for the FPH (12.0%) and FH (14.2%), compared to fibrin (14.8%) in collagen production (micrographs in **Figure 3.6A**), perhaps indicating an anti-fibrotic effect with heparin. These findings were however not significant. Therefore, in a tissue ingrowth model such as the one used in this study; formation of scar tissue was not impeded by heparin.

A

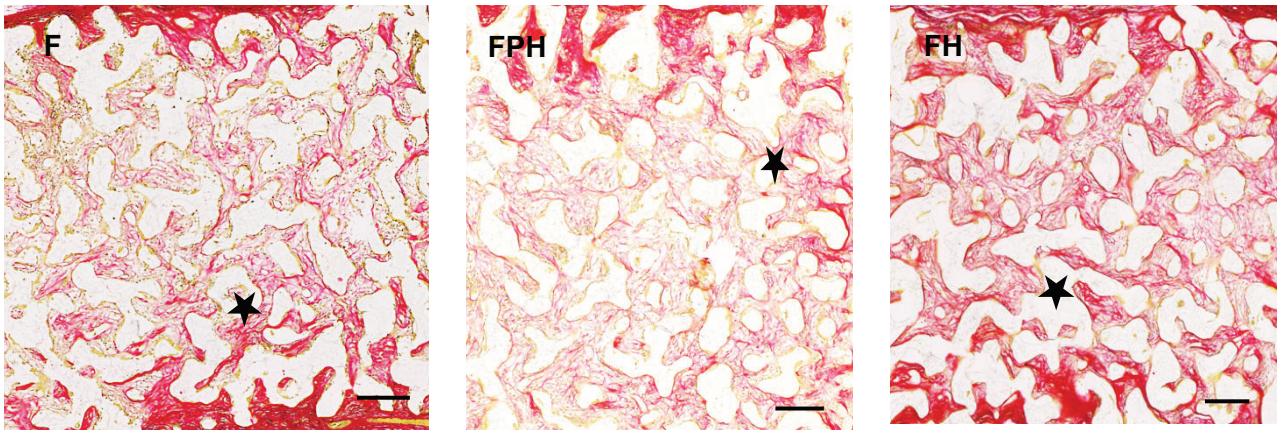

B

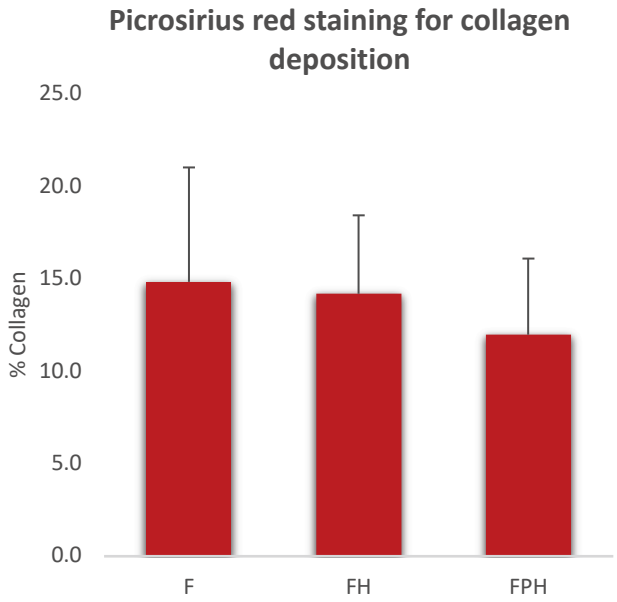

Figure 3.6: Picrosirius red stains for the non-VEGF treated samples. (A) Micrographs showing some collagen deposition (marked with a star) for F, FH and FPH at 10 days. (B) Although a slight downward trend on the % collagen deposition with the presence of heparin was observed, these finding were not significant. Scale bar = 250 μm, n=6 samples per group.

CHAPTER 4: ADIPOSE DERIVED MESENCHYMAL STEM CELL DIFFERENTIATION ON HYDROGELS

4.1 Introduction

Following their discovery by Friedenstein and colleagues in 1976 (381), MSCs were contextualised as a promising cell-based therapy approach due to their self-renewal, immunomodulatory phenotype and multipotency characteristics (381). Their immunomodulatory phenotype has set them apart from all other stem cells as it gives them anti-inflammatory properties and presents them with a unique potential to overcome the immune system's allorecognition due to the absence of MHC class II antigens as well as low levels of MHC class I antigens (363). Because of this characteristic, MSCs do not succumb to immune rejection which is significant for a successful transplant across major histocompatibility barriers (382, 383, 384). Equally, their multipotency distinctly gives them the ability to differentiate into several lineages including osteocytes, chondrocytes, and adipocytes under correct environmental conditions, and this feature is used to characterise isolated MSCs (385). To date, MSCs are sourced from various tissue including bone marrow, Wharton's jelly, and adipose tissue, and have been applied up to and including clinical trials (382, 386). For instance, a four year follow up to a 12-month randomised, double-blind, placebo-controlled phase II trial showed that bone marrow derived MSCs injected intramyocardially could improve myocardial mass as well as infarction for patients with ischaemic heart failure in a dose-dependent manner, and a further significant reduction in scarred tissue, indicating their therapeutic benefit in tissue repair (387).

The therapeutic benefits of MSCs have drawn the attention of researchers, more especially their mechanisms which are yet to be fully understood. A great body of evidence has presented a strong argument that MSCs achieve their regenerative function through paracrine effects with biochemical cues (369, 370). That is, MSCs secrete bioactive factors such as growth factors and cytokines with trophic and chemoattract paracrine effects, capable of inducing and modulating tissue repair signalling pathways

at cellular level (388, 389, 390, 391). In context, both Katagiri et al., 2017 (392) and Kawai et al., 2015 (393) showed that media from bone marrow derived MSCs encouraged angiogenesis by upregulating the expression of angiogenic markers such as VEGF-A. Conditioned media generated from MSCs has also shown *in-vitro* and *in-vivo* to have cardiac repair and healing effects (394). This includes improved endothelial function, inhibition of fibrosis and inflammation, induction of tissue granulation and encouraging angiogenesis (394). While the benefits of MSCs are clear, there are still bottlenecks with transplant application as the effectiveness of MSC-based therapies has been shown to be dependent on cell viability upon administration. Occurrence of cell death and cells directly injected into an injured site can be washed off, and this loss needs to be compensated for (212). For these reasons, hydrogels, as delivery vehicles, are being investigated for their potential to protect, support, and deliver the cells at their target site for application.

The MSC application in tissue regeneration usually targets differentiation that is induced and influenced by several factors biochemically such as media supplements, cytokine cues, and mechanically such as matrix stiffness, elasticity, and forces (395). *In-vitro*, biochemical cues are added to media to form specific differentiation media that directs the MSCs to commit to a specific cell lineage depending on the induction cues added (395). In contrast, mechanical stimulation from matrix elasticity or forces or even a combination thereof in the surrounding matrix induces MSCs to commit to a specific lineage in response to the stimulation (396). This effect is observable during embryonic development where mechanical forces guide tissue patterning and organogenesis (396). For instance, branching morphogenesis for alveolar formation (lung development) relies on actomyosin-mediated cell contraction (in addition to biochemical cues). Equally, this is true for mechanical distention (through breathing) in the foetus, where during the breathing the diaphragm contracts to increase the thoracic cavity volume, which in turn stretches the developing lungs and potentially influence development by increasing cell proliferation (396). The MSCs also exert actomyosin contractile forces to neighbouring cells and the ECM, and equally experience external tensile, shear, and compressive forces from their surroundings. These external forces are transferred to neighbouring cells and ultimately encourage the cells to adhere to the ECM as well as to each other

(cell-cell interactions) to induce intrinsic signalling pathways for differentiation (397, 398). Furthermore, matrix stiffness has been shown to guide MSC differentiation. For instance, naïve human MSCs were seen to commit to lineages specified by matrix elasticity *in-vitro* under specific biochemical cues (399). A soft matrix (1 kPa) that mimics soft tissue such as the brain, was shown to favour neurogenesis. In contrast, a stiffer one that is comparative to collagenous bone tissue (34 kPa) supported osteogenesis, reiterating that the matrix onto which MSCs are cultured on plays a significant role in dictating lineage (399).

Since conventional surfaces such as TCP have been shown to often lead to MSC pluripotency and proliferation loss with time, hydrogels have been proposed as a better matrix for maintaining the pluripotency as they resemble the ECM, (328, 400), while heparin inclusion in culture has been shown to promote proliferation through paracrine mechanisms (401). Simann et al., 2015 (402) demonstrated that free heparin in TCP culture enhanced human bone marrow MSC osteogenic differentiation through BMP-2 induction. It was shown that ALP mRNA levels increased 2.3 higher when 20 U/ml unfractionated heparin was supplemented each day compared to those without heparin supplementation for human bone marrow MSCs cultured for 14 days (402). Although progressive, it is challenging in several ways including the need to continuously supplement culture with the heparin, and susceptibility to pluripotency loss with culture on TCP remains (402). For these reasons, culture on heparinised hydrogel matrices present as a more viable approach.

Investigations of heparinised hydrogel matrices on osteogenic differentiation are still scarce. Heparin acrylated PEG hydrogels (10wt%) were shown to be a better matrix for a five week osteogenic differentiation process of 3D human MSCs (403). This was indicated by a consistent increase of ALP osteogenic biomarker gene expression relative to the control without heparin, and by day 35 this increase was 4-fold higher relative to the control. The lack of hydrogel stiffness evaluation in this experiment was however a limitation. Equally, literature looking into the effect of heparinised hydrogels on MSC adipose differentiation is limited. Kim, Kim & Tae, 2013 (328) demonstrated that heparinised hyaluronic acid hydrogels were a superior environment than TCP for human

ADSCs adipogenic differentiation.. This effect could be modulated by the amount of heparin and elasticity of the hydrogel. Heparin was found to be a good adipogenic differentiation inducer and the softer matrix (± 400 Pa) shown to be a better platform for differentiation than the hard TCP that resulted in gradual loss of pluripotency with culture time. Again, using heparinised hyaluronic acid PEG hydrogels, Gwon et al.,2017 (400) confirmed that a combination of both hydrogel attached heparin and a softer hydrogel encouraged ADSCs differentiation *in-vitro* as indicated by increased adipogenic differentiation markers adiponectin, adipocyte protein 2 and peroxisome proliferator-activated receptor, compared to control hydrogels without heparin and those of higher stiffness (400). Additionally, differentiation on heparin hydrogels proved to be a better environment for maintaining pluripotency compared to TCP, and this was indicated by the upregulation of mRNA markers associated with pluripotency including octamer-binding transcription factor 4, sex determining region Y-box 2 and expression of stage-specific embryonic antigen-4. These findings point towards the benefits of using heparinised hydrogels for differentiating MSCs (400). This chapter thus aimed to evaluate the two hydrogel systems, FH and FPH, for their role in ADSCs differentiation and whether they were superior to TCP.

4.2 Results and discussion

4.2.1 Functional characterisation

The ADSCs previously isolated from epididymal fat pads of male rats using collagenase and subsequent adhesion during culture were obtained from our laboratory's cell repository with ethical approval granted. Prior to storage, these cells had been characterised for ADSC markers (positive for CD29, CD44 and negative for CD31, CD34 and CD49d) and multipotency (404). Their multipotent stem cell nature was re-confirmed in this study by first assaying the ADSCs (passage numbers less than 5 for all experiments) for their ability to differentiate into either adipocytes or osteoblasts. For this, quality control experiments were performed on TCP with adipogenic induction carried out initially for 14 days in adipogenic media (AM) and osteogenic differentiation for 21 days in osteogenic media (OM), with media changes every three days. Experimental controls (normal culture media without induction cues) were cultured along the experiments. At the end of the induction periods, cultured cells were assayed for differentiation using cellular staining methodologies. The extent of adipocyte induction was detected by staining with Oil Red O and that for osteogenic induction with Alizarin Red S. The former and latter detect the presence of lipid droplets and calcium deposits respectively, indicative of adipocyte and osteoblast formation. Oil Red O adipocytes were eluted with 100% isopropanol, while Alizarin Red S stained calcium deposits with 10% acetic acid for quantification.

Adipocyte droplets (indicated with red arrows in **Figure 4.1A, D7**) were more pronounced on day seven and at later time points (day 14) these decreased in quantity perhaps due to cell senescence induced by AM as there were cells that appeared more spindle shaped than circular (indicated with black arrows in **Figure 4.1A, D14**). Due to this, day seven was used as the final time point in later studies. Quantified eluted stain from Oil Red O stained differentiated adipocytes (**Figure 4.1B**) was significantly higher ($p<0.05$) than the control (**Figure 4.1C**), confirming a successful adipocyte differentiation process as observed in the micrographs in **Figure 4.1A**.

A

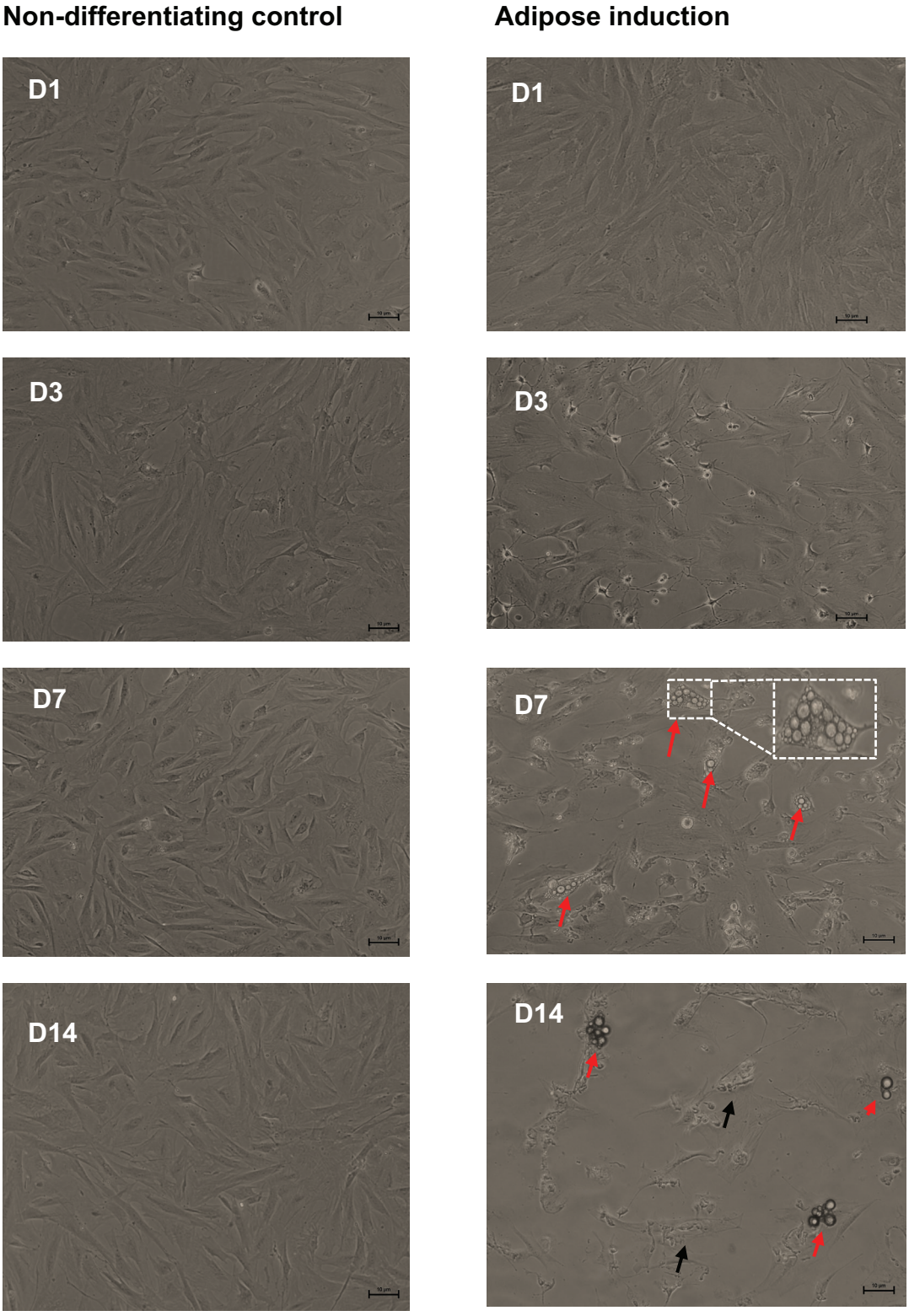
Non-differentiating control
Adipose induction
D1
D1
D3
D3
D7
D7
D14
D14

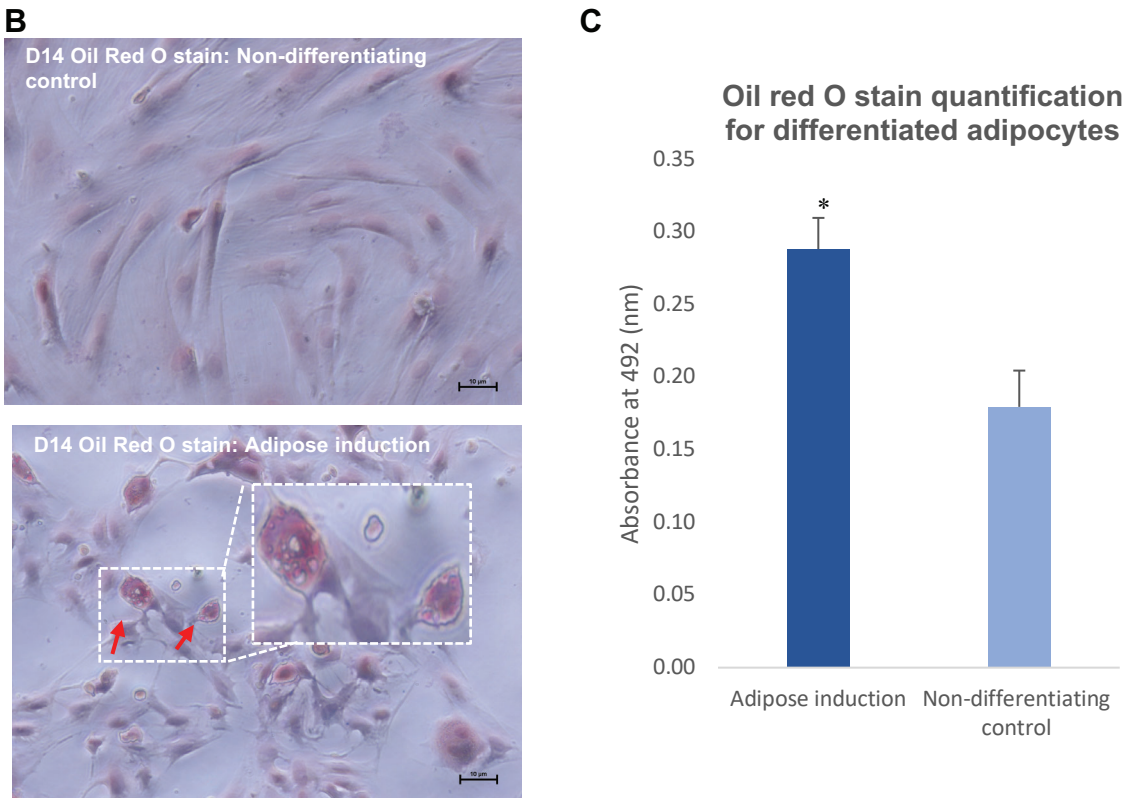

Figure 4.1: ADSC functional characterisation with adipose induction for 14 days. (A) Representative images of non-differentiating (non-differentiating control) and differentiating (adipose induction) ADSCs over 14 days. Adipocytes were more pronounced on day seven (red arrows on day 7) and thereafter decreased, possibly due to senescence, as observed on day 14. Black arrows indicate potential cell senescence at day 14 compared to day 7. (B) Oil Red O stained of adipocytes at day 14. (C) Oil Red O stain significantly higher in the adipose induction experimental group (* $p<0.05$) compared to the non-differentiating control group as indicated by the quantification of eluted stain on day 14, * represent adipogenic induction significant increase against non-osteogenic induced control at $p<0.05$. Scale bar = 10 μm, n=3 technical repeats with each hydrogel set in its individual well.

Osteogenic induction results also showed that the ADSCs were able to differentiate into osteoblasts over 21 days as indicated in **Figure 4.2A,** with calcium deposits (red arrows) that stained positive for Alizarin Red S stain (**Figure 4.2B**). When the stain was quantified after extraction with 10% acetic acid, there was significantly more stain present in the induced group (**Figure 4.2C**), compared to the control group. Therefore, multipotency of the ADSCs was successfully confirmed before proceeding to the next set of experiments with these cells.

A

Non-osteogenic induced control

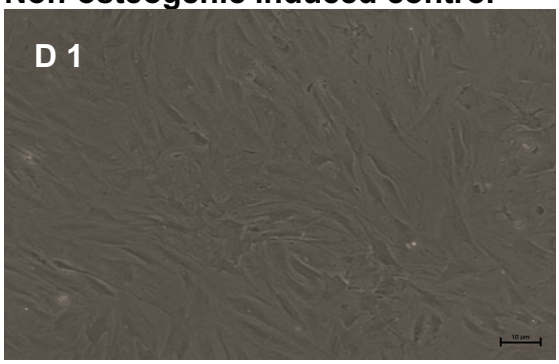

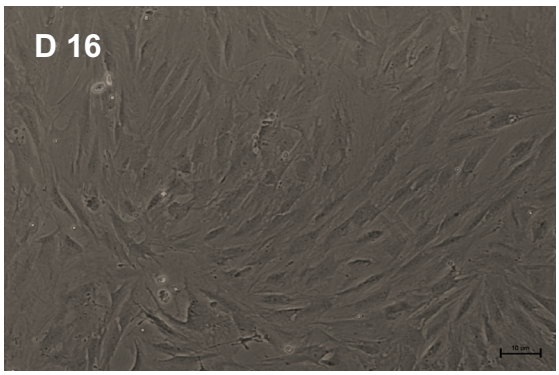

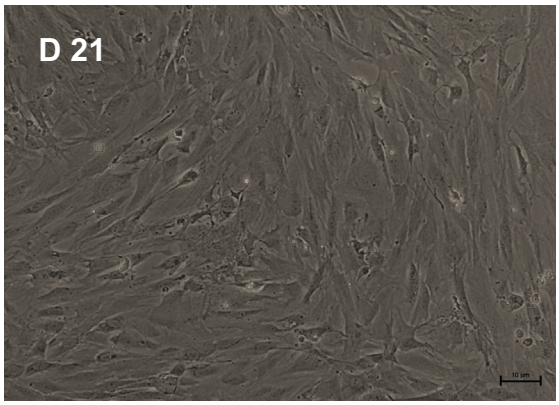

Osteogenic induction

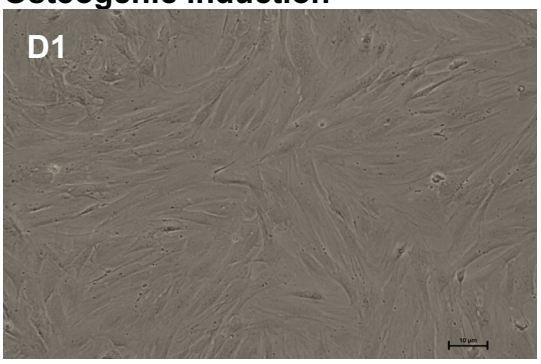

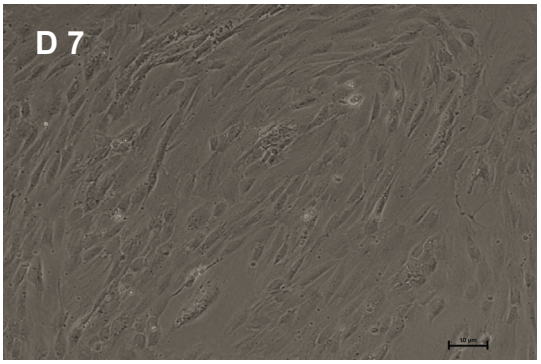

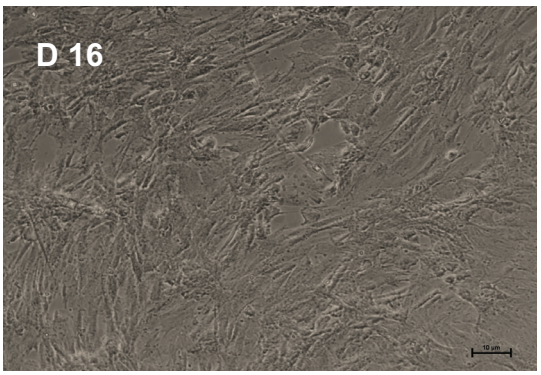

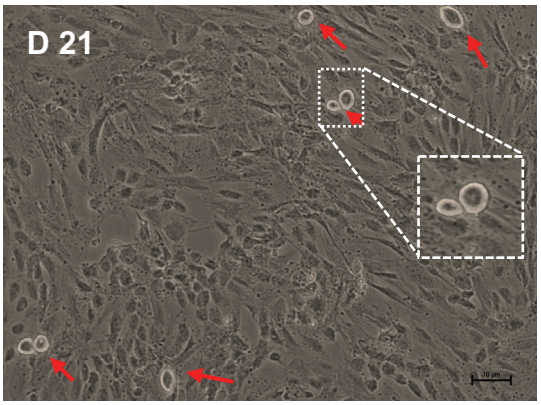

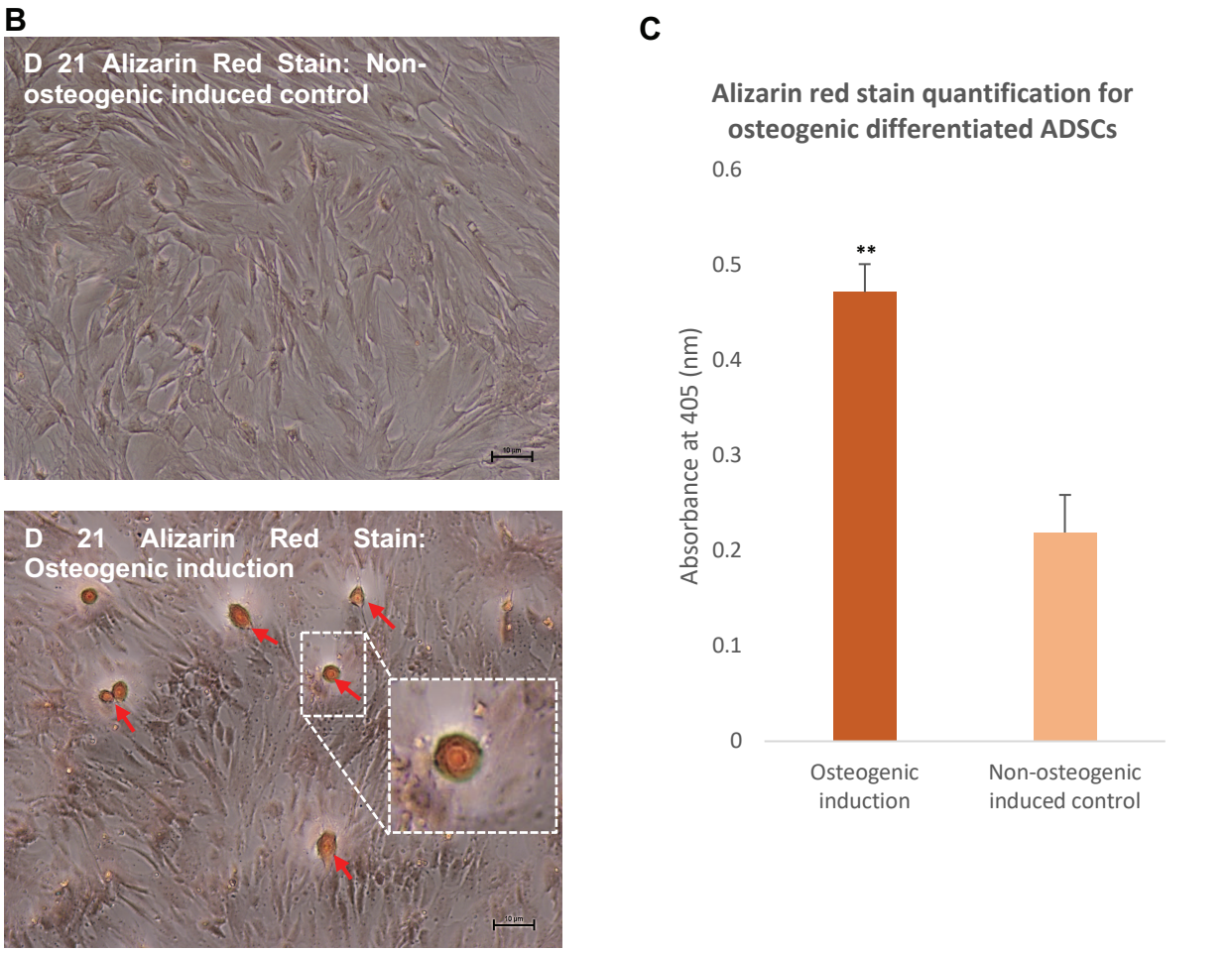

Figure 4.2: ADSC functional characterisation with osteogenic induction for 21 days. (A) Representative images of non-differentiating (non-differentiating control) and differentiating (adipose induction) over 21 days. Red arrows indicate differentiated cells. (B) Alizarin Red stained of adipocytes at day 21. (C) Alizarin Red stain significantly higher in the osteogenic induction experimental group (** $p<0.01$) compared to the non-differentiating control group as indicated by the quantification of eluted stain on day 21. ** represent osteogenic induction significant increase against non-osteogenic induced control at $p<0.01$. Scale bar = 10 µm, n=3 technical repeats with each hydrogel set in its individual well.

4.2.2 *In-vitro* cytocompatibility

To assess cytocompatibility of the modified fibrin hydrogels, ADSCs were encapsulated in the different hydrogel formulations (fibrin and heparinised fibrin) and thereafter cultured for seven days in culture media. A live/day assay (**described in section 2.2.4**) was conducted on days three and seven; with cells imaged with a confocal microscope and images analysed on ImageJ cell counter plugin. Live cells appeared green, and dead cells appeared red.

The results showed that on day three, all hydrogel formulations had high viability (above 80%), indicating their non-cytotoxicity as indicated in **Figure 4.3**. At day three, cells were more spread out in the FH and FPH group compared to the F, FP, and Fand H groups, suggesting that the presence of heparin in these samples potentially contributed to cell spreading. At day seven, viability in all groups decreased by no more than 17%, perhaps due to a decrease in supportive biochemical cues with time (no media change occurred). This decrease was significant for FP ($p<0.01$) and FPH ($p<0.001$). Viability however remained above 70% in all groups, indicative of good cell viability and non-cytotoxicity.

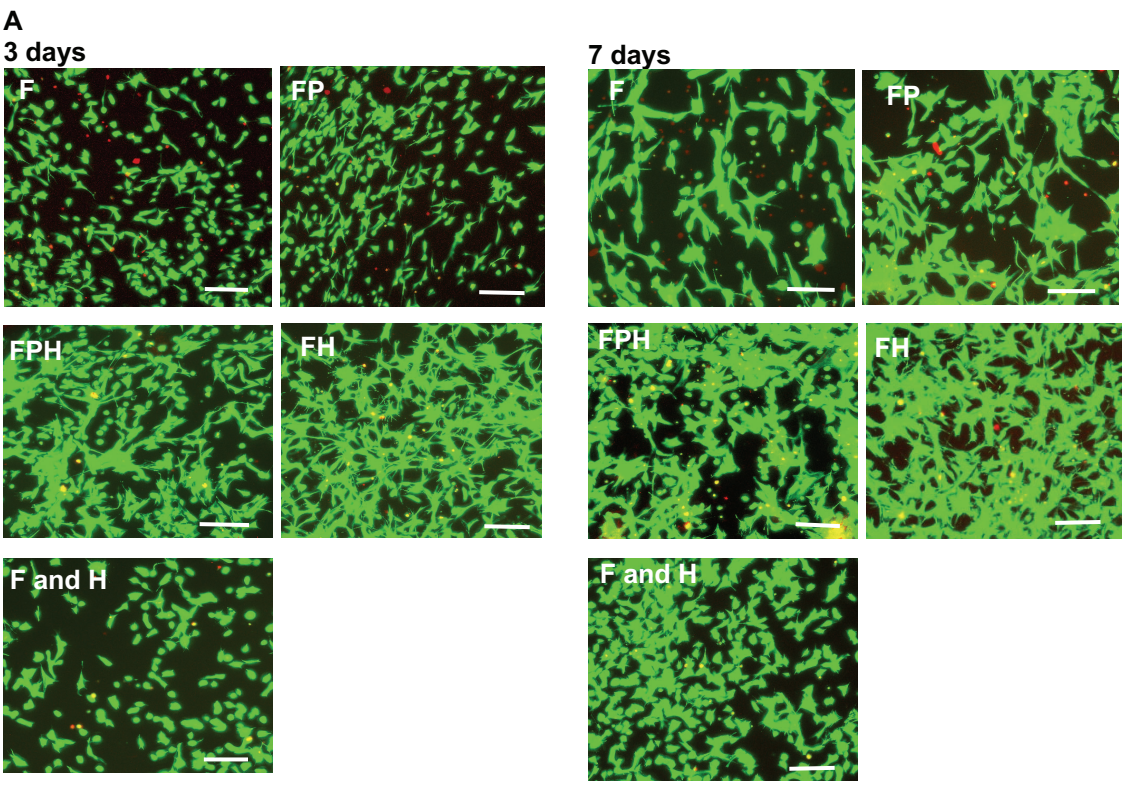

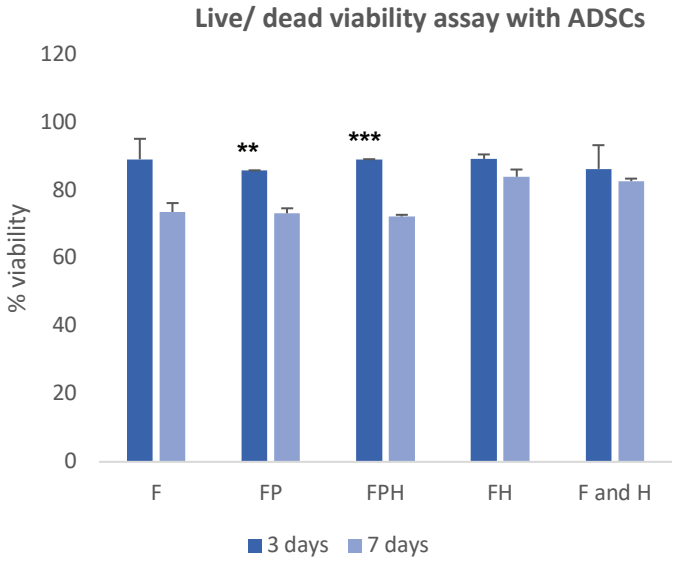

Figure 4.3: Live/ Dead cell viability assay for 3D hydrogel encapsulated ADSCs at 3 and 7 days. (A) Micrographs for live/ dead assay with green = live and red = dead. (B) Cells were viable with no significant decreases between 3 and 7 days. ** and *** represent day 3 significant decrease against day 7 at $p<0.001$ and $p<0.001$. Scale bar = 100 µm, n=3 technical repeats with each hydrogel set in its individual well.

4.2.3 Influence of bound heparin on ADSCs differentiation

Once the ADSCs were characterised and checked for viability in the different hydrogel formulations, the impact of heparin on cell differentiation was evaluated. Although limited, there is some evidence (**section 4.1**) that suggests that hydrogels functionalised with heparin can accelerate the differentiation process compared to hydrogels without heparin (328, 400). For these experiments, 200 µl hydrogels with aprotinin were polymerised in tissue culture well plates, and thereafter 10 000 ADSCs seeded on top of the polymerised hydrogels. For adipogenic differentiation, culture medium was replaced with AM after three days of culture and thereafter changed every three days for seven days. For osteogenic differentiation, culture media was replaced with OM after overnight incubation and changed every three days for 15 days to ensure that fresh and sufficient ingredients were received by the cells. Control wells received only culture media that was also changed every three days for the duration of the experiments.

After 24 hours of incubation, ADSC on PEGylated hydrogels (FP and FPH) surprisingly changed morphology without culture media being changed. They elongated to form tubes connected by colonies/ clusters (black stars) of cells as indicated in **Figure 4.4B**. It was hypothesised that this could have been influenced by the PEGylation process (**see section 1.5.6**) as it has previously been shown that PEGylation increases tube formation and cell migration by covering the RGD cell adhesion sites through the primary amino group of arginine binding to PEG-NHS thus reducing traction forces and in turn enabling cell migration (239, 299). In chapter three, a similar effect was observed with HUVECs cultured in 3D (in 2% FBS), however the difference between the FP to F were not large enough to produce a significant difference. Perhaps the effect is more pronounced in 2D as observed in this chapter where the migration was significantly different (qualitative observation from micrographs, depicted in **Figure 4.4B**) to the F. Furthermore, ADSCs in this current chapter were seeded in 10% FBS containing media as compared to 2% for HUVECs in chapter three. It is possible that the growth factors in media could have accentuated the sensitivity of the migration and tube formation processes (389, 405). Additionally, it was speculated that matrix stiffness could have also had an impact in tube

formation. In this study, FP (18.3 ± 1.3 Pa) and FPH (17.6 ± 2.7 Pa) had no significant differences between them while both were significantly softer than F (42.1 ± 1.5) and FH (36.7 ± 1.9 Pa) (**section 2.2.3.6**). While the influence of stiffness on cell migration and tube formation remains an active area of research, there is increasing evidence that cell migration is highly influenced by matrix stiffness (406, 407, 408). Cells can sense and respond to changes in mechanical properties by releasing specific mechanosensory proteins linking the actin cytoskeleton and ECM. However, though as described above, there are significant differences in stiffnesses between the PEGylated fibrin (FP and FPH) and the stiffnesses investigated in the literature. Those in literature, are almost exclusively higher (>100 Pa) and the relative differences between experimental groups studied much greater (>500 Pa) than present in this study (408). It is thus challenging to determine how stiffness might have impacted on the above.

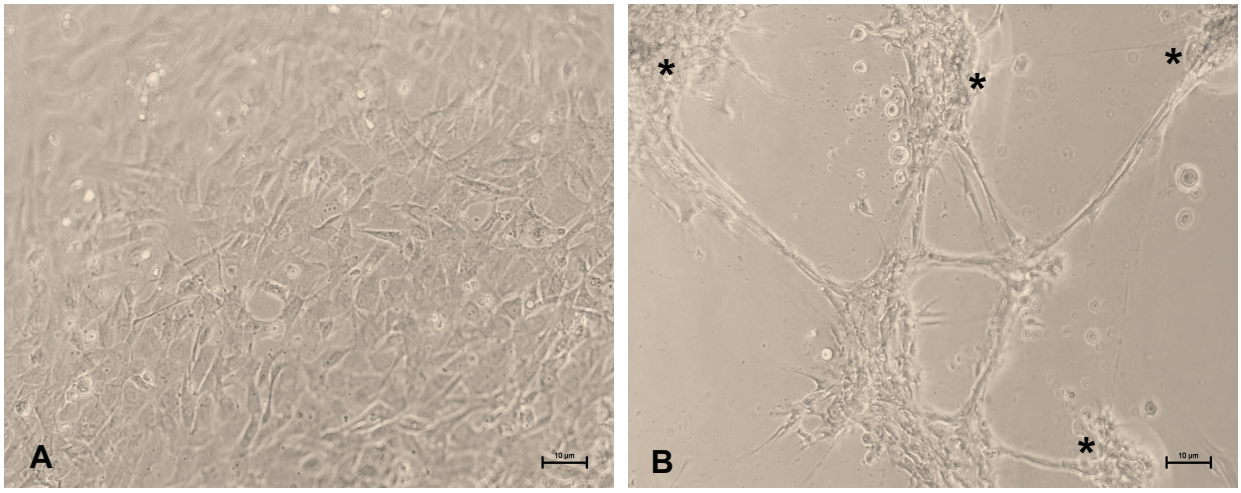

Figure 4.4: **2D seeded ADSCs after 24 hours seeding**. (A) No morphological changes in the stiffer hydrogels, fibrin (F) and fibrin-heparin (FH). (A) Change in morphology in the less stiff PEGylated hydrogels, fibrin-peg (FP) and fibrin-peg-heparin (FPH). Formed clusters marked with a black asterisk. Scale bar = 10 µm.

Regardless of the cell morphological changes that occurred in the FP and FPH, the induction processes proceeded, and these changes did not hinder the differentiation process. At the end of the seven-day induction process and Oil Red O stain, clusters of intense Oil Red O stained droplets were observed on hydrogels (**appendix C**) in all groups at varying degrees. For osteogenic differentiation, the cell clusters in the FP and FPH showed intensely stained but limited numbers of calcium deposits over the 14-day

differentiation period. There was also a substantial retention of both stains within the hydrogels. Therefore, the amount of stain incorporated into cells exposed to induction media was determined by subtracting the absorbance eluted from control cells cultured on the corresponding hydrogel in the absence of induction media.

Spectrophotometric quantification of the eluted Oil Red O and Alizarin Red stains at the end of the induction period showed that differentiation on hydrogels was significantly ($p<0.001$) increased across all groups compared to TCP (**Figure 4.5**). For adipogenesis this likely reflects the well-established influence of soft hydrogels on preferential differentiation of MSC towards adipocytes (210). Though the mechanisms are still under study, according to Mao et al.,2015 (409), Vining et al., 2017 (397), and Hu et al., 2023 (410) mechanical forces contribute in directing MSC differentiation where forces prime signalling pathways, related to the differentiation lineage, by increasing biochemical signalling molecules related to the specific pathway in response to the matrix elasticity. Interestingly, there are a number of studies that have found that fibrin hydrogels, though of low stiffness, stimulate osteogenesis and bone formation of MSCs and this might be the reason for the increased calcium content observed here for all cells cultured in osteogenic differentiation media in all hydrogels (all are fibrin based) (210, 412).

The effect of covalently bound heparin on adipocyte differentiation in this study is suggestive that heparin does have an influence but it is not conclusive. FH hydrogels resulted in a significant increase in lipid accumulation relative to FP hydrogels ($p < 0.05$), and the FPH as well as the F + H hydrogels were trending towards an increase relative to FP ($p=0.073$ for both FPH as well as F + H vs FP) (**Figure 4.5A**). Thus, if there is an influence, it is possibly due to the presence of heparin but not indicative of the need for binding of heparin to a hydrogel. These findings tend to support previous studies (described above) that found heparin to stimulate adipogenesis (328, 400). Interestingly, FH was found to further stimulate osteogenesis above that induced by fibrin itself and was significantly elevated relative to all other fibrin groups ($p<0.05$) (**Figure 4.5B**). FPH had no accumulative effect which indicates that either the increased stiffness of FH or its better-preserved structure was needed in combination with bound heparin to induce this effect. As all the hydrogels here are of very low stiffness, it might be speculated that it is

the structure that may be of greater importance. These findings generally support an enhancement of differentiation of MSCs by heparin particularly for osteogenesis. It is possible that FH may be a promising substrate for delivery of MSC for the regeneration of bone.

It is crucial to delineate the limitations of these present findings. As this was a pilot study designed with limited resources to explore the influence of heparin and the matrix, it is essential that future studies incorporate gene expression studies as well as optimised staining methodologies that account for fibrin binding. Resources were limiting in this study to perfume gene expression studies. The influence of varying the concentrations of both heparin and fibrin would also inform on the nature of the interaction between bound heparin and unPEGylated fibrin on osteogenesis.

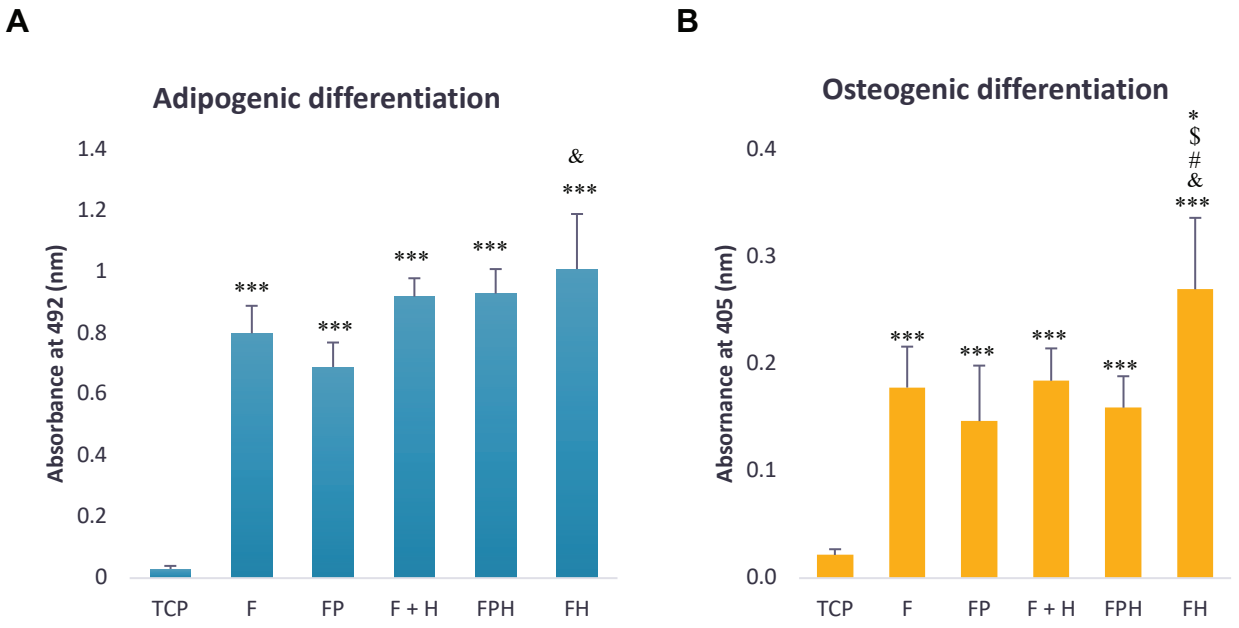

Figure 4.5: Adipogenic and osteogenic ADSC differentiation on hydrogels compared to tissue culture plastic. (A) Adipogenic differentiation indicating all hydrogels being superior to tissue culture plastic as a matrix for differentiation. FH was significantly higher than FP, suggesting a combination effect of a matrix with bound heparin increasing differentiation. (B) Osteogenic differentiation on hydrogels indicating all hydrogels being superior to tissue culture plastic as a matrix for differentiation. Differentiation in FH was also significantly higher than all groups. (* represents FH significance against FPH at $p<0.05$; $ represents FH significance against F + H at $p<0.05$; # represents FH significance against F at $p<0.05$; & represents FH significance against FP at $p<0.05$; *** represents significance of all groups against TCP at $p<0.001$). n=3 technical repeats with each hydrogel set in its individual well.

CHAPTER 5: CONCLUSION

In overall, this study aimed to develop a heparinised fibrin hydrogel as a bioactive delivery reagent, that polymerises without the need for additional fibrinogen, and further characterise the regenerative medicine potential of such a modified hydrogel. With their high-water content and polymeric biomaterial combination, hydrogels can human tissue.. Fibrin is an ideal biomaterial for this due to its FDA approval as well as its inherent biocompatibility and biodegradability with degradation products that are non-cytotoxic.

Fibrin is formed from natural fibrinogen polymerisation by the protease thrombin in the presence of Ca^{2+}. It binds several cell types, and angiogenic growth factors through its natural RGD sequences at positions Aα95–97 and Aα572–574, and the HBD respectively. It thus supports cellular processes such as cell migration, vessel formation and vascular infiltration as demonstrated during the wound healing process. In particular, angiogenic growth factors such as VEGF and bFGF have been of particular interest in regenerative medicine due to their demonstrated role in stimulating neovascularisation during the wound healing process and tissue repair. Fibrin is thus an attractive delivery reagent in regenerative medicine. Although fibrin alone can bind these angiogenic growth factors for delivery, it is only able to release them for a short period of time without any sustained release. Heparinisation of fibrin was proposed in this study to enhance this as heparin is a natural polyanionic ECM polysaccharide that binds VEGF and bFGF through their HBD.

In the first chapter, hep-acr that preferential binds to thiols through spontaneous thiol-acrylate Michael-type addition reactions were successfully utilised to heparinise fibrinogen through two methods that retained its ability to polymerise without the need for additional fibrinogen as in previous studies. Hep-acr was directly bound to fibrinogen in the first method. In the second method, NHS-PEG-SH was used in attempt to increase heparin binding by increasing the amount of free thiol in fibrinogen, and after dialysis 0.8 thiols per fibrinogen molecule were bound which is an increase of more than a hundred-fold relative to unmodified fibrinogen. After removal of unbound heparin through dialysis, two different heparin quantification methods showed that between one heparin molecule

was bound every two to three fibrinogens. The higher binding was derived from the more direct fluorescent Heparin Red® assay and it is possible that this is the more accurate assay relative to the modified MBTH assay developed for this study. Interestingly, no significant difference in heparinisation levels was detected between the one and two step methods and it is not clear why additional free thiols did not increase binding. It should be noted that heparinisation of PEGylated fibrin did result in reduction of free thiols approximately equivalent to heparin molecules bound.

All hydrogels (F, FP, and FH) successfully polymerised with 1 unit/ml without delaying gelation, while the FPH needed 4 units/ ml fibrinogen thus suggesting a possible modification that influenced thrombin action and the polymerisation process. Thromboelastography showed that the anti-thrombotic potential of heparin was preserved after coupling to fibrinogen. These hydrogels were biocompatible as indicated by the viability of HUVECs at 72 hours and HdFBs at seven days. The FH hydrogel allowed for more rapid invasion by sprouting HUVECs in 3D, compared to unmodified fibrin suggesting that this was due to bound heparin as both FP and F and H did not result in similar levels of invasion. Additionally, the more fibrous structural feature of the FH (together with the bound heparin), compared to the sheet like FPH was hypothesised to also contribute to this more rapid invasion. Addition of PEG alone or in combination with hep-acr reduced stiffness significantly in all hydrogels, while heparin neither reduced nor increased stiffness. PEGylation was further found to increase resistance of fibrin to proteolytic degradation where the presence of PEG extended unmodified fibrin's half-life (from complete degradation at day five day nine), and interestingly a more enhanced effect was observed with the combination of PEG and heparin (57.5 ± 6.2% degradation by day 15). This increased stability is desirable as a limitation of fibrin as a regenerative medicine scaffold is its rapid degradation. Addition of PEG molecule also resulted in the formation of more transparent hydrogels relative to fibrin. This transparent feature is advantageous as it enabled phase contrast viewing of cell behavior in 2D and 3D more conveniently compared to the turbid hydrogels.

In the second chapter, heparinisation significantly increased binding of bFGF and VEGF and sustained their release for at least 15 days. Sustained release is crucial for

maintaining therapeutic levels over time. The VEGF was released at higher rate over the 15 days, compared to bFGF and this is likely due to the enhanced affinity of bFGF for heparin. The released growth factors were still bioactive at day 15. *In-vivo*, a rat subcutaneous model study found no significant increase in neovascularisation due to heparinisation and binding of VEGF. It is speculated that this negative finding stems from the high levels of vessel ingrowth stimulated by fibrin itself and the apparent rapid degradation of the hydrogels. Further investigations into higher fibrin and VEGF concentrations are required. Additionally, in this study heparinisation of fibrin did not impede collagen deposition after implantation in the rats.

In the final chapter, fibrin was found to stimulate differentiation of ADSCs towards both adipocytes and osteoblasts compared to TCP, supporting relevant literature in this area. Most compellingly, binding of heparin to fibrin was found to further significantly enhance osteogenesis suggesting that the FH hydrogels may have potential as delivery vehicles for MSC in bone regeneration therapies.

In conclusion, this thesis presents novel ad innovative methods for heparinising fibrin for bioactive delivery hydrogels with potential applications in tissue regeneration for damaged and injured tissues. It contributes to advancing the understanding of growth factor delivery systems in regenerative medicine, emphasising the role of heparin in achieving sustained release, enhancing stem cell differentiation, and promoting tissue regeneration. Future research could build upon this thesis by investigating the specific mechanisms underlying heparin binding to fibrinogen, optimising concentrations of growth factors like VEGF and fibrin to maximize neovascularisation and conducting gene expression studies to quantify biomarkers related to adipogenesis and osteogenesis. Comprehensive preclinical studies will be critical for establishing safety and efficacy profiles in animal models, laying the foundation for subsequent clinical trials aimed at demonstrating therapeutic benefits in human subjects and meeting regulatory standards for clinical adoption. This translational research is essential for addressing clinical needs in conditions such as chronic wounds, myocardial infarction, bone damage, and osteoarthritis.

CHAPTER 6: MATERIALS AND METHODS

6.1 Heparin acrylate preparation

The heparin acrylate (hep-acr) used in this study was previously prepared in Professor Bezuidenhout's Polymer Laboratory as described by Rensburg et al., 2017 (45, 297). Acrylates were desired for their reactivity and highly preferential binding to the thiol groups in cysteine side chains via 1,4- addition Michael type additions. Briefly, a heparin/heparan sulfate solution was deprotonated and reacted with acrolyl chloride for an hour, thereafter, filtered and the hep-acr/heparan sulfate solution precipitated. This mixture was then vacuum dried, purified by dialysing against deionized water and finally freeze-dried for long-term storage. Acrylation was achieved on the secondary hydroxyls of the heparin and ^{1}H NMR revealed that percentage was calculated to be 40% of the heparin disaccharide units were acrylated, with hep-acr molecular weight at 15.9 kDa.

6.2 One step fibrinogen heparinisation

In the first method of fibrinogen heparinisation, we explored direct hep-acr binding to fibrinogen's backbone thiols (-SH) and amines (-NH2) groups through Michael addition reactions. It was targeted that these would act as nucleophiles that react with the α, β-unsaturated carbonyl of the arylates and thus forming 1,4-addition type additions. For this, 40 mg/ml working concentration of fibrinogen was prepared in PBS at pH 7.4, and thereafter diluted such that the working concentration was at 10 mg/ml. A concentration of 0.6 mg/ml hep-acr was then slowly added to this fibrinogen solution at room temperature under sterile conditions. The heparin concentration used in this study was chosen based on lab's previous unpublished data where it was shown that this concentration could bind and release growth factors at a controlled rate, and concentrations higher than this were found to induce serious hemorrhage in rats after implantation. The heparin-fibrinogen mixture was then incubated at 37°C for 6 hours, and thereafter cooled down before dialysis. Incubation times were optimised by comparing four incubation times 0, 2, 4 and 6 hours. After optimization, 6 hours was found to be the optimum time that showed significant hep-acr binding and thus used in this study.

Experiments were conducted in three biological repeats (n=3) and a student's t-test used for statistical analysis.

6.3 Two step fibrinogen Heparinisation

6.3.1 PEGylation

Additional free thiols were added to fibrinogen through PEGylation as it was envisioned that this will ultimately increase heparin binding via the thiol-acrylate Michael-type addition reactions. Four PEG molecules, namely NHS-PEG-SH (3.4 kDa), SG-PEG-SH (3.4 kDa), SPA-PEG-SH (3.5 kDa), and NHS-PEG-SH (10 kDa), were compared for their ability to yield the optimum bound thiols in NHS ester reaction chemistry at 1:10 molar ratio. For this, PEGylation was carried out in phosphate PBS at pH 7.8 for 1.5 hours incubated at 37°C. Fibrinogen stock was prepared at 40 mg/ml for a final working concentration of 10 mg/ml. Bound thiols were quantified using Thiostar® fluorescent detection reagent (below) after overnight dialysis to remove unbound PEG.

6.3.2 Free thiol quantification

Free thiols of the bound PEG molecules were quantified with an optimised Thiostar® fluorescent detection assay according to the manufacturer's instructions. Briefly, thiostar® fluorescent detection agent is a maleimide based fluorescent agent that binds free thiols in a sample and resultantly generates a fluorescence detection signal when the maleimide binds to the free thiols. Upon receipt of the reagent, 50 µg of the detection reagent was reconstituted in 1 ml in dry acetonitrile which had been stored over molecular sieves. This solution was then vortexed and 40 µl (2 µg) was aliquoted into sterile 1.5 ml orange screw cap tubes. These aliquots were then vacuum centrifuged such that the detection mixture evaporates to dryness. When the vacuuming was complete, the caps were screwed on to close the tubes, sealed with parafilm and each tube covered with foil. These aliquots were then stored in a desiccator at -20°C.

To assay samples, the Thiostar® fluorescent detection agent was pre-warmed to room temperature before use and thereafter reconstituted in 875 µl dry DMSO which had been spun down at 15000 rpm for 3 minutes at room temperature so to remove any residues

that could interfere with the assay. The dialysed PEGylated samples were then diluted according to the working range of the assay 625 - 19.5 nM, and 100 µl of this transferred into white 96 microwell plates. A volume of 25 µl of the reconstituted Thiostar® reagent was then added to the dilution solutions in the wells and aspirated up and down once to ensure adequate mixing. The plate was covered with foil, incubated in the dark for 30 minutes and thereafter fluorescence measured with the Molecular Devices SpectraMax iD3 Multi-Mode Microplate Reader at 410 nm excitation and 550 nm emission. Thiol concentration was calculated from the N-acetylcysteine as standard curve assayed along the samples and corrected for dilution.

Because unmodified fibrinogen is known to have thiols in its backbone, it was also assayed as a control to determine their contribution to the detected thiols. For statistical analysis, optimisation experiments were initially conducted with three technical repeats, and thereafter biological repeats conducted in three biological repeats to quantify selected -SH-PEG. A Student's t-test used for statistical analysis.

6.3.3 Heparin acrylate conjugation to free thiols

The second method targeted to attach hep-acr to the free thiols of the FP through Michael addition reaction as it was envisioned that additional free thiols might increase hep-acr binding. Like the one step method, hep-acr was slowly added to FP for a final concentration of 0.6 mg/ml and incubated for 6 hours. at 37°C. Final experiments were conducted in three biological experiments, and a Student's t-test used for statistical analysis.

6.4 Size exclusion chromatography

Size exclusion with sephadex G-100 medium was attempted as a method (three biological repeats) of removing unbound hep-acr before quantification. A 10 ml bed volume with 12.7 cm bed volume height and 1 cm width sterile column was packed and allowed to settle for 30 minutes. It was then washed with sterile PBS three times. Heparinised fibrinogen samples (1 ml) were then loaded into the column and eluted with PBS through gravity. Eluates were collected as sequential fractions of 500 µl. A 2 µl volume of each fraction was then used to measure fibrinogen concentration using a

NanoDrop microvolume spectrophotometer at extinction coefficient (E1%) = 15.1 (280 nm). Heparin in each fraction was quantified with the MBTH assay (**section 6.5.1 3**). This method was however not pursued any further in this thesis as both heparin and fibrinogen had overlapping elusion profiles and heparin could not be accurately quantified from fractions eluted (**Figure 2.6**).

6.5 Dialysis

After optimisation, dialysis was explored and it showed to be the most effective method for removing unbound PEG and heparin molecules. For this, unbound PEG molecules (**section 6.3.1**) were removed by dialysis using a 100 kDa molecular weight cut-off (MWCO) dialysis cellulose ester (CE) membrane for 24 hours. Similarly, unbound heparin was removed by dialysis using a 300 kDa MWCO CE membrane for 36 hours at room temperature in both methods for heparin conjugation. For each, dialysis was against PBS > 1000x PBS dialysate volume at pH 7.4 at room temperature with the buffer changed every 12 hours and once one hour before the end of the dialysis cycle.

6.6 Bound heparin quantification

6.6.1 3-Methyl-2-benzothiazolinone hydrazone hydrochloride hydrate heparin (MBTH) assay

An MBTH calorimetric assay was used to quantity free heparin and was modified to quantify hep-acr bound to fibrinogen. The assay was originally designed to quantify free heparin. This modification required fibrinogen digestion with proteinase K prior to assaying. After dialysis, 0.1 mg/ml proteinase K working concentration was added to dialysed samples (corrected for final volume and concentration) in 1.5 ml Eppendorf tubes. These samples were then covered in foil and incubated for 12 hours at 65°C in the Scientific 400L Digital oven. After the incubation period, proteinase K in the samples was inactivated by increasing the oven temperature to 95°C for 10 minutes. The samples were then removed from the oven to cool down at room temperature. Once the samples had cooled down, they were then assayed in the MBTH according to the protocol developed in the Cardiovascular Research Unit.

Briefly, 250 µl test sample was added to a glass test tube and thereafter 0.025M nitrous acid, and 12.5% w/v ammonium sulfamate solution added to the sample. This mixture was vortexed briefly and 1M NaCl solution added to the mixture and vortexed. A 0.25% w/v MBTH solution was added, and the solution incubated in the Scientific 400L Digital oven at 50°C for 15 minutes. A 0.5% w/v $FeCl_3$ was added to the solution was added without cooling, vortexed and incubated in oven at 50°C for 20mins. This solution was cooled down before the samples were diluted (1:10 or 1:5) in disposable cuvettes and absorbance read with a Shimadzu UV spectrophotometer at 660 nm against air within 20 minutes. The concentration was calculated from the standard curve assayed along the samples.

6.6.2 Heparin Red® assay

Bound heparin was also quantified with a more sensitive fluorescent quenching probe assay, Heparin Red® that changes fluorescence intensity when it binds to heparin. It was ideal (but scarce) as it could directly measure heparin without additional processing steps and required much less sample compared to the MBTH. The assay was conducted according to the manufacturers' instructions. In brief, all reagents were first warmed to room temperature as they had been stored at 4-8°C. A 20 µl volume of the test sample (diluted accordingly e.g. 1:20 dilution) was transferred into white 96 non-tissue culture microplate. A heparin mix solution was then prepared by mixing 22 µl heparin red molecular probe and 2500 µl enhancer solution, and 80 µl of this solution added to each test sample in the microplate. This mixture was then gently shaken for 3 minutes and immediately measured for fluorescence using an ENSPIRE multiplate reader with excitation at 570 nm and emission at 605 nm. Heparin concentration was then calculated from the heparin standard curve ran along the test samples and corrected for dilution.

6.7 Lyophilisation and storage

Once the two methods of heparin conjugation to fibrinogen had been optimised and bound heparin quantified, the products were then upscaled and prepared in larger batches for storage.

After dialysis each batch of samples were collected into a 50 ml tubes. A 250 µl volume was then aliquoted into sterile orange capped tubes. These were then snap frozen with nitrogen and thereafter placed in freeze-dryer glass flasks that were then covered in foil before being placed in a freeze dryer for overnight drying with the pressure below 130 µbar and temperature below -40°C. Once freeze dried, the samples were stored in our lab's nitrogen tank and accessed upon need for use.

For use, each sample was reconstituted in 125 µl sterile Nanopure water (filtered with 0.22 µm filter) to allow working concentration and hydrogel mastermix preparation. To sterilize, especially for subsequent cell culture experiments, the samples were filtered with low protein binding 0.22 µm filter in the laminar flow hood after dialysis. Hydrogel preparations were at 20 nM Ca2+, and in experiments where aprotinin was used, it was at 100 ug/ ml.

6.8 Characterisation

6.8.1 Fourier transform infrared analysis

Lyophilised samples from the nitrogen tank were pre-warmed to room temperature. Once warm, the pallet sample was placed over the diamond stage of the Bruker Alpha FTIR spectrometer and pressed down with the pressure clamp and the red centering dot in the middle of the clamp indicator. The infrared beams were allowed to run through the samples generating the scans, thereafter the sample removed from the stage and cleaned. The PBS background was run first before the test samples.

6.8.2 Thromboelastography

The heparinised fibrin, namely FH and FPH, were evaluated for their clotting kinetics, indicative of potential thrombotic effects. For this, thromboelastography was conducted with TEG® haemostasis analyser (5000 series) using the researcher's own blood (ethics granted, HREC REF 661/2021). The lympholysed F, FP, FH and FPH were placed in the assay's oscillating cups pre-warmed to 37°C, and thereafter a total volume of 340 µl of citrated whole blood with kaolin and 0.2 M $CaCl_2$ added to the samples in the oscillating cups. These were then assayed for 120 minutes in the analyser, monitoring fibrinogen's ability to clot using thrombin present in the blood. The following parameters were

monitored: clotting time R, which is the time from start to when the waveform reaches 2 mm above baseline, clot formation time K, which is time from 2 mm above baseline to 20 mm above baseline, rate of clot strength build-up α, also known as the alpha angle, and clot strength which is the maximal amplitude (MA). Native bovine fibrinogen (referred to as F) and whole blood were assayed as control samples. The Student's t-test was used for any statistical data analysis.

6.8.3 *In-vitro* degradation

In-vitro degradation of fibrin and modified fibrin hydrogels were investigated to understand these profiles for downstream application in tissue culture assays and release studies. A 50 µl volume of hydrogels (with 100 µg/ ml aprotinin and without aprotinin) were prepared in triplicates and set for 30 minutes 1 hour at 37°C in 0.6 ml Eppendorf tubes. Once set, 150µl PBS with a neutral pH was added to each hydrogel and incubated at 37°C for 15 days. Eluates were collected after 1 hour (wash) and every day for 15 days. At each time point of eluate collection, the PBS was replaced with fresh PBS. The collected eluates were snap frozen with liquid nitrogen and stored at -20°C until the end of the 15 days where all samples were assayed. The samples were then assayed (n=3 technical repeats) in a Bradford assay according to the manufacturer's instruction and measured with SPECTRA MAX Molecular Devices Microplate Reader Spectrophotometer at 595 nm. Eluted protein was quantified from fibrinogen standard curve assayed along the test samples.

6.8.4 Turbidity analysis

A turbidity analysis assay was conducted by running a transmission spectrum for all hydrogels. In principle, samples that allow visible light to pass through it have high transmission and absorb less light as absorbance is inversely proportional to transmission. To profile the hydrogels, 100 µl hydrogels were set in clear 96 well microplates and thereafter assayed (n = 3 biological repeats) in a Molecular Devices SpectraMax iD3 Multi-Mode Microplate Reader for a transmission spectrum. A Student's t-test used for statistical analysis.

6.8.5 Scanning electron microscopy

Scanning electron microscopy was used to gain insight on micro-structures of the different hydrogel formulations. Lyomphilised samples were reconstituted in sterile Nanopure water and thereafter added to thrombin in the 96 microwell plates such that a total volume of 50µl is present in the wells. A microporous polyurethane foam disc (previously synthesised in Prof Bezuidenhout's Polymer Lab) that is 2 mm thick with diameter pores between 150 -180 µm and 80 - 90 µm interconnections was then placed swiftly in the hydrogel solution and pressed down using a plunger of a syringe such that the foam absorbed the hydrogel solution and it polymerises within the foam (280, 314) These discs supported the hydrogel during the processing steps for SEM. The hydrogels in the discs were then allowed to set for 30 minutes 1 hour, and thereafter fixed with 2.5% glutaraldehyde for 30 minutes. After this, they were rinsed three times with Nanopure water (with ± 5 minutes incubation in between) and gently freeze dried overnight in sterile orange cap tubes. Following a successful freeze-drying cycle, the samples were sputter coated with gold/palladium and thereafter viewed and micrographs acquired with either Tescan MIRA SEM or Nova NanoSEM.

6.8.6 Rheology

To characterize the hydrogels' stiffness, small strain oscillatory shear rheometry was conducted for each hydrogel type (n=3 biological repeats), set between the upper and the lower geometries of the Kinexus Pro rheometer. The hydrogels were prepared in 1 ml Eppendorf tubes by first adding thrombin into the tube followed by the Nanopure water reconstituted and unpolymerized solutions of F, FP, FPH or FH. A 300 µl volume of this hydrogel solution was then transferred to the center of the lower geometry which had been heated to 37°C, ensuring consistency and no bubble formation. The upper geometry (20 mm diameter) was then swiftly lowered down with the gap set to 0.8 mm. The hood was closed, and hydrogels allowed to fully polymerise for 30 minutes. Frequency sweeps were then run between 0.1 - 10 Hz to obtain G' and G' moduli. The G' was used as an indicator of hydrogel stiffness at 1 Hz (equivalent to a resting heart rate, 60 beats per minutes). Statistical comparisons between the different groups were conducted using a Student's t-test.

6.8.7 Growth factor release

Hydrogels (20 µl) consisting of 10 mg/ml reconstituted hydrogel precursors (F or FP or FPH or FH), 100 µg/ ml aprotinin and 1 µg of either VEGF165 or bFGF were set in triplicates (different biological samples) with thrombin in 0.6 ml Eppendorf tubes at 37°C. Once polymerised, PBS at neutral pH was added. After three hours of incubation, the PBS was aspirated out into a new 0.6 ml collection tube as a wash eluate to remove any unbound growth factor. The PBS was replaced with fresh PBS and further incubated for 15 days. Eluates were collected on day one and every second day for 15 days and thereafter stored at -20°C. Once all samples' eluates were collected, they were assayed with a DuoSet® ELISA Development System kits according to the manufacturer's instructions for released growth factor concentration.

Optical density was read using an iMark microplate reader at 450 nm, with background correction at 570 nm. The standard curve run along the test samples was used to calculate the amount of growth factor released (ng/ml) on each collection day and used to construct cumulative release curves. Bound growth factor was calculated by subtracting the amount of growth factor contained in each wash from the total amount of growth factor loaded into each hydrogel.

6.8.7.1 Bioactivity

The VEGF and bFGF eluates (**from section 6.7.7**) released on day 15 from FH and FPH were evaluated for bioactivity (triplicates; each sample of the eluted growth factor) by measuring their ability to stimulate HUVECs and HdFBs activity respectively. For this, 5000 cells (each cell line conducted separately) were seeded per well in a 96-well tissue culture plates and allowed to attach overnight. After 24 hours, the media was removed, and the cells treated with 10 ng/ ml dosing solutions prepared from the eluted VEGF and bFGF in 2% FBS MCDB 131 for HUVECS and serum free MCDB media for HdFBs respectively. Cells free of growth factors and controlled for PBS were used as negative controls. Fresh VEGF and bFGF at 10 ng/ml were used as positive control samples. The experiments were then incubated for 72 hours. at 37°C, 5% CO_2 and cell activity measured with Cell TitterGlo assay as described in **section 6.8.5.** A Student's t-test and ANOVA were used for statistical significance.

6.9 *In-vitro* cell culture

6.9.1 Cell culture stocks

The use of previously isolated HUVECs, HdFBs and ADSCs stocks in our laboratory's cell repository was obtained, specifically for this study, from the University of Cape Town's Human Ethics Committee in accordance with the Declaration of Helsinki (HREC REF 661/2021).

6.9.2 Cell culture conditions

6.9.2.1 Culture media

The HUVECs were routinely cultured in 10% filtered fetal bovine serum (FBS) MCBD-1 supplemented with 1% penicillin-streptomycin, 100 mg/L hydrocortisone, 292 mg/L L-Glutamine, 10 µg/L EGF and 5 µg/L bFGF. This media is hereafter referred to as culture media and was established in laboratory as a sufficient media for EC culture. For some experiments, basal media consisting of only MCBD-1, 1% penicillin-streptomycin and 2% FBS was used. For HdFBs, culture media was made up of 10% FBS in DMEM supplemented with 1% penicillin-streptomycin, and for ADSCs this was 10% FBS in α-MEM supplemented with 1% penicillin-streptomycin.

6.9.3 Thawing of cells

Cells were removed from the liquid nitrogen tank and thawed swiftly by placing the cryovial in a floating tube holder and thereafter placed in a 37°C water bath for less than a minute (until the icicle had just disappeared). All the contents of the cryovial were then transferred into a T25 flask containing warm 5 ml 20% FBS culture media, placed in the incubator and allowed to attach overnight. After this overnight incubation, the media with dimethyl sulfoxide (DMSO) (**section 6.8.2.3**) was replaced with 10% FBS culture media.

6.9.4 Cell passaging

All cells were cultured in the 37°C, 5% CO_2 incubator. For routine culturing, cells were passaged at 70-90% confluency. For this, the culture media was removed from the flasks, and the flasks washed twice with PBS (3 ml for a 25 cm^2 and 5 ml for a 75 cm^2 flask).

0.25% trypsin-EDTA (1 ml for a 25 cm^2 and 3 ml for a 75 cm^2 flask) was added to the flask and incubated for about 2-3 minutes in the incubator; the HdFBs needed a longer incubation time (about 4 minutes) and a higher trypsin-EDTA volume (1 ml higher) to detach. The cells were then observed under a microscope for detachment. Once they had detached, trypsin-EDTA was inactivated by neutralising it with culture media (5 ml for a 25 cm2 and 6 ml for a 75 cm^2 flask). This solution was then transferred into a 15 ml tube and centrifuged at 1500 rpm for 3 minutes to generate a cell pallet. The media was carefully removed from the 15 ml tube and discarded, leaving behind an intact pallet. This pallet was hereafter resuspended in 1 ml culture media in preparation for cell counting.

For subsequent experiments, cells were counted with a hemocytometer. This was prepared by mixing 20 µl of the cell suspension with 20 µl of Trypan Blue (0.4% (m/v)), and 10 µl of this solution added carefully to the hemocytometer through capillary action. Four corners of the grids were counted, averaged and the number of cells/ml determined using the following equation:

$$Number\ of\ cells\ per\ milliliter = \ Average\ number\ of\ cells\ counted\ x\ 2\ x\ 10\ 000$$

Cell numbers required for an experiment were seeded, and the remaining cells were either divided into different flasks for further culturing or frozen for storage. The passage number was recorded with each passaging.

6.9.5 Cryofreezing of cells

Once cells were counted, 500 000 cells/ ml diluted in 7.5% DMSO (final concentration) culture media were transferred into 1.5 ml cryovials. The cryovials were then transferred into a quick-freeze container, Mr. Frosty™ Freezing Container filled with isopropyl alcohol. This container was then placed in a -80°C freezer for overnight slow freezing at 1 degree of cooling per minute. The cryovials were transferred to a liquid nitrogen tank for long term storage.

6.9.6 Live/Dead® viability assay

A live/ dead assay was conducted according to the manufacturer's instructions to assess cell viability. This assay distinguishes live cells from dead cells based on plasma membrane integrity and esterase activity using EthD-1 and calcein AM. In live cells, intercellular esterase is active, and the plasma membrane is intact. Calcein AM binds to this esterase of live cells and stains them for green fluorescence excited at 495 nm and emits at 515 nm. In contrast, the plasma membrane of dead cells is damaged (lost), and thus EthD-1 can enter the cell and bind to the cell's DNA for a bright red fluorescent signal excited at 525 nm and emits around 617 nm.

For the experiments, respective cells were encapsulated in hydrogels (3D) (in triplicates, with technical as well as biological repeats) and set in the wells of 96 well tissue culture plates, and thereafter cultured for three and seven days in 10% FBS of the respective culture medias. On day seven, a live/ dead solution was prepared in the laminar flow hood by adding 2 µl of the supplied 2 mM EthD-1 stock solution to 1ml sterile PBS and the solution vortexed to ensure thorough mixing. 0.5 µl of the supplied 4 mM calcein AM stock solution was added to this solution and the resultant mixture vortexed. The growth media was then removed from each well with the hydrogels and the hydrogels washed twice with PBS at neutral pH. A 100 µl EthD-1/ calcein AM solution was then added on top of the washed hydrogels, and the plate was then covered with foil before being incubated for 20 minutes at room temperature. When the incubation period was over, the live/ dead solution was removed, and the hydrogels washed twice with PBS. They were then viewed under a Carl Zeiss LSM 880 confocal microscope equipped with Fast Airyscan technology and maximum projections of Z-Stacks micrographs acquired within an hour to avoid over exposure. Images were taken with 10x objective magnification using Cy3 (red) and 10 Alexa Fluor 488 (green) reflectors. ImageJ cell counter plug in was then used for live/ dead cell quantification.

6.9.7 CellTiter-Glo® luminescent cell viability assay

The CellTitterGlo® measures viability based on the ATP present in metabolically active cells. The CellTiter-Glo® reagent lysis the cells to release ATP (if cells are viable) that reacts with luciferase for a luminescent signal. This assay was conducted according to

the manufacturer's instructions with minor modifications to measure cell activity in for cells encapsulated in hydrogels. 5000 cells were encapsulated per 50 µl hydrogel, in triplicates (different samples), and allowed to fully polymerise for 30 minutes 1 hour in the tissue culture incubator at 37°C. Once the hydrogels had completely polymerised, 100 µl culture media was added to the hydrogels and these were incubated for the different specific time points. At the end of the incubation period, the experiments were removed from the incubator and 100 µl of CellTiter-Glo® Reagent added to each well, covered with foil, and the contents mixed on an orbital shaker for 3 minutes to induce cell lysis. 150 µl of this solution was then transferred to a new an opaque, non-sterile, 96-well flat-bottomed white plate for each test sample and luminescence read immediately using a Molecular Devices SpectraMax iD3 Multi-Mode Microplate Reader equipped with a luminometer. Wells with media alone and without cells (with CellTitre-Glo® reagent) were used as blanks. Student's t-test was used for statistical analysis.

6.9.8 3D spheroid sprouting invasion assay

6.9.8.1 Methylcellulose preparation

A 20% methylcellulose solution was used in this study to generate spheroids. To prepare this, 3.6 g methylcellulose was weighed using filter paper, transferred into a 500 ml Schott bottle containing a magnetic stirrer bar and sterilised using an autoclave. This preparation was thereafter allowed to cool down completely overnight at room temperature. Once cooled, 150 ml of sterile basal MCDB 131 (without any enrichments) at pH 7.4 media was pipetted into a measuring cylinder, covered with foil and pre-warmed to 60°C for 15 minutes in a water bath. This media was then added into the 500 ml Schott bottle, with the methylcellulose, in the laminar flow hood and stirred on a magnetic stirrer for 20 minutes at room temperature. A further 150 ml of the media was then added in the laminar flow hood for a 300 ml total volume. This methylcellulose solution was then stirred overnight at 4°C. Following this, the methylcellulose solution was aliquoted into centrifuge tubes, and thereafter spun for 2 hours at 5000 g at room temperature on fixed head centrifuge. It was then spun again for 40 mins at 3500 g at room temperature using a swing out centrifuge. The clear supernatant was collected into a sterile Schott bottle and stored at 4°C until used for spheroids.

6.9.8.2 Siliconising plates

The 24-well plates used for spheroid assays were siliconised with Sigmacote® to increase hydrophobicity. This was to ensure that the hydrogels do not adhere to the plates and thus becoming flat to sink the spheroids, but instead form smooth 3D droplets that enable 3D spheroids to be assayed. In short, 500 µl Sigmacote® was added to cover each well and thereafter incubated for half a minute. The Sigmacote® was then removed and allowed to dry overnight in the laminar flow hood. The wells were then rinsed twice with sterile Nanopure water and allowed to air dry in the laminar flow hood. The plates were then sterilized using ethylene oxide in sterilisation bags.

6.9.8.3 Assaying spheroids

Endothelial cell invasion into the different hydrogel formulations was then assessed. 750 Spheroids were prepared from HUVECs with passage number used below P5. A total of 750 cells/well in 20% methylcellulose were seeded into each well of sterile 96 well, non-tissue culture treated and round bottom plates and incubated overnight at 37°C, 5% CO_2 to generate spheroids. Intact and without debris spheroids were then harvested, and about 4 – 6 individual spheroids were encapsulated into each hydrogel (n=3 per group) type namely F, FP, FHP and FH at 10 mg/ml fibrinogen, 100 µg/ ml aprotinin and 1 unit/ ml thrombin for F, FP, and FH, and 4 units for FPH. A pre-mixture was made with each hydrogel's components using sterile PBS with the harvested spheroids. Thrombin was added to each siliconised 24-well plate of the and thereafter the pre-mixture (with selected spheroids) added to the thrombin such that 50 µl hydrogel polymerises with 4 – 6 spheroids encapsulated. The hydrogels were allowed to fully polymerise at 37°C for 30 minutes 1 hour. Once fully polymerised, 300 µl of 2% FBS MCDB -131media was added on top of each hydrogel and incubated at 37°C with 5% CO_2. Spheroid sprouts were then tracked for 48 hours, with micrographs taken 24 hours and 48-hours' time points using a Nikon Light microscope (Nikon Eclipse Ti-S) at 10x magnification. ImageJ was then used to quantify sprout number and length with a straight line used to measure all individual sprout lengths. Spheroids that were touching each other or near the side of the hydrogel were excluded.

For data analysis, a two-way ANOVA was conducted with two-tailed Student t-tests employed for between-group comparisons.

6.9.8.4 Fixation, staining, and visualisation

For better visualization, sprouted spheroids in the hydrogels were stained with ActinRed and counterstained with Hoechst 33258 at 48 hours. For this, the media was removed, and the hydrogels washed twice with PBS. They were then fixed in 4% formalin (in PBS) and incubated for 30 minutes at room temperature. The formalin was then removed, and the hydrogels washed again twice with PBS. The cells were then permeabilised with 0.1% Triton-X in PBS for 4 minutes, removed, and washed again three times with PBS. Actin red (prepared by adding one drop of ActinRed 555 Ready Probes reagent to 5 ml PBS) was then added to each hydrogel and incubated for 20 minutes at room temperature. It was thereafter removed and washed with PBS twice to remove any residual reagent. Hoechst 33258 nuclear stain was then added for counterstaining and incubated for 10 minutes at room temperature, followed by a wash with PBS three times. The hydrogels were thereafter viewed and imaged (Z-stacks) with a Carl Zeiss LSM 880 confocal microscope equipped with Fast Airyscan technology. Plates were stored at 4°C slightly covered in PBS and the plates wrapped in parafilm.

6.9.9 Adipose derived mesenchymal stem cell characterisation

Rat primary ADSCs obtained from our laboratory cell repository were assessed their ability to differentiate into either adipocytes or osteoblasts for functional characterisation. For osteogenic differentiation, 10 000 ADSCs were seeded into 24 well tissue culture plates and incubated overnight at 37°C with 5% CO_2. The culture media was then replaced with OM which consisted of 10% DMEM culture medium supplemented with 10 nM dexamethasone, 10mM glycerol-2-phosphate and 0.05 mM ascorbic acid that was weighed out and added fresh each time OM was replaced. The OM replacement occurred every three days for 21 days. Experimental controls were grown in normal culture media without supplements with induction cues and run along each experiment.

For adipogenic differentiation, 15 000 ADSCs were seeded into 24 well tissue culture plates and allowed to grow for three days in 10% FBS DMEM culture medium at 37°C

with 5% CO_2. The culture media was then removed and replaced with AM which was changed every three days for 14 days. The AM was ADSC culture media supplemented with 1 µM dexamethasone, 56 µM indomethacin, 500 µM 3-isobutylmethylxanthine and 10 µM insulin. A large stock of AM, without indomethacin, was prepared fresh to use for the duration of the experiment, and indomethacin added separately each time the medium was replaced. Control samples were those treated with culture media without AM supplements. These experiments were done in triplicates.

6.9.9.1 Alizarin Red Stain

At the end of the differentiation period, OM was removed from each well with cells, cells rinsed two times with PBS and thereafter fixed in 4% formalin for an hour at room temperature. The formalin was removed, and the cells rinsed again twice with sterile deionized water. A 1 ml volume of 40 mM Alizarin Red S stain was then added to each well with cells and incubated in the dark for 45 minutes. The stain was then removed, cells washed five times with deionized water, and all the deionized water removed. Micrographs were then taken immediately using a phase contrast Nikon Light microscope (Nikon Eclipse Ti-S).

The stain was extracted by adding 200 µl of 10% acetic acid to each well and incubated at room temperature for 30 minutes. A pipette tip was used as a scrapper to collect all the cells in the well into a 1.5 ml microcentrifuge tube which was then vortexed for a minute to ensure thorough mixing. The solution was then heated to 85°C for 10 minutes, with the microtubes covered in parafilm and foil to prevent evaporation. The samples were then cooled down by incubating them on ice for 5 minutes and thereafter centrifuged at 20 000 g for 15 minutes. A volume of 150 µl was then transferred to new clear 96 well plate and the absorbance read at 405 nm with a SPECTRA MAX Molecular Devices Microplate Reader Spectrophotometer. A 10% acetic acid solution was run along as a negative control.

6.9.9.2 Oil Red O Stain

The extent of adipogenic differentiation was quantified with an Oil Red O stain. The AM was removed from the wells and the cells rinsed with PBS without disturbing the

monolayer culture. The cells were then fixed in 10% formalin for one hour at room temperature. A 500 µl 60% isopropanol volume was then added to the wells to dehydrate and thereafter incubated for 3 minutes, and then removed and replaced with 1 ml Oil Red O working solution (prepared in isopropanol). The Oil Red O stain was then incubated at room temperature for 30 minutes. The stain was removed, and the wells thoroughly rinsed with water, ensuring no residual stain remains. For 2D differentiation, the cells were counterstained with Hematoxylin. The stained cells were then imaged with a phase contrast Nikon Light microscope (Nikon Eclipse Ti-S).

The stain was extracted, for quantification, with 250 µl 100% isopropanol in each well. This was shaken (by moving the plate on the bench up, down, and sideways) well to ensure adequate extraction and thereafter incubated at room temperature for 15 minutes. A volume of 200 µl of the extracted solution was then transferred into a new clear 96 well plate and the absorbance read at 492 nm with a SPECTRA MAX Molecular Devices Microplate Reader Spectrophotometer. A 100% isopropanol was used as a negative control.

6.9.10 Adipose derived mesenchymal stem cell differentiation on hydrogels

The same protocol as described above was followed with the exception that the cells were seeded on top of 200 µl hydrogels with 100 µg/ ml aprotinin. For adipogenic differentiation, the differentiation process was conducted for seven days as this time point showed to be optimum during the characterization phase. For osteogenic differentiation, differentiation was carried out for 15 days. Control wells received culture media without the differentiation supplements in the medias, and it was also changed every three days for the duration of the experiments. The plates were stored at stored at -20°C. Data analysis was done with a two-way ANOVA with two-tailed student t-tests for between group comparisons. This was followed by a Tukey post-hoc test for significance

6.10 *In-vivo* rat subcutaneous implant assay

Male Wistar rats obtained from the UCT Animal Unit were used in this study and all experiments were conducted under aseptic conditions. Ethical approval was attained from the University of Cape Town's Animal Research and Ethics Committee (HSF AEC

020_028). The study adhered to the Principles of Laboratory Care and the guidelines within the National Research Council's Guide for the Care and Use of Laboratory Animals.

6.10.1 Porous polyurethane discs sterilisation

For structural support, hydrogels were set in porous PU discs previously described in **section 2.2.3.5,** as developed in Prof Bezuidenhout's Polymer Lab (314). These discs were 2 mm x 5.4 mm (thickness x diameter) with 82% porosity and pores between 150 - 180 µm and 80 - 90 µm interconnections. Prior to their use, they were sterilised by sonication in 70% ethanol for 30 minutes and thereafter incubated at room temperature for 24 hours. They were then air dried in the tissue culture laminar flow hood.

6.10.2 Hydrogel preparation in polyurethane discs

Hydrogels of 40 µl with either 1 µg VEGF or bFGF for treatment groups or no growth factor as controls were set in the PU discs. Briefly, unpolymerised hydrogel constituents (reconstituted heparinised fibrin or native fibrinogen, 1 µg VEGF or bFGF or no growth factor, and sterile PBS) were mixed and aspirated into a well plate with thrombin at the center. The PU discs were swiftly placed on top of this mixture whereafter pressed down, once, consistently with a 1 ml syringe plunger and the hydrogel allowed to infiltrate the disc through absorption as the plunger was released off the disc, ensuring that any air trapped in the disc is removed completely. These hydrogels were then allowed to completely polymerise at 37°C, 5% CO_2 for 30 minutes 1 hour in the tissue culture incubator.

6.10.3 *In-vivo* Subcutaneous implants

A power analysis was performed to determine the number of animals required for the study. For n=6, expected effect-size at 30% increase degradation, expected variability/variance of measured values 15 %, statistical power selected 0.8, and significance threshold (p value) selected 0.05.

All surgical procedures were conducted under aseptic technique. Implants were done in Wistar rats (n=6) according to the protocol described by Goetsch et al., 2015 (376). Once the rats were monitored for welfare, analgesic (0.05 mg/ kg buprenorphine) was

administered, and the animals were ready for surgical procedures. Anesthesia was induced by placing the rats in an inhalation chamber with 5% isoflurane air flow for about 3 min and maintained for the procedures with nose cone delivery of about 1.5% Isoflurane, 1.5 l/min oxygen output, 750 mmHg, 21°C. When anesthesia was achieved, the surgical area where incisions would be done was shaved and disinfected with povidine. Longitudinal incisions (six) of about 1 cm were then made subcutaneously on either side of the dorsal midline (three on each side, six in total per rat) and with a pocket of about 1.5 cm in depth for each disc was secured by gentle blunt dissection (**Figure 6.1**). The prepared hydrogels in discs were then implanted into the pockets, with each rat receiving only one disc of each group (n=6). Body temperature was maintained throughout the surgeries with a heating pad at 37°C. Once complete, the incisions were sutured using surgical stapples and the animals carefully transferred to their recovery cages. They were monitored until fully conscious whereafter they received the analgesic again (0.05 mg/ kg, buprenorphine) after 24 hours operation.

After 10 days, the rats were euthanised with rising isoflurane concentration with CO_2 and death confirmed with 1 ml saturated potassium chloride injection (cardiac puncture) and rigor mortis. The discs were then explanted with their surrounding tissue capsules and each disc cut in half longitudinally to generate two semi-cylindrical sections. One half was fixed in a zinc fixative for CD31 staining, while the other half was fixed in 10% formalin for picrosirius red stain for about 24 hours and processed in graded 70% ethanol.

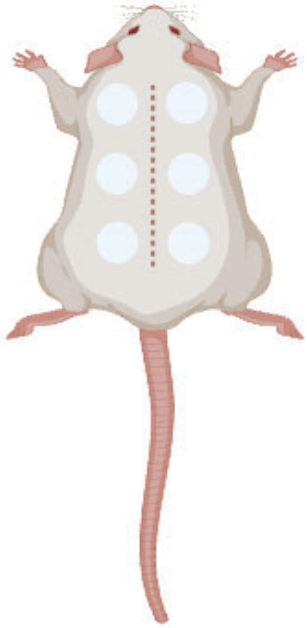

Figure 6.1: Illustration of the positions for the subcutaneous implant model in rats. Incision of 1 cm subcutaneous pockets were made, and PU discs impregnated with hydrogels (with or without growth factor) and implanted subcutaneously in the dorsal region of the rat. Six discs were placed per rat, with three discs on each side separated by a dorsal midline. Generated with Biorender.com.

6.10.4 Histology

6.10.4.1 Wax processing and embedding

Half PU discs were removed from the ethanol, inserted into histology cassettes, and thereafter placed into wire mesh baskets. These were then dehydrated by immersion in 70 – 90% graded alcohol for 60 minutes each, followed by immersion in 100% alcohol three times for 60 minutes each. The samples thereafter had three consecutive changes of iso-octane and paraffin wax for 60 minutes each at 60°C, followed by a final change for 120 minutes. Once this was complete, the cassettes were opened, and samples embedded in paraffin wax using embedding molds. These samples were then sectioned across the entire cut face of the half discs using a microtome and transferred onto microscope slides.

6.10.4.2 Staining

The sections mounted on the slides were stained for vascular differentiation CD31 biomarker and the vessels quantified. Embedded sample sections (from zinc fixative) were first dewaxed twice with trimethylpentane for 10 minutes, and thereafter dehydrated in alcohols by first immersing them in 100% alcohol three times, then 96% alcohol two times, and finally 70% alcohol twice. They were then rinsed and hydrated by immersion in distilled water.

To stain for CD31 biomarker, sections were then incubated with a 1:25 diluted mouse anti-rat CD31 primary antibody (in 1% bovine serum albumin) for 2 hours at room temperature, and then rinsed twice in 0.1% tween20 (prepared in PBS) for 10 minutes. An ALP Biocare Medical kit was then used, according to the manufacturer's instructions with minor modification to detect the primary antibody. Briefly, the sample sections were incubated with a rodent antibody for 30 minutes, followed by two 10-minute washes with tris buffered saline. A mouse on rat ALP polymer was then added and incubated for 30 minutes and thereafter washed twice with 0.1% tween 20. This was then followed by an incubation of the sections with BCIP/NBT DAKO until color development was complete. They were then rinsed in running tap water, dehydrated, cleared in 2,2,4 trimethylpentane, and finally mounted with Entellan.

For collagen fiber detection, a picrosirius red stain was conducted to visualize and quantify the collagen deposition. Sample sections that had been fixed in formalin were dewaxed, as described above, and thereafter stained with Weigert's hematoxylin for 8 minutes before being washed in running tap water for 10 minutes. The sections were then stained with Picrosirius Red stain for 1 hour and washed twice with acidified water. The water was thereafter removed from the slides by physically and vigorously shaking the slides. The sections were dehydrated using three changes of 100% ethanol and thereafter cleared in xylene before mounting the coverslips onto the samples and allowed to dry.

6.10.5 Microscopic analysis

The stained samples were viewed, and images captured using a Nikon Eclipse 90i microscope with a Nikon Eclipse software for stitching. Micrographs covering the entire

cross-sections across the mid-region of the explanted disc were captured and stitched together to form one image. These images were then analysed by a blinded observer on Visiopharm Integrated Systems software. Vessel quantification was performed by training the Visiopharm Integrated Systems software to automatically detect CD31 stained vessel structures in the outline the Region of Interest (ROI) Following this, % vessel was calculated as the % of vessels detected in the ROI/ area using Visiopharm Integrated Systems software. A fold increase was calculative for the growth factor group, relative to the no growth factor group,

For picrosirius red stains, the images were also trained to detect picrosirius red staining for collagen content, using the forest classifier machine learning model. All analyses were done by a blinded observer to eliminate any biases. % collagen was calculated as the % of collagen that stained positive for picrosirius red in the ROI using Visiopharm Integrated Systems software.

6.10.6 Statistical analysis

Comparison between multiple groups was done by means of one-way ANOVA followed by Tukey post-hoc testing for significance, where appropriate. Analyses of all other data were conducted using Student's t-tests (two-sample equal variance [homoscedastic]) in Excel (Microsoft Office). All data are expressed as mean ± standard deviation, and error bars generated from standard deviations.

6.11 Data analysis

Comparison between multiple groups was done by means of one-way and two-way ANOVAs followed by Tukey or Neuman-Keuls post-hoc testing for significance, where appropriate. Analyses of all other data were conducted using Student's t-tests (two-sample equal variance [homoscedastic]) in Excel (Microsoft Office). All data in this thesis are expressed as mean ± standard deviation, and error bars generated from standard deviations.

6.12 Reagents, equipment, and consumables

Table 6.1: Table of reagents

Reagent	Producer/ Supplier	Catalogue/ Product No
ActinRed™ ReadyProbes® Reagent	Life Technologies, Carlsbad, CA, USA	R37112
Alkaline phosphatase Biocare Medical kit	Sigma-Aldrich, St Louis, MO, USA	AP0100-1KT
Aprotinin	Roche, Basel, Switzerland	70257723
bFGF	Peprotech, Rocky Hill, NJ	100-18B-100UG
Biotech grade CE Dialysis Membrane Tubing (100 KD MWCO)	Spectrum Laboratories™, USA	11500980
Biotech grade CE Dialysis Membrane Tubing (300 KD MWCO)	Spectrum Laboratories™, USA	11550970
Bovine fibrinogen	Sigma-Aldrich, St Louis, MO, USA	F8630-5G
Bovine serum albumin (IgGfree, Protease-free)	Jackson ImmunoResearch, Westgrove, PA	LS004174
Bradford reagent	Sigma-Aldrich, St Louis, MO, USA	B6916
Calcium chloride ($CaCl_2$)	Sigma-Aldrich, St Louis, MO, USA	C4901
CellTiter-Glo® luminescent Cell Viability Assay	Promega (WI, USA)	G7571 (10 × 10 ml)
Dimethyl sulfoxide (DMSO)	Sigma-Aldrich, St Louis, MO, USA	D2650
DMEM media	Sigma-Aldrich, St Louis, MO, USA	D5648
DuoSet® ELISA Development system – Human bFGF	R&D Systems, Minneapolis, MN	DY233-05
DuoSet® ELISA Development system – Human VEGF	R&D Systems, Minneapolis, MN	DY293B-05
Entellan	Merck, Darmstadt, Germany	1079610500
Ethanol	Servochem (PTY) LTD, Montague Gardens, Cape Town, South Africa	-
Fibrinogen		

Foetal bovine serum (FBS) (gamma irradiated)	Gibco® by Life Technologies™, Paisley, UK	10499-044
Heparin Red®	Redprobes, Münster Deutschland, Germany	HR001
Hoechst 33258	ThermoFischer Scientific, OR	H3569 – 10 ml
Human epidermal growth factor (EGF)	Peprotech, Rocky Hill, NJ, USA	AF-100-15
Hydrochloric acid (HCl), 25% w/v	Honeywell Riedel-deHaën, Seelze, Germany	30723 – 2.5L
Hydrocortisone	Sigma-Aldrich, St Louis, MO, USA	H0396
L-Glutamine	Sigma-Aldrich, St Louis, MO, USA	G-8540
LIVE/DEAD ® Viability/Cytotoxicity Kit	Molecular Probes, Invitrogen detection technologies, USA	MP03224
Live/Dead™ cell viability assay kit	Molecular Probes Inc. (Eugene, OR)	
MBTH reagant	Merck, Darmstadt, Germany,	65875
MCDB-131 media	Sigma-Aldrich, St Louis, MO, USA	M8537
Methyl cellulose: 4000 centipoises	Sigma-Aldrich, St Louis, MO, USA	M0512
Mouse anti-human CD31 primary antibody (monoclonal)	Dako, Agilent Technologies, C.A.	M0823
Penicillin Streptomycin (10 000 U/ml / 10 000 µg/ml)	Gibco® by Life Technologies, Carlsbad, CA	15140-122 (100 ml)
Penicillin streptomycin (10 000 U penicillin and 10 mg streptomycin/ml	Sigma-Aldrich, St Louis, MO, USA	P0781
Picrosirius red solution: - Sirus red F3B (Direct Red 80) - Saturated aqueos solution of picric acid	Sigma-Aldrich, St Louis, MO, USA	- 365548 or 43665 - P6744-1GA
Picrosirius Red stain		
Potassium chloride (KCl)	Sigma-Aldrich, St Louis, MO, USA	P9541

Potassium phosphate monobasic ($KH2PO_4$)	Sigma-Aldrich, St Louis, MO, USA	P5655
Proteinase K	Sigma-Aldrich, St Louis, MO, USA	P2308
Reagent Diluent Concentrate 2 (10X, 5 x 21 mL)	R&D Systems, Minneapolis, MN	DY995
Sephadex® G-100	Sigma-Aldrich, St Louis, MO, USA	S6147
Sigmacote®	Sigma-Aldrich, St Louis, MO, USA	SL2
Sodium azide	Sigma-Aldrich, St Louis, MO, USA	S2002
Sodium bicarbonate ($NaHCO_3$)	Sigma-Aldrich, St Louis, MO, USA	S5761
Sodium chloride (NaCl)	Sigma-Aldrich, St Louis, MO, USA	S7653
Sodium dihydrogen phosphate ($NaH2PO_4$)	Sigma-Aldrich, St Louis, MO, USA	S3139
Sodium hydroxide (NaOH)	Sigma-Aldrich, St Louis, MO, USA	S-5881
Sodium phosphate dibasic dodecahydrate ($Na_2HPO_4.12H_2O$)	Sigma-Aldrich, St Louis, MO, USA	71649
Substrate BCIP/NBT DAKO)	DAKO, A/S, Glostrup, Denmark	11681451001
ThioStar® Thiol Detection Reagant	Arbor Assays, Ann Arbor, Michigan, USA	L002-50UG
Thrombin from bovine plasma	Sigma-Aldrich, St Louis, MO, USA	T4648
Trypan Blue	Sigma-Aldrich, St Louis, MO, USA	T8154
Trypsin-EDTA (10X)	Sigma-Aldrich, St Louis, MO, USA	59427C
Tween® 20	Sigma-Aldrich, St Louis, MO, USA	P1379
$VEGF_{165}$	Peprotech, Rocky Hill, NJ	100-20-10UG

Table 6.2: Table of equipment

Equipment	**Manufacturer**
Bruker Alpha FTIR spectrometer	Bruker, Karlsruhe, Germany

Carl Zeiss LSM 880 confocal microscope equipped with Fast Airyscan technology	Carl Zeiss, Oberkochen, Baden-Württemberg, Germany
Centrifuge: 5415R (for microcentrifuge tubes)	Eppendorf, Hamburg, Germany
Centrifuge: 5810R	Eppendorf, Hamburg, Germany
Centrifuge: J2-21 with a JA20 rotor (for centrifuging methylcellulose)	Beckman Coulter Life Sciences, Indianapolis, IN, USA
Centrifuge: Megafuge 1.0R	Heraeus, Hanau, Germany
ENSPIRE multiplate reader	PerkinElmer, Inc., Connecticut, USA
Fluorescent spectrophotometer: Cary Eclipse serial no. e101124662	Agilent Technologies, Santa Clara, CA, USA
Freeze Dryer - Virtis	SP Industries, Gardiner, NY
Glomax 96 Luminometer	Promega, Madison, WI
Haemocytometer	Improved Neubauer, Baxter Scientific, Deerfield, IL, USA
HERA cell incubator (for all 37 °C cell culture)	Bio-Rad, Hercules, CA, USA
iMark plate reader	Bio-Rad, Hercules, CA, USA
Kinexus Pro rheometer	Malvern Instruments, U.K.
Laminar Flow Hood (Microbiological Safety Cabinet Class II, model 4B2)	Labaire Manufacturing Company, (Pty), Ltd, Mt Edgcombe, South Africa
Microscope: Nikon fluorescent microscope (Nikon Eclipse 90i DS-Ri1)	Nikon, Tokyo, Japan
Microscope: Nikon light microscope (Nikon Eclipse Ti-S)	Nikon, Tokyo, Japan
Microscope: ZEISS LSM510 Confocal microscope with MaiTai two photon laser	Carl Zeiss Microscopy GmbH, Göttingen, Germany
Molecular Devices SpectraMax iD3 Multi-Mode Microplate Reader	Molecular Devices SpectraMax, San Jose, USA
NanoDrop: NanoDrop 2000	Thermo Fisher Scientific, Waltham, MA, USA
pH meter: Jenway 3510	Bibby Scientific, Staffordshire, UK
Pipettes	Gilson Inc., Middleton, WI

Rheometer - Kinexus Pro	Malvern Instruments, UK
Scientific 400L Digital Oven	Scientific Manufacturing CC, South Africa
Sonicator: Virsonic 100 probe	Virtis, Gardiner, NY, USA
SPECTRA MAX Molecular Devices Microplate Reader Spectrophotometer	Molecular Devices SpectraMax, San Jose, USA
Sputter coater	Quorum Technologies, Lewes, UK
Sturdy Autoclave SA-300MB	Sturdy, New Taipei City, Taiwan
TEG® haemostasis analyser (5000 series)	Haemonetics Hospital, Boston, USA
Tescan MIRA SEM	Tescan, Brno, Czech Republic
UV spectrophotometer (660 nm, Shimadzu UV 1601-PC)	Shimadzu, Kyoto, Japan
Visiopharm Integrated Systems software	Visiopharm A/S, Hørsholm, Denmark
Water bath: Grant Y14	Grant Instruments, Cambridge, UK

Table 6.3: Table of general consumables

Consumables	**Producer/ Supplier**	**Product/ Catalogue Number**
24-well tissue culture treated plates	Costar® by Corning Incorporated, NY	3524
96-well clear, round bottomed, sterile plate, non-tissue culture treated	Nunc® MicroWell, Roskilde, Denmark by Sigma,	268200
96-well non-tissue culture treated	Nunc® MicroWell Roskilde, Denmark by Sigma	260887
96-well opaque flat bottomed nonsterile plate	Nunc® MicroWell, Roskilde, Denmark by Sigma,	Z688665 or P8616
96-well opaque, flat bottomed, non-sterile	Nunc® MicroWell, Roskilde, Denmark	Z688665
96-well tissue culture treated plates	Costar by Corning Incorporated, NY	3595
Acetic acid	Sigma-Aldrich, St Louis, MO, USA	320099-500ML
Alizarin Red S	Sigma-Aldrich, St Louis,	A5533-25G

	MO, USA	
Cell culture flask, surface area 25 cm2, canted neck, cap (vented)	Corning Inc. Corning, NY	CLS430639
Centrifuge tube (15 ml)	Falcon by BD Biosciences, San Jose, CA	352096
Centrifuge tube (50 ml)	Falcon by BD Biosciences, San Jose, CA	352070
ELISA plates: Maxisorp 96-well plates, non-sterile	Nunc, Roskilde, Denmark	44-2404-21
Filter, low-protein binding (0.22 µm PES, 250 ml) for cell culture media	Millipore® Stericup™ (Polyethersulfone membrane, Millipore Express PLUS), Merck KGaA, Darmstadt, Germany	Z660493 – Sigma SCGPU02RE – Merck
Filter, syringe filter unit (0.22 µm)	Abluo™, GVS Lifesciences, Sanford, ME	FJ25ASCCA002DL01
Isopropanol	Sigma-Aldrich, St Louis, MO, USA	24137-2.5L-R
Micro centrifuge tube (graduated) with flat cap (1.5 ml)	Thermo Scientific QSP, San Diego, CA	509-GRD-Q
Micro centrifuge tube (with orange screw cap) for freeze-drying samples	Corning Incorporated, Nuevo Leon, Mexico	430909
Mr Frosty freezing container	Nalgene, Sigma-Aldrich®, St Louis, MO, USA	C1562
Oil Red O	Sigma-Aldrich, St Louis, MO, USA	O0625-25G
Parafilm M® 4 in. X 250 ft. roll	Bemis NA, Neenah, WI	PM 999
Sephadex® G-100	Sigma-Aldrich, St Louis, MO, USA	G100120
SH-PEG-NHS (10K)	Biochempeg, Watertown, MA, USA	HE003023-10K
SH-PEG-NHS (3.4K)	Biochempeg, Watertown, MA, USA	HE003023-3.4K
SH-PEG-SG (10K)	Biochempeg, Watertown, MA, USA	HE003027-3.4K
SH-PEG-SPA (3.5K)	Jenkem Technology, USA	HS-PEG3500-SPA
Sringe	Codan Medical Apl., Rodby, DK	RLSMED-SYRC02

Whatman No.1 filter paper	Sigma-Aldrich, St Louis, MO, USA	WHA1001325

References

1. Mukherjee S, Venugopal JR, Ravichandran R, Ramakrishna S, Raghunath M. Multimodal biomaterial strategies for regeneration of infarcted myocardium. J Mater Chem. 2010;20(40):8819-31.

2. Venugopal JR, Prabhakaran MP, Mukherjee S, Ravichandran R, Dan K, Ramakrishna S. Biomaterial strategies for alleviation of myocardial infarction. J Royal Soc Interface. 2012;9(66):1-19.

3. Mason C, Dunnill P. A brief definition of regenerative medicine. 2008.

4. Nelson TJ, Behfar A, Terzic A. Strategies for therapeutic repair: the “R3” regenerative medicine paradigm. Clinical and translational science. 2008;1(2):168-71.

5. Sampogna G, Guraya SY, Forgione A. Regenerative medicine: Historical roots and potential strategies in modern medicine. Journal of Microscopy and Ultrastructure. 2015;3(3):101-7.

6. Mitchell AC, Briquez PS, Hubbell JA, Cochran JR. Engineering growth factors for regenerative medicine applications. Acta biomaterialia. 2016;30:1-12.

7. Bajaj P, Schweller RM, Khademhosseini A, West JL, Bashir R. 3D biofabrication strategies for tissue engineering and regenerative medicine. Annual review of biomedical engineering. 2014;16:247-76.

8. Wichterle O, Lim D. Hydrophilic gels for biological use. Nature. 1960;185(4706):117-8.

9. Kopeček J, Yang J. Hydrogels as smart biomaterials. Polymer international. 2007;56(9):1078-98.

10. Chai Q, Jiao Y, Yu X. Hydrogels for biomedical applications: their characteristics and the mechanisms behind them. Gels. 2017;3(1):6.

11. Li R, Guan X, Lin X, Guan P, Zhang X, Rao Z, et al. Poly (2-hydroxyethyl methacrylate)/β-cyclodextrin-hyaluronan contact lens with tear protein adsorption resistance and sustained drug delivery for ophthalmic diseases. Acta Biomaterialia. 2020;110:105-18.

12. Bahram M, Mohseni N, Moghtader M. An introduction to hydrogels and some recent applications. Emerging concepts in analysis and applications of hydrogels: IntechOpen; 2016.

13. Ahmed EM. Hydrogel: Preparation, characterization, and applications: A review. JAR. 2015;6(2):105-21.

14. Peppas NA, Hoffman AS. Hydrogels. Biomaterials science: Elsevier; 2020. p. 153-66.

15. Kalhapure A, Kumar R, Singh VP, Pandey D. Hydrogels: a boon for increasing agricultural productivity in water-stressed environment. Current science. 2016:1773-9.

16. Wong V. Hydrogels water absorbing polymers. Catalyst. 2007;18(1):4.

17. Peters JT, Wechsler ME, Peppas NA. Advanced biomedical hydrogels: molecular architecture and its impact on medical applications. Regenerative Biomaterials. 2021;8(6):rbab060.

18. Ahmed TA, Dare EV, Hincke M. Fibrin: A versatile scaffold for tissue engineering applications. Tissue Eng Part B Rev. 2008;14(2):199-215.

19. Jiang Y, Guo S, Jiao J, Li L. A Biphasic Hydrogel with Self-Healing Properties and a Continuous Layer Structure for Potential Application in Osteochondral Defect Repair. Polymers. 2023;15(12):2744.

20. Bashir S, Hina M, Iqbal J, Rajpar A, Mujtaba M, Alghamdi N, et al. Fundamental concepts of hydrogels: Synthesis, properties, and their applications. Polymers. 2020;12(11):2702.

21. Carletti E, Motta A, Migliaresi C. Scaffolds for tissue engineering and 3D cell culture. 3D Cell Culture: Methods and Protocols. 2011:17-39.

22. Vedadghavami A, Minooei F, Mohammadi MH, Khetani S, Kolahchi AR, Mashayekhan S, et al. Manufacturing of hydrogel biomaterials with controlled mechanical properties for tissue engineering applications. Acta biomaterialia. 2017;62:42-63.

23. Guan X, Avci-Adali M, Alarçin E, Cheng H, Kashaf SS, Li Y, et al. Development of hydrogels for regenerative engineering. Biotechnology journal. 2017;12(5):1600394.

24. Alonso JM, Andrade del Olmo J, Perez Gonzalez R, Saez-Martinez V. Injectable hydrogels: From laboratory to industrialization. Polymers. 2021;13(4):650.

25. Atkinson JB, Gomperts ED, Kang R, Lee M, Arensman RM, Bartlett RH, et al. Prospective, randomized evaluation of the efficacy of fibrin sealant as a topical hemostatic agent at the cannulation site in neonates undergoing extracorporeal membrane oxygenation. The American journal of surgery. 1997;173(6):479-84.

26. Foudazi R, Zowada R, Manas-Zloczower I, Feke DL. Porous Hydrogels: Present Challenges and Future Opportunities. Langmuir. 2023;39(6):2092-111.

27. Ji W, Chang B, Yu H, Li Y, Song W. Effect of Polymer and Crosslinker Concentration on Static and Dynamic Gelation Behavior of Phenolic Resin Hydrogel. Gels. 2024;10(5):325.

28. Garg S, Garg A, Vishwavidyalaya R. Hydrogel: Classification, properties, preparation and technical features. Asian J Biomater Res. 2016;2(6):163-70.

29. Zhang T, Yang R, Yang S, Guan J, Zhang D, Ma Y, et al. Research progress of self-assembled nanogel and hybrid hydrogel systems based on pullulan derivatives. Drug delivery. 2018;25(1):278-92.

30. Wang C, Stewart RJ, KopeČek J. Hybrid hydrogels assembled from synthetic polymers and coiled-coil protein domains. Nature. 1999;397(6718):417-20.

31. Lau HK, Kiick KL. Opportunities for multicomponent hybrid hydrogels in biomedical applications. Biomacromolecules. 2015;16(1):28-42.

32. Cho Y-W, Jang J, Park CR, Ko S-W. Preparation and solubility in acid and water of partially deacetylated chitins. Biomacromolecules. 2000;1(4):609-14.

33. Zhu D, Cheng H, Li J, Zhang W, Shen Y, Chen S, et al. Enhanced water-solubility and antibacterial activity of novel chitosan derivatives modified with quaternary phosphonium salt. Materials Science and Engineering: C. 2016;61:79-84.

34. Bhaladhare S, Das D. Cellulose: a fascinating biopolymer for hydrogel synthesis. Journal of Materials Chemistry B. 2022.

35. Haque MO, Mondal MIH. Cellulose-Based Hydrogel for Personal Hygiene Applications. Cellulose-Based Superabsorbent Hydrogels. 2018:1-21.

36. Tao F, Cheng Y, Shi X, Zheng H, Du Y, Xiang W, et al. Applications of chitin and chitosan nanofibers in bone regenerative engineering. Carbohydrate polymers. 2020;230:115658.

37. Davoodi P, Lee LY, Xu Q, Sunil V, Sun Y, Soh S, et al. Drug delivery systems for programmed and on-demand release. Advanced drug delivery reviews. 2018;132:104-38.

38. Sun Y, Nan D, Jin H, Qu X. Recent advances of injectable hydrogels for drug delivery and tissue engineering applications. Polymer Testing. 2020;81:106283.

39. Bordbar-Khiabani A, Gasik M. Smart hydrogels for advanced drug delivery systems. International Journal of Molecular Sciences. 2022;23(7):3665.

40. Madduma-Bandarage US, Madihally SV. Synthetic hydrogels: Synthesis, novel trends, and applications. Journal of Applied Polymer Science. 2021;138(19):50376.

41. Silva M, Ferreira FN, Alves NM, Paiva MC. Biodegradable polymer nanocomposites for ligament/tendon tissue engineering. Journal of nanobiotechnology. 2020;18(1):1-33.

42. Lawlor D. Absorption of polyethylene glycols by plants and their effects on plant growth. New phytologist. 1970;69(2):501-13.

43. Kopeček J. Hydrogel biomaterials: a smart future? Biomaterials. 2007;28(34):5185-92.

44. Davies NH, Schmidt C, Bezuidenhout D, Zilla P. Sustaining neovascularization of a scaffold through staged release of vascular endothelial growth factor-A and platelet-derived growth factor-BB. Tissue engineering Part A. 2012;18(1-2):26-34.

45. van Rensburg AJ, Davies NH, Oosthuysen A, Chokoza C, Zilla P, Bezuidenhout D. Improved vascularization of porous scaffolds through growth factor delivery from heparinized polyethylene glycol hydrogels. Acta Biomaterialia. 2017;49:89-100.

46. Lin C-C, Anseth KS. PEG hydrogels for the controlled release of biomolecules in regenerative medicine. Pharmaceutical research. 2009;26(3):631-43.

47. Lutolf M, Hubbell J. Synthesis and physicochemical characterization of end-linked poly (ethylene glycol)-co-peptide hydrogels formed by Michael-type addition. Biomacromolecules. 2003;4(3):713-22.

48. Lutolf MP, Weber FE, Schmoekel HG, Schense JC, Kohler T, Müller R, et al. Repair of bone defects using synthetic mimetics of collagenous extracellular matrices. Nature biotechnology. 2003;21(5):513-8.

49. Chokoza C, Gustafsson CA, Goetsch KP, Zilla P, Thierfelder N, Pisano F, et al. Tuning Tissue Ingrowth into Proangiogenic Hydrogels via Dual Modality Degradation. ACS Biomaterials Science & Engineering. 2019;5(10):5430-8.

50. Kumar A, Han SS. PVA-based hydrogels for tissue engineering: A review. International journal of polymeric materials and polymeric biomaterials. 2017;66(4):159-82.

51. Sciarretta FV. 5 to 8 years follow-up of knee chondral defects treated by PVA-H hydrogel implants. European Review for Medical & Pharmacological Sciences. 2013;17(22).

52. Chen K, Chen G, Wei S, Yang X, Zhang D, Xu L. Preparation and property of high strength and low friction PVA-HA/PAA composite hydrogel using annealing treatment. Materials Science and Engineering: C. 2018;91:579-88.

53. Wang M, Bai J, Shao K, Tang W, Zhao X, Lin D, et al. Poly (vinyl alcohol) hydrogels: The old and new functional materials. International Journal of Polymer Science. 2021;2021:1-16.

54. Jia Z, Zhu F, Li X, Liang Q, Zhuo Z, Huang J, et al. Repair of osteochondral defects using injectable chitosan-based hydrogel encapsulated synovial fluid-derived mesenchymal stem cells in a rabbit model. Materials Science and Engineering: C. 2019;99:541-51.

55. Bikiaris ND, Koumentakou I, Samiotaki C, Meimaroglou D, Varytimidou D, Karatza A, et al. Recent advances in the investigation of poly (lactic acid)(PLA) nanocomposites: incorporation of various nanofillers and their properties and applications. Polymers. 2023;15(5):1196.

56. Basu A, Kunduru KR, Doppalapudi S, Domb AJ, Khan W. Poly (lactic acid) based hydrogels. Advanced Drug Delivery Reviews. 2016;107:192-205.

57. Kaliaraj GS, Shanmugam DK, Dasan A, Mosas KKA. Hydrogels—A Promising Materials for 3D Printing Technology. Gels. 2023;9(3):260.

58. Zhu J. Bioactive modification of poly (ethylene glycol) hydrogels for tissue engineering. Biomaterials. 2010;31(17):4639-56.

59. Catoira MC, Fusaro L, Di Francesco D, Ramella M, Boccafoschi F. Overview of natural hydrogels for regenerative medicine applications. Journal of Materials Science: Materials in Medicine. 2019;30(10):1-10.

60. Cui R, Zhang L, Ou R, Xu Y, Xu L, Zhan X-Y, et al. Polysaccharide-based hydrogels for wound dressing: Design considerations and clinical applications. Frontiers in Bioengineering and Biotechnology. 2022;10.

61. Gounden V, Singh M. Hydrogels and Wound Healing: Current and Future Prospects. Gels. 2024;10(1):43.

62. Chatterjee S, Sharma S, Prasad RK, Datta S, Dubey D, Meghvansi MK, et al. Cellulase enzyme based biodegradation of cellulosic materials: an overview. Cellulose. 2015;5(6):271-82.

63. Keshk S. Bacterial cellulose production and its industrial applications. J Bioprocess Biotech. 2014;4(2):150.

64. Klemm D, Heublein B, Fink HP, Bohn A. Cellulose: fascinating biopolymer and sustainable raw material. Angewandte chemie international edition. 2005;44(22):3358-93.

65. Baer EL, Davies MW, Easterbrook K. Disposable nappies for preventing napkin dermatitis in infants. Cochrane Database of Systematic Reviews. 2006(3).

66. Simeoni RB, Mogharbel BF, Francisco JC, Miyague NI, Irioda AC, Souza CM, et al. Beneficial roles of cellulose patch-mediated cell therapy in myocardial infarction: a preclinical study. Cells. 2021;10(2):424.

67. Koike T, Sha J, Bai Y, Matsuda Y, Hideshima K, Yamada T, et al. Efficacy of bacterial cellulose as a carrier of BMP-2 for bone regeneration in a rabbit frontal sinus model. Materials. 2019;12(15):2489.

68. Bao C, Chen J, Wang Y, Yang T, Xu X, Zhang Q. Cellulose-based functional polycarbonates as degradable enzyme carriers. Cellulose. 2022;29(16):8769-80.

69. Elieh-Ali-Komi D, Hamblin MR. Chitin and chitosan: production and application of versatile biomedical nanomaterials. International journal of advanced research. 2016;4(3):411.

70. Hajji S, Younes I, Ghorbel-Bellaaj O, Hajji R, Rinaudo M, Nasri M, et al. Structural differences between chitin and chitosan extracted from three different marine sources. International journal of biological macromolecules. 2014;65:298-306.

71. Lloyd L, Kennedy J, Methacanon P, Paterson M, Knill C. Carbohydrate polymers as wound management aids. Carbohydrate Polymers. 1998;37(3):315-22.

72. Ahmadi F, Oveisi Z, Samani SM, Amoozgar Z. Chitosan based hydrogels: characteristics and pharmaceutical applications. Research in pharmaceutical sciences. 2015;10(1):1.

73. Aziz MA, Cabral JD, Brooks HJ, Moratti SC, Hanton LR. Antimicrobial properties of a chitosan dextran-based hydrogel for surgical use. Antimicrobial Agents and Chemotherapy. 2012;56(1):280-7.

74. Muthu M, Gopal J, Chun S, Devadoss AJP, Hasan N, Sivanesan I. Crustacean waste-derived chitosan: Antioxidant properties and future perspective. Antioxidants. 2021;10(2):228.

75. Mori T, Murakami M, Okumura M, Kadosawa T, Uede T, Fujinaga T. Mechanism of macrophage activation by chitin derivatives. Journal of veterinary medical science. 2005;67(1):51-6.

76. Aranaz I, Alcántara AR, Civera MC, Arias C, Elorza B, Heras Caballero A, et al. Chitosan: An overview of its properties and applications. Polymers. 2021;13(19):3256.

77. Fu J, Yang F, Guo Z. The chitosan hydrogels: From structure to function. New Journal of Chemistry. 2018;42(21):17162-80.

78. Krefting A. An improved method of treating seaweed to obtain valuable products therefrom. Br Patent. 1896;11:538.

79. Sandford PA, Baird J. Industrial utilization of polysaccharides. The polysaccharides: Elsevier; 1983. p. 411-90.

80. Hirst E, Jones J, Jones WO. Structure of alginic acid. Nature. 1939;143(3629):857-.

81. Ye S, Xie C, Agar OT, Barrow CJ, Dunshea FR, Suleria HA. Alginates from Brown Seaweeds as a Promising Natural Source: A Review of Its Properties and Health Benefits. Food Reviews International. 2024:1-29.

82. Burdick JA, Stevens MM. Biomedical hydrogels. Biomaterials, artificial organs and tissue engineering: Elsevier; 2005. p. 107-15.

83. Aderibigbe BA, Buyana B. Alginate in wound dressings. Pharmaceutics. 2018;10(2):42.

84. Abasalizadeh F, Moghaddam SV, Alizadeh E, Akbari E, Kashani E, Fazljou SMB, et al. Alginate-based hydrogels as drug delivery vehicles in cancer treatment and their

applications in wound dressing and 3D bioprinting. Journal of biological engineering. 2020;14:1-22.

85. Krzyszczyk P, Schloss R, Palmer A, Berthiaume F. The role of macrophages in acute and chronic wound healing and interventions to promote pro-wound healing phenotypes. Frontiers in physiology. 2018;9:419.

86. Balakrishnan B, Mohanty M, Umashankar P, Jayakrishnan A. Evaluation of an in situ forming hydrogel wound dressing based on oxidized alginate and gelatin. Biomaterials. 2005;26(32):6335-42.

87. Soon-Shiong P, Heintz R, Merideth N, Yao Q, Yao Z, Zheng T, et al. Insulin independence in a type 1 diabetic patient after encapsulated islet transplantation. Lancet (London, England). 1994;343(8903):950-1.

88. Tuch BE, Keogh GW, Williams LJ, Wu W, Foster JL, Vaithilingam V, et al. Safety and viability of microencapsulated human islets transplanted into diabetic humans. Diabetes care. 2009;32(10):1887-9.

89. Hogrebe NJ, Ishahak M, Millman JR. Developments in stem cell-derived islet replacement therapy for treating type 1 diabetes. Cell Stem Cell. 2023;30(5):530-48.

90. Qin T. Enhancing Pancreatic β-Cell Viability and Longevity Through Novel Microencapsulation Strategies and Stromal Cell Support. 2024.

91. Keymeulen B, De Groot K, Jacobs-Tulleneers-Thevissen D, Thompson DM, Bellin MD, Kroon EJ, et al. Encapsulated stem cell–derived β cells exert glucose control in patients with type 1 diabetes. Nature Biotechnology. 2023:1-8.

92. Lee LC, Wall ST, Klepach D, Ge L, Zhang Z, Lee RJ, et al. Algisyl-LVR™ with coronary artery bypass grafting reduces left ventricular wall stress and improves function in the failing human heart. International journal of cardiology. 2013;168(3):2022-8.

93. Lee RJ, Hinson A, Bauernschmitt R, Matschke K, Fang Q, Mann DL, et al. The feasibility and safety of Algisyl-LVR™ as a method of left ventricular augmentation in patients with dilated cardiomyopathy: initial first in man clinical results. International journal of cardiology. 2015;199:18-24.

94. Anker SD, Coats AJ, Cristian G, Dragomir D, Pusineri E, Piredda M, et al. A prospective comparison of alginate-hydrogel with standard medical therapy to determine impact on functional capacity and clinical outcomes in patients with advanced heart failure (AUGMENT-HF trial). European heart journal. 2015;36(34):2297-309.

95. Leor J, Tuvia S, Guetta V, Manczur F, Castel D, Willenz U, et al. Intracoronary injection of in situ forming alginate hydrogel reverses left ventricular remodeling after myocardial infarction in Swine. Journal of the American College of Cardiology. 2009;54(11):1014-23.

96. Landa N, Miller L, Feinberg MS, Holbova R, Shachar M, Freeman I, et al. Effect of injectable alginate implant on cardiac remodeling and function after recent and old infarcts in rat. Circulation. 2008;117(11):1388-96.

97. Paloschi V, Sabater-Lleal M, Middelkamp H, Vivas A, Johansson S, van der Meer A, et al. Organ-on-a-chip technology: a novel approach to investigate cardiovascular diseases. Cardiovascular research. 2021;117(14):2742-54.

98. Zhang H, Cheng J, Ao Q. Preparation of alginate-based biomaterials and their applications in biomedicine. Marine Drugs. 2021;19(5):264.

99. Geckil H, Xu F, Zhang X, Moon S, Demirci U. Engineering hydrogels as extracellular matrix mimics. Nanomedicine. 2010;5(3):469-84.

100. Golebiowska AA, Intravaia JT, Sathe VM, Kumbar SG, Nukavarapu SP. Decellularized extracellular matrix biomaterials for regenerative therapies: Advances, challenges and clinical prospects. Bioactive Materials. 2024;32:98-123.

101. Saldin LT, Cramer MC, Velankar SS, White LJ, Badylak SF. Extracellular matrix hydrogels from decellularized tissues: Structure and function. Acta biomaterialia. 2017;49:1-15.

102. Song JJ, Ott HC. Organ engineering based on decellularized matrix scaffolds. Trends in molecular medicine. 2011;17(8):424-32.

103. Zhang W, Du A, Liu S, Lv M, Chen S. Research progress in decellularized extracellular matrix-derived hydrogels. Regenerative Therapy. 2021;18:88-96.

104. Crapo PM, Gilbert TW, Badylak SF. An overview of tissue and whole organ decellularization processes. Biomaterials. 2011;32(12):3233-43.

105. Gilbert TW, Sellaro TL, Badylak SF. Decellularization of tissues and organs. Biomaterials. 2006;27(19):3675-83.

106. Drake M, Davison tP, Bump S, Schmitt F. Action of proteolytic enzymes on tropocollagen and insoluble collagen. Biochemistry. 1966;5(1):301-12.

107. Hulmes D. Collagen diversity, synthesis and assembly. Collagen: structure and mechanics: Springer; 2008. p. 15-47.

108. Brightman A, Rajwa B, Sturgis J, McCallister M, Robinson J, Voytik-Harbin S. Time-lapse confocal reflection microscopy of collagen fibrillogenesis and extracellular matrix assembly in vitro. Biopolymers: Original Research on Biomolecules. 2000;54(3):222-34.

109. Wang RM, Christman KL. Decellularized myocardial matrix hydrogels: In basic research and preclinical studies. Advanced drug delivery reviews. 2016;96:77-82.

110. Johnson TD, Christman KL. Injectable hydrogel therapies and their delivery strategies for treating myocardial infarction. Expert opinion on drug delivery. 2013;10(1):59-72.

111. Ungerleider J, Johnson T, Rao N, Christman K. Fabrication and characterization of injectable hydrogels derived from decellularized skeletal and cardiac muscle. Methods. 2015;84:53-9.

112. Singelyn JM, DeQuach JA, Seif-Naraghi SB, Littlefield RB, Schup-Magoffin PJ, Christman KL. Naturally derived myocardial matrix as an injectable scaffold for cardiac tissue engineering. Biomaterials. 2009;30(29):5409-16.

113. Singelyn JM, Sundaramurthy P, Johnson TD, Schup-Magoffin PJ, Hu DP, Faulk DM, et al. Catheter-deliverable hydrogel derived from decellularized ventricular extracellular matrix increases endogenous cardiomyocytes and preserves cardiac function post-myocardial infarction. Journal of the American College of Cardiology. 2012;59(8):751-63.

114. Chen WC, Wang Z, Missinato MA, Park DW, Long DW, Liu H-J, et al. Decellularized zebrafish cardiac extracellular matrix induces mammalian heart regeneration. Science advances. 2016;2(11):e1600844.

115. Traverse J, Henry T, Dib N, Patel A, Pepine C, Schaer G, et al. First-in-man study of a cardiac extracellular matrix hydrogel in early and late myocardial infarction patients. JACC Basic Transl Sci. 2019; 4: 659–69. Epub 2019/11/12. https://doi. org/10.1016/j. jacbts. 2019.07. 012 PMID: 31709316.

116. Diaz MD, Tran E, Spang M, Wang R, Gaetani R, Luo CG, et al. Injectable myocardial matrix hydrogel mitigates negative left ventricular remodeling in a chronic myocardial infarction model. Basic to Translational Science. 2021;6(4):350-61.

117. Sasikumar S, Chameettachal S, Cromer B, Pati F, Kingshott P. Decellularized extracellular matrix hydrogels—Cell behavior as a function of matrix stiffness. Current Opinion in Biomedical Engineering. 2019;10:123-33.

118. Davari N, Bakhtiary N, Khajehmohammadi M, Sarkari S, Tolabi H, Ghorbani F, et al. Protein-based hydrogels: promising materials for tissue engineering. Polymers. 2022;14(5):986.

119. Shoulders MD, Raines RT. Collagen structure and stability. Annual review of biochemistry. 2009;78:929-58.

120. Meyer M. Processing of collagen based biomaterials and the resulting materials properties. Biomedical engineering online. 2019;18(1):1-74.

121. Harris J. Fibroblasts and their transformations: the connective-tissue cell family. Molecular Biology of the Cell. 1994:1179-93.

122. Harris CA, Hamilton PB, Runnalls TJ, Vinciotti V, Henshaw A, Hodgson D, et al. The consequences of feminization in breeding groups of wild fish. 2011.

123. Mathew-Steiner SS, Roy S, Sen CK. Collagen in wound healing. Bioengineering. 2021;8(5):63.

124. Thomas A, Farah K, Millis RM. Epigenetic influences on wound healing and hypertrophic-keloid scarring: a review for basic scientists and clinicians. Cureus. 2022;14(3).

125. Liu X, Zheng C, Luo X, Wang X, Jiang H. Recent advances of collagen-based biomaterials: Multi-hierarchical structure, modification and biomedical applications. Materials Science and Engineering: C. 2019;99:1509-22.

126. Simon H, Van Agthoven M, Lam P, Floris F, Chiron L, Delsuc M-A, et al. Uncoiling collagen: a multidimensional mass spectrometry study. Analyst. 2016;141(1):157-65.

127. Achilli M, Mantovani D. Tailoring mechanical properties of collagen-based scaffolds for vascular tissue engineering: the effects of pH, temperature and ionic strength on gelation. Polymers. 2010;2(4):664-80.

128. Zhu J, Kaufman LJ. Collagen I self-assembly: revealing the developing structures that generate turbidity. Biophysical journal. 2014;106(8):1822-31.

129. Furusawa K, Sato S, Masumoto J-i, Hanazaki Y, Maki Y, Dobashi T, et al. Studies on the formation mechanism and the structure of the anisotropic collagen gel prepared by dialysis-induced anisotropic gelation. Biomacromolecules. 2012;13(1):29-39.

130. Antoine EE, Vlachos PP, Rylander MN. Review of collagen I hydrogels for bioengineered tissue microenvironments: characterization of mechanics, structure, and transport. Tissue Engineering Part B: Reviews. 2014;20(6):683-96.

131. Sarrigiannidis SO, Rey JM, Dobre O, González-García C, Dalby MJ, Salmeron-Sanchez M. A tough act to follow: Collagen hydrogel modifications to improve mechanical and growth factor loading capabilities. Materials Today Bio. 2021;10:100098.

132. Sanz-Ramos P, Mora G, Vicente-Pascual M, Ochoa I, Alcaine C, Moreno R, et al. Response of sheep chondrocytes to changes in substrate stiffness from 2 to 20 Pa: effect of cell passaging. Connective tissue research. 2013;54(3):159-66.

133. Schuh E, Hofmann S, Stok K, Notbohm H, Müller R, Rotter N. Chondrocyte redifferentiation in 3D: the effect of adhesion site density and substrate elasticity. Journal of Biomedical Materials Research Part A. 2012;100(1):38-47.

134. Schuh E, Hofmann S, Stok KS, Notbohm H, Müller R, Rotter N. The influence of matrix elasticity on chondrocyte behavior in 3D. Journal of tissue engineering and regenerative medicine. 2012;6(10):e31-e42.

135. Mandal A, Clegg JR, Anselmo AC, Mitragotri S. Hydrogels in the clinic. Bioengineering & translational medicine. 2020;5(2):e10158.

136. Salvatore L, Natali ML, Brunetti C, Sannino A, Gallo N. An Update on the Clinical Efficacy and Safety of Collagen Injectables for Aesthetic and Regenerative Medicine Applications. Polymers. 2023;15(4):1020.

137. Brown-Etris M, Milne CT, Hodde JP. An extracellular matrix graft (Oasis® wound matrix) for treating full-thickness pressure ulcers: A randomized clinical trial. Journal of tissue viability. 2019;28(1):21-6.

138. Li Y, Meng H, Liu Y, Lee BP. Fibrin gel as an injectable biodegradable scaffold and cell carrier for tissue engineering. Sci World J. 2015;2015.

139. Weisel JW, Litvinov RI. Fibrin formation, structure and properties. Fibrous proteins: structures and mechanisms. 2017:405-56.

140. Jensen T, Kierulf P, Sandset PM, Klingenberg O, Joø GB, Godal HC, et al. Fibrinogen and fibrin induce synthesis of proinflammatory cytokines from isolated peripheral blood mononuclear cells. Thrombosis and haemostasis. 2007;97(05):822-9.

141. Jennewein C, Tran N, Paulus P, Ellinghaus P, Eble JA, Zacharowski K. Novel aspects of fibrin (ogen) fragments during inflammation. Molecular medicine. 2011;17:568-73.

142. Yeromonahos C, Polack B, Caton F. Nanostructure of the fibrin clot. Biophysical journal. 2010;99(7):2018-27.

143. Litvinov RI, Weisel JW. Fibrin mechanical properties and their structural origins. Matrix Biology. 2017;60:110-23.

144. Fish RJ, Neerman-Arbez M. Fibrinogen gene regulation. Thrombosis and haemostasis. 2012;108(09):419-26.

145. Asselta R, Spena S, Duga S, Tenchini M. Molecular genetics of quantitative fibrinogen disorders. Cardiovascular & Hematological Agents in Medicinal Chemistry (Formerly Current Medicinal Chemistry-Cardiovascular & Hematological Agents). 2007;5(2):163-73.

146. Hu C-H, Harris JE, Davie EW, Chung DW. Characterization of the 5′-flanking region of the gene for the α chain of human fibrinogen. Journal of Biological Chemistry. 1995;270(47):28342-9.

147. Dalmon J, Laurent M, Courtois G. The human beta fibrinogen promoter contains a hepatocyte nuclear factor 1-dependent interleukin-6-responsive element. Molecular and Cellular Biology. 1993;13(2):1183-93.

148. Mizuguchi J, Hu C-H, Cao Z, Loeb KR, Chung DW, Davie EW. Characterization of the 5′-Flanking Region of the Gene for the γChain of Human Fibrinogen. Journal of Biological Chemistry. 1995;270(47):28350-6.

149. Fort A, Borel C, Migliavacca E, Antonarakis SE, Fish RJ, Neerman-Arbez M. Regulation of fibrinogen production by microRNAs. Blood, The Journal of the American Society of Hematology. 2010;116(14):2608-15.

150. Bailey K, Astbury W, Rudall K. Fibrinogen and fibrin as members of the keratin-myosin group. Nature. 1943;151(3843):716-7.

151. Velnar T, Bailey T, Smrkolj V. The wound healing process: an overview of the cellular and molecular mechanisms. Journal of international medical research. 2009;37(5):1528-42.

152. Enoch S, Leaper DJ. Basic science of wound healing. Surgery (Oxford). 2008;26(2):31-7.

153. Periayah MH, Halim AS, Saad AZM. Mechanism action of platelets and crucial blood coagulation pathways in hemostasis. International journal of hematology-oncology and stem cell research. 2017;11(4):319.

154. Chaudhry R, Usama SM, Babiker HM. Physiology, coagulation pathways. 2018.

155. Mackman N, Tilley RE, Key NS. Role of the extrinsic pathway of blood coagulation in hemostasis and thrombosis. Arteriosclerosis, thrombosis, and vascular biology. 2007;27(8):1687-93.

156. Achyuthan K, Slaughter T, Santiago M, Enghild J, Greenberg C. Factor XIIIa-derived peptides inhibit transglutaminase activity. Localization of substrate recognition sites. Journal of Biological Chemistry. 1993;268(28):21284-92.

157. Rijken DC, Uitte de Willige S. Inhibition of fibrinolysis by coagulation factor XIII. BioMed research international. 2017;2017.

158. Schultz GS, Chin GA, Moldawer L, Diegelmann RF. 23 principles of wound healing. Mechanisms of vascular disease: a reference book for vascular specialists. 2011:423.

159. Trinh X-T, Long N-V, Van Anh LT, Nga PT, Giang NN, Chien PN, et al. A Comprehensive Review of Natural Compounds for Wound Healing: Targeting Bioactivity Perspective. International Journal of Molecular Sciences. 2022;23(17):9573.

160. Li Y, Meng H, Liu Y, Lee BP. Fibrin gel as an injectable biodegradable scaffold and cell carrier for tissue engineering. The Scientific World Journal. 2015;2015.

161. Yurina L, Vasilyeva A, Indeykina M, Bugrova A, Biryukova M, Kononikhin A, et al. Ozone-induced damage of fibrinogen molecules: Identification of oxidation sites by high-resolution mass spectrometry. Free radical research. 2019;53(4):430-55.

162. Yang Z, Mochalkin I, Doolittle RF. A model of fibrin formation based on crystal structures of fibrinogen and fibrin fragments complexed with synthetic peptides. Proceedings of the National Academy of Sciences. 2000;97(26):14156-61.

163. Weisel JW, Litvinov RI. Mechanisms of fibrin polymerization and clinical implications. Blood, The Journal of the American Society of Hematology. 2013;121(10):1712-9.

164. Stamboroski S, Joshi A, Noeske PLM, Köppen S, Brüggemann D. Principles of fibrinogen fiber assembly in vitro. Macromolecular Bioscience. 2021;21(5):2000412.

165. Martino MM, Briquez PS, Ranga A, Lutolf MP, Hubbell JA. Heparin-binding domain of fibrin (ogen) binds growth factors and promotes tissue repair when incorporated within a synthetic matrix. Proceedings of the National Academy of Sciences. 2013;110(12):4563-8.

166. Sabban AMA. Characterisation of the fibrinogen RGD sequence in erythrocyte binding and clot structure: University of Leeds; 2019.

167. Martinez J, Ferber A, Bach TL, Yaen CH. Interaction of fibrin with VE-cadherin. Annals of the New York Academy of Sciences. 2001;936(1):386-405.

168. Laurens N, Koolwijk Pd, De Maat M. Fibrin structure and wound healing. Journal of Thrombosis and Haemostasis. 2006;4(5):932-9.

169. Bennett JS. Platelet-fibrinogen interactions. Annals of the New York Academy of Sciences. 2001;936(1):340-54.

170. Ugarova TP, Yakubenko VP. Recognition of fibrinogen by leukocyte integrins. Annals of the New York Academy of Sciences. 2001;936(1):368-85.

171. Chapin JC, Hajjar KA. Fibrinolysis and the control of blood coagulation. Blood reviews. 2015;29(1):17-24.

172. Bailey K, Bettelheim FR, Lorand L, Middlebrook W. Action of thrombin in the clotting of fibrinogen. Nature. 1951;167(4241):233-4.

173. Latallo ZS, Fletcher AP, Alkjaersig N, Sherry S. Inhibition of fibrin polymerization by fibrinogen proteolysis products. American Journal of Physiology-Legacy Content. 1962;202(4):681-6.

174. Senior RM, Skogen WF, Griffin GL, Wilner GD. Effects of fibrinogen derivatives upon the inflammatory response. Studies with human fibrinopeptide B. The Journal of clinical investigation. 1986;77(3):1014-9.

175. Richardson D, Pepper D, Kay A. Chemotaxis for human monocytes by fibrinogen-derived peptides. British Journal of Haematology. 1976;32(4):507-14.

176. Lalla RV, Tanzer ML, Kreutzer DL. Identification of a region of the fibrin molecule involved in upregulation of interleukin-8 expression from human oral squamous cell carcinoma cells. Archives of oral biology. 2003;48(4):263-71.

177. Roesner JP, Petzelbauer P, Koch A, Tran N, Iber T, Vagts DA, et al. Bβ15-42 (FX06) reduces pulmonary, myocardial, liver, and small intestine damage in a pig model of hemorrhagic shock and reperfusion. Critical care medicine. 2009;37(2):598-605.

178. Hense D, Strube OI. Fibrillogenesis and hydrogel formation from fibrinogen induced by calcium salts. Gels. 2023;9(3):175.

179. Rowe SL, Lee S, Stegemann JP. Influence of thrombin concentration on the mechanical and morphological properties of cell-seeded fibrin hydrogels. Acta biomaterialia. 2007;3(1):59-67.

180. Leonidakis KA, Bhattacharya P, Patterson J, Vos BE, Koenderink GH, Vermant J, et al. Fibrin structural and diffusional analysis suggests that fibers are permeable to solute transport. Acta biomaterialia. 2017;47:25-39.

181. Chernysh IN, Weisel JW. Dynamic imaging of fibrin network formation correlated with other measures of polymerization. Blood, The Journal of the American Society of Hematology. 2008;111(10):4854-61.

182. Kubota K, Kogure H, Masuda Y, Toyama Y, Kita R, Takahashi A, et al. Gelation dynamics and gel structure of fibrinogen. Colloids and Surfaces B: Biointerfaces. 2004;38(3-4):103-9.

183. Naski M, Shafer J. A kinetic model for the alpha-thrombin-catalyzed conversion of plasma levels of fibrinogen to fibrin in the presence of antithrombin III. Journal of Biological Chemistry. 1991;266(20):13003-10.

184. Mihalyi E. Clotting of bovine fibrinogen. Calcium binding to fibrin during clotting and its dependence on release of fibrinopeptide B. Biochemistry. 1988;27(3):967-76.

185. Okada M, Blombäck B. Factors influencing fibrin gel structure studied by flow measurement. Annals of the New York Academy of Sciences. 1983;408(1):233-53.

186. Di Stasio E, Nagaswami C, Weisel JW, Di Cera E. Cl− regulates the structure of the fibrin clot. Biophysical journal. 1998;75(4):1973-9.

187. McKee PA, Mattock P, Hill RL. Subunit structure of human fibrinogen, soluble fibrin, and cross-linked insoluble fibrin. Proceedings of the National Academy of Sciences. 1970;66(3):738-44.

188. Waugh DF, Livingstone BJ. Clotting time and reaction velocity in the interaction of bovine fibrinogen and thrombin. Science. 1951;113(2927):121-4.

189. Fogelson AL, Keener JP. Toward an understanding of fibrin branching structure. Physical Review E. 2010;81(5):051922.

190. Kelley MA, Leiderman K. Mathematical modeling to understand the role of bivalent thrombin-fibrin binding during polymerization. PLoS Computational Biology. 2022;18(9):e1010414.

191. Ho W, Tawil B, Dunn JC, Wu BM. The behavior of human mesenchymal stem cells in 3D fibrin clots: dependence on fibrinogen concentration and clot structure. Tissue Engineering. 2006;12(6):1587-95.

192. Cox S, Cole M, Tawil B. Behavior of human dermal fibroblasts in three-dimensional fibrin clots: dependence on fibrinogen and thrombin concentration. Tissue engineering. 2004;10(5-6):942-54.

193. Britton S, Kim O, Pancaldi F, Xu Z, Litvinov RI, Weisel JW, et al. Contribution of nascent cohesive fiber-fiber interactions to the non-linear elasticity of fibrin networks under tensile load. Acta biomaterialia. 2019;94:514-23.

194. Kim OV, Litvinov RI, Weisel JW, Alber MS. Structural basis for the nonlinear mechanics of fibrin networks under compression. Biomaterials. 2014;35(25):6739-49.

195. Salam N, Toumpaniari S, Gentile P, Marina Ferreira A, Dalgarno K, Partridge S. Assessment of migration of human mscs through fibrin hydrogels as a tool for formulation optimisation. Materials. 2018;11(9):1781.

196. Spotnitz WD. Fibrin sealant: the only approved hemostat, sealant, and adhesive—a laboratory and clinical perspective. International Scholarly Research Notices. 2014;2014.

197. Insert P. Tisseel. Westlake Village, CA: Baxter. 2009.

198. Spotnitz WD, Burks S. Hemostats, sealants, and adhesives: components of the surgical toolbox. Transfusion. 2008;48(7):1502-16.

199. Thompson DF, Letassy NA, Thompson GD. Fibrin glue: a review of its preparation, efficacy, and adverse effects as a topical hemostat. Drug intelligence & clinical pharmacy. 1988;22(12):946-52.

200. De Hert S, Ouattara A, Royston D, van der Linden J, Zacharowski K. Use and safety of aprotinin in routine clinical practice: A European postauthorisation safety study conducted in patients undergoing cardiac surgery. European Journal of Anaesthesiology. 2022;39(8):685.

201. Mandell SP, Gibran NS. Fibrin sealants: surgical hemostat, sealant and adhesive. Expert opinion on biological therapy. 2014;14(6):821-30.

202. Bao Z, Gao M, Sun Y, Nian R, Xian M. The recent progress of tissue adhesives in design strategies, adhesive mechanism and applications. Materials Science and Engineering: C. 2020;111:110796.

203. Choudhuri AH, Uppal R. Predictors of septic shock following anastomotic leak after major gastrointestinal surgery: An audit from a tertiary care institute. Indian Journal of Critical Care Medicine: Peer-reviewed, Official Publication of Indian Society of Critical Care Medicine. 2013;17(5):298.

204. Roy C, Tamura R, McDonald L, Gabra H. Successful management of anastomotic leakage with endoscopic fibrin glue injection after primary repair of pure oesophageal atresia. BMJ Case Reports CP. 2021;14(1):e238823.

205. Abbade LP, Barraviera SRCS, Silvares MRC, Lima ABBdC, Haddad GR, Gatti MA, et al. Treatment of chronic venous ulcers with heterologous fibrin sealant: a phase I/II clinical trial. Frontiers in immunology. 2021;12:627541.

206. Sileshi B, Achneck HE, Lawson JH. Management of surgical hemostasis: topical agents. Vascular. 2008;16(1_suppl):22-8.

207. Rousou J, Levitsky S, Gonzalez-Lavin L, Cosgrove D, Magilligan D, Weldon C, et al. Randomized clinical trial of fibrin sealant in patients undergoing resternotomy or reoperation after cardiac operations: a multicenter study. The Journal of thoracic and cardiovascular surgery. 1989;97(2):194-203.

208. Schwartz M, Madariaga J, Hirose R, Shaver TR, Sher L, Chari R, et al. Comparison of a new fibrin sealant with standard topical hemostatic agents. Archives of Surgery. 2004;139(11):1148-54.

209. Reddy KS, Chittoria RK, Babu P, Marimuthu SK, Kumar SH, Subbarayan EK, et al. Effectiveness of fibrin glue in adherence of skin graft. Journal of Cutaneous and Aesthetic Surgery. 2017;10(2):72.

210. Ortiz AdC, Fideles SOM, Pomini KT, Reis CHB, Bueno CRdS, Pereira EdSBM, et al. Effects of Therapy with Fibrin Glue combined with Mesenchymal Stem Cells (MSCs) on Bone Regeneration: A Systematic Review. Cells. 2021;10(9):2323.

211. Kim I, Lee SK, Yoon JI, Kim DE, Kim M, Ha H. Fibrin glue improves the therapeutic effect of MSCs by sustaining survival and paracrine function. Tissue engineering part a. 2013;19(21-22):2373-81.

212. Dow J, Simkhovich BZ, Kedes L, Kloner RA. Washout of transplanted cells from the heart: a potential new hurdle for cell transplantation therapy. Cardiovascular research. 2005;67(2):301-7.

213. Baldari S, Di Rocco G, Piccoli M, Pozzobon M, Muraca M, Toietta G. Challenges and strategies for improving the regenerative effects of mesenchymal stromal cell-based therapies. International journal of molecular sciences. 2017;18(10):2087.

214. Abdelwahid E, Kalvelyte A, Stulpinas A, De Carvalho KAT, Guarita-Souza LC, Foldes G. Stem cell death and survival in heart regeneration and repair. Apoptosis. 2016;21:252-68.

215. van den Akker F, Feyen DA, van den Hoogen P, van Laake LW, van Eeuwijk EC, Hoefer I, et al. Intramyocardial stem cell injection: go (ne) with the flow. European heart journal. 2017;38(3):184-6.

216. Christman KL, Vardanian AJ, Fang Q, Sievers RE, Fok HH, Lee RJ. Injectable Fibrin Scaffold Improves Cell Transplant Survival, Reduces Infarct Expansion, and Induces Neovasculature Formation in Ischemic Myocardium. J Am Coll Cardiol. 2004;44(3):654-60.

217. Ryu JH, Kim I-K, Cho S-W, Cho M-C, Hwang K-K, Piao H, et al. Implantation of bone marrow mononuclear cells using injectable fibrin matrix enhances neovascularization in infarcted myocardium. Biomaterials. 2005;26(3):319-26.

218. Falanga V, Iwamoto S, Chartier M, Yufit T, Butmarc J, Kouttab N, et al. Autologous bone marrow–derived cultured mesenchymal stem cells delivered in a fibrin spray accelerate healing in murine and human cutaneous wounds. Tissue engineering. 2007;13(6):1299-312.

219. Spicer PP, Mikos AG. Fibrin glue as a drug delivery system. Journal of controlled release. 2010;148(1):49-55.

220. Hameed H, Faheem S, Paiva-Santos AC, Sarwar HS, Jamshaid M. A comprehensive review of hydrogel-based drug delivery systems: classification, properties, recent trends, and applications. AAPS PharmSciTech. 2024;25(4):64.

221. Liu B, Chen K. Advances in Hydrogel-Based Drug Delivery Systems. Gels. 2024;10(4):262.

222. Wong C, Inman E, Spaethe R, Helgerson S. Fibrin-based biomaterials to deliver human growth factors. Thrombosis and haemostasis. 2003;89(03):573-82.

223. Zisch AH, Schenk U, Schense JC, Sakiyama-Elbert SE, Hubbell JA. Covalently conjugated VEGF–fibrin matrices for endothelialization. Journal of Controlled Release. 2001;72(1-3):101-13.

224. Sacchi V, Mittermayr R, Hartinger J, Martino MM, Lorentz KM, Wolbank S, et al. Long-lasting fibrin matrices ensure stable and functional angiogenesis by highly tunable, sustained delivery of recombinant VEGF164. Proceedings of the National Academy of Sciences. 2014;111(19):6952-7.

225. Arkudas A, Tjiawi J, Saumweber A, Beier J, Polykandriotis E, Bleiziffer O, et al. Evaluation of blood vessel ingrowth in fibrin gel subject to type and concentration of growth factors. Journal of cellular and molecular medicine. 2009;13(9a):2864-74.

226. Arkudas A, Pryymachuk G, Hoereth T, Beier JP, Polykandriotis E, Bleiziffer O, et al. Dose-finding study of fibrin gel-immobilized vascular endothelial growth factor 165 and basic fibroblast growth factor in the arteriovenous loop rat model. Tissue Engineering Part A. 2009;15(9):2501-11.

227. Dozier JK, Distefano MD. Site-specific PEGylation of therapeutic proteins. International journal of molecular sciences. 2015;16(10):25831-64.

228. Gupta V, Bhavanasi S, Quadir M, Singh K, Ghosh G, Vasamreddy K, et al. Protein PEGylation for cancer therapy: bench to bedside. Journal of Cell Communication and Signaling. 2019;13(3):319-30.

229. Hoffman AS. The early days of PEG and PEGylation (1970s–1990s). Acta biomaterialia. 2016;40:1-5.

230. Drinnan CT, Zhang G, Alexander MA, Pulido AS, Suggs LJ. Multimodal release of transforming growth factor-β1 and the BB isoform of platelet derived growth factor from PEGylated fibrin gels. Journal of controlled release. 2010;147(2):180-6.

231. Geuss LR, Allen AC, Ramamoorthy D, Suggs LJ. Maintenance of HL-1 cardiomyocyte functional activity in PEGylated fibrin gels. Biotechnology and bioengineering. 2015;112(7):1446-56.

232. Rytlewski JA, Aldon MA, Lewis EW, Suggs LJ. Mechanisms of tubulogenesis and endothelial phenotype expression by MSCs. Microvascular research. 2015;99:26-35.

233. Zhang G, Wang X, Wang Z, Zhang J, Suggs L. A PEGylated fibrin patch for mesenchymal stem cell delivery. Tissue engineering. 2006;12(1):9-19.

234. Rytlewski JA, Geuss LR, Anyaeji CI, Lewis EW, Suggs LJ. Three-dimensional image quantification as a new morphometry method for tissue engineering. Tissue Engineering Part C: Methods. 2012;18(7):507-16.

235. Zhang G, Hu Q, Braunlin EA, Suggs LJ, Zhang J. Enhancing efficacy of stem cell transplantation to the heart with a PEGylated fibrin biomatrix. Tissue Engineering Part A. 2008;14(6):1025-36.

236. Dadashzadeh A, Moghassemi S, Amorim C. Evaluation of PEGylated fibrin as a three-dimensional biodegradable scaffold for ovarian tissue engineering. Materials Today Chemistry. 2021;22:100626.

237. Hammers DW, Sarathy A, Pham CB, Drinnan CT, Farrar RP, Suggs LJ. Controlled release of IGF-I from a biodegradable matrix improves functional recovery of skeletal muscle from ischemia/reperfusion. Biotechnology and bioengineering. 2012;109(4):1051-9.

238. Zamora DO, Natesan S, Becerra S, Wrice N, Chung E, Suggs LJ, et al. Enhanced wound vascularization using a dsASCs seeded FPEG scaffold. Angiogenesis. 2013;16:745-57.

239. Chung E, Rytlewski JA, Merchant AG, Dhada KS, Lewis EW, Suggs LJ. Fibrin-based 3D matrices induce angiogenic behavior of adipose-derived stem cells. Acta biomaterialia. 2015;17:78-88.

240. Ricles LM, Hsieh P-L, Dana N, Rybalko V, Kraynak C, Farrar RP, et al. Therapeutic assessment of mesenchymal stem cells delivered within a PEGylated fibrin gel following an ischemic injury. Biomaterials. 2016;102:9-19.

241. Rabenstein DL. Heparin and heparan sulfate: structure and function. Natural product reports. 2002;19(3):312-31.

242. McLean J. The thromboplastic action of cephalin. American Journal of Physiology-Legacy Content. 1916;41(2):250-7.

243. Capila I, Linhardt RJ. Heparin–protein interactions. Angewandte Chemie International Edition. 2002;41(3):390-412.

244. Paluck SJ, Nguyen TH, Maynard HD. Heparin-mimicking polymers: synthesis and biological applications. Biomacromolecules. 2016;17(11):3417-40.

245. Best CH. Preparation of heparin and its use in the first clinical cases. Circulation. 1959;19(1):79-86.

246. Hao C, Xu H, Yu L, Zhang L. Heparin: an essential drug for modern medicine. Progress in molecular biology and translational science. 2019;163:1-19.

247. Koch A, Bouges S, Ziegler S, Dinkel H, Daures J, Victor N. Low molecular weight heparin and unfractionated heparin in thrombosis prophylaxis after major surgical intervention: update of previous meta-analyses. British journal of surgery. 1997;84(6):750-9.

248. Eikelboom JW, Anand SS, Malmberg K, Weitz JI, Ginsberg JS, Yusuf S. Unfractionated heparin and low-molecular-weight heparin in acute coronary syndrome without ST elevation: a meta-analysis. The Lancet. 2000;355(9219):1936-42.

249. Merli GJ, Groce JB. Pharmacological and clinical differences between low-molecular-weight heparins: implications for prescribing practice and therapeutic interchange. Pharmacy and Therapeutics. 2010;35(2):95.

250. Sakiyama-Elbert SE. Incorporation of heparin into biomaterials. Acta biomaterialia. 2014;10(4):1581-7.

251. Jha AK, Mathur A, Svedlund FL, Ye J, Yeghiazarians Y, Healy KE. Molecular weight and concentration of heparin in hyaluronic acid-based matrices modulates growth factor retention kinetics and stem cell fate. Journal of Controlled Release. 2015;209:308-16.

252. Faham S, Hileman R, Fromm J, Linhardt R, Rees D. Heparin structure and interactions with basic fibroblast growth factor. Science. 1996;271(5252):1116-20.

253. Munoz EM, Linhardt RJ. Heparin-binding domains in vascular biology. Arteriosclerosis, thrombosis, and vascular biology. 2004;24(9):1549-57.

254. Pearson RG. Hard and soft acids and bases. Journal of the American Chemical society. 1963;85(22):3533-9.

255. Caldwell EE, Nadkarni VD, Fromm JR, Linhardt RJ, Weiler JM. Importance of specific amino acids in protein binding sites for heparin and heparan sulfate. The international journal of biochemistry & cell biology. 1996;28(2):203-16.

256. Fromm J, Hileman R, Caldwell E, Weiler J, Linhardt RJ. Pattern and spacing of basic amino acids in heparin binding sites. Archives of biochemistry and biophysics. 1997;343(1):92-100.

257. Ornitz DM, Itoh N. Fibroblast growth factors. Genome biology. 2001;2(3):1-12.

258. Yun Y-R, Won JE, Jeon E, Lee S, Kang W, Jo H, et al. Fibroblast growth factors: biology, function, and application for tissue regeneration. Journal of tissue engineering. 2010;1(1):218142.

259. Ornitz DM, Itoh N. The fibroblast growth factor signaling pathway. Wiley Interdisciplinary Reviews: Developmental Biology. 2015;4(3):215-66.

260. Uciechowska-Kaczmarzyk U, Babik S, Zsila F, Bojarski KK, Beke-Somfai T, Samsonov SA. Molecular dynamics-based model of VEGF-A and its heparin interactions. Journal of Molecular Graphics and Modelling. 2018;82:157-66.

261. Apte RS, Chen DS, Ferrara N. VEGF in signaling and disease: beyond discovery and development. Cell. 2019;176(6):1248-64.

262. Reynolds CM, Eguchi S, Frank GD, Motley ED. Signaling mechanisms of heparin-binding epidermal growth factor-like growth factor in vascular smooth muscle cells. Hypertension. 2002;39(2):525-9.

263. Mehta VB, Zhou Y, Radulescu A, Besner GE. HB-EGF stimulates eNOS expression and nitric oxide production and promotes eNOS dependent angiogenesis. Growth factors. 2008;26(6):301-15.

264. Khan SA, Nelson MS, Pan C, Gaffney PM, Gupta P. Endogenous heparan sulfate and heparin modulate bone morphogenetic protein-4 signaling and activity. American Journal of Physiology-Cell Physiology. 2008;294(6):C1387-C97.

265. Halloran D, Durbano HW, Nohe A. Bone morphogenetic protein-2 in development and bone homeostasis. Journal of developmental biology. 2020;8(3):19.

266. Hettiaratchi MH, Krishnan L, Rouse T, Chou C, McDevitt TC, Guldberg RE. Heparin-mediated delivery of bone morphogenetic protein-2 improves spatial localization of bone regeneration. Science advances. 2020;6(1):eaay1240.

267. McCaffrey TA, Falcone DJ, Du B. Transforming growth factor-β1 is a heparin-binding protein: identification of putative heparin-binding regions and isolation of heparins with varying affinity for TGF-β1. Journal of cellular physiology. 1992;152(2):430-40.

268. Lee J, Wee S, Gunaratne J, Chua R, Smith RA, Ling L, et al. Structural determinants of heparin–transforming growth factor-β1 interactions and their effects on signaling. Glycobiology. 2015;25(12):1491-504.

269. Rider CC, Mulloy B. Heparin, heparan sulphate and the TGF-β cytokine superfamily. Molecules. 2017;22(5):713.

270. Bikle DD, Tahimic C, Chang W, Wang Y, Philippou A, Barton ER. Role of IGF-I signaling in muscle bone interactions. Bone. 2015;80:79-88.

271. Ahmad SS, Ahmad K, Lee EJ, Lee Y-H, Choi I. Implications of insulin-like growth factor-1 in skeletal muscle and various diseases. Cells. 2020;9(8):1773.

272. Bergers G, Song S. The role of pericytes in blood-vessel formation and maintenance. Neuro-oncology. 2005;7(4):452-64.

273. Rolny C, Spillmann D, Lindahl U, Claesson-Welsh L. Heparin amplifies platelet-derived growth factor (PDGF)-BB-induced PDGF α-receptor but not PDGF β-receptor tyrosine phosphorylation in heparan sulfate-deficient cells: effects on signal transduction and biological responses. Journal of Biological Chemistry. 2002;277(22):19315-21.

274. Sakata H, Stahl SJ, Taylor WG, Rosenberg JM, Sakaguchi K, Wingfield PT, et al. Heparin binding and oligomerization of hepatocyte growth factor/scatter factor isoforms: heparan sulfate glycosaminoglycan requirement for Met binding and signaling. Journal of Biological Chemistry. 1997;272(14):9457-63.

275. Salbach PB, Brückmann M, Turovets O, Kreuzer J, Kübler W, Walter-Sack I. Heparin-mediated selective release of hepatocyte growth factor in humans. British journal of clinical pharmacology. 2000;50(3):221-6.

276. Nakamura T, Mizuno S. The discovery of hepatocyte growth factor (HGF) and its significance for cell biology, life sciences and clinical medicine. Proceedings of the Japan Academy, Series B. 2010;86(6):588-610.

277. Hauser S, Weich HA. A heparin-binding form of placenta growth factor (PlGF-2) is expressed in human umbilical vein endothelial cells and in placenta. Growth factors. 1993;9(4):259-68.

278. Bottomley M, Webb N, Watson C, Holt L, Bukhari M, Denton J, et al. Placenta growth factor (PlGF) induces vascular endothelial growth factor (VEGF) secretion from mononuclear cells and is co-expressed with VEGF in synovial fluid. Clinical & Experimental Immunology. 2000;119(1):182-8.

279. McLaughlin K, Hobson SR, Chandran AR, Agrawal S, Windrim RC, Parks WT, et al. Circulating maternal placental growth factor responses to low-molecular-weight heparin in pregnant patients at risk of placental dysfunction. American Journal of Obstetrics and Gynecology. 2022;226(2):S1145-S56. e1.

280. Bezuidenhout D, Davies N, Black M, Schmidt C, Oosthuysen A, Zilla P. Covalent surface heparinization potentiates porous polyurethane scaffold vascularization. Journal of biomaterials applications. 2010;24(5):401-18.

281. Pennel T, Bezuidenhout D, Koehne J, Davies NH, Zilla P. Transmural capillary ingrowth is essential for confluent vascular graft healing. Acta biomaterialia. 2018;65:237-47.

282. Zieris A, Prokoph S, Levental KR, Welzel PB, Grimmer M, Freudenberg U, et al. FGF-2 and VEGF functionalization of starPEG–heparin hydrogels to modulate biomolecular and physical cues of angiogenesis. Biomaterials. 2010;31(31):7985-94.

283. Ciuffreda MC, Malpasso G, Chokoza C, Bezuidenhout D, Goetsch KP, Mura M, et al. Synthetic extracellular matrix mimic hydrogel improves efficacy of mesenchymal stromal cell therapy for ischemic cardiomyopathy. Acta Biomaterialia. 2018;70:71-83.

284. Sakiyama-Elbert SE, Hubbell JA. Development of fibrin derivatives for controlled release of heparin-binding growth factors. Journal of controlled release. 2000;65(3):389-402.

285. Yang HS, Bhang SH, Hwang JW, Kim D-I, Kim B-S. Delivery of basic fibroblast growth factor using heparin-conjugated fibrin for therapeutic angiogenesis. Tissue Eng Part A. 2010;16(6):2113-9.

286. Kim B-S, Jeon O-J, Yang H-S. Heparin-conjugated fibrin gel and method and kit for preparing same. Google Patents; 2011.

287. Yang HS, La W-G, Bhang SH, Jeon J-Y, Lee JH, Kim B-S. Heparin-conjugated fibrin as an injectable system for sustained delivery of bone morphogenetic protein-2. Tissue Eng Part A. 2010;16(4):1225-33.

288. Yang HS, Shin J, Bhang SH, Shin J-Y, Park J, Im G-I, et al. Enhanced skin wound healing by a sustained release of growth factors contained in platelet-rich plasma. Experimental & molecular medicine. 2011;43(11):622.

289. Sarsenova M, Raimagambetov Y, Issabekova A, Karzhauov M, Kudaibergen G, Akhmetkarimova Z, et al. Regeneration of Osteochondral Defects by Combined Delivery of Synovium-Derived Mesenchymal Stem Cells, TGF-β1 and BMP-4 in Heparin-Conjugated Fibrin Hydrogel. Polymers. 2022;14(24):5343.

290. Tusipkhan Toktarov BS, Yerik Raimagambetov, Bagdat Balbossynov1, Gulzhanat Korganbekova, Marat Urazayev, Assel Issabekova, Gulsamal Zhubanova, Guldarigash Kaukabayeva, Aliya Sekenova, Gulshakhar Kudaibergen, Zhanar Akhmetkarimova, Saule Eskendirova, Yerlan Ramankulov2,3, Olzhas Bekarissov, Arman Batpen, Vyacheslav Ogay. Heparin-Conjugated Fibrin Hydrogel with Chondroinductive Growth Factors and Human Synovium-Derived Mesenchymal Stem Cells for the Treatment of Articular Cartilage Defects: Evaluation of Clinical Safety. INTERNATIONAL JOURNAL

OF BIOMEDICINE. 2022;12(4):5399-547.

291. Meneghetti MC, Hughes AJ, Rudd TR, Nader HB, Powell AK, Yates EA, et al. Heparan sulfate and heparin interactions with proteins. Journal of the Royal Society Interface. 2015;12(110):20150589.

292. Briquez P, Tortelli F, Martino M, Pisano M, Hubbell J. Extracellular matrix molecules regulate growth factor and cytokine delivery through their heparin-binding domains and promote wound healing. Journal Of Tissue Engineering And Regenerative Medicine. 2014;8(EPFL-CONF-201375):189-.

293. Wissink M, Beernink R, Pieper J, Poot A, Engbers G, Beugeling T, et al. Immobilization of heparin to EDC/NHS-crosslinked collagen. Characterization and in vitro evaluation. Biomaterials. 2001;22(2):151-63.

294. ThermoFischer. Bioconjugation and crosslinking technical handbook. 2022:8.

295. Yang HS, La W-G, Cho Y-M, Shin W, Yeo G-D, Kim B-S. Comparison between heparin-conjugated fibrin and collagen sponge as bone morphogenetic protein-2 carriers for bone regeneration. Experimental & molecular medicine. 2012;44(5):350.

296. Jayachandran B, Parvin TN, Alam MM, Chanda K, Mm B. Insights on Chemical Crosslinking Strategies for Proteins. Molecules. 2022;27(23):8124.

297. Janse van Rensburg A. Heparanoid hydrogels for cardiovascular tissue regeneration: University of Cape Town; 2015.

298. Seetharaman S, Natesan S, Stowers RS, Mullens C, Baer DG, Suggs LJ, et al. A PEGylated fibrin-based wound dressing with antimicrobial and angiogenic activity. Acta biomaterialia. 2011;7(7):2787-96.

299. Shpichka A, Konarev P, Efremov YM, Kryukova A, Aksenova N, Kotova S, et al. Digging deeper: structural background of PEGylated fibrin gels in cell migration and lumenogenesis. RSC advances. 2020;10(8):4190-200.

300. Maulik V, Jennifer S, Teruna J. The role of thiols and disulfides in protein chemical and physical stability. Curr Protein Pept Sci. 2009;10:614-25.

301. Berne D, Ladmiral V, Leclerc E, Caillol S. Thia-Michael Reaction: The Route to Promising Covalent Adaptable Networks. Polymers. 2022;14(20):4457.

302. ThermoFischer. Separation Characteristics of Dialysis Membranes. 2006-2023.

303. Macheboeuf M, Lacaille P, Rebeyrotte P. Studies of the xanthoproteic reaction. Application to colorimetric micro-estimation of proteins in blood serum. Bulletin de la Societe de chimie biologique. 1947;29:402-11.

304. Inada Y, Blombäck B. Four states of tyrosine residues in the fibrinogen molecule. Biochimica et Biophysica Acta (BBA)-Protein Structure. 1978;533(1):74-9.

305. Gustafsson CA. Modified polyethylene glycol hydrogels for growth factor delivery and controlled tissue invasion: Faculty of Health Sciences; 2019.

306. Chokoza C. Stimulation of angiogenesis through growth factor delivery from synthetic heparinised hydrogels: University of Cape Town; 2017.

307. Elbert DL, Pratt AB, Lutolf MP, Halstenberg S, Hubbell JA. Protein delivery from materials formed by self-selective conjugate addition reactions. Journal of Controlled Release. 2001;76(1-2):11-25.

308. Shpichka A, Koroleva A, Deiwick A, Timashev P, Semenova E, Moiseeva IY, et al. Evaluation of the vasculogenic potential of hydrogels based on modified fibrin. Cell and Tissue Biology. 2017;11:81-7.

309. Stani C, Vaccari L, Mitri E, Birarda G. FTIR investigation of the secondary structure of type I collagen: New insight into the amide III band. Spectrochimica Acta Part A: Molecular and Biomolecular Spectroscopy. 2020;229:118006.

310. Kunwong D, Sumanochitraporn N, Kaewpirom S. Curing behavior of a UV-curable coating based on urethane acrylate oligomer: the influence of reactive monomers. Sonklanakarin Journal of Science and Technology. 2011;33(2):201.

311. Tugut F, Turgut M, Saraydin D. Influence of concentrations of methacrylate and acrylate monomers on the properties of fiber reinforced polymethyl methacrylate denture base materials. Acta Chemica Iasi. 2018;26(2):329-50.

312. Veronese FM, Pasut G. PEGylation, successful approach to drug delivery. Drug discovery today. 2005;10(21):1451-8.

313. Turecek PL, Bossard MJ, Schoetens F, Ivens IA. PEGylation of biopharmaceuticals: a review of chemistry and nonclinical safety information of approved drugs. Journal of pharmaceutical sciences. 2016;105(2):460-75.

314. Bezuidenhout D, Davies N, Zilla P. Effect of well defined dodecahedral porosity on inflammation and angiogenesis. ASAIO journal. 2002;48(5):465-71.

315. Benavides OM, Quinn JP, Pok S, Petsche Connell J, Ruano R, Jacot JG. Capillary-like network formation by human amniotic fluid-derived stem cells within fibrin/poly (ethylene glycol) hydrogels. Tissue Engineering Part A. 2015;21(7-8):1185-94.

316. Koroleva A, Deiwick A, Nguyen A, Narayan R, Shpichka A, Kufelt O, et al. Hydrogel-based microfluidics for vascular tissue engineering. BioNanoMaterials. 2016;17(1-2):19-32.

317. Zhang G, Drinnan CT, Geuss LR, Suggs LJ. Vascular differentiation of bone marrow stem cells is directed by a tunable three-dimensional matrix. Acta biomaterialia. 2010;6(9):3395-403.

318. Hurley-Novatny AC, Allbritton-King JD, Jha S, Cowen EW, Colbert RA, Navid F, et al. Fibroblasts from Patients with Melorheostosis Promote Angiogenesis in Healthy Endothelial Cells through Secreted Factors. Journal of Investigative Dermatology. 2022;142(9):2406-14. e5.

319. Zorova LD, Popkov VA, Plotnikov EY, Silachev DN, Pevzner IB, Jankauskas SS, et al. Mitochondrial membrane potential. Analytical biochemistry. 2018;552:50-9.

320. Yeh Y-T, Hur SS, Chang J, Wang K-C, Chiu J-J, Li Y-S, et al. Matrix stiffness regulates endothelial cell proliferation through septin 9. PloS one. 2012;7(10):e46889.

321. Cavo M, Fato M, Peñuela L, Beltrame F, Raiteri R, Scaglione S. Microenvironment complexity and matrix stiffness regulate breast cancer cell activity in a 3D in vitro model. Scientific reports. 2016;6(1):35367.

322. Hui L, Zhang J, Ding X, Guo X, Jiang X. Matrix stiffness regulates the proliferation, stemness and chemoresistance of laryngeal squamous cancer cells. International journal of oncology. 2017;50(4):1439-47.

323. Klein EA, Yin L, Kothapalli D, Castagnino P, Byfield FJ, Xu T, et al. Cell-cycle control by physiological matrix elasticity and in vivo tissue stiffening. Current biology. 2009;19(18):1511-8.

324. Handorf AM, Zhou Y, Halanski MA, Li W-J. Tissue stiffness dictates development, homeostasis, and disease progression. Organogenesis. 2015;11(1):1-15.

325. Korff T, Augustin HG. Integration of endothelial cells in multicellular spheroids prevents apoptosis and induces differentiation. The Journal of cell biology. 1998;143(5):1341-52.

326. Bracher M, Bezuidenhout D, Lutolf MP, Franz T, Sun M, Zilla P, et al. Cell specific ingrowth hydrogels. Biomaterials. 2013;34(28):6797-803.

327. Viji R, Kumar VS, Kiran M, Sudhakaran P. Angiogenic response of endothelial cells to heparin-binding domain of fibronectin. The International Journal of Biochemistry & Cell Biology. 2008;40(2):215-26.

328. Kim M, Kim YH, Tae G. Human mesenchymal stem cell culture on heparin-based hydrogels and the modulation of interactions by gel elasticity and heparin amount. Acta Biomaterialia. 2013;9(8):7833-44.

329. Isali I, Al-Sadawi MAA, Qureshi A, Khalifa AO, Agrawal MK, Shukla S. Growth factors involve in cellular proliferation, differentiation and migration during prostate cancer metastasis. International journal of cell biology and physiology. 2019;2(1-2):1.

330. Folkman J. Tumor angiogenesis: therapeutic implications. The New England journal of medicine. 1971;285(21):1182-6.

331. Takeshita S, Zheng L, Brogi E, Kearney M, Pu L, Bunting S, et al. Therapeutic angiogenesis. A single intraarterial bolus of vascular endothelial growth factor augments

revascularization in a rabbit ischemic hind limb model. The Journal of clinical investigation. 1994;93(2):662-70.

332. Folkman J, Long Jr DM, Becker FF. Growth and metastasis of tumor in organ culture. Cancer. 1963;16(4):453-67.

333. Lenzi P, Bocci G, Natale G. John Hunter and the origin of the term “angiogenesis”. Angiogenesis. 2016;19:255-6.

334. Folkman J. Angiogenesis in cancer, vascular, rheumatoid and other disease. Nature medicine. 1995;1(1):27-30.

335. Jaffe RB, editor Importance of angiogenesis in reproductive physiology. Seminars in perinatology; 2000: Elsevier.

336. Colpaert C, Vermeulen P, Benoy I, Soubry A, Van Roy F, Van Beest P, et al. Inflammatory breast cancer shows angiogenesis with high endothelial proliferation rate and strong E-cadherin expression. British journal of cancer. 2003;88(5):718-25.

337. Shinkaruk S, Bayle M, Lain G, Deleris G. Vascular endothelial cell growth factor (VEGF), an emerging target for cancer chemotherapy. Current Medicinal Chemistry-Anti-Cancer Agents. 2003;3(2):95-117.

338. Carmeliet P. Angiogenesis in health and disease. Nature medicine. 2003;9(6):653-60.

339. Mayer G. Capillary rarefaction, hypoxia, VEGF and angiogenesis in chronic renal disease. Nephrology Dialysis Transplantation. 2011;26(4):1132-7.

340. Senger DR, Galli SJ, Dvorak AM, Perruzzi CA, Harvey VS, Dvorak HF. Tumor cells secrete a vascular permeability factor that promotes accumulation of ascites fluid. Science. 1983;219(4587):983-5.

341. Dvorak HF. Reconciling VEGF with VPF: the importance of increased vascular permeability for stroma formation in tumors, healing wounds, and chronic inflammation. Frontiers in Cell and Developmental Biology. 2021;9:660609.

342. Maglione D, Guerriero V, Viglietto G, Delli-Bovi P, Persico MG. Isolation of a human placenta cDNA coding for a protein related to the vascular permeability factor. Proceedings of the National Academy of Sciences. 1991;88(20):9267-71.

343. Joukov V, Pajusola K, Kaipainen A, Chilov D, Lahtinen I, Kukk E, et al. A novel vascular endothelial growth factor, VEGF-C, is a ligand for the Flt4 (VEGFR-3) and KDR (VEGFR-2) receptor tyrosine kinases. The EMBO journal. 1996;15(2):290-8.

344. Olofsson B, Pajusola K, Kaipainen A, Von Euler G, Joukov V, Saksela O, et al. Vascular endothelial growth factor B, a novel growth factor for endothelial cells. Proceedings of the National Academy of Sciences. 1996;93(6):2576-81.

345. Orlandini M, Marconcini L, Ferruzzi R, Oliviero S. Identification of a c-fos-induced gene that is related to the platelet-derived growth factor/vascular endothelial growth factor family. Proceedings of the National Academy of Sciences. 1996;93(21):11675-80.

346. Li X, Eriksson U. Novel vegf family members: Vegf-b, vegf-c and vegf-d. The international journal of biochemistry & cell biology. 2001;33(4):421-6.

347. Ferrara N, Gerber HP. Vascular endothelial growth factor molecular and biological aspects. Advances in organ biology. 1999;7:25-57.

348. Stacker SA, Achen MG. The VEGF signaling pathway in cancer: the road ahead. Chinese Journal of Cancer. 2013;32(6):297.

349. Carmeliet P, Ferreira V, Breier G, Pollefeyt S, Kieckens L, Gertsenstein M, et al. Abnormal blood vessel development and lethality in embryos lacking a single VEGF allele. Nature. 1996;380(6573):435-9.

350. Park JE, Keller G-A, Ferrara N. The vascular endothelial growth factor (VEGF) isoforms: differential deposition into the subepithelial extracellular matrix and bioactivity of extracellular matrix-bound VEGF. Molecular biology of the cell. 1993;4(12):1317-26.

351. Shibuya M. Vascular endothelial growth factor (VEGF) and its receptor (VEGFR) signaling in angiogenesis: a crucial target for anti-and pro-angiogenic therapies. Genes & cancer. 2011;2(12):1097-105.

352. Shaw P, Dwivedi SKD, Bhattacharya R, Mukherjee P, Rao G. VEGF signaling: Role in angiogenesis and beyond. Biochimica et Biophysica Acta (BBA)-Reviews on Cancer. 2024:189079.

353. Fu Y, Zhang Z, Webster KA, Paulus YM. Treatment Strategies for Anti-vegf Resistance in Neovascular Age-Related Macular Degeneration by Targeting Arteriolar Choroidal Neovascularization. Biomolecules. 2024;14(3):252.

354. Fani N, Moradi M, Zavari R, Parvizpour F, Soltani A, Arabpour Z, et al. Current advances in wound healing and regenerative medicine. Current stem cell research & therapy. 2024;19(3):277-91.

355. Itoh N, Ornitz DM. Evolution of the Fgf and Fgfr gene families. TRENDS in Genetics. 2004;20(11):563-9.

356. Beenken A, Mohammadi M. The FGF family: biology, pathophysiology and therapy. Nature reviews Drug discovery. 2009;8(3):235-53.

357. Dai S, Zhou Z, Chen Z, Xu G, Chen Y. Fibroblast growth factor receptors (FGFRs): structures and small molecule inhibitors. Cells. 2019;8(6):614.

358. Xie Y, Su N, Yang J, Tan Q, Huang S, Jin M, et al. FGF/FGFR signaling in health and disease. Signal transduction and targeted therapy. 2020;5(1):1-38.

359. GRAŻYNA CHODOROWSKA MJ-B, WAWRZYCKI DWaB. Serum levels ofbasic Fibroblast Growth Factor in patients

with chronic plaque psoriasis. ANNALES. 2006;LXI(2):132.

360. Zhang F, Zhang Z, Lin X, Beenken A, Eliseenkova AV, Mohammadi M, et al. Compositional analysis of heparin/heparan sulfate interacting with fibroblast growth factor· fibroblast growth factor receptor complexes. Biochemistry. 2009;48(35):8379-86.

361. Sarabipour S, Hristova K. Mechanism of FGF receptor dimerization and activation. Nature communications. 2016;7(1):1-12.

362. Presta M, Dell'Era P, Mitola S, Moroni E, Ronca R, Rusnati M. Fibroblast growth factor/fibroblast growth factor receptor system in angiogenesis. Cytokine & growth factor reviews. 2005;16(2):159-78.

363. Laestander C, Engström W. Role of fibroblast growth factors in elicitation of cell responses. Cell proliferation. 2014;47(1):3-11.

364. Hariawala MD, Horowitz JR, Esakof D, Sheriff DD, Walter DH, Keyt B, et al. VEGF improves myocardial blood flow but produces EDRF-mediated hypotension in porcine hearts. Journal of Surgical Research. 1996;63(1):77-82.

365. Laham RJ, Rezaee M, Post M, Sellke FW, Braeckman RA, Hung D, et al. Intracoronary and intravenous administration of basic fibroblast growth factor: myocardial and tissue distribution. Drug Metabolism and Disposition. 1999;27(7):821-6.

366. Haroun RI, Brem H. Local drug delivery. Current opinion in oncology. 2000;12(3):187-93.

367. Annex BH, Simons M. Growth factor-induced therapeutic angiogenesis in the heart: protein therapy. Cardiovascular Research. 2005;65(3):649-55.

368. Yang HS, Bhang SH, Hwang JW, Kim D-I, Kim B-S. Delivery of basic fibroblast growth factor using heparin-conjugated fibrin for therapeutic angiogenesis. Tissue Engineering Part A. 2010;16(6):2113-9.

369. Sahni A, Francis CW. Vascular endothelial growth factor binds to fibrinogen and fibrin and stimulates endothelial cell proliferation. Blood, The Journal of the American Society of Hematology. 2000;96(12):3772-8.

370. Lee K, Silva EA, Mooney DJ. Growth factor delivery-based tissue engineering: general approaches and a review of recent developments. Journal of the Royal Society Interface. 2011;8(55):153-70.

371. Martino MM, Briquez PS, Güç E, Tortelli F, Kilarski WW, Metzger S, et al. Growth factors engineered for super-affinity to the extracellular matrix enhance tissue healing. Science. 2014;343(6173):885-8.

372. Ibrahimi OA, Zhang F, Lang Hrstka SC, Mohammadi M, Linhardt RJ. Kinetic model for FGF, FGFR, and proteoglycan signal transduction complex assembly. Biochemistry. 2004;43(16):4724-30.

373. Zustiak SP, Leach JB. Hydrolytically degradable poly (ethylene glycol) hydrogel scaffolds with tunable degradation and mechanical properties. Biomacromolecules. 2010;11(5):1348-57.

374. Davies N, Dobner S, Bezuidenhout D, Schmidt C, Beck M, Zisch AH, et al. The dosage dependence of VEGF stimulation on scaffold neovascularisation. Biomaterials. 2008;29(26):3531-8.

375. Schmidt C, Bezuidenhout D, Beck M, Van der Merwe E, Zilla P, Davies N. Rapid three-dimensional quantification of VEGF-induced scaffold neovascularisation by microcomputed tomography. Biomaterials. 2009;30(30):5959-68.

376. Goetsch K, Bracher M, Bezuidenhout D, Zilla P, Davies N. Regulation of tissue ingrowth into proteolytically degradable hydrogels. Acta biomaterialia. 2015;24:44-52.

377. Sefton MV, Babensee JE, Woodhouse KA, editors. Innate and adaptive immune responses in tissue engineering. Seminars in Immunology; 2008.

378. Naranjo JD, Scarritt ME, Huleihel L, Ravindra A, Torres CM, Badylak SF. Regenerative medicine: lessons from mother nature. Regenerative Medicine. 2016;11(8):767-75.

379. Rozenfel'd MA, Leonova, V. B., Khavkina, L. S., & Meshkov, B. B. Antifibrinoliticheskoe deĭstvie geparina [Antifibrinolytic effect of heparin]. Biokhimiia. 1984;49(10):1672-8.

380. Kolev K, Komorowicz E, Machovich R. Heparin modulation of the fibrinolytic activity of plasmin, miniplasmin and neutrophil leukocyte elastase in the presence of plasma protease inhibitors. Blood Coagulation & Fibrinolysis: an International Journal in Haemostasis and Thrombosis. 1994;5(6):905-11.

381. Friedenstein AJ, Gorskaja J, Kulagina N. Fibroblast precursors in normal and irradiated mouse hematopoietic organs. Experimental hematology. 1976;4(5):267-74.

382. Badimon L, Onate B, Vilahur G. Adipose-derived mesenchymal stem cells and their reparative potential in ischemic heart disease. Revista Española de Cardiología (English Edition). 2015;68(7):599-611.

383. Kot M, Baj-Krzyworzeka M, Szatanek R, Musiał-Wysocka A, Suda-Szczurek M, Majka M. The importance of HLA assessment in “off-the-shelf” allogeneic mesenchymal stem cells based-therapies. International Journal of Molecular Sciences. 2019;20(22):5680.

384. Ankrum JA, Ong JF, Karp JM. Mesenchymal stem cells: immune evasive, not immune privileged. Nature biotechnology. 2014;32(3):252-60.

385. Fitzsimmons RE, Mazurek MS, Soos A, Simmons CA. Mesenchymal stromal/stem cells in regenerative medicine and tissue engineering. Stem cells international. 2018;2018.

386. Davies JE, Walker JT, Keating A. Concise review: Wharton's jelly: the rich, but enigmatic, source of mesenchymal stromal cells. Stem cells translational medicine. 2017;6(7):1620-30.

387. Mathiasen AB, Jørgensen E, Qayyum AA, Haack-Sørensen M, Ekblond A, Kastrup J. Rationale and design of the first randomized, double-blind, placebo-controlled trial of intramyocardial injection of autologous bone-marrow derived Mesenchymal Stromal Cells in chronic ischemic Heart Failure (MSC-HF Trial). American heart journal. 2012;164(3):285-91.

388. Liang Y, Kiick KL. Heparin-functionalized polymeric biomaterials in tissue engineering and drug delivery applications. Acta Biomaterialia. 2014;10(4):1588-600.

389. Gnecchi M, Danieli P, Malpasso G, Ciuffreda MC. Paracrine mechanisms of mesenchymal stem cells in tissue repair. Mesenchymal stem cells. 2016:123-46.

390. Walter MN, Wright KT, Fuller HR, MacNeil S, Johnson WEB. Mesenchymal stem cell-conditioned medium accelerates skin wound healing: an in vitro study of fibroblast and keratinocyte scratch assays. Experimental cell research. 2010;316(7):1271-81.

391. Timmers L, Lim SK, Arslan F, Armstrong JS, Hoefer IE, Doevendans PA, et al. Reduction of myocardial infarct size by human mesenchymal stem cell conditioned medium. Stem cell research. 2008;1(2):129-37.

392. Katagiri W, Kawai T, Osugi M, Sugimura-Wakayama Y, Sakaguchi K, Kojima T, et al. Angiogenesis in newly regenerated bone by secretomes of human mesenchymal stem cells. Maxillofacial Plastic and Reconstructive Surgery. 2017;39(1):1-8.

393. Kawai T, Katagiri W, Osugi M, Sugimura Y, Hibi H, Ueda M. Secretomes from bone marrow–derived mesenchymal stromal cells enhance periodontal tissue regeneration. Cytotherapy. 2015;17(4):369-81.

394. Lee DE, Ayoub N, Agrawal DK. Mesenchymal stem cells and cutaneous wound healing: novel methods to increase cell delivery and therapeutic efficacy. Stem cell research & therapy. 2016;7(1):1-8.

395. Pittenger MF, Discher DE, Péault BM, Phinney DG, Hare JM, Caplan AI. Mesenchymal stem cell perspective: cell biology to clinical progress. NPJ Regenerative medicine. 2019;4(1):22.

396. Gjorevski N, Nelson CM. The mechanics of development: Models and methods for tissue morphogenesis. Birth Defects Research Part C: Embryo Today: Reviews. 2010;90(3):193-202.

397. Vining KH, Mooney DJ. Mechanical forces direct stem cell behaviour in development and regeneration. Nature reviews Molecular cell biology. 2017;18(12):728-42.

398. Murrell M, Oakes PW, Lenz M, Gardel ML. Forcing cells into shape: the mechanics of actomyosin contractility. Nature reviews Molecular cell biology. 2015;16(8):486-98.

399. Engler AJ, Sen S, Sweeney HL, Discher DE. Matrix elasticity directs stem cell lineage specification. Cell. 2006;126(4):677-89.

400. Gwon K, Kim E, Tae G. Heparin-hyaluronic acid hydrogel in support of cellular activities of 3D encapsulated adipose derived stem cells. Acta biomaterialia. 2017;49:284-95.

401. Ling L, Camilleri ET, Helledie T, Samsonraj RM, Titmarsh DM, Chua RJ, et al. Effect of heparin on the biological properties and molecular signature of human mesenchymal stem cells. Gene. 2016;576(1):292-303.

402. Simann M, Schneider V, Le Blanc S, Dotterweich J, Zehe V, Krug M, et al. Heparin affects human bone marrow stromal cell fate: Promoting osteogenic and reducing adipogenic differentiation and conversion. Bone. 2015;78:102-13.

403. Benoit DS, Durney AR, Anseth KS. The effect of heparin-functionalized PEG hydrogels on three-dimensional human mesenchymal stem cell osteogenic differentiation. Biomaterials. 2007;28(1):66-77.

404. Fraser JK, Schreiber RE, Zuk PA, Hedrick MH. Adult stem cell therapy for the heart. The international journal of biochemistry & cell biology. 2004;36(4):658-66.

405. Hocking AM, Gibran NS. Mesenchymal stem cells: paracrine signaling and differentiation during cutaneous wound repair. Experimental cell research. 2010;316(14):2213-9.

406. Nasrollahi S, Walter C, Loza AJ, Schimizzi GV, Longmore GD, Pathak A. Past matrix stiffness primes epithelial cells and regulates their future collective migration through a mechanical memory. Biomaterials. 2017;146:146-55.

407. Janmey PA, Fletcher DA, Reinhart-King CA. Stiffness sensing by cells. Physiological reviews. 2020;100(2):695-724.

408. Lv H, Wang H, Zhang Z, Yang W, Liu W, Li Y, et al. Biomaterial stiffness determines stem cell fate. Life sciences. 2017;178:42-8.

409. Mao AS, Mooney DJ. Regenerative medicine: Current therapies and future directions. Proceedings of the National Academy of Sciences. 2015;112(47):14452-9.

410. Hu D, Dong Z, Li B, Lu F, Li Y. Mechanical Force Directs Proliferation and Differentiation of Stem Cells. Tissue Engineering Part B: Reviews. 2023;29(2):141-50.

411. Mao AS, Shin J-W, Mooney DJ. Effects of substrate stiffness and cell-cell contact on mesenchymal stem cell differentiation. Biomaterials. 2016;98:184-91.

412. Colley H, McArthur SL, Stolzing A, Scutt A. Culture on fibrin matrices maintains the colony-forming capacity and osteoblastic differentiation of mesenchymal stem cells. Biomedical Materials. 2012;7(4):045015.

Appendices

Appendix A: Slow heparin release from FH and FPH quantified from degradation eluates.

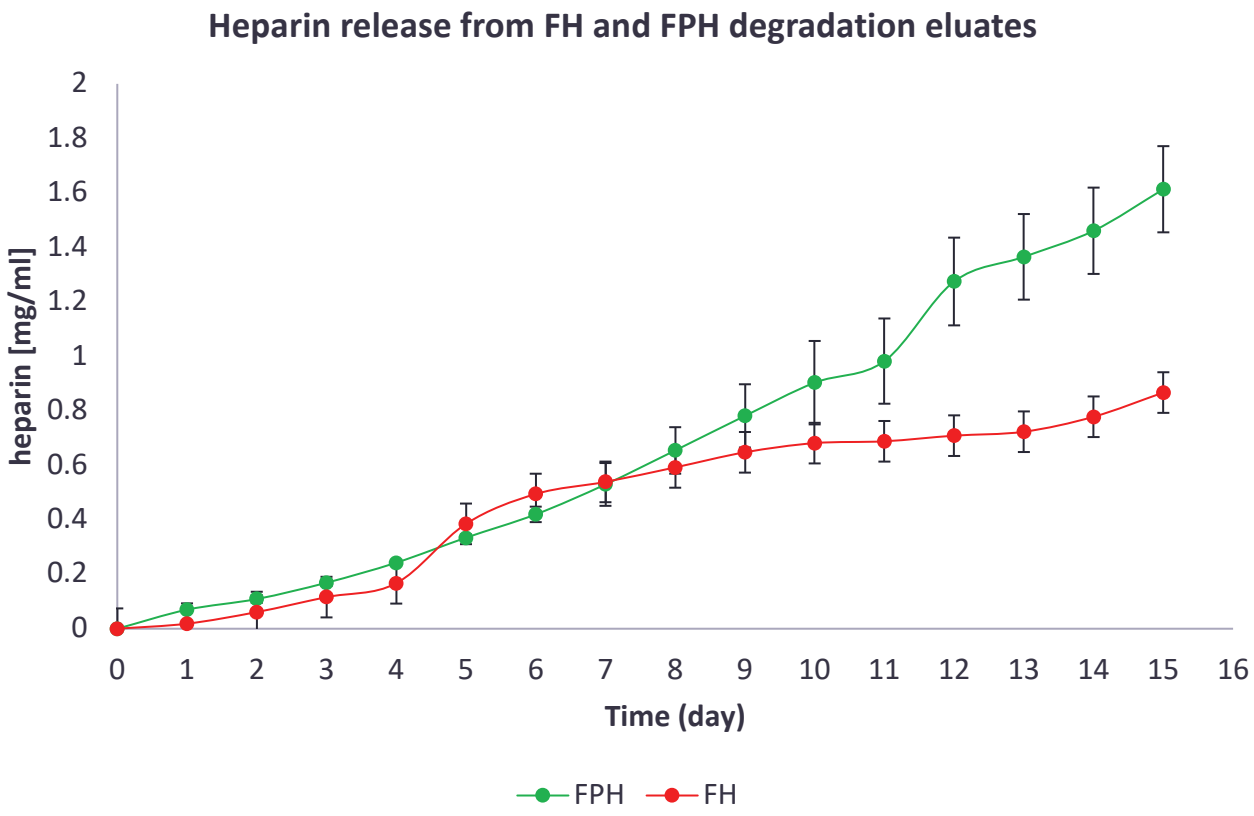

Figure A1: Slow heparin release from FH and FPH quantified from degradation eluates. Degradation eluates assayed in the MBTH showed a slow cumulative heparin release over time confirming the presence of heparin in the original hydrogels. n=3 technical repeats.

Appendix B: Example rheology Scans

	A	B	C	D	E	F	G	H	I	J	K
1	F										
2	Time (action)(s)	Temperature(Â°C)	Frequency(Hz)	Complex shear strain(%	Complex shear stress(Pa)	Shear modulus (complex component)(Pa	Shear modulus (elastic component)(Pa	Shear modulus (viscous component)(Pa	Shear viscosity (complex component)(Pa s	Phase angle(Â°)	Gap(mm)
3	11,000000	37,440000	10,000000	1,002110	0,257600	25,710000	24,490000	7,836000	0,409200	-162,250000	0,800000
4	22,340000	37,490000	7,943000	0,971533	0,048770	5,019000	3,689000	3,404000	0,100600	90,000000	0,800000
5	34,090000	37,470000	6,310000	0,992474	0,141100	14,220000	13,640000	4,010000	0,358600	16,390000	0,800000
6	46,280000	37,420000	5,012000	0,998468	0,229200	22,960000	22,720000	3,279000	0,729000	8,210000	0,800000
7	58,850000	37,360000	3,981000	1,001520	0,299300	29,880000	29,770000	2,650000	1,195000	5,090000	0,800000
8	72,160000	37,300000	3,162000	0,996775	0,336400	33,750000	33,690000	2,008000	1,699000	3,410000	0,800000
9	86,510000	37,240000	2,512000	1,000620	0,361600	36,140000	36,100000	1,779000	2,290000	2,820000	0,800000
10	101,500000	37,200000	1,995000	1,003040	0,378100	37,700000	37,660000	1,628000	3,007000	2,470000	0,800000
11	118,000000	37,160000	1,585000	1,001620	0,387800	38,710000	38,680000	1,503000	3,887000	2,230000	0,800000
12	136,300000	37,130000	1,259000	1,002930	0,393300	39,220000	39,200000	1,314000	4,958000	1,920000	0,800000
13	156,300000	37,100000	1,000000	0,999552	0,399700	39,990000	39,960000	1,362000	6,364000	1,950000	0,800000
14	179,000000	37,080000	0,794300	1,001060	0,402200	40,170000	40,150000	1,311000	8,049000	1,870000	0,800000
15	205,900000	37,060000	0,631000	1,000990	0,405200	40,480000	40,460000	1,359000	10,210000	1,920000	0,800000
16	237,900000	37,040000	0,501200	0,999994	0,406600	40,660000	40,640000	1,225000	12,910000	1,730000	0,800000
17	273,000000	37,030000	0,398100	1,000700	0,408500	40,820000	40,800000	1,216000	16,320000	1,710000	0,800000
18	317,300000	37,020000	0,316200	1,000380	0,409300	40,910000	40,890000	1,237000	20,590000	1,730000	0,800000
19	369,100000	37,010000	0,251200	0,999950	0,410400	41,040000	41,020000	1,247000	26,000000	1,740000	0,800000
20	429,300000	37,010000	0,199500	1,000650	0,410800	41,050000	41,040000	1,166000	32,750000	1,630000	0,800000
21	501,900000	37,000000	0,158500	1,000700	0,413100	41,280000	41,260000	1,149000	41,450000	1,590000	0,800000
22	577,800000	37,000000	0,125900	1,000380	0,416100	41,590000	41,580000	1,182000	52,580000	1,630000	0,800000
23	647,860000	37,000000	0,100000	1,000040	0,420100	42,010000	41,990000	1,232000	66,860000	1,680000	0,800000
24	FH										
25	Time (action)(s)	Temperature(Â°C)	Frequency(Hz)	Complex shear strain(%	Complex shear stress(Pa)	Shear modulus (complex component)(Pa	Shear modulus (elastic component)(Pa	Shear modulus (viscous component)(Pa	Shear viscosity (complex component)(Pa s	Phase angle(Â°)	Gap(mm)
26	11,000000	36,950000	10,000000	0,853283	0,104500	12,240000	8,076000	9,200000	0,194800	90,000000	0,800000
27	22,350000	37,130000	7,943000	0,972534	0,055000	5,655000	0,410900	5,640000	0,113300	85,830000	0,800000
28	34,090000	37,230000	6,310000	0,995709	0,165400	16,610000	15,830000	5,038000	0,419000	17,650000	0,800000
29	46,280000	37,250000	5,012000	1,002410	0,232800	23,220000	22,730000	4,766000	0,737500	11,840000	0,800000
30	58,860000	37,230000	3,981000	1,001880	0,275600	27,510000	27,240000	3,829000	1,100000	8,000000	0,800000
31	72,160000	37,180000	3,162000	0,996988	0,300700	30,160000	29,980000	3,289000	1,518000	6,260000	0,800000
32	86,500000	37,140000	2,512000	1,000410	0,317900	31,780000	31,620000	3,185000	2,014000	5,750000	0,800000
33	101,600000	37,110000	1,995000	1,003150	0,326400	32,530000	32,390000	2,995000	2,595000	5,280000	0,800000
34	118,000000	37,090000	1,585000	1,001580	0,331700	33,120000	32,990000	2,944000	3,326000	5,100000	0,800000
35	136,300000	37,070000	1,259000	1,002180	0,335700	33,500000	33,380000	2,816000	4,235000	4,820000	0,800000
36	156,300000	37,060000	1,000000	0,999759	0,337800	33,790000	33,670000	2,761000	5,377000	4,690000	0,800000
37	179,000000	37,050000	0,794300	1,000640	0,340300	34,010000	33,900000	2,717000	6,814000	4,580000	0,800000
38	205,900000	37,040000	0,631000	1,001210	0,343600	34,310000	34,200000	2,785000	8,656000	4,650000	0,800000
39	237,900000	37,030000	0,501200	0,999611	0,341400	34,150000	34,050000	2,566000	10,840000	4,310000	0,800000
40	273,000000	37,020000	0,398100	1,001010	0,343400	34,310000	34,220000	2,459000	13,720000	4,110000	0,800000
41	317,300000	37,010000	0,316200	1,000250	0,341300	34,120000	34,050000	2,299000	17,170000	3,860000	0,800000
42	369,100000	37,010000	0,251200	0,999886	0,340300	34,040000	33,970000	2,157000	21,570000	3,630000	0,800000
43	429,300000	37,010000	0,199500	0,999856	0,346800	34,680000	34,600000	2,401000	27,670000	3,970000	0,800000
44	501,900000	37,000000	0,158500	0,999979	0,347900	34,790000	34,710000	2,317000	34,940000	3,820000	0,800000
45	577,800000	37,000000	0,125900	1,000130	0,346200	34,620000	34,550000	2,260000	43,770000	3,740000	0,800000
46	647,800000	37,000000	0,100000	1,000280	0,345300	34,520000	34,450000	2,177000	54,940000	3,620000	0,800000
47	FP										
48	Time (action)(s)	Temperature(Â°C)	Frequency(Hz)	Complex shear strain(%	Complex shear stress(Pa)	Shear modulus (complex component)(Pa	Shear modulus (elastic component)(Pa	Shear modulus (viscous component)(Pa	Shear viscosity (complex component)(Pa s	Phase angle(Â°)	Gap(mm)
49	11,000000	37,290000	10,000000	0,942421	0,239700	25,430000	24,580000	6,515000	0,404800	-165,160000	0,800000
50	22,350000	37,330000	7,943000	0,971397	0,181300	18,660000	17,710000	5,871000	0,373900	90,000000	0,800000
51	34,090000	37,320000	6,310000	0,993915	0,065760	6,617000	3,411000	5,670000	0,166900	90,000000	0,800000
52	46,270000	37,280000	5,012000	0,998815	0,054760	5,482000	2,146000	5,045000	0,174100	66,960000	0,800000
53	58,850000	37,230000	3,981000	1,003740	0,083890	8,357000	7,107000	4,397000	0,334100	31,750000	0,800000
54	72,150000	37,180000	3,162000	0,998138	0,117000	11,720000	11,090000	3,807000	0,589900	18,950000	0,800000
55	86,500000	37,150000	2,512000	1,000260	0,145600	14,560000	14,110000	3,574000	0,922400	14,210000	0,800000
56	101,600000	37,120000	1,995000	1,002180	0,170400	17,010000	16,670000	3,348000	1,357000	11,350000	0,800000
57	118,000000	37,100000	1,585000	1,000980	0,191700	19,160000	18,880000	3,245000	1,924000	9,750000	0,800000
58	136,300000	37,080000	1,259000	1,000840	0,214100	21,400000	21,140000	3,322000	2,705000	8,930000	0,800000
59	156,300000	37,060000	1,000000	0,998724	0,229000	22,930000	22,710000	3,197000	3,649000	9,120000	0,800000
60	179,000000	37,050000	0,794300	0,999949	0,239100	23,910000	23,730000	2,959000	4,791000	7,110000	0,800000
61	205,900000	37,030000	0,631000	1,000130	0,252500	25,250000	25,060000	3,065000	6,368000	6,970000	0,800000
62	237,900000	37,020000	0,501200	0,999278	0,263100	26,330000	26,160000	3,020000	8,362000	6,590000	0,800000
63	273,100000	37,020000	0,398100	1,000350	0,272100	27,200000	27,050000	2,924000	10,880000	6,170000	0,800000
64	317,400000	37,010000	0,316200	1,000340	0,280800	28,070000	27,930000	2,858000	14,130000	5,840000	0,800000
65	369,100000	37,000000	0,251200	0,999824	0,288600	28,870000	28,730000	2,799000	18,290000	5,560000	0,800000
66	429,300000	37,000000	0,199500	0,999670	0,295300	29,540000	29,420000	2,658000	23,560000	5,160000	0,800000
67	502,000000	37,000000	0,158500	1,000410	0,300800	30,070000	29,960000	2,552000	30,200000	4,870000	0,800000
68	577,900000	37,000000	0,125900	1,000340	0,306300	30,620000	30,510000	2,569000	38,710000	4,810000	0,800000
69	647,900000	37,000000	0,100000	0,999247	0,309600	30,980000	30,880000	2,527000	49,310000	4,680000	0,800000
70	FPH										
71	Time (action)(s)	Temperature(Â°C)	Frequency(Hz)	Complex shear strain(%	Complex shear stress(Pa)	Shear modulus (complex component)(Pa	Shear modulus (elastic component)(Pa	Shear modulus (viscous component)(Pa	Shear viscosity (complex component)(Pa s	Phase angle(Â°)	Gap(mm)
72	11,000000	37,150000	10,000000	0,928009	0,401100	43,230000	42,580000	7,466000	0,688000	90,000000	0,800000
73	22,350000	37,130000	7,943000	0,972157	0,207300	21,320000	20,990000	3,767000	0,427200	90,000000	0,800000
74	34,100000	37,100000	6,310000	0,994684	0,054130	5,442000	3,852000	3,844000	0,137300	90,000000	0,800000
75	46,270000	37,090000	5,012000	0,997886	0,058670	5,879000	4,511000	3,770000	0,186700	39,880000	0,800000
76	58,850000	37,070000	3,981000	1,001470	0,116000	11,590000	11,150000	3,148000	0,463200	15,770000	0,800000
77	72,150000	37,070000	3,162000	0,997904	0,152500	15,280000	15,060000	2,603000	0,769000	9,810000	0,800000
78	86,500000	37,060000	2,512000	1,000380	0,175600	17,550000	17,380000	2,499000	1,112000	8,180000	0,800000
79	101,500000	37,050000	1,995000	1,002450	0,190500	19,000000	18,860000	2,324000	1,516000	7,030000	0,800000
80	118,000000	37,040000	1,585000	1,001110	0,201400	20,120000	19,990000	2,310000	2,021000	6,590000	0,800000
81	136,300000	37,030000	1,259000	1,002390	0,213200	21,270000	21,110000	2,582000	2,689000	6,970000	0,800000
82	156,300000	37,030000	1,000000	0,999300	0,218700	21,880000	21,740000	2,524000	3,483000	6,620000	0,800000
83	179,000000	37,020000	0,794300	1,000330	0,223900	22,380000	22,240000	2,476000	4,484000	6,350000	0,800000
84	205,900000	37,020000	0,631000	1,000400	0,229600	22,950000	22,820000	2,439000	5,789000	6,100000	0,800000
85	237,800000	37,010000	0,501200	0,999684	0,236800	23,680000	23,560000	2,457000	7,521000	5,960000	0,800000
86	273,000000	37,010000	0,398100	1,000750	0,245200	24,500000	24,390000	2,347000	9,794000	5,500000	0,800000
87	317,300000	37,000000	0,316200	1,000420	0,254100	25,400000	25,290000	2,340000	12,780000	5,290000	0,800000
88	369,100000	37,000000	0,251200	0,999963	0,263900	26,390000	26,290000	2,306000	16,720000	5,010000	0,800000
89	429,200000	37,000000	0,199500	1,000410	0,276500	27,640000	27,540000	2,300000	22,050000	4,770000	0,800000
90	501,900000	37,000000	0,158500	1,000470	0,289700	28,960000	28,850000	2,430000	29,080000	4,810000	0,800000
91	577,800000	37,000000	0,125900	0,999802	0,304800	30,490000	30,390000	2,443000	38,540000	4,600000	0,800000

Figure A2: Example data scan generated from the rheometer.

Appendix C: 2D ADSC differentiation on gels – adipogenic 7 days

TCP adipose induction

Day 1

Day 7

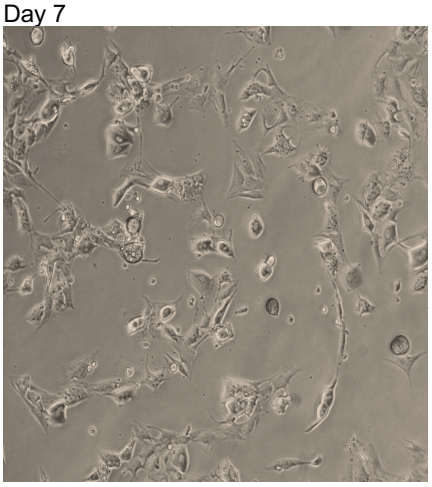

Day 7 Oil Red O

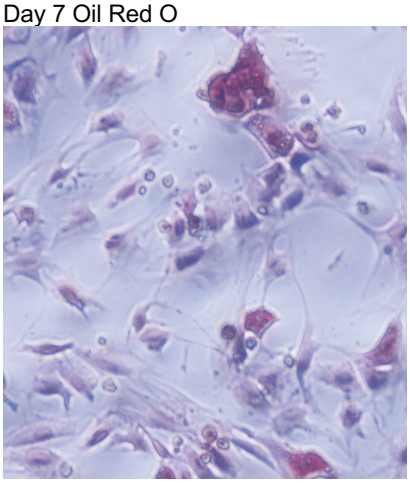

TCP non-induction control

Day 1

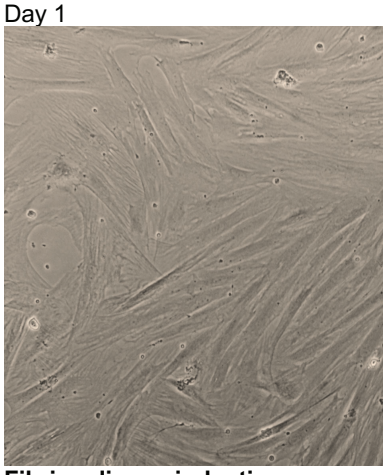

Day 7

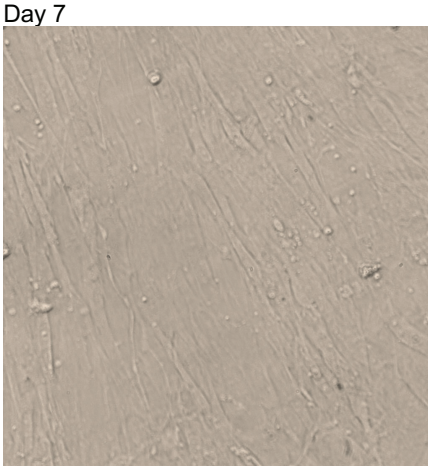

Day 7 Oil Red O

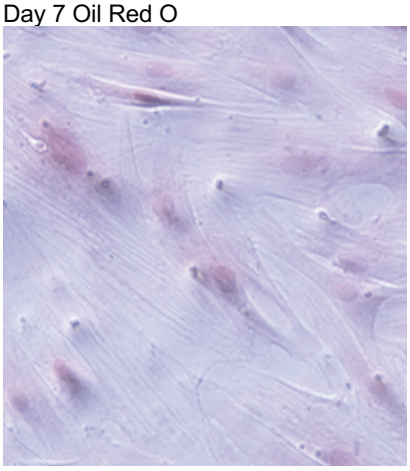

Fibrin adipose induction

Day 1

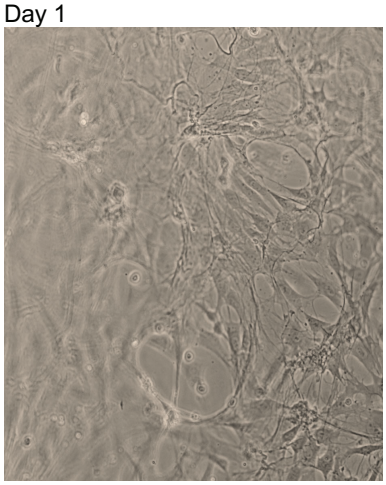

Day 7

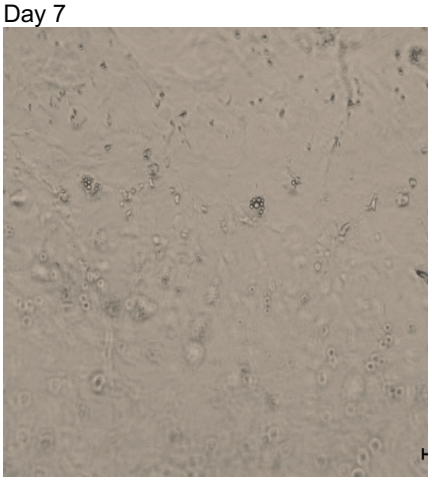

Day 7 Oil Red O

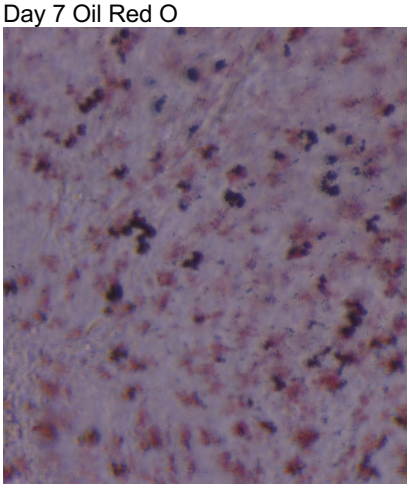

Fibrin non- induction control

Day 1

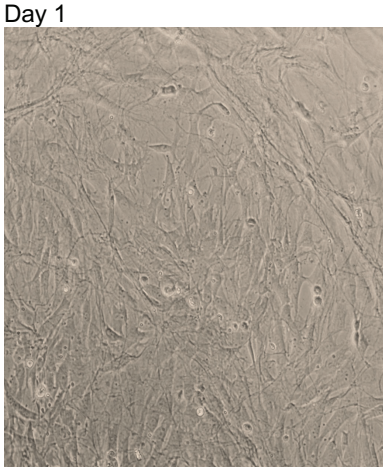

Day 7

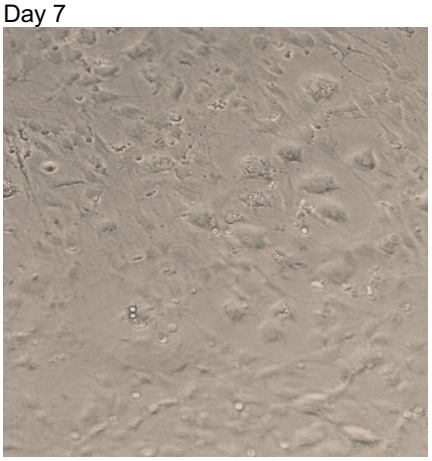

Day 7 Oil Red O

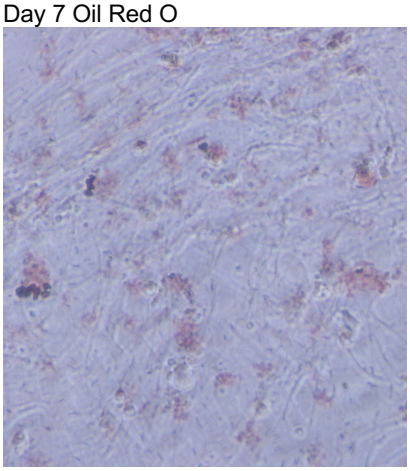

FP adipose induction

Day 1

Day 7

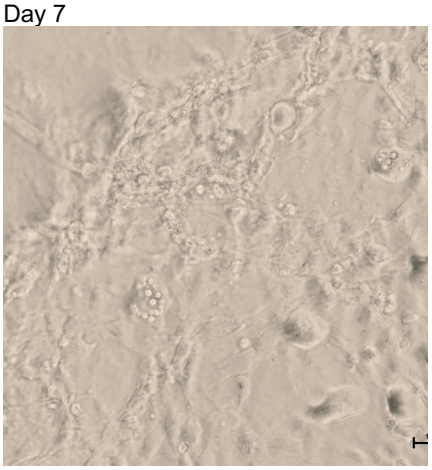

Day 7 Oil Red O

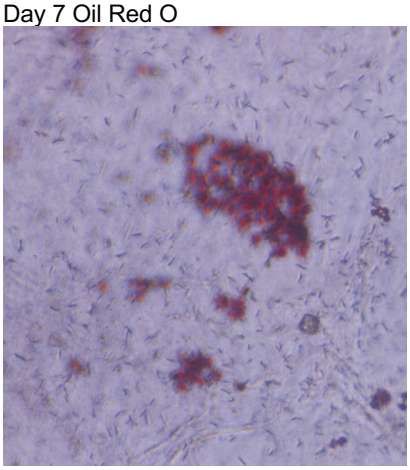

FP non-induction control

Day 1

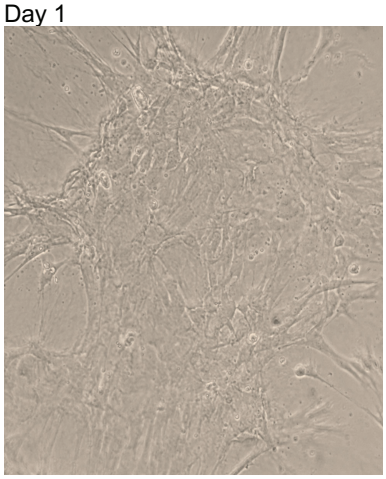

Day 7

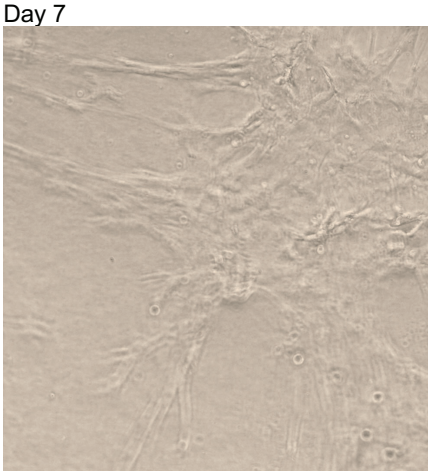

Day 7 Oil Red O

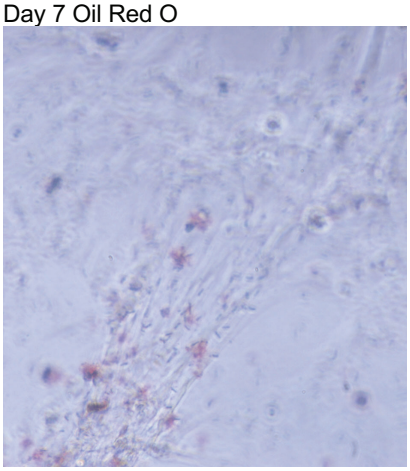

FPH: adipose induction

Day 1

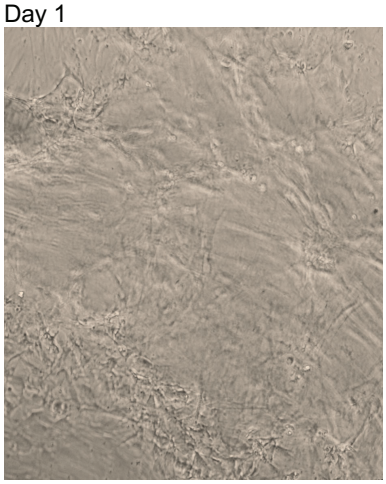

Day 7

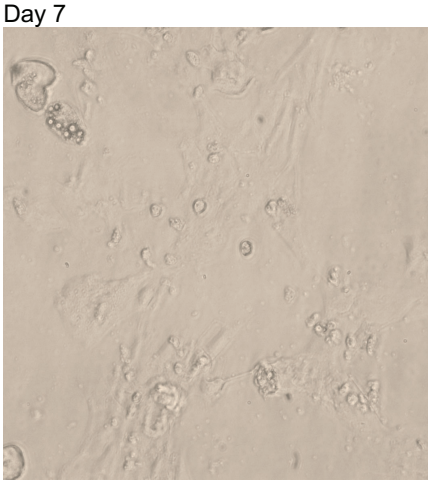

Day 7 Oil Red O

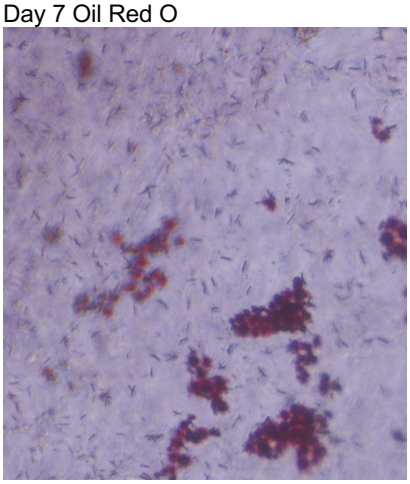

FPH non-induction control

Day 1

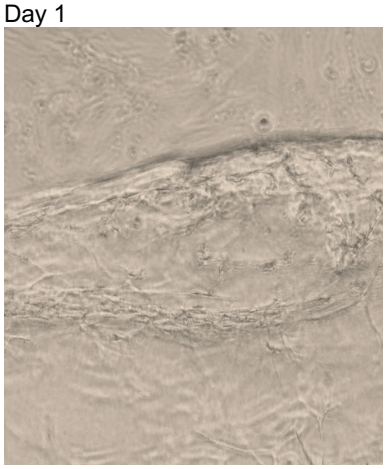

Day 7

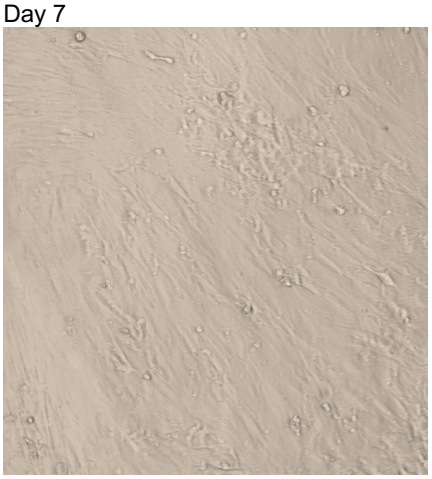

Day 7 Oil Red O

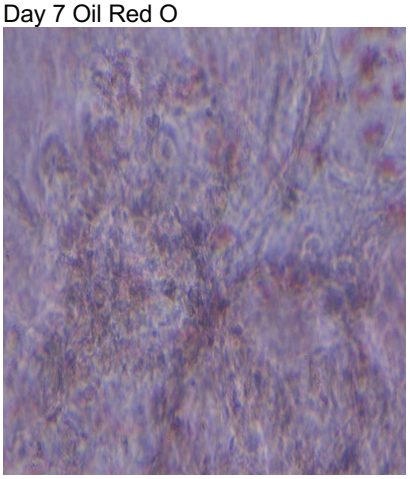

FH Adipose induction

Day 1

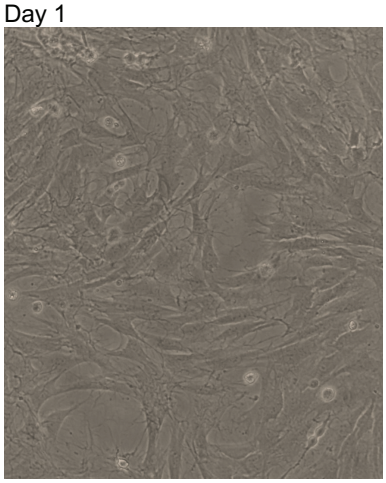

Day 7

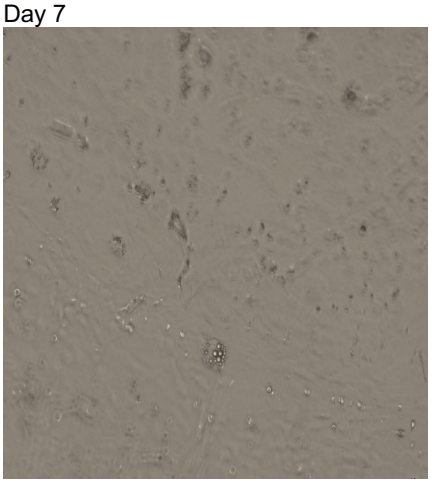

Day 7 Oil Red O

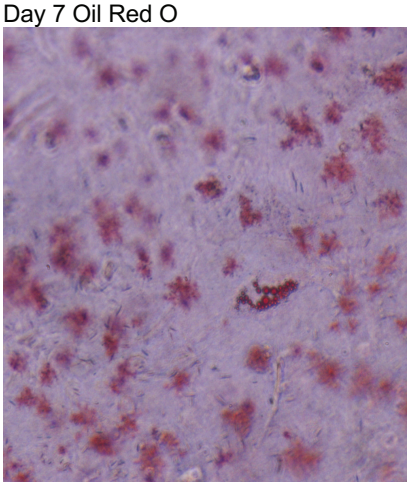

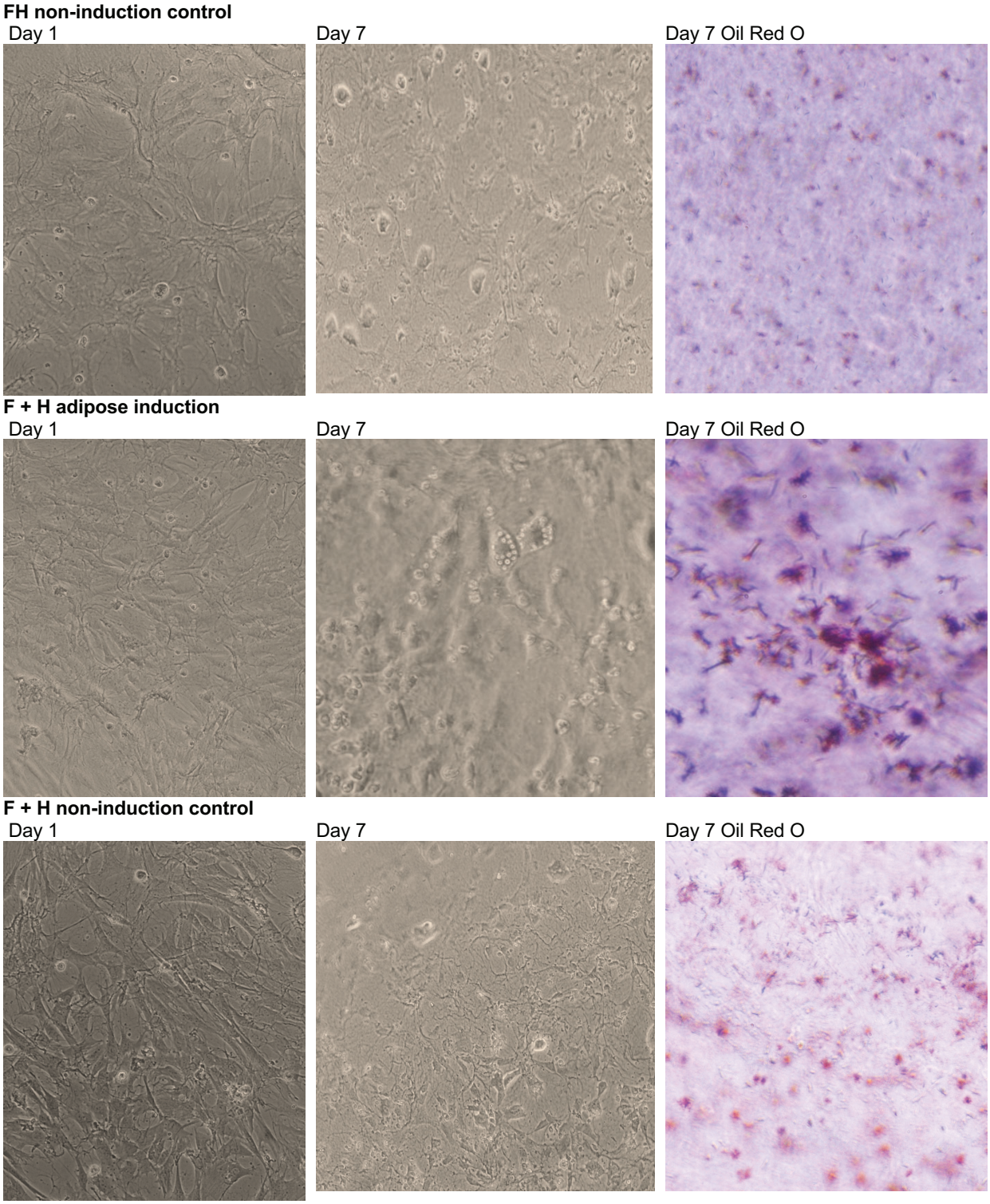

Figure A3: Micrographs of adipogenic induction on hydrogels, n=3 technical repeats

Appendix D: 2D ADSC differentiation on hydrogels – osteogenic 14 days

TCP osteogenic induction

Day 1

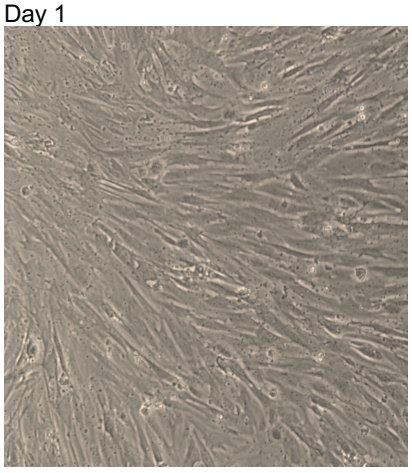

Day 14

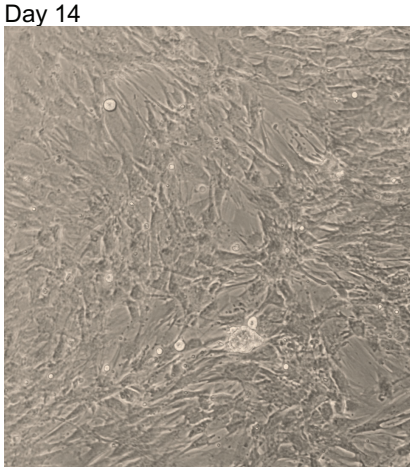

Day 14 Alizarin Red S

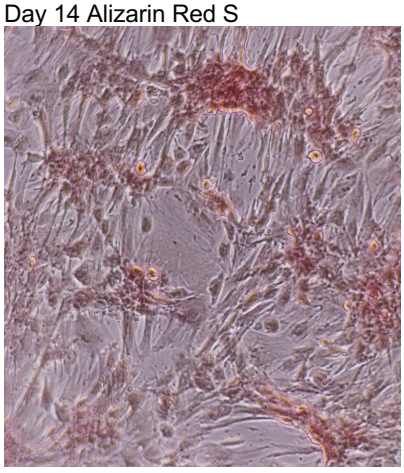

TCP non-induction control

Day 1

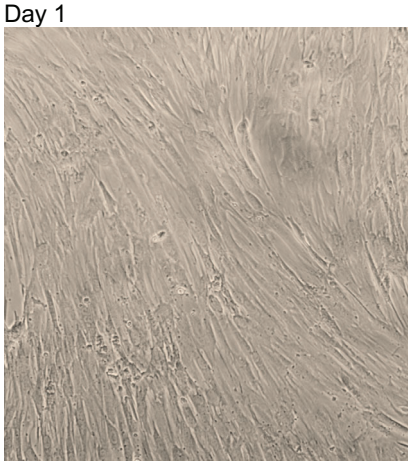

Day 14

Day 14 Alizarin Red S

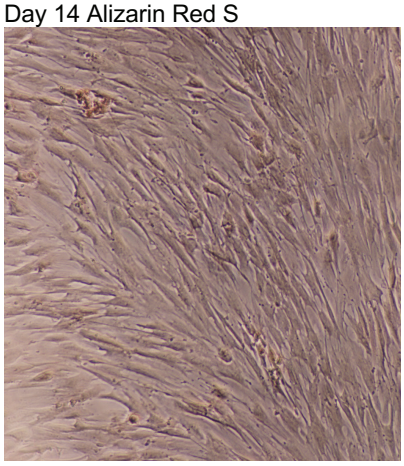

Fibrin adipose induction

Day 1

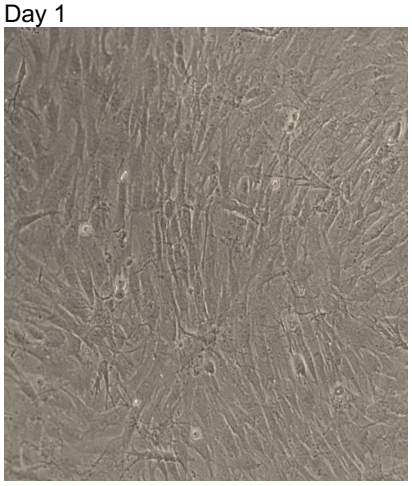

Day 14

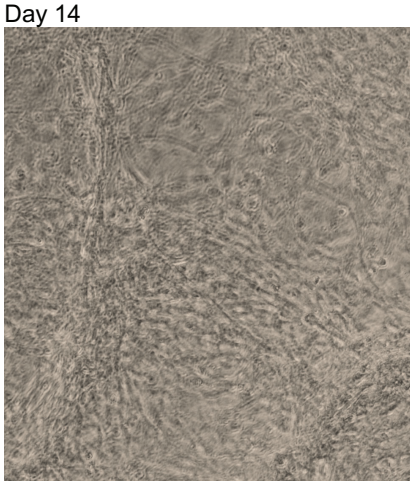

Day 14 Alizarin Red S

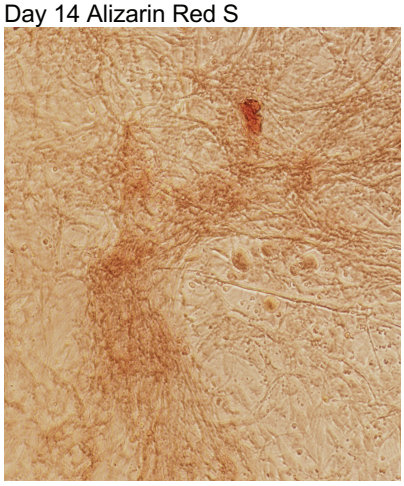

Fibrin non- induction control

Day 1

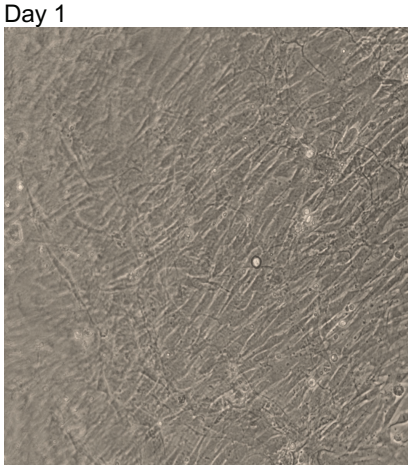

Day 14

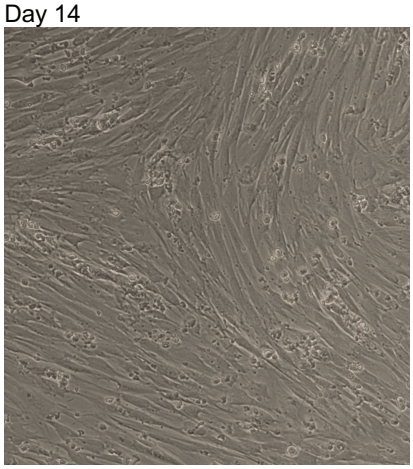

Day 14 Alizarin Red S

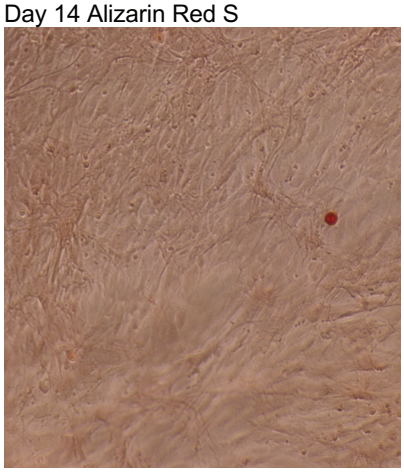

FP adipose induction

Day 1

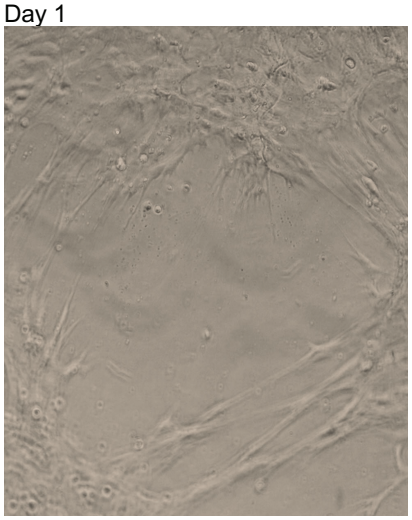

Day 14

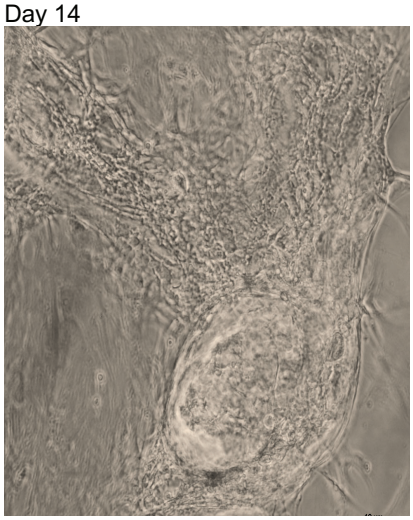

Day 14 Alizarin Red S

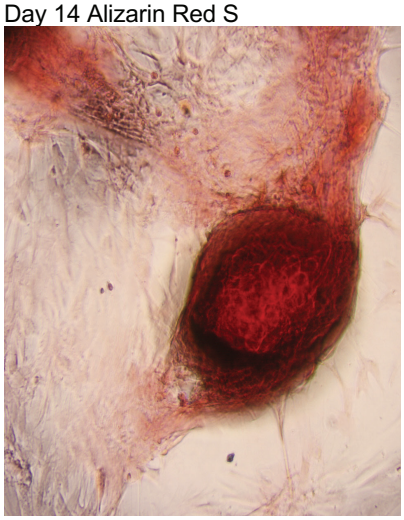

FP non-induction control

Day 1

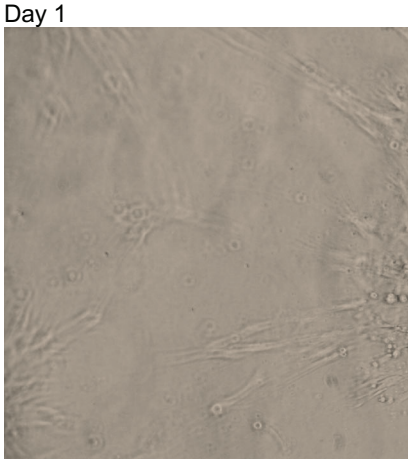

Day 14

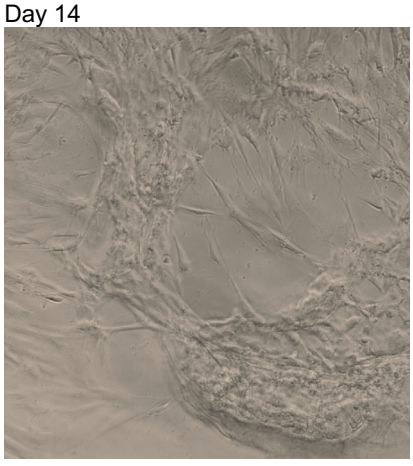

Day 14 Alizarin Red S

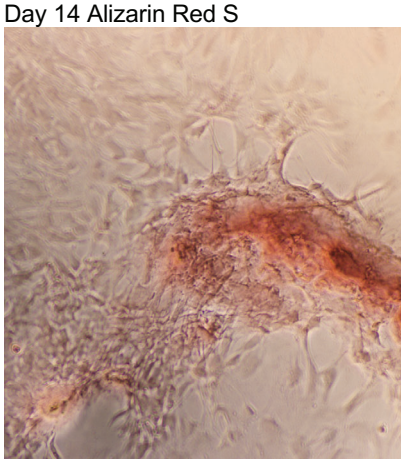

FPH: osteogenic induction

Day 1

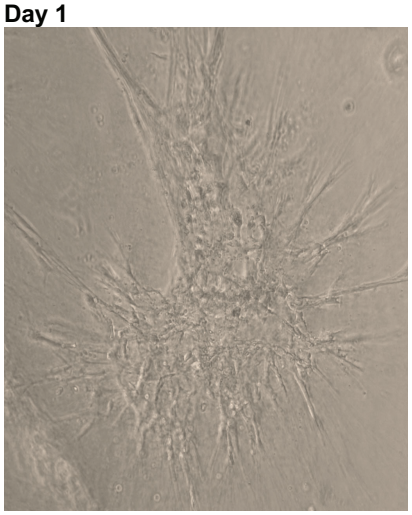

Day 14

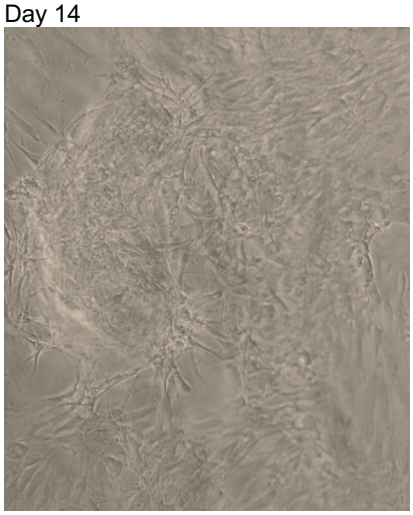

Day 14 Alizarin Red S

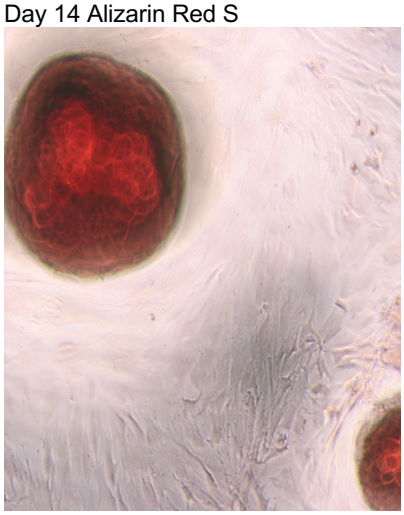

FPH non-induction control

Day 1

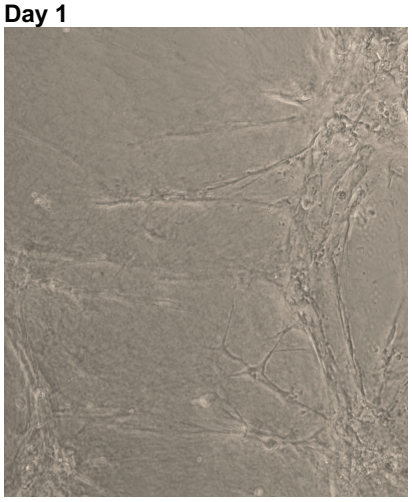

Day 14

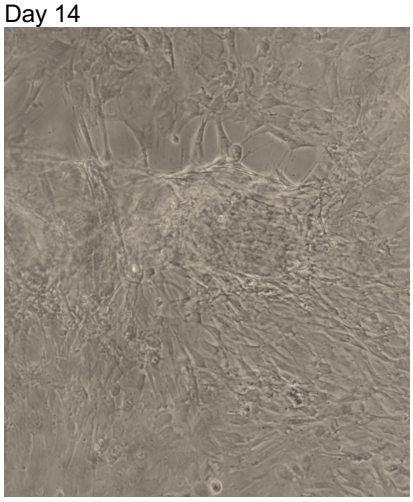

Day 14 Alizarin Red S

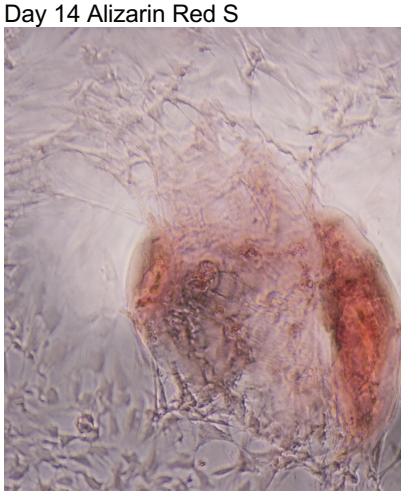

FH osteogenic induction

Day 1

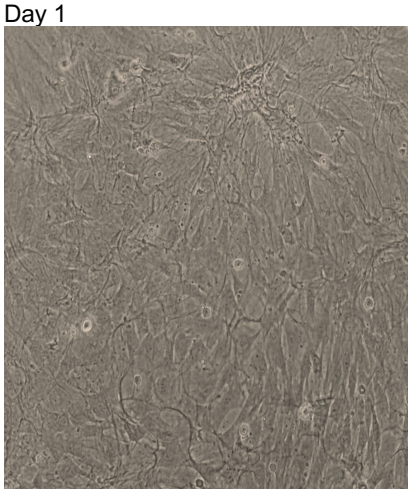

Day 14

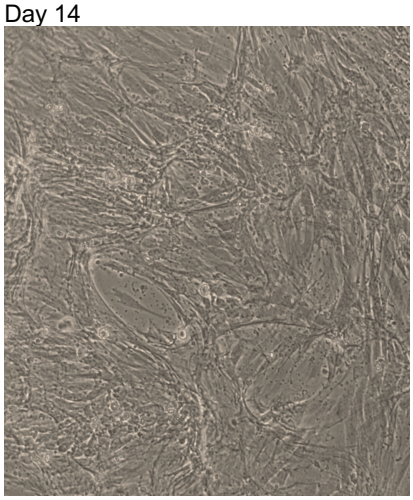

Day 14 Alizarin Red S

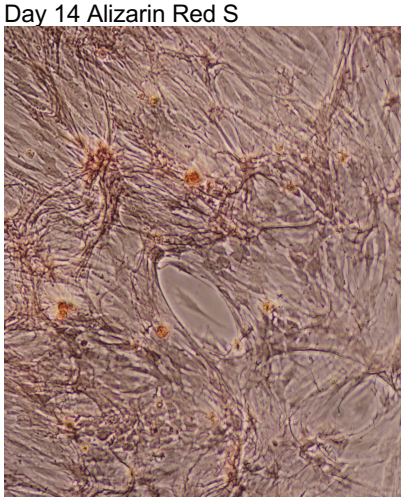

FH non-induction control

Day 1 | Day 14 | Day 14 Alizarin Red S

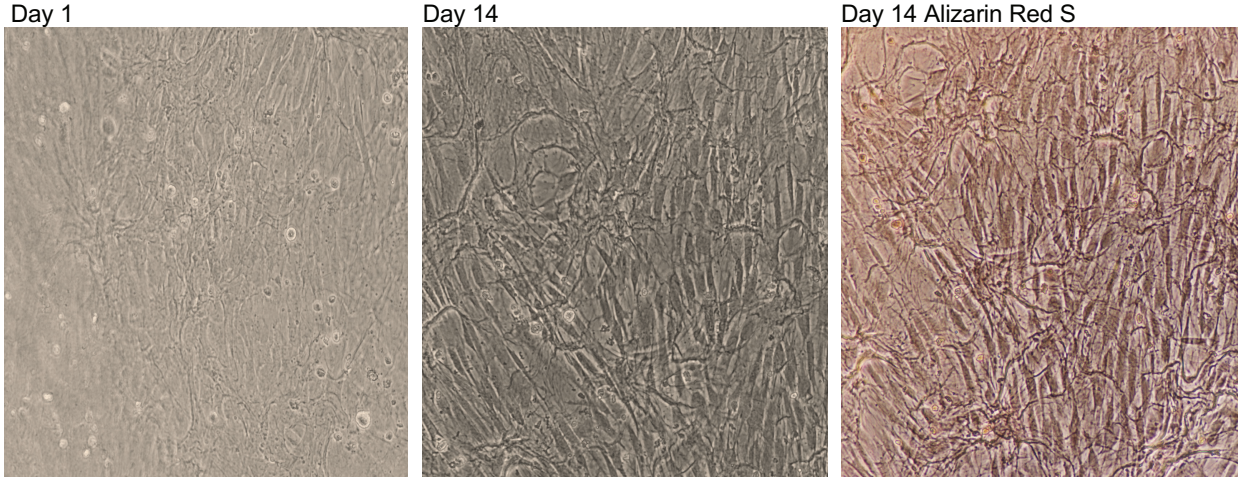

F + H osteogenic induction

Day 1 | Day 14 | Day 14Alizarin Red S

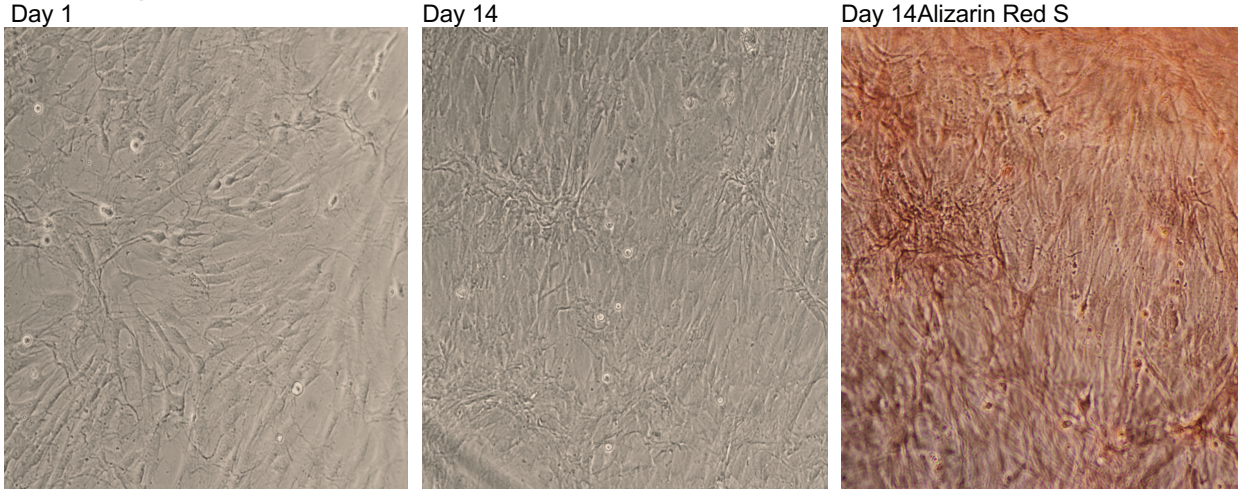

F + H non-induction control

Day 1 | Day 14 | Day 14 Alizarin Red S

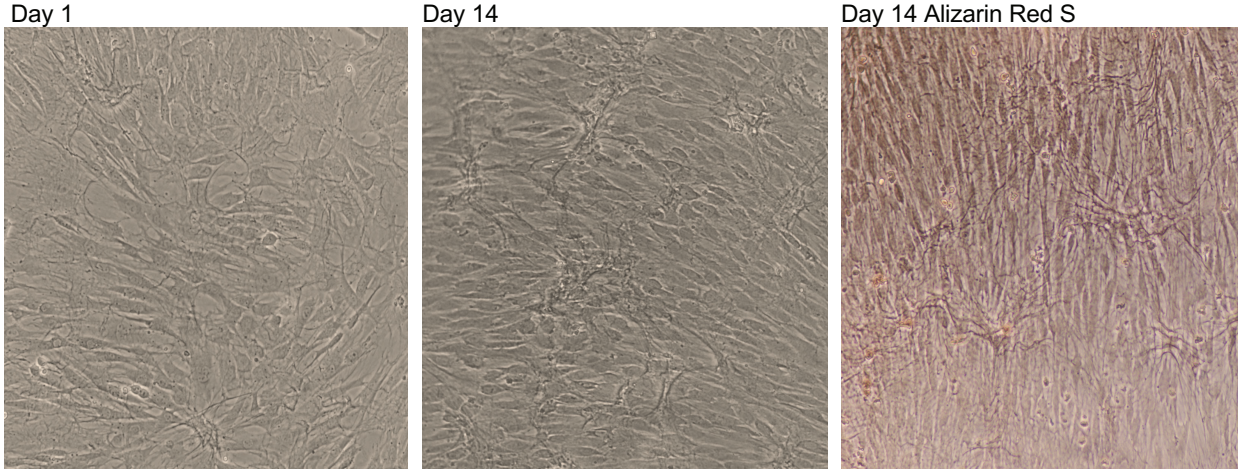

Figure A4: Micrographs of osteogenic induction on hydrogels for 14 days, n=3 technical repeats